UNREINFORCED MASONRY ITALIAN MEDIEVAL CHURCHES: A HOLISTIC FRAMEWORK FOR SEISMIC RISK ASSESSMENT FROM THE NATIONAL SCALE TO THE BUILDING SCALE

A Thesis

Submitted to the Graduate School

of the University of Notre Dame

in Partial Fulfillment of the Requirements

for the Degree of

Master of Science in Civil Engineering

by

David Pirchio

____

Kevin Quinn Walsh, Co-Director

____

Yahya Kurama, Co-Director

Graduate Program in Civil and Environmental Engineering and Earth Science

Notre Dame, Indiana

July 2020

© Copyright 2020

David Pirchio

UNREINFORCED MASONRY ITALIAN MEDIEVAL CHURCHES: A HOLISTIC FRAMEWORK FOR THE SEISMIC RISK ASSESSMENT FROM THE NATIONAL SCALE TO THE BUILDING SCALE

Abstract

by

David Pirchio

On-site surveys were conducted of 72 unreinforced masonry (URM) medieval churches across Italy. Following a hierarchical approach for the surveys, each component of risk – hazard, vulnerability, exposure, and consequence – was defined throughout by the development of indices resulting in a holistic seismic risk assessment methodology. Regarding the risk component of vulnerability specifically, a “macro-block” analysis was applied to all 28 geometric components of each surveyed church that have been identified empirically as common collapse mechanisms in historic earthquakes. To improve the efficacy of subsequent assessments, an aggregation of commonly applied non-destructive testing (NDT) techniques was proposed to address the problematic acquisition of mechanical property of heritage URM buildings sans destructive testing. Finally, a case study church selected amongst the most critical churches was both geometrically and structurally modeled by applying photogrammetric techniques based on an unmanned aircraft system (UAS) survey, building information modeling (BIM) approach, and finite

element model (FEM) analysis. The following goals of the seismic risk assessment were targeted in this study:

- Developing an appropriate and cost-efficient methodology for seismic risk assessments for large portfolios of churches;
- Quantifying the exposure and consequence components of risk by recording occupancy rates, heritage components, and equivalent replacement value of the churches;
- Developing a risk ranking of churches surveyed in order to assist stakeholders by prioritizing churches for futher detailed assessment and potentially retrofit intervention;
- Contributing to the innovation of engineering investigation techniques by introducing a rapid and reliable assessment methodology both on a regional or national scale, as well as on a higher resolution building scale;
- Recording in a rapid and dependable way the geometry and material properties with respect to complex URM churches when the lack of architectural and structural drawing represents a significant obstacle to assessment; and
- Developing a structural modeling approach for complex URM churches that is accessible by a significant portion of the practicing engineering community, based on the availability of the software utilized and the simplification of the robust analytical methods.

CONTENTS

FIGURES

TABLES

PREFACE

To my family, without whose support I would not have reached any of my results.

To Chiara, without whose help I could not have made it through my tougher periods.

To Riccardo, I hope you will be proud of me as much I was of you.

A special thanks to all who helped and advised me throughout the completion of my research including Dr. Elizabeth Kerr, Dr. Ivan Giongo, Dr. Kevin Q. Walsh, Dr. Marta Giaretton, Dr. Brad Weldon, and Dr. Luigi Sorrentino.

Last, but not least, a special thanks to the undergrads that made my summer much less stressful and much more fun: Elizabeth, Emily, Lily, Marie, and Patricia.

ACKNOWLEDGMENTS

This research was primarily funded by a Global Gateways Faculty Research Award at the University of Notre Dame (grant FY18RGG03). Undergraduate students at the University of Notre Dame who assisted with the surveys include Elizabeth DePaola, Emily Brady, Lily Polster, Marie Bond, and Patricia Dirlam. These students were supported by research scholarship funding from various programs, institutes, and centers at the University of Notre Dame, including the Fitzgerald Institute for Real Estate, the Grand Challenges Scholars Program, the Women in Engineering Program, and the Flatley Center for Undergraduate Scholarly Engagement.

The authors are thankful for the assistance of the cultural heritage offices of the involved dioceses, as well as the assistance of Dr. Federica Romiti (diocese of Anagni – Alatri), the Bishop Stefano Manetti and the Surveyor Marco Cortellessa (diocese of Montepulciano – Chiusi – Pienza), Don Francesco Valentini and the Dr. Giovanna Bandinu (diocese of Orvieto – Todi), the Arch. Agapito Fornari (diocese of Palestrina), Don Riccardo Pascolini (diocese of Perugia – Città della Pieve), Don Fabio Sottoriva (diocese of Vicenza), the Dr. Monia Sartori (archdiocese of Trento), the Arch. Graziana Santamaria, and the Surveyor Marco Cherubini. The first author would like to thank his parents Valter Pirchio and Lorena Trentini for their assistance with logistics, as well as an undergraduate student at the University of Trento, Chiara Meloni. The following priests are thanked for granting access to their churches and for assisting during the data collection:

- Diocese of Anagni – Alatri: Deacon Massimiliano Floridi, Don Alessandro De Sanctis, Don Antonio Castagnacci, Don Pierino Giacomi, Don Roberto Martufi, Don Virginio De Rocchis, and the parishes' collaborators.
- Diocese of Montepulciano – Chiusi – Pienza: Don Andrea Malacarne, Don Antonio Nutarelli, Don Azelio Mariani, Don Carlo Sensani, Don Elia Sartori, Don Francesco Monachini, Don Kishor Uppalapati, Don Manlio Sodi, Don Sergio Graziani, Don Silvano Nardi, Don Stefano Cinelli, and the parishes' collaborators.
- Diocese of Nocera Inferiore – Sarno: Friar Damiano Antonino, Friar Felice Petrone, Friar Michele Alfano, Friar Raffaele Panopio, Friar Renato Sapere, and the parishes' collaborators.
- Diocese of Orvieto – Todi: Don Claudio Calzoli, Don Jeremiah Joseph Kelly, Don Marcello Sargeni, Don Marco Gasparri, Don Piero Grassi, and Don Zeffiro Tordi.
- Diocese of Palestrina: Monsignor Andrea Leonardo, Don Davide Maria Martinelli, and the parishes' collaborators.
- Diocese of Perugia – Città della Pieve: Don Augusto Martelli, Don Fabio Quaresima, Don Gianni Pollini, Don Giuseppe Piccioni, Don Marco Merlini, Don Matteo Rubechini, Don Vincenzo Esposito, and the parishes' collaborators.

- Diocese of Sorrento – Castellammare di Stabia: Don Antonino Lazzazzara, Don Beniamino Di Martino, Don Ciro Esposito, Don Maurizio Esposito, and the parishes' collaborators.
- Diocese of Trento: Don Ferdinando Murari, Don Maurizio Toldo, and the parishes' collaborators.
- Diocese of Vicenza: Don Adriano Preto Martini, Don Fabio Ogliani, Don Francesco Strazzari, Don Giacomo Viali, Don Giovanni Campagnolo, Don Giovanni Imbonati, Don Giovanni Sandonà, Don Giuseppe Mattiello, Don Luigi Spadetto, Don Paolo Zampiva, and the parishes' collaborators.

CHAPTER 1:

INTRODUCTION

1.1 Overview

Unreinforced masonry (URM) Italian Medieval churches represent a fundamental component of the architectural and artistic heritage panorama in Italy both in terms of the countless and invaluable artworks housed within these buildings and for the architectural value of the churches themselves as expressions of the mastery of Italian architects throughout the Middle Ages. However, while several studies on post-earthquake damage have been conducted to analyze the behavior of URM churches and develop assessment methodologies with respect to church vulnerability during earthquakes (e.g., Doglioni, Moretti and Petrini 1994, Marotta, et al. 2017, Gàlvez, et al. 2018), the author is aware of no previous investigation performed with a nationwide footprint to address a holistic risk assessment encompassing both structural and non-structural risk criteria for Medieval churches in Italy. A previous nationwide study conducted on URM churches in New Zealand was limited to accounting primarily for seismic hazard and structural vulnerability (A. Marotta et al. 2018) with a limited implementation of the exposure and consequences compared to the study presented herein.

In addition to the addressed structural fragility of URM churches, there are geotechnical, historical, cultural, and economical reasons that represent an inherent predisposition of Italian churches to be exposed to larger overall risks of damage and collapse compared to churches in other countries. Three primary reasons were identified as follows:

- The hazard component of risk is enhanced by the severe level of seismicity in Italy;
- After the Lateran Treaty in 1929, Catholicism was no longer officially the sole state-supported religion in Italy; therefore, the Catholic Church was deprived of state financing as well as the formal ownership of several religious buildings (Wright 1944). As a direct consequence, resources for retrofitting interventions on churches were subjected to drastic reductions and, currently, the dioceses often have limited budgets available to invest on retrofitting interventions, intended only for existing buildings older than 20 years (CEI 2018), and with several restrictions (e.g., ordinary maintenance and any intervention less expensive than 50,000€ cannot be funded);
- Italy had been the early center of Christianity for centuries (MacCulloch 2010); thus, a significant number of churches was constructed within the current borders of Italy enhancing the amount of exposed heritage and augmenting the complications of having a sustainable and systematic program of maintenance and intervention;

In the following manuscript, a holistic seismic risk assessment methodology accounting for the four components of risk (i.e. hazard, vulnerability, exposure, and consequences) was developed, as extensively discussed in Chapter 2:. Reproducibility, rapid implementation, and generalizability were targeted as critical features of the proposed methodology. The ultimate goal of the proposed seismic risk assessment methodology was to provide the dioceses with a scientific and objective basis for the management of their buildings portfolio and to support their decision-making process with respect to the allocation of the limited funds at their disposal for an efficient prioritization of detailed assessment and future retrofitting interventions.

Due to their status as critical heritage buildings, URM Italian Medieval churches are often subjected to regulatory and architectural constraints that prohibit the extraction of specimens to be studied in laboratory testing using destructive techniques. A national-scale provisional seismic risk assessment of the portfolio, as well as more detailed structural analysis, are likely to be affected by these uncertainties in material properties. With the aim of enhancing the dependability of non-destructive testing (NDT) techniques without losing the rapidity and cost-efficiency of their application, a review of some NDT techniques commonly applied to URM buildings was conducted and a methodology for the aggregation of the reviewed NDT techniques was proposed.

Finally, a select case study church was chosen for detailed assessment based on its high risk ranking in the provisional regional assessment. The church case study was subjected to a three-step detailed assessment procedure, identified as follows:

- Step 1: Acquisition of the geometry of the church via photogrammetry-based surveys using unmanned aircraft systems (UAS) and development of the dense point cloud (given that structural and architectural drawings almost never exists for Medieval churches);
- Step 2: Development of a 3D model comprising geometric information, material properties, and various other risk-related information collected from site

investigations, and their aggregation into a complete building information model (BIM); and

- Step 3: Detailed structural analysis of the church, with respect to both global and local behavior, using finite element model (FEM) analysis software and supplemented with “macro-block” element analysis.

1.2 Thesis Format

The manuscript is presented in the “thesis by publications” format wherein each body chapter represents a paper that has been (or will be at the time of the final thesis submission) submitted to a peer-reviewed journal publication. Given the similar subjects, intents, and objectives of the included papers, and the “thesis by publications” format, some intrinsic repetition of information might be observed throughout the manuscript. The following subsections offer a rapid overview of each chapter and references the included papers and their submission status.

1.2.1 Chapter 2. Seismic Risk Assessment and Intervention Prioritization for Italian Medieval Churches

Given the limited funds allocated to dioceses to perform retrofitting interventions on their buildings portfolio (CEI 2018), the decision-making process to achieve a fair and efficient prioritization with respect of the allocation of funds to the dioceses might result quite uncertain and without a scientific basis. On-site surveys of 72 URM Italian Medieval churches were conducted with the aim of developing a rapid, generalizable, and dependable national-scale seismic assessment methodology to help the dioceses in the management of their building portfolio. To achieve a holistic approach to the risk assessment, several components of risk (i.e., hazard, vulnerability, exposure, and consequences) were accounted, defined, parametrized, and aggregated.

Included publication:

Pirchio, D., Walsh, K. Q., Kerr, E., Giongo, I., Giaretton, M., Weldon, B. D., Ciocci, L., Sorrentino, L. 2020a. Seismic risk assessment and intervention prioritization for Italian Medieval churches (Submitted). *International Journal of Architectural Heritage*.

1.2.2 Chapter 3. An Aggregated Non-destructive Testing (NDT) Methodology for the Assessment of Mechanical Properties of Unreinforced Masonry Italian Medieval Churches

Given the drawbacks of destructive and semi-destructive testing techniques of heritage buildings, they are not feasible procedure for assessing the mechanical properties of URM churches without causing damage to the structure. An aggregation of different commonly applied non-destructive testing (NDT) techniques was proposed to overcome the practical limitations of more invasive testing techniques. The aggregated method was proposed with the aim of being more dependable of the single addressed NDT techniques without relevant loss in terms of cost-efficiency of the testing procedure.

Included publication:

Pirchio, D., Walsh, K. Q., Kerr, E., Giongo, I., Giaretton, M., Weldon, B. D., Ciocci, L., Sorrentino, L. 2020b. An aggregated non-destructive testing (NDT) methodology for the assessment of mechanical properties of unreinforced masonry Italian Medieval churches (In preparation). *Construction and Building Materials*.

1.2.3 Chapter 4. Integrated Framework to Structurally Model Unreinforced Masonry Italian Medieval Churches: From Photogrammetry to Finite Element Model Analysis through Building Information Modeling

Given the inherent complexity of the unreinforced masonry as a non-homogeneous and discrete material, and the complicated structure (both in terms of geometry and dynamic behaviour) of Italian Medieval churches, the structural analysis of URM churches might often require highly specialized software and a niche expertise to be performed. Given the practice limitations of the above mentioned highly specialized analysis, a three-steps procedure involving the acquisition of geometric information via drones and photogrammetric techniques, the development of a solid three-dimensional BIM-based model, and the analysis of the latter based on modal response spectrum in a finite element modeling environment was performed on a case study. The intent of the case study was to provide professional engineers with a basic framework to be followed in all those cases where extensive geometric information is missing, and highly specialized analysis are not viable.

Included publication:

Pirchio, D., Walsh, K. Q., Kerr, E., Giongo, I., Giaretton, M., Weldon, B. D., Ciocci, L., Sorrentino, L. 2020c. Integrated framework to structurally model unreinforced masonry Italian Medieval churches: from photogrammetry to finite element model analysis through building information modeling (In preparation). *Engineering Structures*.

CHAPTER 2:

SEISMIC RISK ASSESSMENT AND INTERVENTION PRIORITIZATION FOR ITALIAN MEDIEVAL CHURCHES

Rapid and reliable seismic risk assessment are critical to help practicing engineers, facility stakeholders, and insurance companies in their asset management decision-making processes. In particular, the integrity of the Italian church portfolio has been often threatened by intense earthquake. The Italian church portfolio includes thousands of religious buildings, often representing milestones of the Italian art and architecture, therefore, it requires an assessment methodology which accounts for the structural, architectural, cultural, and functional complexities of churches. The methodology proposed herein combined both widely applied assessment techniques for structural vulnerability (e.g., "macro-blocks") with a newly developed framework accounting for other important variables (e.g., the heritage value of a church) to produce a rapid, quantifiable, and holistic approach to the seismic risk assessment of historic masonry churches. On-site surveys of 72 unreinforced masonry medieval churches across Italy were conducted. Following a hierarchical approach for the surveys, each risk component – hazard, vulnerability, exposure, and consequence – was defined throughout by the development of 13 different indices. Using the fuzzy set theory, the indices were aggregated into a final risk rating useful to provide the stakeholders with a scientific-based prioritization list for the maintenance and retrofit intervention of their church portfolios.

2.1 Introduction

Churches retain a dominating importance among Italian cultural and spiritual life as they represent and contain a relevant component of Italian architectural and artistic heritage. However, this built heritage undergoes significant risk during seismic events. During most of the major earthquakes in recent history, churches suffered significant damage and even partial or complete collapse (Doglioni, Moretti, and Petrini 1994; Lagomarsino 2012; Parisi, Tardini, and Maritato 2016). Thus, it is relevant to prevent the structural failure of churches to avoid significant losses in terms of cultural heritage, economic value, and human lives. In theses terms, the Italian church portfolio, with its immense architectural, cultural, and functional value, is the perfect case study for a research with aim of addressing holistically the risk as function of several components (i.e., hazard, vulnerability, exposure, and consequences).

Several studies have been conducted regarding structural behavior, vulnerability assessment, and retrofitting intervention on churches (Doglioni, Moretti, and Petrini 1994; Lagomarsino and Podestà 2004). However, most of the historical research has focused on advanced modeling for single case studies (e.g., Valente and Milani 2019). Several empirical studies were also conducted after strong earthquakes at a regional scale (Doglioni, Moretti, and Petrini 1994; Lagomarsino et al. 1997; Lagomarsino and Podestà 2004; da Porto et al. 2012; Sorrentino et al. 2014; De Matteis et al. 2019; Penna et al. 2019), Furthermore, nationwide studies to predict the vulnerability of unreinforced masonry (URM) churches were performed as well outside of Italy (Abeling et al. 2018; Marotta et al. 2018). However, previous research generally was limited to considering the structural vulnerability of churches. The authors are not aware of any previous investigation of church seismic risk that encompass the Italian nationwide geographic footprint accounting holistically for all general risk components (i.e., hazard, vulnerability, exposure, and consequences).

2.2 Scope, Objectives, and Novelties

The current research focused on developing a holistic and generalizable seismic risk assessment methodology, developing a prioritization of churches for asset management decisions and retrofitting intervention. Developing a prioritization listing based on comparative risk was considered a useful way to help the dioceses in their property portfolio management decision-making processes. The dioceses often have limited budgets available to invest on retrofitting interventions on existing buildings older than 20 years (CEI 2018); therefore it is necessary to prioritize churches for interventions.

72 URM churches were assessed in nine different dioceses, distributed amongst six regions in North, Central and South Italy (Figure 2.1). The selected churches were surveyed for the existing masonry geometry, existing damage (i.e., cracking), and material properties to develop a suite of data for simulated models that may forecast possible collapse mechanisms. Some prototypical examples of the chosen churches are represented in Figure 2.2. To make the developed methodology generalizable, a representative range of medieval churches was selected. Some of the information collected for each individual church can be found in Table A.1 of Appendix A.

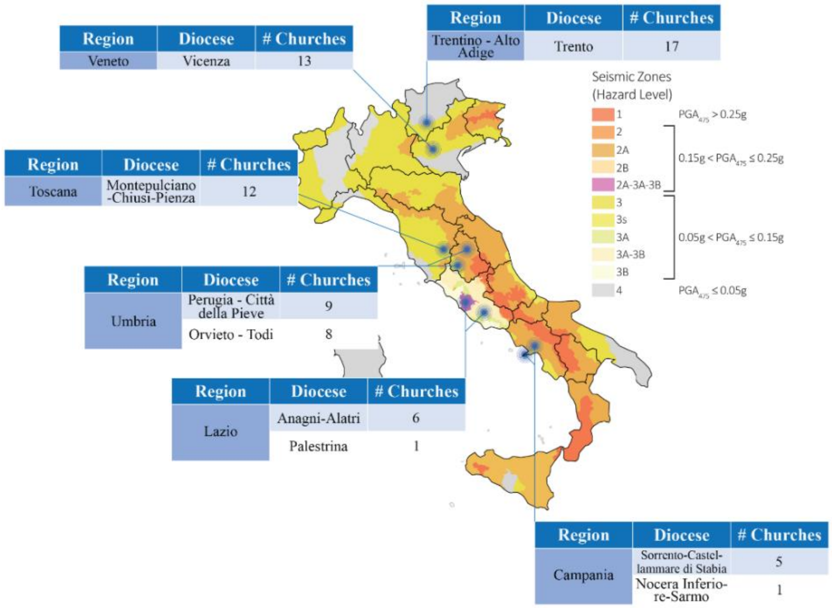

Figure 2.1: Map of Italy indicating the nine dioceses in which churches were surveyed superimposed atop the national seismic hazard map. PGA_{475} = peak ground acceleration for a 475-years average return period, units of gravity acceleration (*g*). Seismic zones adopted from the Italian National Civil Protection (Protezione Civile Nazionale 2019).

Figure 2.2: Examples of prototypical churches surveyed: a) Santa Maria Assunta (Dasindo, Trentino – Alto Adige); b) San Matteo Apostolo (Cavazzale, Veneto); c) Santi Leonardo e Cristoforo (Monticchiello, Toscana); d) Sant’Ansano Martire (Petrignano del Lago, Umbria); e) Maddalena (Alatri, Lazio); f) Santa Maria di Casarlano (Casarlano, Campania).

The scope of the research was to provide the church stakeholders and practicing engineers with a holistic and comprehensive seismic risk assessment methodology to be used as a scientific, objective basis in guiding the dioceses through their decision-making process for the allocation of maintenance and retrofitting intervention funds. Rather than proposing advanced techniques for addressing any specific risk component (i.e., hazard, vulnerability, exposure, and consequences), the authors focused on the identification of all the possible factors contributing to overall seismic risk (i.e., risk subcomponents), their definition, and the development of an index-based procedure for quantification.

Pre-existing and established assessment techniques, where available, were applied to quantify the risk subcomponents (e.g., the macro-block vulnerability assessment per DPCM 2011), while a statistically based analysis was performed to quantify the subcomponents not explicitly defined within current literature. The subcomponents were aggregated through the application of the fuzzy set theory (FST; Zadeh 1965) resulting in a final relative risk rating for each church.

Each risk subcomponent was quantified through the use of easily accessible and/or widely accepted metrics. While future research and advances in the assessment of each risk subcomponent are desirable and encouraged, the authors' goal was to develop an applicable framework combining the state of the art in a holistic and readily applied seismic risk assessment methodology for provisionally determining which churches will warrant more sophisticated analysis.

2.3 Selection Criteria

Churches chosen for consideration in this study were required to meet the following criteria impacting life safety and the cultural heritage of the churches:

- The geographic location (i.e., the researchers sought a range of geographic locations and seismicity zones);
- Active functionality within the community based on the church housing regular churchgoers, and the church's dominant role as a focal point of the spiritual life within the parish, given the relatively small sizes of the communities included in this study. This characteristic is represented by the term "community church";
- A construction period approximately between the years 1000 and 1500 (but occasionally slightly outside this timeframe); and
- A building planimetric layout preferably – but not exclusively – typical of stand-alone churches in city squares (i.e., piazzas).

2.3.1 Geographic Location

To obtain a large variety of in-site conditions, the geographic location for the case studies of the current research was based on a representative range of seismicity, density of churches, climate and geologic/topographic environments, and cultural/historic background.

2.3.1.1 Seismicity

Churches were chosen so as to achieve a wide variety of locations across the spectrum of codified seismic hazards (Figure 2.1) to ensure the development of a generalizable assessment methodology. The diocese of Perugia-Città della Pieve in the Umbria region, the diocese of Anagni-Alatri in Lazio, and the diocese of Vicenza in Veneto are generally associated with higher seismicity compared to the other considered dioceses.

2.3.1.2 Density Churches

Another critical parameter that affected the geographical criteria is the density of churches within the regions, as quantified in Equation 2.1, Table 2.1, and Figure 2.3. There is still no known complete record of the number of churches in each region, but a census of all the Italian churches is currently ongoing (Chiesa Cattolica 2018). Based on this census the number of parishes and the number of priests per 10,000 residents (Figure 2.3) was used to define an "index of exposure proxies" i_{ep}. This index was used to classify the ecclesiastical regions (i.e., how Italy is divided from the Church administration point of view) by the perceived importance and density of the church services for the community. Regions with a larger density of parishes and priests were considered more exposed to the possible consequences of natural disasters, since the spiritual services and safety of the residents may be more heavily affected by church collapse. The resulting index i_{ep} was calculated using Equation 2.1:

$$i_{ep} = \frac{1}{2}\left(\frac{N_{pa,i}}{N_{pa,max}} + \frac{N_{pr,i}}{N_{pr,max}}\right) \tag{2.1}$$

where: i_{ep} is the index of exposure proxies;

$N_{pa,i}$ represents the number of parishes per 10,000 residents in region i;

$N_{pa,max}$ represents the maximum value of $N_{pa,i}$ among the 16 ecclesiastical regions (whole Italy);

$N_{pr,i}$ represents the number of priests per 10,000 residents in region i;

$N_{pr,max}$ represents the maximum value of $N_{pr,i}$ among the 16 ecclesiastical regions (whole Italy).

These parameters are quantified for the 16 ecclesiastical regions of Italy in Table 2.1. The regions named in bolded text represent the regions in which churches were surveyed in the current study.

The selected ecclesiastical regions offer a wide range in terms of both the density of parishes and priests. As shown in Table 2.1, Umbria and Tuscany are regions with higher large parish density (respectively, 7.06 and 6.78 per 10,000 residents), while Lazio has the largest density of priests (14.37 per 10,000 residents). Triveneto (including the administrative regions of Trentino – Alto Adige, Veneto, and Friuli Venezia-Giulia) has a mid-range density both for parishes and priests, while Campania has the lowest density of parishes and priests over the population amongst the surveyed regions.

TABLE 2.1

THE NUMBER OF PARISHES AND PRIESTS PER 10,000 RESIDENTS IN THE 16 ITALIAN ECCLESIASTICAL REGIONS IN DESCENDING ORDER OF THE INDEX OF EXPOSURE PROXIES I_{EP}

Ecclesiastical region (bolded were included in this study)	**Parishes per 10,000 residents**	**Priests per 10,000 residents**	$\boldsymbol{i_{ep}}$
Umbria	**7.06**	**12.21**	**0.92**
Abruzzo-Molise	6.95	10.15	0.80
Toscana	**6.78**	**8.63**	**0.78**
Liguria	6.47	8.71	0.76
Triveneto	**5.11**	**10.15**	**0.72**
Lazio	**2.52**	**14.37**	**0.68**
Marche	5.61	7.04	0.64
Emilia-Romagna	6.06	5.97	0.64
Piemonte	4.90	8.27	0.63
Basilicata	4.46	6.82	0.55
Calabria	4.79	5.03	0.51
Lombardia	3.16	8.10	0.51
Sardegna	3.72	6.63	0.49
Sicilia	3.36	6.08	0.45
Campania	**3.08**	**6.04**	**0.43**
Puglia	2.51	6.05	0.39

NOTE: The regions named in bolded text represent the regions in which churches were surveyed in the current study; Triveneto represents the ecclesiastical region grouping the three administrative regions of Friuli-Venezia Giulia, Trentino-Alto Adige, and Veneto.

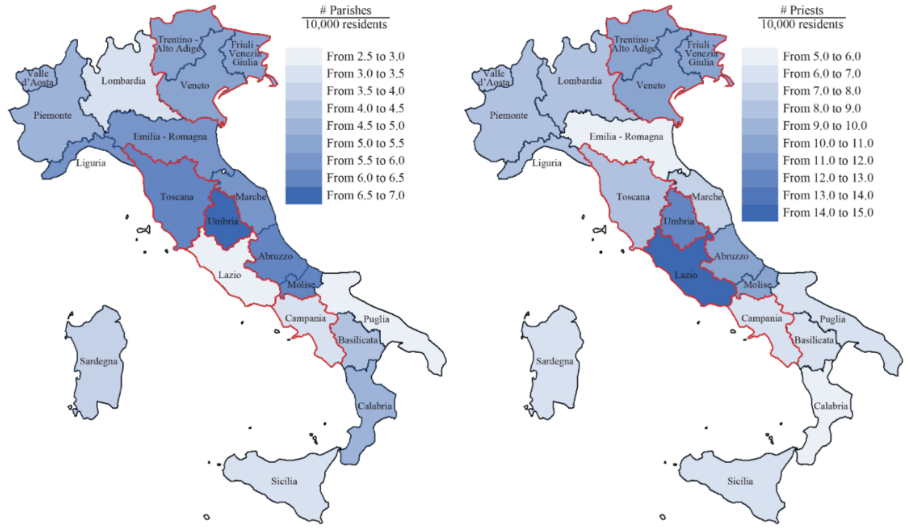

Figure 2.3: Number of parishes and priests for every 10,000 residents. Data adopted from the Italian Episcopal Conference (Conferenza Episcopale Italiana 2019).

2.3.1.3 Climate and Geologic/Topographic Conditions

The distinctive climatic and geologic/topographic condition of each diocese plays an important role in the original choice of building materials. Churches surveyed in the current study were constructed using different techniques and materials, which represents a key variable for developing a generalizable risk assessment. Thus, the range of surveyed dioceses (Figure 2.1) was also selected to account for the significant climatic and geologic/topographic differences between the various regions of the country:

- The diocese of Trento, in the region of Trentino – Alto Adige, is a mountainous area full of valleys within the alpine mountain range;
- The diocese of Vicenza, in the region of Veneto, occupies an ample part of the "Po Valley", the largest Italian plain region;

- The diocese of Montepulciano-Chiusi-Pienza, in the ecclesiastical region of Toscana, is an area covered by steep hills;
- The dioceses of Perugia-Città della Pieve and Orvieto-Todi, in the ecclesiastical region of Umbria, are hilly areas;
- The dioceses of Anagni-Alatri and Palestrina, in the ecclesiastical region of Lazio, have been founded on the hills and crossed by the Apennine mountains; and
- The dioceses of Sorrento-Castellammare di Stabia and Nocera Inferiore-Sarno, in the ecclesiastical region of Campania, comprehend several churches located on the sea cliffs and hills close to the seaside.

2.3.1.4 Culture and History

The selected locations are well tied to Church history. Trento was the seat of one of the most important councils in Church annals, the Council of Trento from 1545 – 1563 (Yates 1944). Vicenza, as a part of the former Republic of Venice, was a bulwark for Christianity throughout the Middle Ages and beyond. Toscana has always had close relationship with the Church; in particular, the area of Montepulciano, Chiusi, and Pienza was for a long time a border zone with the Church's territory establishing contacts with several popes and members of the clergy resulting in a significant amount of relics that is still preserved there. Perugia was one of the key cities of the Papal States until 1860. Lazio, where Vatican resides, has been the center of the whole Christianity, since the founding of the Church. Finally, Campania has always had profound catholic roots that are still alive and strong, especially in Sorrento, where the priests are democratically chosen by the communities, a privilege that only few other communities in the world have (Ferraioulo 1991).

Within each diocese, the churches chosen for assessment were generally geographically near to each other, for the following reasons: 1) efficiency of field surveying, 2) usefulness of results to specific parishes, and 3) consistency of structural and architectural forms for purposes of identifying common vulnerabilities and for efficiency in future modelling.

2.3.2 Active Functionality

The churches were selected based on their role as a focal point in the spiritual life of the surrounding communities by identifying consecrated churches regularly utilized. In the context of the current research, the term “community churches” represents churches which are not primary cathedrals, in regard to size and fame, but are still actively visited and utilized by residents. The more famous cathedrals in Italy have often already been extensively assessed by others, and the stakeholders for cathedrals generally have access to more resources. In contrast, the “community churches” assessed in the current study have not often been extensively assessed by others. Finally, the architectural and cultural value of churches was considered in this phase as a discriminant. In selecting for assessment between two churches with similar functionality and occupancy rates, the church with a more qualitatively significant historical and heritage value was selected.

2.3.3 Original Construction Period

Medieval churches were the primary focus of this research due to their prominent presence within the Italian territory, their vulnerability as observed in past earthquakes, such as in Friuli-Venezia Giulia in 1976 (Doglioni, Moretti, and Petrini 1994), in Basilicata and Campania in 1980 (Proietti 1994), in Umbria-Marche in 1997 (Doglioni 2000; Lagomarsino and Podestà 2004), in L'Aquila in 2009 (Cimellaro et al. 2010; da Porto et al. 2012; Lagomarsino 2012), and in central Italy in 2016 (Hofer et al. 2018; Penna et al. 2019). Furthermore, medieval churches generally represent high levels of cultural and historic value, including by housing invaluable artwork.

Churches chosen for assessment in the current study were generally constructed between the 11th and the 15th centuries, corresponding to the High and Late Middle Ages (Pirenne and Wallace 1963; Jordan 2002). This time period was chosen to achieve a greater homogeneity among sample churches in terms of construction techniques. Note that the timeframe refers to the original construction year, since many churches have been retrofitted, expanded, and modified in other fashions over time. Furthermore, churches originally constructed during the High and Late Middle Ages in Italy and still existing today are usually URM structures (Cagnana 1997). A few exceptions to the time period criteria for selection were made by assessing churches explicitly requested by the dioceses, and some other churches that were typologically similar to medieval ones as shown in Table A.1 of Appendix A.

2.3.4 Urban and Planimetric Layout

The urban and planimetric layout of churches was also considered amongst the selection criteria, and churches were generally only selected for assessment if they were structurally isolated (i.e., stand-alone) from all neighboring buildings. The reason for focusing on structurally isolated churches is due to the greater simplicity and precision of quantifying all risk components of the church (especially vulnerability) as explicit from neighboring structures that may not even belong to the Church. Furthermore, the interaction between adjacent buildings during an earthquake leads to highly variable predictions in structural models (Magenes and Penna 2009). Most "community churches", due to their importance and strategical position within the community, are usually isolated buildings located in town main squares (i.e., piazzas).

2.4 Church Typologies

The 72 selected churches surveyed as listed in Table A.1 of Appendix A were classified based on their general geometric attributes into various typological groupings as shown in Table 2.2. Although a large variety of typologies was addressed in the current studychurches with the basilican plan and simple nave represented the majority of the analyzed cases, corresponding to 59.8% of the total number of churches.

TABLE 2.2

CHURCHES TYPOLOGIES

	No vaults		Partially vaulted		Fully vaulted	
Basilican plan and simple nave			N.A.			
	# Churches	% Churches	# Churches	% Churches	# Churches	% Churches
	13	18.1%	N.A.	N.A.	30	41.7%
Basilican plan and main nave with aisles	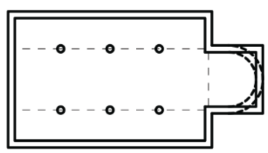		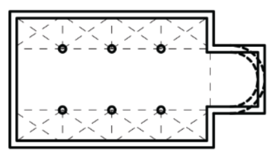		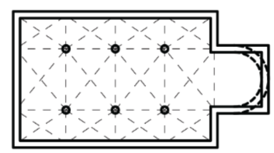	
	# Churches	% Churches	# Churches	% Churches	# Churches	% Churches
	3	4.2%	2	2.8%	10	13.8%
Latin cross plan and simple nave	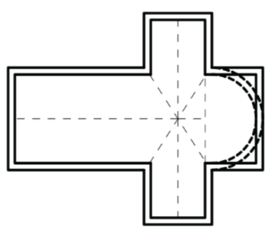		N.A.		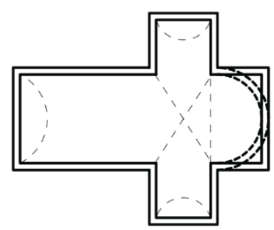	
	# Churches	% Churches	# Churches	% Churches	# Churches	% Churches
	1	1.4%	N.A.	N.A.	10	13.8%
Latin cross plan and main nave with aisles	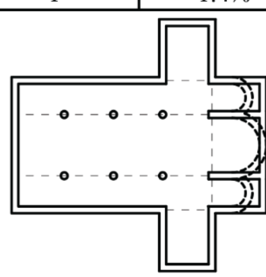		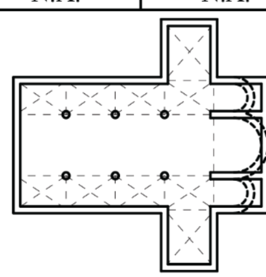		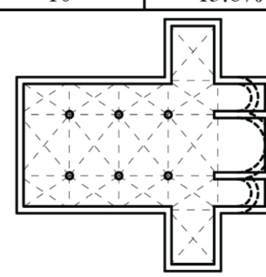	
	# Churches	% Churches	# Churches	% Churches	# Churches	% Churches
	1	1.4%	1	1.4%	1	1.4%

2.5 Seismic Risk Assessment

For purposes of this study, risk (R) was defined as the product of hazard (H), vulnerability (V), exposure (E), and consequences (C) (Romão and Paupério 2019; Basaglia et al. 2018; The National Academies 2012; Parducci 2011). With respect to earthquakes, these four different factors defined as “Risk Components” are described as follows:

- Hazard (H) refers to the probability that an earthquake of a particular magnitude and associated intensity will occur;
- Vulnerability (V) represents the expected performance and damage of a given structure caused by shaking of a certain intensity;
- Exposure (E) refers to the social and spiritual values, as well as to the loss of lives that may be related to buildings damage in each region;
- Consequences (C) addresses the costs that may be incurred in terms of economic value, social and urban capital, and, most importantly, the loss of the heritage value comprised of the churches themselves and the pieces of art contained within them.

2.6 Risk Components: Definition and Quantification

Given the primary goal of the research to develop a generalizable, rapid, and reliable seismic risk assessment methodology for churches, the definition of the risk components was based upon data that was both easily accessible and based on dependable proxies for desired attributes. The four factors of risk were each divided into several subcomponents (Table 2.3), which are defined in the following sections.

TABLE 2.3

RISK SUBCOMPONENTS

Risk Component	Subcomponent	Variable
Hazard	Index of hazard for 90 years average return period	$i_{H,90}$
	Index of hazard for 151 years average return period	$i_{H,151}$
	Index of hazard for 1424 years average return period	$i_{H,1424}$
	Index of hazard for 2475 years average return period	$i_{H,2475}$
Vulnerability	Index of vulnerability in the best-case scenario	$i_{V,min}$
	Index of vulnerability in the worst-case scenario	$i_{V,max}$
Exposure	Index of average occupancy during the week	$i_{OR,AO}$
	Index of maximum occupancy throughout the year	$i_{OR,MO}$
	Index of community utilization during the regular weeks' masses (i.e., from Monday to Sunday)	$i_{CU,RW}$
	Index of community utilization during the highest attended holy days' masses (i.e., Christmas or Easter)	$i_{CU,HD}$
Consequences	Index of minimum equivalent economic value	$i_{EEV,min}$
	Index of maximum equivalent economic value	$i_{EEV,max}$
	Index of susceptible heritage	i_{SH}

To prevent any outliers from disproportionately affecting the calculation of the indices, the data collected from the 72 surveyed churches was fit to lognormally distributed functions. Each data set was normalized from 0 to 1 using as the normalizing bounds the values of the 5th and 95th percentiles (Frantzich 1988; Martinez 2009; ACI Committee and International Organization for Standardization 2019). All the values exceeding the 95th percentile where assigned with an index of 1. All the values lower than the 5th percentile where assigned to an index equal to the ratio between the 5th and the 95th percentiles. Intermediate values were linearly interpolated between the two bounds.

2.6.1 Hazard

The peak ground acceleration (PGA) at various average return periods was selected as the hazard metric for the proposed methodology because of its familiarity to practitioners, its being commonly quantified for any location, and its independence from structural performance leading to its wide applicability across a wide range of structural typologies. Several different hazard metrics have been used in other research such as the Modified Mercalli Intensity *MMI* (Abeling et al. 2018), the spectral acceleration S_a (Tesfamaraim and Saatcioglu 2008), and the Mercalli Scale *MCS* (Lagomarsino and Podestà 2004; Lagomarsino 2006). However, these aforementioned indicators are dependent on both intensity and structural performance, and are thus unreliably applied to large, dispersed building portfolios that have not been extensively studied in the context of such measures. Other hazard metrics have been successfully correlated with damage, such as the Arias intensity or the Saragoni factor (Cosenza and Manfredi 2000). Furthermore, recent studies has shown the peak ground velocity (PGV) to have a stronger correlation with the damage prediction of URM buildings (Zucconi, Ferlito, and Sorrentino 2020), although PGA was also determined to have a strong correlation with damage in this same study. However, PGVs have not yet been widely determined across the country for various average return periods. To account for aggregated seismic hazards, the values of the PGAs for four different average return periods of the earthquakes, T_R, (90, 151, 1424, and 2475 years, respectively) were determined based on the Italian High Council of Public Work (MIT and CSLP 2020) and the Italian Standards for Construction (MIT 2018). The values of PGAs for the surveyed church locations were normally distributed as shown in Figure 2.4.

The minimum of the distributions shown in Figure 2.4 was determined as the 5th percentile of the 90 years average return period PGA, corresponding to ln(PGA_{5th})= -3.144 (PGA_{5th} = 0.043g), while the maximum was set as the 95th percentile of the 2475 years average return period PGA, corresponding to ln(PGA_{95th}) = -1.068 (PGA_{95th} = 0.344g). Cumulative distributions for the PGAs are shown in (Figure 2.5).

Finally, the indices of hazard $\boldsymbol{i_{H,i}}$ were determined using Equations 2.2 – 2.5.

$$\frac{PGA_{5th}}{PGA_{95th}} \leq i_{H,90,i} = \frac{PGA_{90,i}}{PGA_{95th}} \leq 1 \qquad (2.2)$$

$$\frac{PGA_{5th}}{PGA_{95th}} \leq i_{H,151,i} = \frac{PGA_{151,i}}{PGA_{95th}} \leq 1 \qquad (2.3)$$

$$\frac{PGA_{5th}}{PGA_{95th}} \leq i_{H,1424,i} = \frac{PGA_{1424,i}}{PGA_{95th}} \leq 1 \qquad (2.4)$$

$$\frac{PGA_{5th}}{PGA_{95th}} \leq i_{H,2475,i} = \frac{PGA_{2475,i}}{PGA_{95th}} \leq 1 \qquad (2.5)$$

where: $i_{H,90,i}$ is the index of hazard of the church *i* for $T_R = 90\ years$;

$i_{H,151,i}$ is the index of hazard of the church *i* for the $T_R = 151\ years$;

$i_{H,1424,i}$ is the index of hazard of the church *i* for $T_R = 1424\ years$;

$i_{H,2475,i}$ is the index of hazard of the church *i* for $T_R = 2475\ years$.

The resulting indices of hazard $i_{H,i}$ are shown in Figure 2.6 subdivided based on the considered return period scenario and sorted by region.

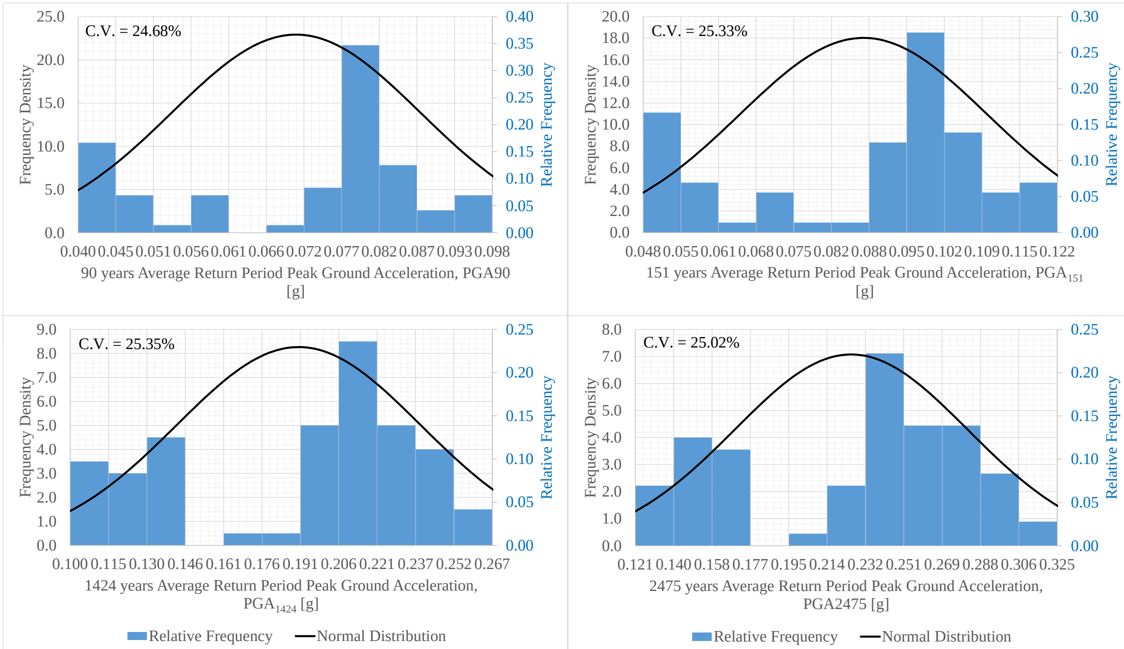

Figure 2.4: Normal distribution and relative frequency of the PGA corresponding to PGA_{90}, PGA_{151}, PGA_{1424}, and PGA_{2475}

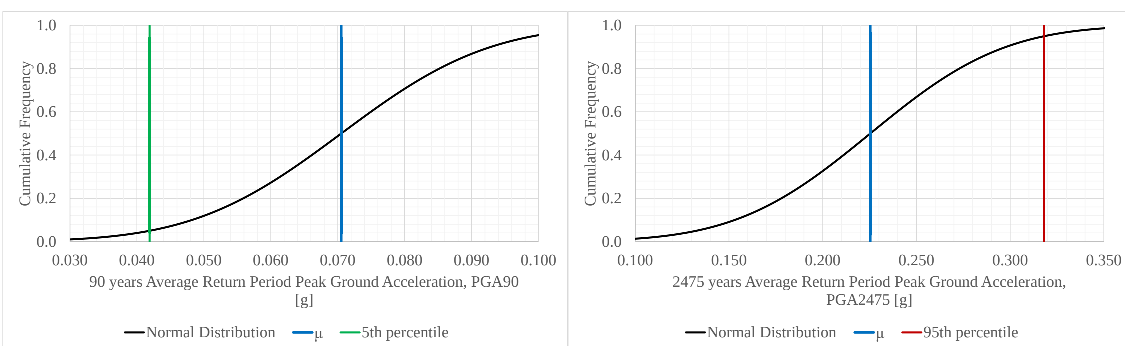

Figure 2.5: On the left: cumulative distribution of PGA_{90} with the corresponding average (μ) and the 5th percentile; On the right: cumulative distribution of PGA_{2475} with the corresponding average (μ) and the 95rd percentile.

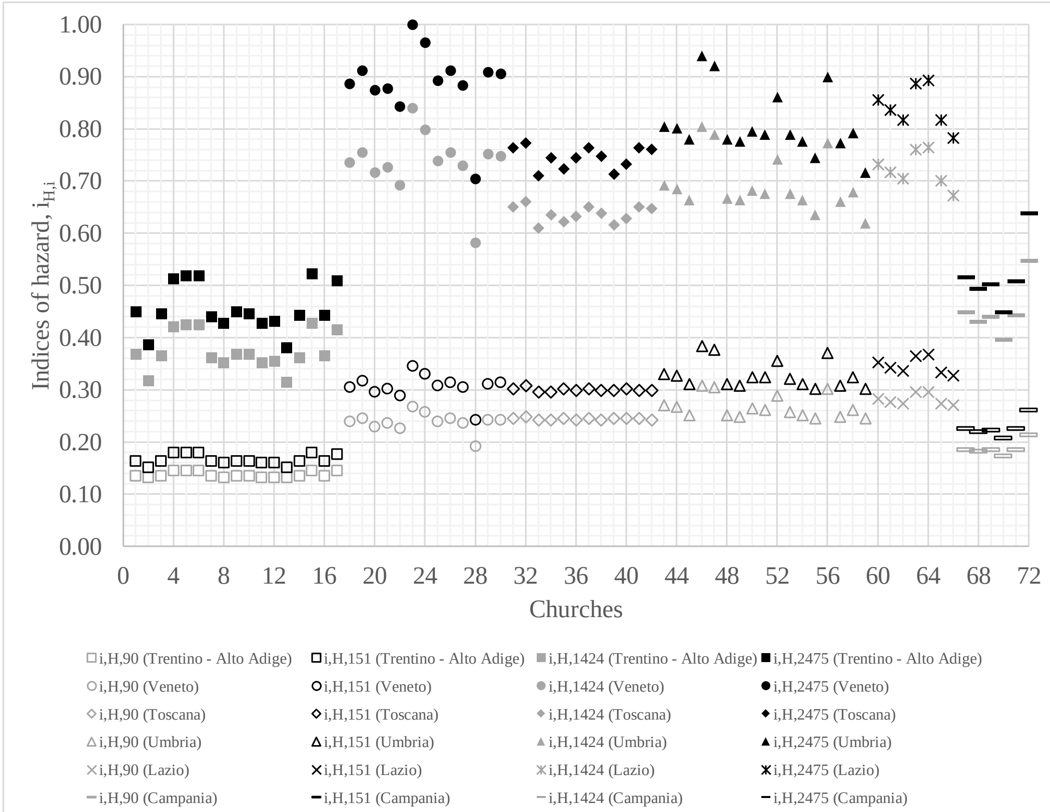

Figure 2.6: Indices of hazard $i_{H,i}$.

2.6.2 Vulnerability

Due to the slenderness of church walls compared to most other types of buildings, subdividing URM churches into units called "macro-blocks" is the preferred method to assess churches and other complex URM buildings (Giuffrè 1989; Doglioni, Moretti, and Petrini 1994; DPCM 2011; Marotta et al. 2017; Gàlvez et al. 2018). The macro-blocks considered in the current research are shown in Figure 2.7. Particularly vulnerable collapse mechanisms were identified through empirical observations during past earthquakes (Doglioni, Moretti, and Petrini 1994; Doglioni 2000; Cimellaro et al. 2010) and can be numerically predicted using virtual work principles. The Italian Guideline on the Built Heritage (DPCM 2011), which is based on the work of Lagomarsino et al. (2004), identified nine different macro-blocks comprising 28 total collapse mechanisms. However, the authors considered the roof as a macro-block itself, given its relevant structural function as illustrated in Figure 2.7, bringing the number of considered macro-blocks to 10.

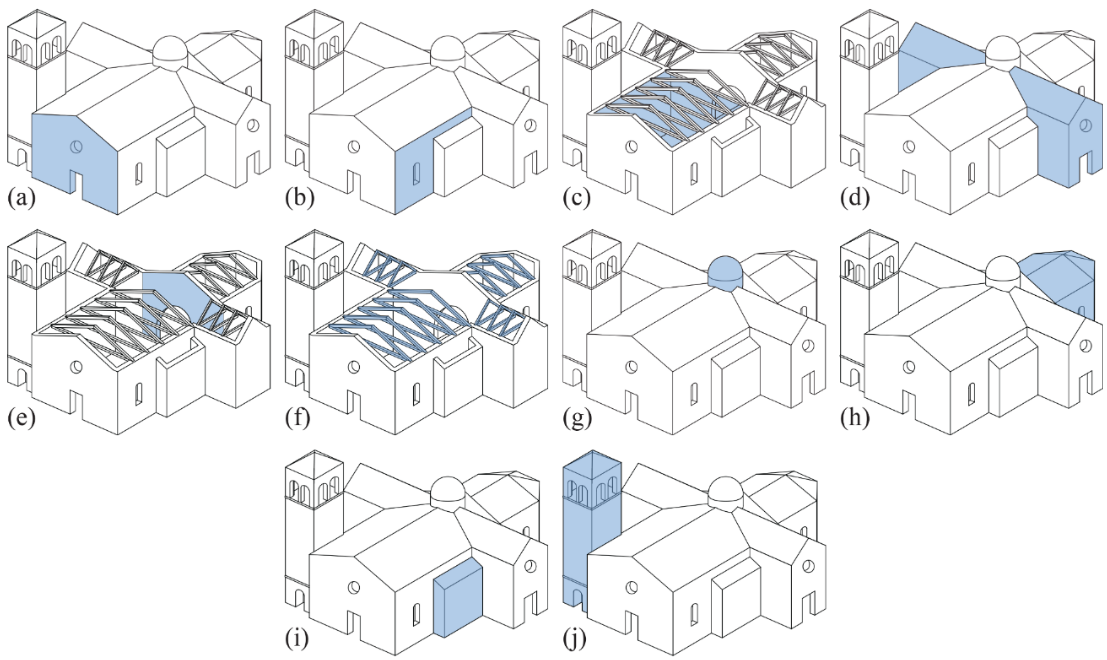

Figure 2.7: Macro-blocks considered: (a) Façade; (b) Lateral Walls; (c) Naves; (d) Transept; (e) Triumphal arch; (f) Roof; (g) Dome; (h) Apse; (i) Chapels; (j) Bell Tower.

According to the Italian Guideline on the Built Heritage (DPCM 2011), the global seismic behavior of any church may be represented by a vulnerability index i_V (ranging from 0 to 1) which accounts for the contribution of each macro-block collapse mechanism. The presence of structural elements that could affect (positively or negatively) each macro-block collapse mechanism was documented in the current research for each of the 72 churches surveyed shown in Table A.1 of Appendix A. Thus, the vulnerability index was determined using Equation 2.6:

$$i_{V,i} = \frac{1}{6}\frac{\sum_{k=1}^{28}\rho_{k,i}(v_{ki,i}-v_{kp,i})}{\sum_{k=1}^{28}\rho_{k,i}} + \frac{1}{2} \quad (2.6)$$

where: $i_{V,i}$ is the vulnerability index of the church ***i*** determined using the macro-blocks approach;

$\rho_{k,i}$ is the influence factor ($0 \leq \rho_{k,i} \leq 1$) of the *k*-th collapse mechanism on the global seismic behavior of the church *i*;

$v_{ki,i}$ is the score ($0 \leq v_{ki,i} \leq 3$) obtained by the evaluation of the vulnerability indicators;

$v_{kp,i}$ is the score ($0 \leq v_{kp,i} \leq 3$) obtained by the evaluation of the seismic robustness improvers.

Other researchers (Lagomarsino 2012; De Matteis, Criber, and Brando 2016) proposed a methodology for the exact evaluation of the influence factor, $\rho_{k,i}$, based on the observable damage on the macro-blocks of the churches. However, given the pre-damage states of the churches surveyed in thecurrent research, no relevant damage was observable on the selected churches, and thus, $\rho_{k,i}$ could not be directly calculated. Given the uncertainties regarding the $\rho_{k,i}$ values, both the worst and the best case scenarios were considered assuming the limit values proposed by the DPCM (2011) set as $\rho_{k,min,i} = 0.5$ and $\rho_{k,max,i} = 0.5$ or 1.0 (depending on the collapse mechanism). Thus, the indices of minimum and maximum vulnerability ($i_{V,min,i}$ and $i_{V,max,i}$) were determined using Equations 2.7 and 2.8, respectively.

$$i_{V,min,i} = \frac{1}{6}\frac{\sum_{k=1}^{28}\rho_{k,best,i}(v_{ki,min,i}-v_{kp,max,i})}{\sum_{k=1}^{28}\rho_{k,best,i}} + \frac{1}{2} \quad (2.7)$$

$$i_{V,max,i} = \frac{1}{6}\frac{\sum_{k=1}^{28}\rho_{k,worst,i}(v_{ki,max,i}-v_{kp,min,i})}{\sum_{k=1}^{28}\rho_{k,worst,i}} + \frac{1}{2} \quad (2.8)$$

where: $i_{V,min,i}$ is the index of vulnerability of the church *i* for the best-case scenario;

$\rho_{k,best,i}$ is equal to $\rho_{k,max,i}$ if $v_{ki,min,i} \leq v_{kp,max,i}$, while $\rho_{k,best,i}$ is equal to $\rho_{k,min,i}$ if $v_{ki,min,i} \geq v_{kp,max,i}$;

$i_{V,max,i}$ is the index of vulnerability of the church *i* for the worst-case scenario;

$\rho_{k,worst,i}$ is equal to $\rho_{k,min,i}$ if $v_{ki,min,i} \leq v_{kp,max,i}$, while $\rho_{k,worst,i}$ is equal to $\rho_{k,max,i}$ if $v_{ki,min,i} \geq v_{kp,max,i}$.

A possible modification to the Italian Guidelines on the Built Heritage (DPCM 2011) procedure parameters was proposed by De Matteis et al. (2019). wherein the vulnerability and robustness scores, $v_{ki,i}$ and $v_{kp,i}$, were determined using Equations 2.9 and 2.10.

$$v_{ki,i} = \frac{3}{5n_{ki}} \sum_{j=1}^{n_{ki}} I_{i,ki,j} \tag{2.9}$$

$$v_{kp,i} = \frac{3}{5n_{kp}} \sum_{j=1}^{n_{kp}} I_{e,kp,j} \tag{2.10}$$

where: n_{ki} and n_{kp} are, respectively, the number of vulnerability indicators, and the number of seismic robustness improvers associated with the *k*-th collapse mechanism, defined in Table B.1 of Appendix B;

$I_{i,ki,j}$ is the influence score (varying from 1 to 5) of the *j*-th vulnerability indicators, defined in Table B.2 of Appendix B;

$I_{e,kp,j}$ is the effectiveness score (varying from 1 to 5) of the *j*-th robustness improver, defined in Table B.3 of Appendix B.

The criteria for assigning the influence and the effectiveness score ($I_{i,ki}$ and $I_{e,kp}$) are detailed in Table B.2 and Table B.3 of Appendix B. When $I_{i,ki}$ and $I_{e,kp}$ could not properly determined (e.g., judging the quality of the masonry was impossible when the observed macro-block was entirely plastered), both limit cases (i.e., a score of 1 or 5) were considered, resulting in the possible scores for the vulnerability indicators and the robustness improvers, $v_{ki,max,i}$, $v_{ki,min,i}$, $v_{kp,max,i}$, and $v_{kp,min,i}$. The authors emphasize that the criteria shown in Table B.2 and Table B.3 of Appendix B were developed for the purposes of a rapid and effective visual survey, based on the recurrent characteristics of the analyzed churches, the input of the DPCM (2011), and consistently with the observations of previous researchers (Doglioni, Moretti, and Petrini 1994; Lagomarsino 2012; Marotta et al. 2017; De Matteis et al. 2019). The criteria retain a subjective component and further research to achieve more objective criteria is desirable.

The resulting indices of hazard $i_{V,i}$ are shown in Figure 2.8 subdivided based on the considered scenario and sorted by region.

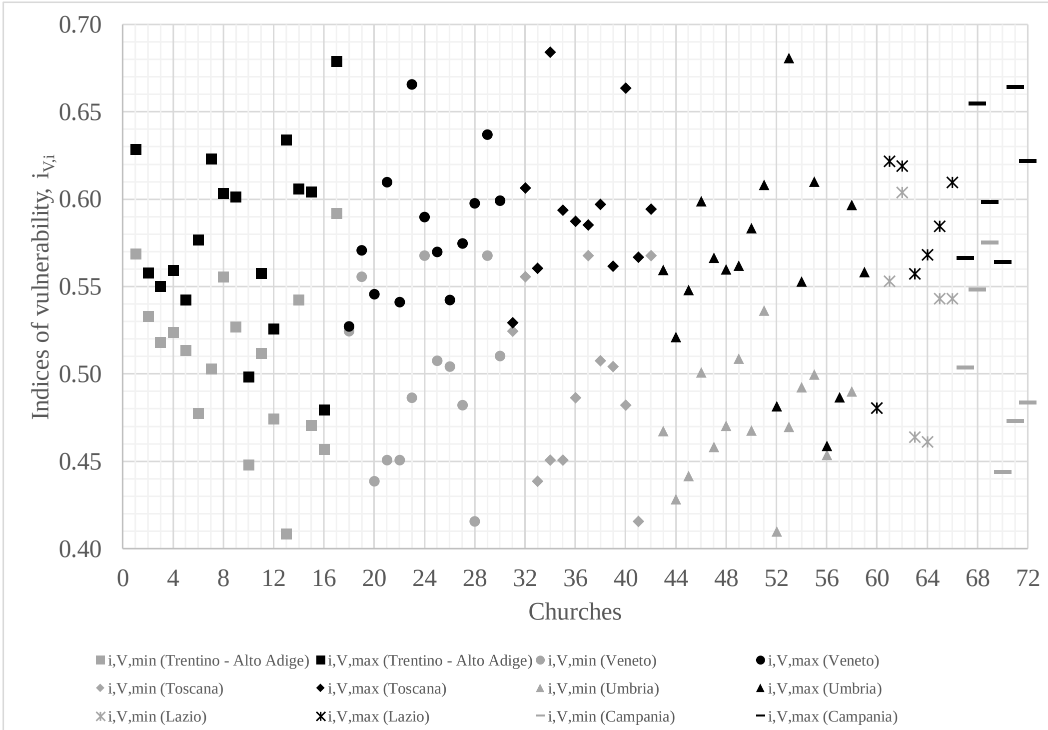

Figure 2.8: Indices of vulnerability $i_{V,i}$.

2.6.3 Exposure

Two main subcomponents were considered to quantify the exposure of each church:

- The "Occupancy Rate" subcomponent accounts for the possible loss of lives due to the potential collapse of the church. Two occupancy rates were utilized in the risk assessment: 1) the average occupancy during the week; and 2) the maximum occupancy throughout the year;
- The "Community Utilization" subcomponent accounts for the utility of the church as a proportion of the size of the surrounding community. The loss of a church with a high community utilization may correspond with a significant functional service loss (i.e., interruption of the service of the Holy Mass for a large portion of the community). This parameter was considered an acceptable proxy of the spiritual

value and the importance of the church as perceived by its community. Two scenarios were investigated during the surveys: 1) the community utilization during the regular weeks' masses (i.e., from Monday to Sunday); and 2) the community utilization during the highest attended holy days' masses (i.e., Christmas or Easter).

2.6.4 Indices of Occupancy Rate

Since official attendance records at masses are not publicly available, the numbers of churchgoers were recorded by interviewing priests associated with each church. The priests were asked to convey the average number of churchgoers per each day of the week, $p_{j,i}$, and the maximum attendance during the most crowded days of the year (i.e., Christmas and Easter), $p_{max,i}$. To determine the average occupancy rate in the church i ($p_{av,i}$), Equation 2.11 was used

$$p_{av,i} = \frac{\sum_{j=1}^{7} p_{j,i}}{7} \tag{2.11}$$

where: $p_{j,i}$ is the number of churchgoers during the j-th day of the week in the church i.

Since the corresponding values of $p_{av,i}$ resulted in a skew normal distribution, the log-normal distribution was determined (Figure 2.9) to proceed with the identification of the 5th and the 95th percentiles. The minimum was determined as the 5th percentile, corresponding to $\ln(p_{av,5th}) = 0.72$ ($p_{av,5th}$ = 2.05 people/day), while the maximum was set as the 95th, corresponding to $\ln(p_{av,95th}) = 4.91$ ($p_{av,95th}$ = 136.20 people/day) as shown in Figure 2.10.

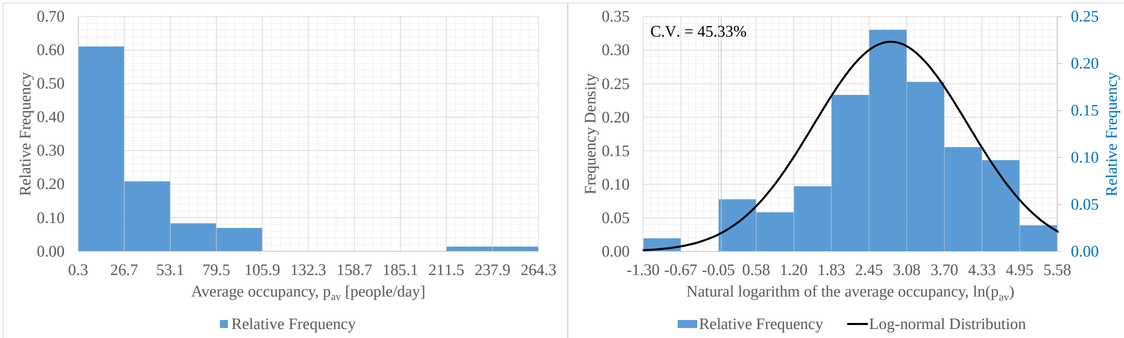

Figure 2.9: On the left: relative frequency of $p_{av,i}$; On the right: log-normal distribution and relative frequency of ln($p_{av,i}$).

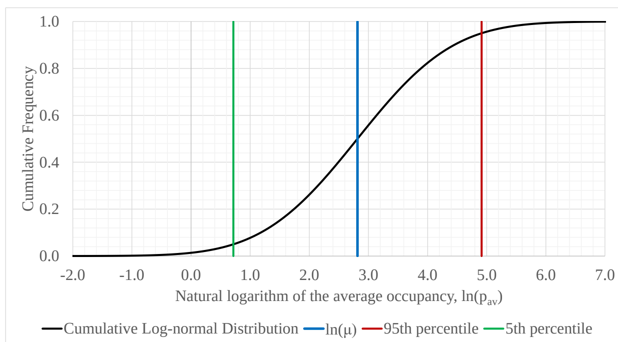

Figure 2.10: Cumulative distribution of ln($p_{av,i}$) with the corresponding average μ, the 5th percentile, and the 95th percentile.

Since the corresponding values of $p_{max,i}$ resulted in a skew normal distribution, the log-normal distribution was determined (Figure 2.11) to proceed with the measurement of the 5th and the 95th percentiles. The minimum was determined as the 5th percentile, corresponding to ln($p_{max,5th}$) = 3.89 ($p_{max,5th}$ = 49.03 people), while the maximum was set as the 95th percentile, corresponding to ln($p_{max,95th}$) = 6.44 ($p_{max,95th}$ = 624.64 people) as shown in Figure 2.12.

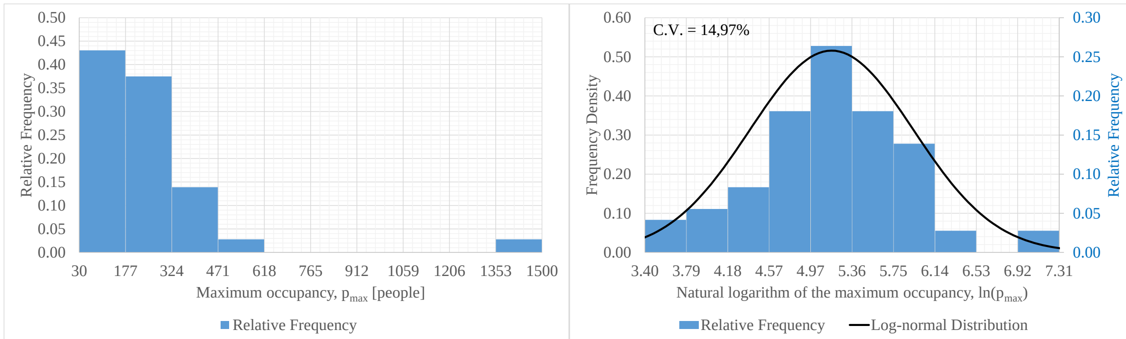

Figure 2.11: On the left: relative frequency of $p_{max,i}$; On the right: log-normal distribution and relative frequency of $\ln(p_{max,i})$.

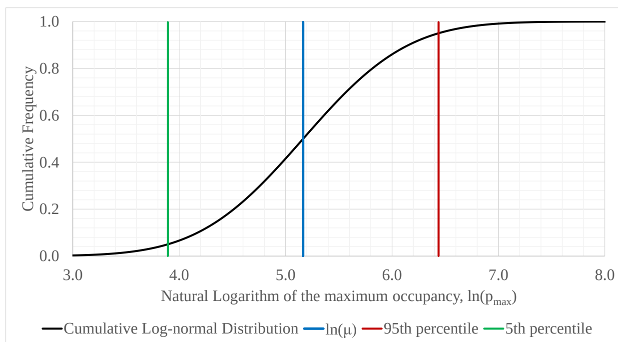

Figure 2.12: Log-normal and cumulative distribution of $\ln(p_{max,i})$ with the corresponding average μ, the 5th percentile, and the 95th percentile.

Finally, the indices of average and maximum occupancy rate ($i_{OR,AO,i}$ and $i_{OR,MO,i}$) were determined using Equations 2.12 and 2.13, respectively.

$$\frac{p_{av,5th}}{p_{av,95th}} \leq i_{OR,AO,i} = \frac{p_{av,i}}{p_{av,95th}} \leq 1 \tag{2.12}$$

$$\frac{p_{max,5th}}{p_{max,95th}} \leq i_{OR,MO,i} = \frac{p_{max,i}}{p_{max,95th}} \leq 1 \tag{2.13}$$

where: $i_{OR,AO,i}$ is the index of average life presence of the church i;

$i_{OR,MO,i}$ is the index of maximum life presence of the church i.

The resulting indices of occupancy rate $i_{OR,i}$ are shown in Figure 2.13 subdivided based on the considered scenario and sorted by region.

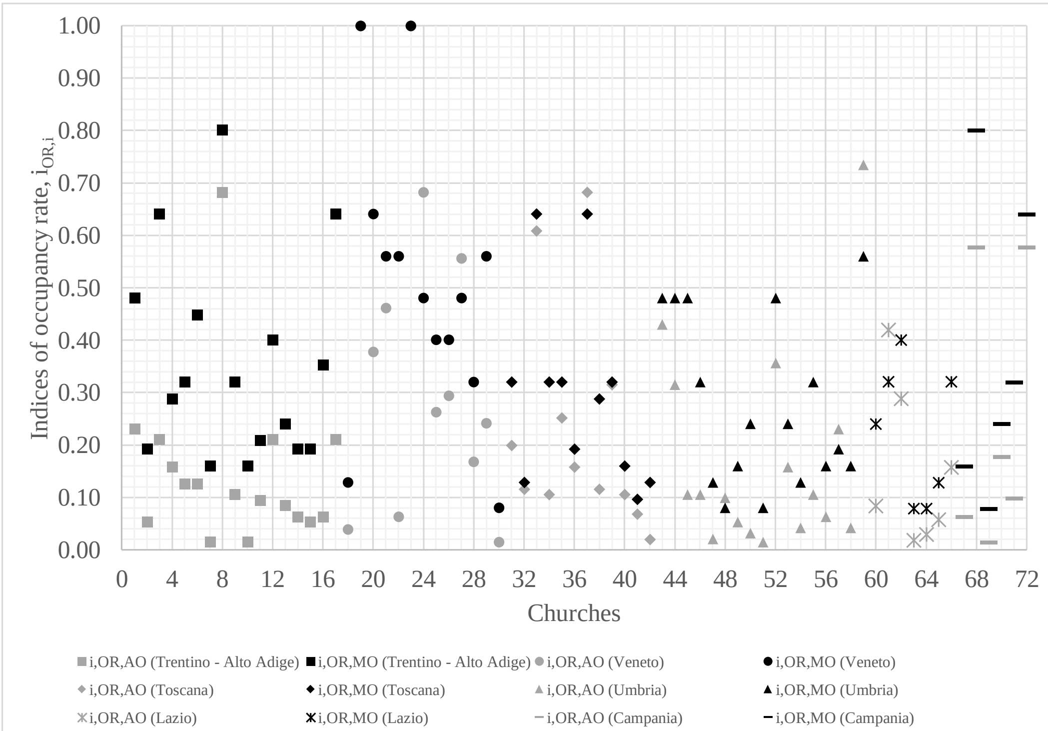

Figure 2.13: Indices of occupancy rate $i_{OR,i}$.

2.6.5 Indices of Community Utilization

To determine the community utilization during the regular weeks' masses of the church i ($k_{av,i}$), Equation 2.14 was used

$$k_{av,i} = \frac{p_{av,i}}{N_{set,i}} \tag{2.14}$$

where: $N_{set,i}$ is the number of residents of the city or settlement ("frazione") where the church i is located.

Since the corresponding values of $k_{av,i}$ resulted in a skew normal distribution, the log-normal distribution was determined (Figure 2.14) to proceed with the measurement of the 5th and the 95th percentiles. The minimum was determined as the 5th percentile, corresponding to $\ln(k_{av,5th})$ = -6.42 ($k_{av,5th}$ = 0.0016), while the maximum was set as the 95th percentile, corresponding to $\ln(k_{av,95th})$ = -1.647 ($k_{av,95th}$ = 0.193) as shown in Figure 2.15.

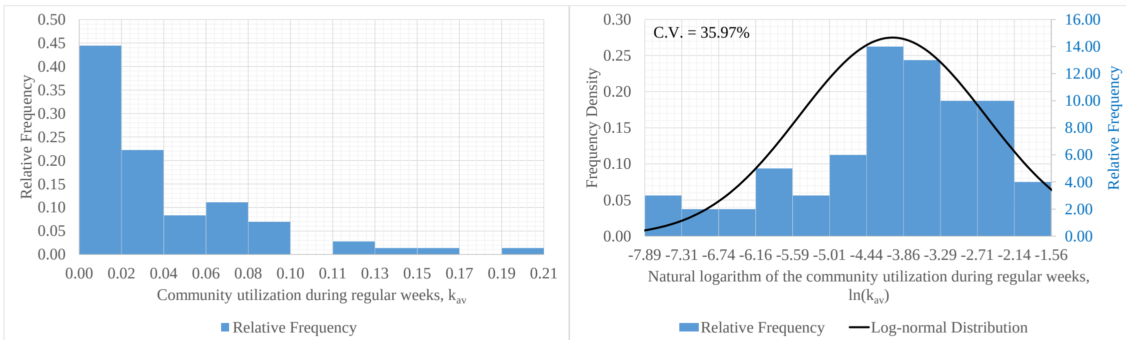

Figure 2.14: On the left: relative frequency of $k_{av,i}$; On the right: log-normal distribution and relative frequency of $\ln(k_{av,i})$.

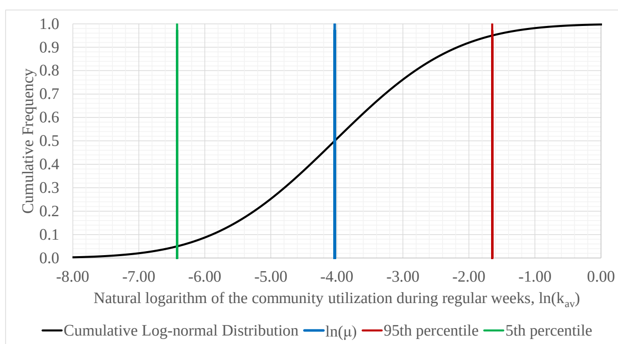

Figure 2.15: Cumulative distribution of $\ln(k_{av,i})$ with the corresponding average μ, the 5th percentile, and the 95th percentile.

To determine the community utilization during the holy days' masses of the church i ($k_{max,i}$), Equation 2.15 was used

$$k_{max,i} = \frac{p_{max,i}}{N_{set,i}} \tag{2.15}$$

Since the corresponding values of $k_{max,i}$ resulted in a skew asymmetric normal distribution, the log-normal distribution was determined (Figure 2.16) to proceed with the measurement of the 5th and the 95th percentiles. In Figure 2.16, it might be noticed that $k_{max,i}$ may be larger than 1, which might be true for small settlements whose residents usually have an older average age. In fact, in this kind of villages the Christmas and Easter masses are regularly attended by the whole family, while, throughout the rest of the year, the younger members of the family live and attend masses in different cities. The minimum was determined as the 5th percentile, corresponding to $\ln(k_{max,5th}) = -4.230$ ($k_{max,5th} = 0.015$), while the maximum was set as the 95th, corresponding to $\ln(k_{max,95th}) = 0.862$ ($k_{max,95th} = 2.368$) as shown in Figure 2.17.

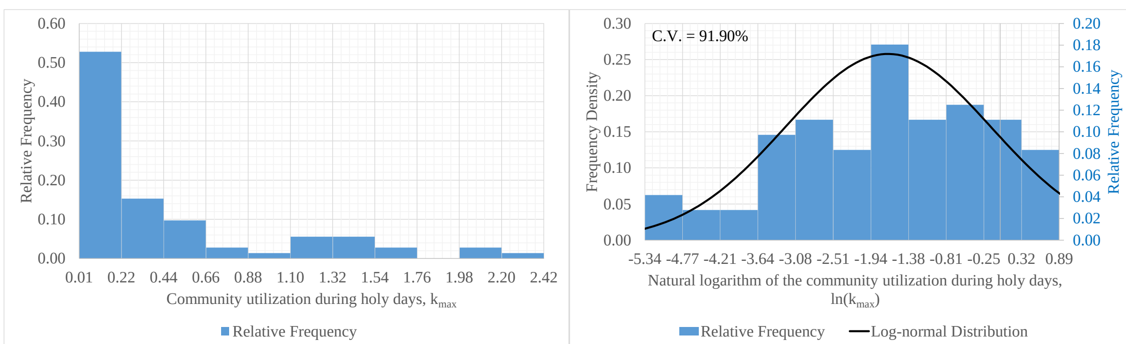

Figure 2.16: On the left: relative frequency of $k_{max,i}$; On the right: log-normal distribution and relative frequency of $\ln(k_{max,i})$.

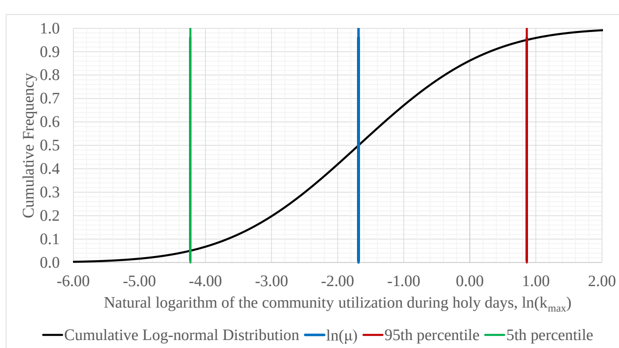

Figure 2.17: Log-normal and cumulative distribution of $\ln(k_{max,i})$ with the corresponding average μ, the 5th percentile, and the 95th percentile.

Finally, the indices of the community utilization during the regular weeks' masses and the holy days' masses ($i_{CU,RW,i}$ and $i_{CU,HD,i}$) were determined using Equations 2.16 and 2.17, respectively.

$$\frac{k_{av,5th}}{k_{av,95th}} \leq i_{CU,RW,i} = \frac{k_{av,i}}{k_{av,95th}} \leq 1 \tag{2.16}$$

$$\frac{k_{max,5th}}{k_{max,95th}} \leq i_{CU,HD,i} = \frac{k_{max,i}}{k_{max,95th}} \leq 1 \tag{2.17}$$

where: $i_{CU,RW,i}$ is the index of community utilization during the regular weeks' mass of the church i;

$i_{CU,HD,i}$ is the index of community utilization during the holy days' mass of the church i.

The resulting indices of community utilization $i_{CU,i}$ are shown in Figure 2.18 subdivided based on the considered scenario and sorted by region.

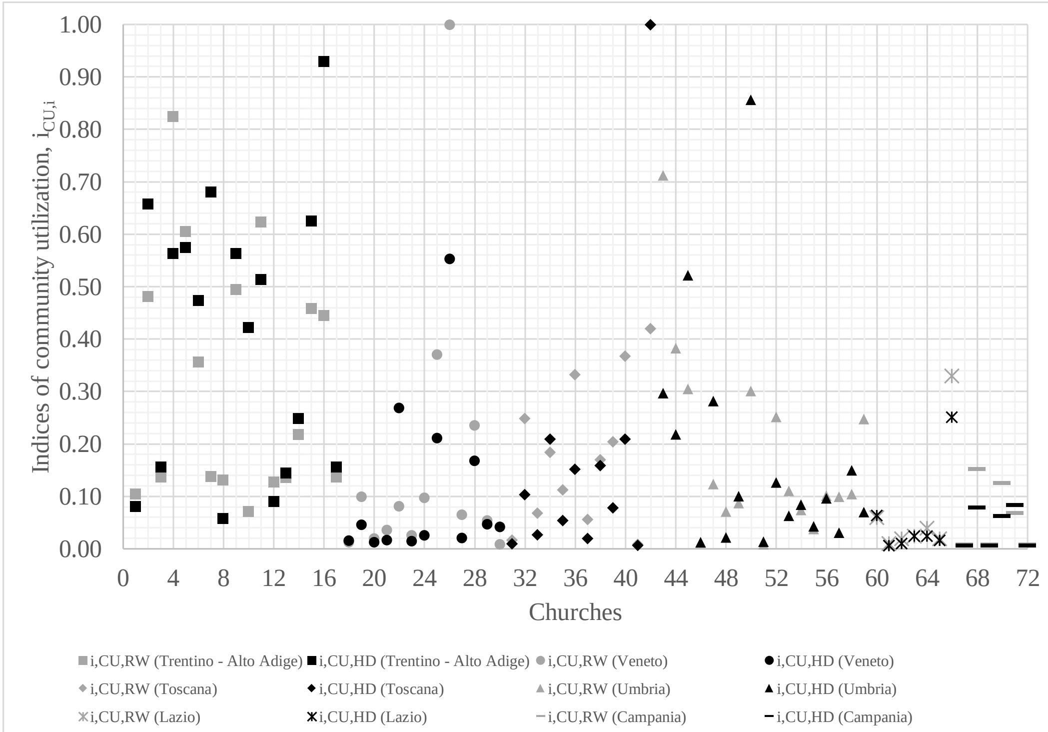

Figure 2.18: Indices of community utilization $i_{CU,i}$.

2.6.6 Consequences

Two main aspects were considered to address the consequences component of risk:

- The “Equivalent Economic Value” (EEQ) accounts for the possible cost of reconstruction of the church due to its hypothetical collapse; and
- The “Susceptible Heritage” subcomponent accounts for the presence of heritage art and architecture within the church (e.g., paintings, sculptures, architectural value).

2.6.7 Indices of Equivalent Economic Value

The authors are aware that the total economic value of the artistic, cultural, and architectural heritage elements contained in each church is not feasible to evaluate and should not be estimated with a high degree of confidence. To address the lack of service capacity (both social and spiritual) offered to the communities because of a hypothetical destructive event leading to the irreparable collapse of the church, the EEQ as used in the current research was mainly intended to represent the cost of reconstruction of a new building, rather than the total economic value of the current churches and all of their components. Given the lack of data regarding the cost of construction of churches, the equivalent value was based on the value per square meter (€/m^2) of a residential three-story building having the same footprint as each church. The equivalency with a three-story building was chosen based on approximating the equivalent volume of a church. The EEQ was also adjusted to account for the value of the land, $i_{a,i}$. This approach was considered reasonable for three main reasons:

- The data regarding the value per square meter of residential buildings are easily accessible for each church location, thus enhancing the speed and the generalizability of the proposed methodology;
- Given the relative index scoring of the proposed methodology, the actual price of construction of each church is less relevant than its proportional values between different churches, furthermore, estimating the price of construction requires more detailed geometric information regarding the building (e.g., Regione Lazio 2012) which would heavily affect the speed of the proposed methodology; and
- The equivalent value of a new residential building construction represents the material cost, the labor cost, and the construction cost within the geographical region where the church is located and, thus, adequately represents the proportional comparison for the construction of a new church in different Italian geographic regions.

The minimum and the maximum value per square meter of the residential buildings ($C_{eq,min,i}$ and $C_{eq,max,i}$) were based on the data collected by the Italian Real Estate Market Observatory (Agenzia delle Entrate 2019) and by the local Chambers of Commerce (CCIAA 2019). The value of the land was based on its economic impact on the total value of the church $i_{a,i}$. Although the value of $i_{a,i}$ is highly variable, several researchers have recommended the use of values between 0.1 and 0.3 (Benvenuti and Simonotti 2005; Stanghellini, Mascarello, and Ruaro 2009; Ciuna 2010; Made 2018). For purposes of the current research, the economic impact of the land $i_{a,i}$ was assigned in accordance with the commercial value of the examined area as follows:

- $i_{a,i} = 0.30$ for the downtown of main cities and valuable areas;
- $i_{a,i} = 0.20$ for the downtown of minor cities;
- $i_{a,i} = 0.15$ for suburban areas;
- $i_{a,i} = 0.10$ for rural areas.

Thus, to determine the minimum and the maximum equivalent values of church *i* ($V_{EEQ,min,i}$ and $V_{EEQ,max,i}$), Equations 2.18 and 2.19 were used.

$$V_{EEQ,min,i} = 3S_i C_{eq,min,i}(1 - i_{a,i}) \tag{2.18}$$

$$V_{EEQ,max,i} = 3S_i C_{eq,max,i}(1 - i_{a,i}) \tag{2.19}$$

where: S_i is the surface of the church *i*;

$C_{eq,min,i}$ is the minimum value per square meter of the church *i*;

$C_{eq,max,i}$ is the maximum value per square meter of the church *i*;

$i_{a,i}$ is the economic impact of the land on the total value of the church *i*.

Since the corresponding values of $V_{EEQ,min,i}$ and $V_{EEQ,max,i}$ resulted in a skew normal distribution, the log-normal distribution was determined (Figure 2.19 and Figure 2.20) to proceed with the measurement of the 5th and the 95th percentiles. The minimum was determined as the 5th percentile of $V_{EEQ,min}$, corresponding to $\ln(V_{EEQ,5th}) = 12.24$ ($V_{EEQ,5th}$ = 207,225 €), while the maximum was set as the 95th percentile of $V_{EEQ,max}$, corresponding to $\ln(V_{EEQ,95th}) = 14.79$ ($V_{EEQ,5th}$ = 2,656,528 €) (Figure 2.21).

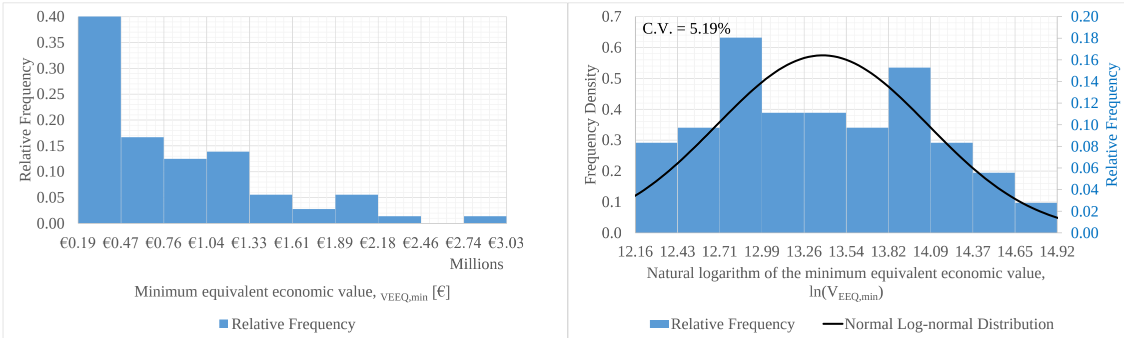

Figure 2.19: On the left: relative frequency of $V_{EEQ,min,i}$; On the right: log-normal distribution and relative frequency of $\ln(V_{EEQ,min,i})$.

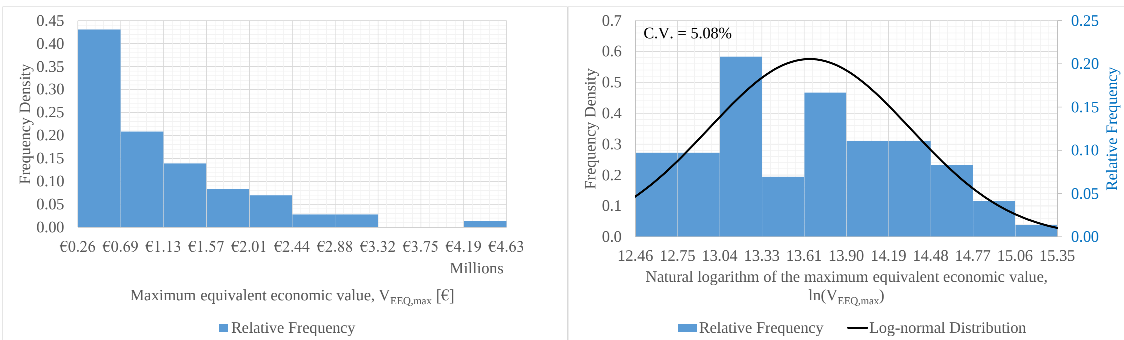

Figure 2.20: On the left: relative frequency of $V_{EEQ,max,i}$; On the right: log-normal distribution and relative frequency of $\ln(V_{EEQ,max,i})$.

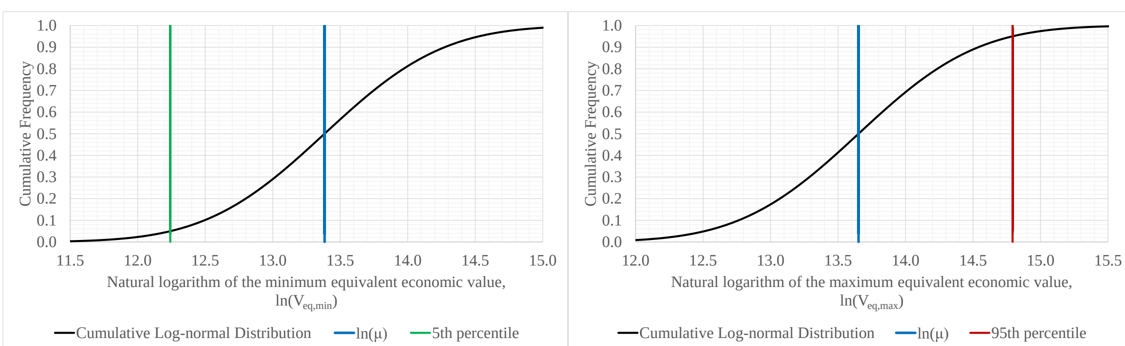

Figure 2.21: On the left: cumulative distribution of $\ln(V_{EEQ,min,i})$ with the corresponding average μ, and the 5th percentile; on the right: cumulative distribution of $\ln(V_{EEQ,max,i})$ with the corresponding average μ, and the 95th percentile.

Finally, the indices of minimum and maximum equivalent economic value ($i_{EEV,min,i}$ and $i_{EEV,max,i}$) were determined using Equations 2.20 and 2.21, respectively.

$$\frac{i_{EEV,5th}}{i_{EEV,95th}} \leq i_{EEV,min,i} = \frac{i_{EEV,min,i}}{i_{EEV,95th}} \leq 1 \tag{2.20}$$

$$\frac{i_{EEV,5th}}{i_{EEV,95th}} \leq i_{EEV,max,i} = \frac{i_{EEV,max,i}}{i_{EEV,95th}} \leq 1 \tag{2.21}$$

where: $i_{EEV,min,i}$ is the index of minimum equivalent economic value of the church i;

$i_{EEV,max,i}$ is the index of maximum equivalent economic value of the church i.

The resulting indices of equivalent economic value $i_{EEV,i}$ are shown in

Figure 2.22 subdivided based on the considered scenario and sorted by region.

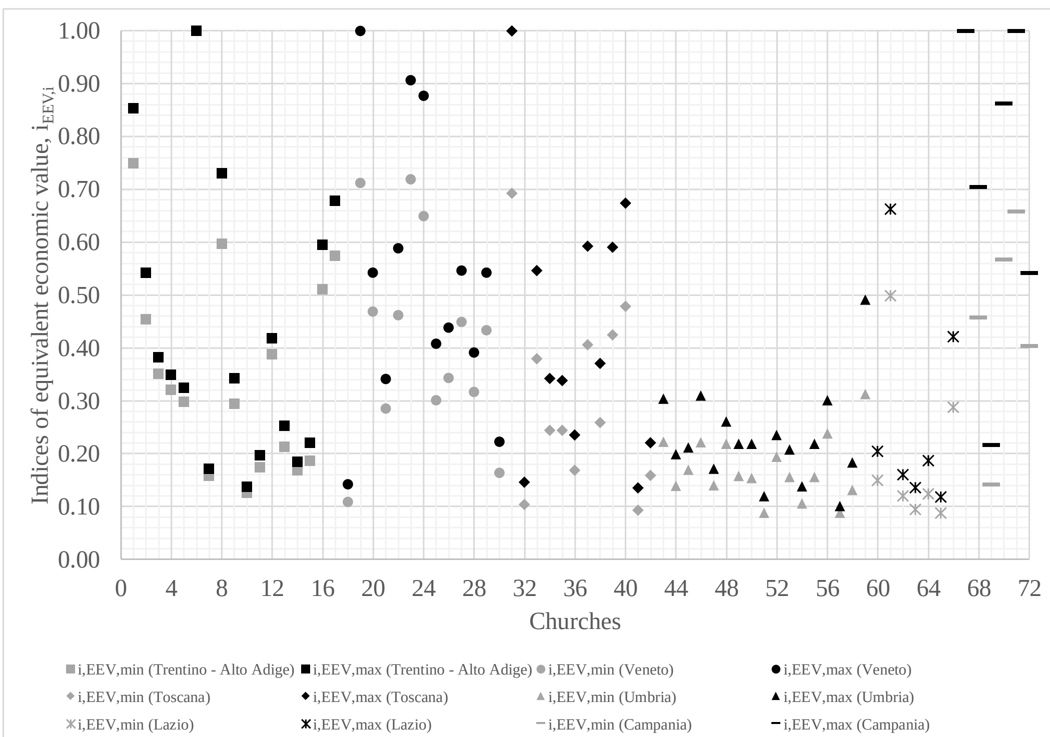

Figure 2.22: Indices of equivalent economic value $i_{EEV,i}$.

2.6.8 Index of Susceptible Heritage

The presence of heritage art and architectural features within the several assessed churches was based on a proposed scoring system (Table 2.4).

TABLE 2.4

CRITERIA FOR THE SCORING SYSTEM OF THE SUSCEPTIBLE HERITAGE

Qualitative Question	Qualitative Parameter	Parameter Score	Max Score
Are there ornaments on the façade?	There is no ornamentation	+0 points	10 points
	Architectural ornamentation	+2 points	
	Sculptured ornamentation	+3 points	
	Painted ornamentation	+3 points	
	Other	+2 points	
Is the vault painted?	There is no vault	+0 points	5 points
	There are no frescoes	+2 point	
	The vault has frescoes	+5 points	
Are there ornaments on the internal walls or chapels?	There is no ornamentation on the walls and there are no chapels	+0 points	10 points
	There is no ornamentation on the walls nor in the chapels	+1 points	
	Architectural ornamentation	+2 points	
	Sculptured ornamentation	+3 points	
	The walls/chapels have frescoes	+3 points	
	Other	+2 points	
Are there paintings in the church?	There are no paintings within the church	+0 points	5 points
	Less than 5	+1 point	
	Less than 10	+2 points	
	Less than 15	+3 points	
	Less than 20	+4 points	
	More than 20	+5 points	
Is there any recognizable piece of art (e.g., paintings or sculptures made by famous artists)?	Number of recognizable pieces of art	Based on educated judgment (The manual "Guida Rossa" might be used to help in the judgment)	15 points
MAXIMUM TOTAL SCORE			**45 points**

In these terms, the discriminating feature that helped in comparing the churches was their ornamental systems which characterized and distinguished the Italian Romanesque and Gothic architecture from the rest of the western Europe (White 1993). The creation of figural art (e.g., sculptures, paintings, and mosaics) was not an aesthetic formality, especially during the Middle Ages, but rather a means to transmit knowledge about the sacred writings to the churchgoers (Lavin 1990). Thus, the presence, the quality, and the quantity of the decorative features were considered and compared following what was perceived as their most important attributes:

- The façade is the main face of a church designed to guide the churchgoers towards their spiritual journey (Altman 1980). The role of welcoming the churchgoers and to make the church's façade recognizable from the other buildings was usually enhanced using different types of ornamentations (e.g., sculptures, painted glasses, architectural ornament, and others) (Lavin 1990), and the comparative quantities of façade ornamentation were surveyed as part of the current study;
- The vaults required a deep understanding of the structure and a significant amount of labor (Fitchen 1981), therefore, their presence represents an added value to the church, and increasingly so in the case of frescoes;
- The figurative apparatus on the internal walls was considered the natural extension of the spiritual journey initiated by the façade, representing a crucial component in leading the devotees through the mass (Lavin 1990);
- Given the lack of information for comparing the values of paintings, their quantity was recorded; and

- One-third of the total subcomponent index score was left flexible to the user in case of recognizable pieces of art made by famous masters (e.g., the rare tridimensional painting of the holy Mary with the Child in the church of San Giovanni Evangelista in Vico Equense, or the Michelangelo's lion sculpture in the church of Santa Maria Maddalena in Capranica Prenestina). Each case was evaluated and judged following in-depth research on the artefact. The authors suggest making use of the "Guide Rosse" (Touring Club Italiano From 1982 to 2015) or, if available, the archives of the dioceses as a guide for identifying artworks of cultural and historical importance.

Since the minimum and the maximum of the scoring method for the index of susceptible heritage were well defined (respectively 0 and 45 points), no statistical analysis to determine the 5th and the 95th percentiles was required. Therefore, the index of susceptible heritage $i_{SH,i}$ was determined using Equation 2.22.

$$i_{SH,i} = \frac{Score_i}{45} \tag{2.22}$$

where: $Score_i$ is the total score reached by the church i with respect of Table 2.4.

The resulting indices of susceptible heritage $i_{SH,i}$ are shown in Figure 2.23 sorted by region.

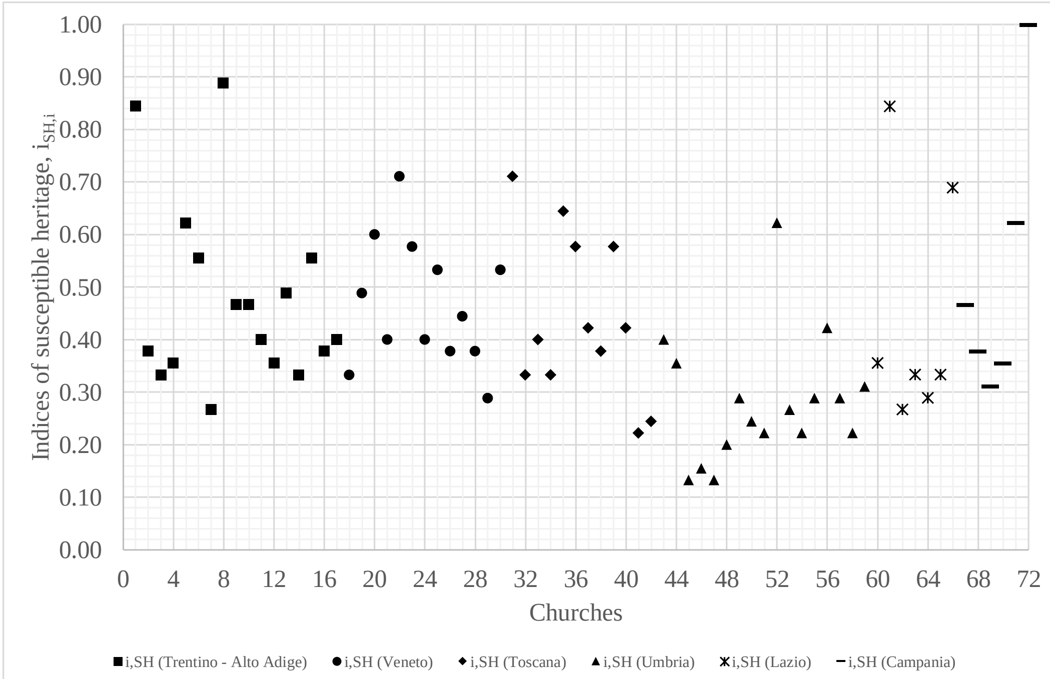

Figure 2.23: Indices of susceptible heritage $i_{SH,i}$.

2.7 Fuzzy Set Theory: Definition and Application Methodology

The "Fuzzy Set Theory" (FST) is a statistical procedure developed for combining variables with a large component of uncertainty (Zadeh 1965). In contrast to the classic set theory, which postulates that a variable x can be part of a set A or not, the FST provides a membership ratio μ_i (ranging from 0 to 1) to one or more sets A_i, addressing the variability of x by leaving room for the inherent uncertainties and the complexity of the assessing procedure. Thus, the sets used for compressing the inputs x_i (i.e., the risk component indices) are applied in order to consider two variables simultaneously in an iterative procedure resulting in one single output (i.e., the seismic risk rating) (Ross 2005). A schematic representation of the iterative procedure is shown in Figure 2.24.

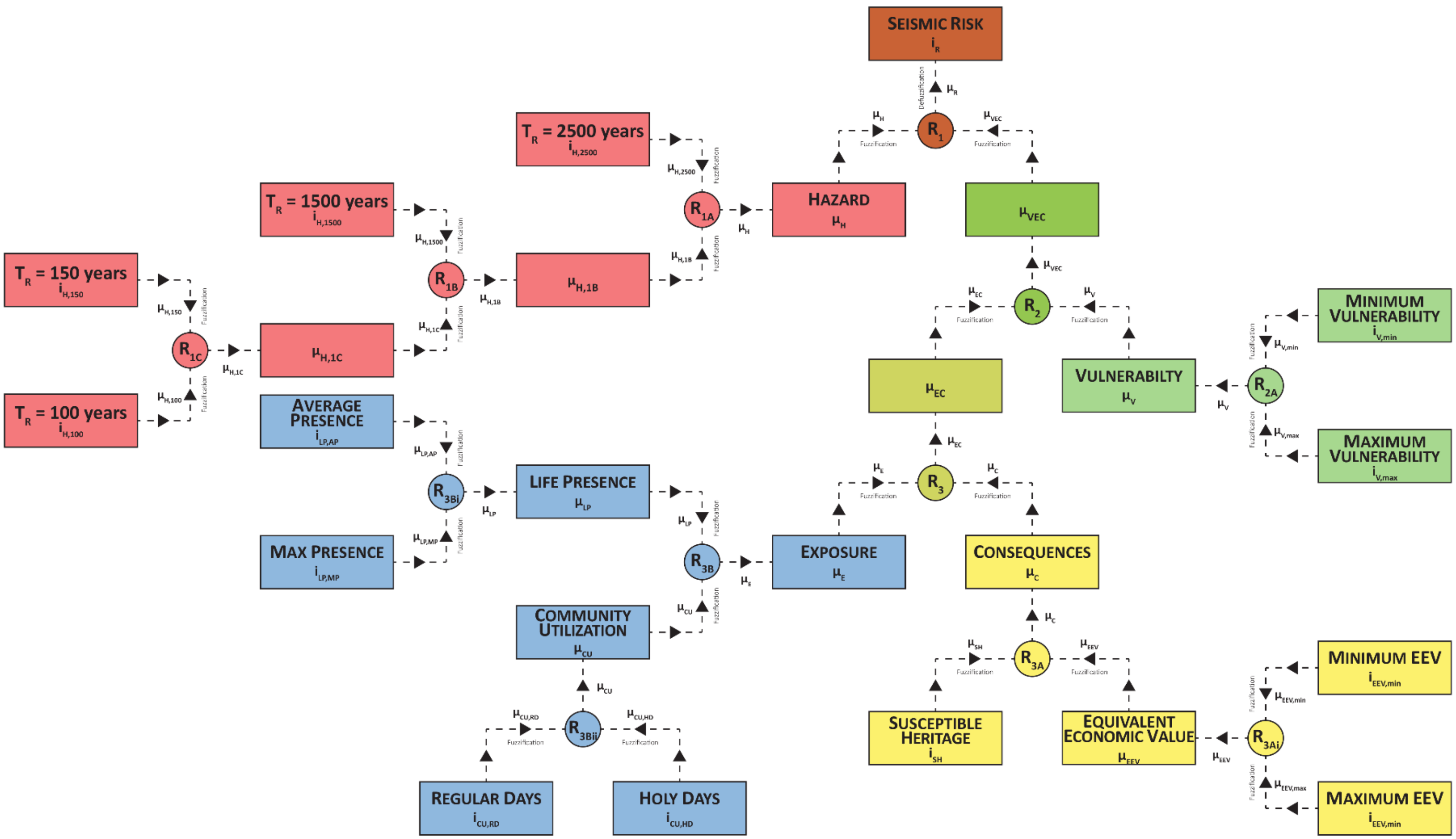

Figure 2.24: The FST procedure for determining the seismic risk rating in the current study.

Differently from other assessment techniques, such as the models for macroseismic vulnerability and damage assessment based on the fragility and capacity curves (Lagomarsino and Giovinazzi 2006; Pitilakis, Crowley, and Kaynia 2014; Kappos 2016), the FST allows to account more than two variable at the same time, including the four components of risk instead of limiting the assessment to the hazard and the vulnerability.

The aggregation procedure comprises four steps. A worked example for a church case study implementing all steps is included in Appendix C.

2.7.1 Step 1: Membership Ratio and Fuzzification of the Risk Subcomponents

Accordingly with previous research (Dong 1987; Tah and Carr 2000; Sánchez-Silva and Garcia 2001; Mistakidis and Georgiou 2003; Tesfamaraim and Saatcioglu 2008; Abeling et al. 2018), the sets A_i were defined as risk categories related with the different components of risk. Five membership ratio elements (corresponding to 5 risk categories) were used to aggregate the probabilistic range of risk variables: VL (Very Low), L (Low), M (Medium), H (High), and VH (Very High). Therefore, the input risk subcomponents (e.g., $i_{H,90}$) were "fuzzified" into a five-tuple $\boldsymbol{\mu_i} = [\ \mu_{VL,i}\ ;\ \mu_{L,i}\ ;\ \mu_{M,i}\ ;\ \mu_{H,i}\ ;\ \mu_{VH,i}\ ]$ known as the membership ratio set wherein each element represents the sensitivity of the variable value to each category from VL to VH. The membership ratio can be assigned following different methods (Ross 2005; Medasani, Kim, and Krishnapuram 1998); however, only the "Heuristic Method" was used to define the membership ratio set $\boldsymbol{\mu_i}$ since it is commonly applied for engineering risk assessment (Tesfamaraim and Saatcioglu 2008; Abeling et al. 2018). The heuristic method defines each set using a "Triangular Fuzzy Number" (TFN). The TFN is characterized by a three-tuple array $\boldsymbol{TFN^j} = [\ a_1^j;\ a_2^j;\ a_3^j\ ]$ where a_1^j, a_2^j, and a_3^j represent, respectively, where the membership to the given j-th set starts, reaches its maximum, and ends (with j = *VL*, *L*, *M*, *H*, *VH*). Thus, the membership ratio can be determined in accordance with equation 2.23.

$$\mu_i{}^j{}_{(i_i)} = \begin{cases} 0, \; i_i \leq a_1{}^j \\ \frac{i_i - a_1{}^j}{a_2{}^j - a_1{}^j}, \; a_1{}^j < i_i \leq a_2{}^j \\ \frac{a_3{}^j - i_i}{a_3{}^j - a_2{}^j}, \; a_2{}^j < i_i \leq a_3{}^j \\ 0, \; i_i > a_3{}^j \end{cases} \tag{2.23}$$

where: i_i is the index related to the i-th risk component;

$\mu_i{}^j{}_{(i_i)}$ is the j-th component of the fuzzified five-tuple array corresponding to the index i_i;

$a_1{}^j$, $a_2{}^j$, and $a_3{}^j$ are the components of $\boldsymbol{TFN^j}$.

The values of $\boldsymbol{TFN^j}$ are shown in Table 2.5.

TABLE 2.5

TRIANGULAR FUZZY NUMBERS (TFNS) OF THE MEMBERSHIP RATIO

SET	Very Low [VL]	Low [L]	Medium [M]	High [H]	Very High [VH]
Triangular Fuzzy Number	TFN^{VL} [0; 0; 0.25]	TFN^{L} [0; 0.25; 0.5]	TFN^{VL} [0.25; 0.5; 0.75]	TFN^{VL} [0.5; 0.75; 1]	TFN^{VL} [0.75; 1; 1]

An example of the TFN application is graphed in Figure 2.25 wherein the different elements (VL, L, M, H, and VH) are distributed with equivalent amplitudes with respect to each risk subcomponent without accounting for possible outliers, since they were removed based on the log-normal procedure applied in the previous sections. Similarly to Sanchez-Silva and Garcia (2001), Dickmen, Nirgonul and Han (2007), and Tesfamaraim and Saatcioglu (2008), five sets (i.e., VL, L, M, H, and VH), instead of three (Abeling et al. 2018), were considered to avoid an excessive discretization of the results. As an example the graphic fuzzification of the indices of susceptible heritage for each church is shown in Appendix D.

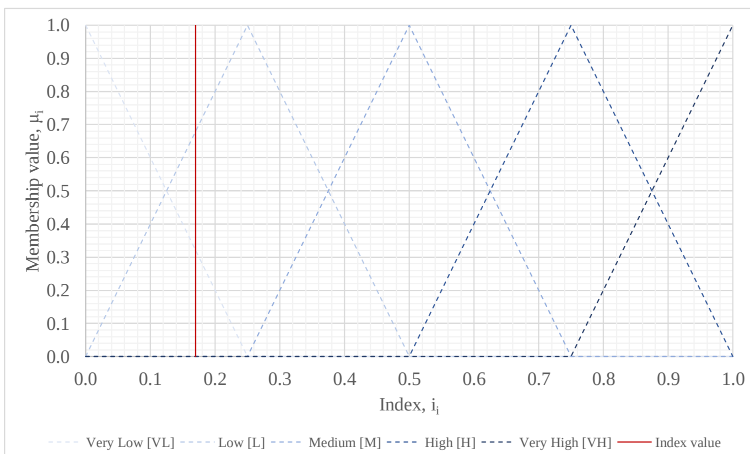

Figure 2.25: Graphical fuzzification of a general variable i_i.

2.7.2 Step 2: Aggregation of a Couple of Five-tuple Sets

According to Zadeh (1965) and Mamdani (1976), two five-tuple sets can be combined into a resulting five-tuple set using a procedure called “aggregation” by Ross (2005). Thus, to result in one single seismic risk rating, 13 five-tuple sets (determined starting from the risk subcomponents) were aggregated in couples until one single five-tuple set remained. Since the aggregation is commutative, the order of aggregation is irrelevant. The aggregation of the components of two five-tuple sets $\boldsymbol{\mu_1}$ = [$\mu_{VL,1}$; $\mu_{L,1}$; $\mu_{M,1}$; $\mu_{H,1}$; $\mu_{VH,1}$] and $\boldsymbol{\mu_2}$ = [$\mu_{VL,2}$; $\mu_{L,2}$; $\mu_{M,2}$; $\mu_{H,2}$; $\mu_{VH,2}$] should be based on rules $\boldsymbol{r^k}$ that combine the two five-tuple sets' components into a single aggregated five-tuple set $\boldsymbol{\mu_r}$ = [$\mu_{VL,r}$; $\mu_{L,r}$; $\mu_{M,r}$; $\mu_{H,r}$; $\mu_{VH,r}$]. Since each five-tuple set $\boldsymbol{\mu_i}$ has five components, each set of rules $\boldsymbol{r^k}$ was constituted of 25 elements ($\boldsymbol{k}$ = [*1, 2, 3, …, 25*]), accounting for any possible combination as shown in Table 2.6.

TABLE 2.6

COMBINATION RULES RK

Rule Set [r]	Set input 1 [μ_1^{jk}]	Set input 2 [μ_2^{jk}]	Set output [μ_r^j]	Rule Set [r]	Set input 1 [μ_1^{jk}]	Set input 2 [μ_2^{jk}]	Set output [μ_r^j]
r^1	VL	VL	VL	r^{14}	M	H	H
r^2	VL	L	L	r^{15}	M	VH	H
r^3	VL	M	L	r^{16}	H	VL	M
r^4	VL	H	M	r^{17}	H	L	M
r^5	VL	VH	M	r^{18}	H	M	H
r^6	L	VL	L	r^{19}	H	H	H
r^7	L	L	L	r^{20}	H	VH	VH
r^8	L	M	M	r^{21}	VH	VL	M
r^9	L	H	M	r^{22}	VH	L	H
r^{10}	L	VH	H	r^{23}	VH	M	H
r^{11}	M	VL	L	r^{24}	VH	H	VH
r^{12}	M	L	M	r^{25}	VH	VH	VH
r^{13}	M	M	M				

The combinations in Table 2.6 are resolved by means of the Boolean rule of set intersection (Whitehead 1898) in Equation 2.24:

$$[\mu_r{}^j]_k = \mu_1{}^{jk} \cap \mu_2{}^{jk} \tag{2.24}$$

where: $[\mu_r{}^j]_k$ is the result of the k-th rule having $\boldsymbol{j}$ as set output for $\boldsymbol{j} = [VL, L, M, H, VH]$ and $\boldsymbol{k} = [1, 2, 3, \ldots, 25]$;

$\mu_1{}^{jk}$ is the j-th component of the first input μ_1 corresponding to the k-th rule (e.g., $\mu_1{}^{jk} = \mu_{M,1}$ for $k = 11$);

$\mu_2{}^{jk}$ is the j-th component of the second input μ_2 corresponding to the k-th rule (e.g., $\mu_2{}^{jk} = \mu_{VL,2}$ for $k = 11$);

The algebraic operation corresponding to the abovementioned Boolean intersection, according to the Mamdani and Zadeh implications, is the minimum value of the two considered components of the five-tuple sets. Thus, Equation 2.24 is converted into Equation 2.25 as follows:

$$[\mu_r{}^j]_k = \min\left(\mu_1{}^{jk}; \mu_2{}^{jk}\right) \tag{2.25}$$

Since the resulting set will have *n* elements *j* within a single component (e.g., rules r^2, r^3, r^6, r^7, r^{11} all contribute to component L) the actual member is resolved by means of the Boolean union rule in Equation 2.26:

$$\mu_{j,r} = [\mu_r{}^j]_{k,1} \cup [\mu_r{}^j]_{k,2} \cup \ldots \cup [\mu_r{}^j]_{k,n} \tag{2.26}$$

where: $\mu_{j,r}$ is the j-th component of the output $\boldsymbol{\mu_r}$;

n is the number of rules $\boldsymbol{r^k}$ having j as result (e.g., $n = 5$ for $j = L$);

the k-th rule (e.g., $\mu_2{}^{jk} = \mu_{VL,2}$ for $k = 11$).

The algebraic operation corresponding to the abovementioned Boolean intersection, according to Zadeh (1965) and the Mamdani (1976) implications, is the minimum value of the two considered components of the five-tuple sets. Thus, Equation 2.26 is translated into Equation 2.27 as follows:

$$\mu_{j,r} = \max\left(\left[{\mu_r}^j\right]_{k,1}; \left[{\mu_r}^j\right]_{k,2}; \dots \left[{\mu_r}^j\right]_{k,n} \right) \tag{2.27}$$

Equation 2.25 and Equation 2.27 were used to determine the components of the resulting five-tuple set $\boldsymbol{\mu_r}$ = [$\mu_{VL,r}\,;\mu_{L,r}\,;\mu_{M,r}\,;\mu_{H,r}\,;\mu_{VH,r}$].

2.7.3 Step 3: Iteration

The third step of the FST procedure consisted in iterating steps 1 and 2 for each couple of input subcomponents (Figure 2.26). The result of step 2, $\boldsymbol{\mu_r}$, was used as input for the iteration. The process was iterated reflecting the hierarchy shown in Figure 2.24 until the final seismic risk ratings i_R were determined for each church.

2.7.4 Step 4: Defuzzification

Finally, the five-tuple set $\boldsymbol{\mu_r}$ was converted back to a rating i_r between 0 and 1 using the inverse procedure defined as “defuzzification” (Abeling et al. 2018). Although several techniques are available for the defuzzification process (Klir and Yuan 1995; Ross 2005), the “Weighted Average Method” was applied accordingly with similar risk assessments (Tesfamaraim and Saatcioglu 2008; Abeling et al. 2018). The resulting rating i_r was determined using 2.28.

$$i_{j,r} = \sum_j q_j \mu_{j,r} \tag{2.28}$$

where: $i_{j,r}$ represents the defuzzified value of $\mu_{j,r}$;

q_j is the weighting factor of the j-th component of the output $\boldsymbol{\mu_r}$;

$\mu_{j,r}$ is the j-th component of the output $\boldsymbol{\mu_r}$.

Tesfamaraim and Saatcioglu (2008) proposed the q_j factors to be, respectively, q_{VL} = 0, q_L = 0.25, q_M = 0.50, q_H = 0.75, and q_{VH} = 1.00, however, in the current research, q_{VL} was modified to assume the value of 0.10 so as not to disregard completely the importance of the Very Low risk category.

2.8 FST Results and Multilinear Regression of Ratings

The seismic risk ratings $i_{R,i}$ are shown in Figure 2.26. Veneto was determined to be the region with the largest average risk rating across its surveyed portfolio of churches. Also, the average risk rating for churches in Lazio was comparatively high, mostly because of index ratings of hazard and susceptible heritage of the churches within this region. The lowest regional average risk rating was determined to be in Toscana. The lowest risk rating for a single church was determined to occur in Trentino – Alto Adige due to the comparatively low seismicity of this region (Figure 2.1). Note that the church determined to have the highest comparative risk rating in the Lazio region was independently identified by the diocese of Anagni-Alatri to be prioritized for retrofit within their portfolio.

Given the large amount of uncertainties inherent to the risk subcomponents, the variability of the risk ratings, $\mathrm{i}_{\mathrm{R,i}}$, was also charted in Figure 2.26. Greater uncertainty in parameters (e.g., the quality of the masonry of a plastered wall), corresponds to to wider ranges between the lower and the upper risk rating limit. However, the implementation of the risk aggregation procedure resulted in the final risk ratings, $\mathrm{i}_{\mathrm{R,i}}$, being generally closer to the upper limit. Therefore, the methodology accounted for the unknowns (depending on the conditions of each inspected church) throughout using a comparatively conservative approach, in accordance with common engineering practice.

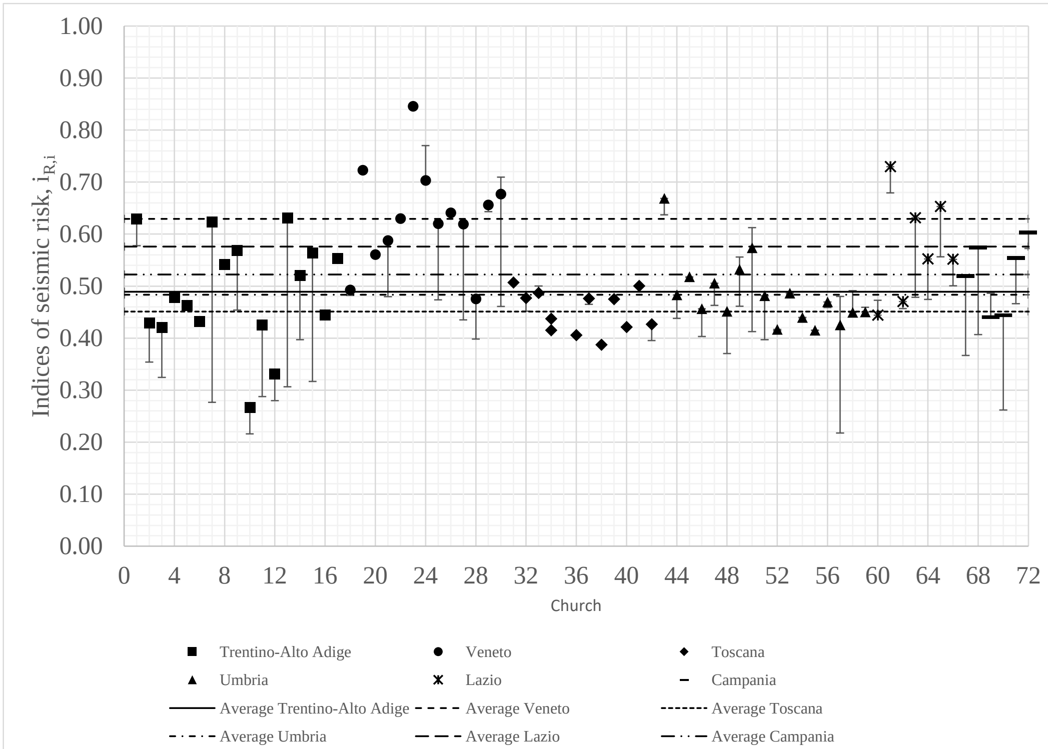

Figure 2.26: Seismic risk ratings $i_{R,i}$.

Acknowledging that the FST procedure can be prohibitively complex for use by general practitioners who wish to carry our preliminary portfolio risk analyses of similar churches in Italy, a multilinear regression was applied to the intermediate and the final outcomes of the FST analysis determined in the current study to provide a direct correlation between the risk components and the final seismic risk ratings (see Equations 2.29 – 2.33). The coefficient of determination, R^2, and the standard errors of the regression, S, are listed in Table 2.7.

TABLE 2.7

COEFFICIENT OF DETERMINATION, R^2, AND STANDARD DEVIATION OF THE REGRESSION, *S*

Equation	**Ratings**	$\mathbf{R^2}$	**Standard deviation, S**
2.29	Hazard, $\mathbf{i_{H,i}}$	0.957	0.091
2.30	Vulnerability, $\mathbf{i_{V,i}}$	0.981	0.038
2.31	Exposure, $\mathbf{i_{E,i}}$	0.939	0.069
2.32	Consequences, $\mathbf{i_{C,i}}$	0.967	0.064
2.33	Seismic risk, $\mathbf{i_{R,i}}$	0.973	0.059

$$i_{H,i} = -4.822 i_{H,90,i} + 8.778 i_{H,151,i} - 7.256 i_{H,1424,i} + 5.020 i_{H,2475,i} \leq 1 \tag{2.29}$$

$$i_{V,i} = 0.103 i_{V,min,i} + 0.892 i_{V,max,i} \leq 1 \tag{2.30}$$

$$i_{E,i} = 0.029 i_{OR,AO,i} + 0.522 i_{OR,MO,i} + 0.302 i_{CU,RD,i} + 0.154 i_{CU,HD,i} \leq 1 \tag{2.31}$$

$$i_{C,i} = -0.111 i_{EEV,min,i} + 0.593 i_{EEV,max,i} + 0.511 i_{SH,i} \leq 1 \tag{2.32}$$

$$i_{R,i} = 0.297 i_{H,i} + 0.474 i_{V,i} + 0.155_{E,i} + 0.104 i_{C,i} \leq 1 \tag{2.33}$$

Given that the coefficient of determination, R^2, is by itself not sufficient to represent the quality of the fitting, the authors suggest referring to the standard deviation of the regression, S, to quantify the discrepancy between the proposed multilinear equations and the FST analysis. A detailed worked example is shown in Appendix C.

2.9 Applications

The developed methodology was based on a sample composed of URM Italian medieval churches with an average footprint surface area of 410 m^2 and maximum footprint surface of 1340 m^2, located in settlements with an average of 4,000 residents and a maximum of 46,000 residents. If the proposed methodology were to be applied to larger URM non-medieval churches located in larger cities (e.g., cathedrals of main cities such as Rome or Milan), the authors recommend re-calibrating the limits given by the 5th and the 95th percentiles of the following indices:

- Index of average and maximum occupancy ratio, $i_{OR,AP}$ and $i_{OR,MP}$;
- Index of community utilization during the regular weeks' masses and holy days' masses, $i_{CU,RW}$ and $i_{CU,HD}$; and
- Index of minimum and maximum equivalent economic value, $i_{EEV,min}$ and $i_{EEV,max}$.

Furthermore, the methodology might also be applied in non-seismic hazard scenarios by defining an appropriate index (from 0 to 1) to account for the considered hazard (e.g., flooding, or hurricanes). Lastly, the proposed methodology may be applied for determining the risk rating associated with non-URM churches (i.e., churches constructed with other materials), but a procedure for quantifying vulnerability different from the macro-blocks approach should be applied.

2.10 Summary, Conclusion, and Future Work

In this paper, a holistic and generalizable seismic risk assessment methodology was established based on surveys of 72 URM Italian medieval churches. Indices to address the different components of risk (i.e., hazard, vulnerability, exposure, and consequences) were developed and assessed with statistical bases. The indices were then processed through the "Fuzzy Set Theory" (FST) to account for statistical variations (including unknowns) result in a final comparative rating of seismic risk for each church. Finally, a set of ready-to-use multilinear equations was developed to facilitate further assessment for similar scenarios conducted by others.

All the proposed indices were based on easily accessible data, resulting in efficient and effective surveys for each church. Using this procedure, one single person could survey several churches per day to obtain the necessary information for the assessment, saving time and money for portfolio managers. Given the limited funding at the disposal of the selected communities, the developed seismic risk ratings are expected to offer a reliable but provisional basis to assist the decision-making process resulting in a cost-efficient management of the dioceses' property portfolio and funding allocations. The seismic risk ratings shown in Figure 2.26 will be provided to the portfolio managers of the respective dioceses and used to prioritize the churches for further detailed analysis and retrofits of the identified vulnerabilities.

In addition to the final seismic risk rating, the indices of risk subcomponent shown in Figure 2.6, Figure 2.8, Figure 2.18, Figure 2.22, and Figure 2.23 and the indices of risk component obtainable using Equations 2.29 through 2.32 may have an applicable value as well pertaining to which type of intervention may be most a. A non-exhaustive list of generic intervention options is offered below:

- High risk subcomponent indices of hazard and/or vulnerability: More sophisticated structural analysis and a structural retrofit may be appropriate to enhance the capacity of the most critical macro-blocks of the church. The current literature offers a large variety of viable solutions depending on the conditions and the vulnerability of each church (e.g., Doglioni 2000; Vinci 2012);

- High risk subcomponent index of exposure: A viable and relatively inexpensive policy to reduce the exposure in a church – mainly in regard to life safety – may be to limit the number of churchgoers that can attend a single mass. Similar results could be achieved by increasing the number of masses available during the holy days in order to spread the attendance temporally; and
- High risk subcomponent index of consequences: The stipulation of insurance for asset damage may be a viable policy to reduce the amount of monetary losses where the level of hazard is considerably high. Furthermore, for "priceless" pieces of art that enrich the churches' artistic and heritage value, some consideration regarding the substitution of copies may be evaluated, while the originals may be stored in more secure local venues.

Material analysis based on non-destructive techniques (NDT) is currently developing to achieve a better understanding of the mechanical properties of URM (e.g., compressive strength). Furthermore, photogrammetric tri-dimensional models of select case study churches are developing to achieve more precise geometric measures. The mechanical and geometric properties will be further used to develop complete structural building information models (BIM) of select case study churches, and to achieve an exhaustive structural analysis to compare the results of the detailed analysis with the results of the current provisional assessment.

CHAPTER 3:
AGGREGATED NON-DESTRUCTIVE TEST TECHNIQUE FOR THE ASSESSMENT OF MECHANICAL PROPERTIES OF UNREINFORCED MASONRY ITALIAN MEDIEVAL CHURCHES

Medieval churches constructed of unreinforced masonry (URM) represent critical assets of Italian architectural heritage. In order to preserve these churches in spite of severe seismic hazards, obtaining reliable information regarding their material mechanical characteristics is necessary as part of a reliable structural analysis and retrofitting intervention. Given the drawbacks of semi-destructive or destructive testing of heritage material, non-destructive testing (NDT) is the most viable approach to obtain data regarding the mechanical characteristics of the material composing the structure of the churches. However, NDT presents several uncertainties based on the current state of the art. Thus, four different NDT techniques (two qualitative and two quantitative) were applied to 170 URM specimens belonging to 72 URM Italian medieval churches to develop a low-impact, rapid, and complete mechanical properties' assessment methodology.

3.1 List of Notations

URM is the abbreviation for "unreinforced masonry";

NDT is the abbreviation for "non-destructive testing";

MQI is the abbreviation for "masonry quality index";

f'_m is the URM compressive strength (MPa);

E_m is the URM Young's modulus (MPa);

E_{dm} is the URM dynamic modulus of elasticity (MPa);

G_m is the URM shear modulus (MPa);

c is the URM cohesion (MPa);

μ is the URM friction coefficient;

w is the URM density (kN/m^3);

ν is the URM Poisson's ratio;

g is the gravitational acceleration (m/s^2);

R is the rebound number; and

v_i is the indirect pulse velocity (m/s).

3.2 Introduction

Unreinforced masonry (URM) has been one of the most largely utilized construction materials in Italy since the early major civilizations (e.g., Etruscan and Roman) and remained so until the introduction of reinforced concrete in the late 1800s (Galliani 1832; Gloria 1976; Adam et al. 1984; Narendra 2010). Furthermore, given the durability of masonry, most of the historic structures still in existence are partially or totally composed of URM. The High and Late Middle Ages represent periods of intense masonry construction during which a large proportion of Italian architectural heritage was constructed (Cagnana 1997). Some examples of the prototypical considered churches considered in the current study are shown in Figure 3.1.

Figure 3.1: Prototypical examples of churches surveyed: a) Santa Maria Assunta (Dasindo, Trentino – Alto Adige); b) San Matteo Apostolo (Cavazzale, Veneto); c) Santi Leonardo e Cristoforo (Monticchiello, Toscana); d) Sant'Ansano Martire (Petrignano del Lago, Umbria); e) Maddalena (Alatri, Lazio); f) Santa Maria di Casarlano (Casarlano, Campania).

Given the cultural importance of URM Medieval churches, and the vulnerability of this construction type observed in past earthquakes, such as in Friuli-Venezia Giulia in 1976 (Doglioni, Moretti, and Petrini 1994), in Basilicata and Campania in 1980 (Proietti 1994), in Umbria-Marche in 1997 (Doglioni 2000; Lagomarsino 2012), in L'Aquila in 2009 (Cimellaro et al. 2010; da Porto et al. 2012), and in central Italy in 2016 (Penna et al. 2019), a holistic risk assessment methodology to justify the decision-making process of the dioceses concerning the retrofitting interventions was developed (Pirchio et al., 2020a). In regard to improving the risk assessment methodology, and as a basis for further studies, a more sophisticated analysis regarding the mechanical material properties of the considered churches was conducted as reported herein.

While component geometry (e.g., wall height-to-thickness ratio) is the dominating variable for the out-of-plane behavior of URM structures (Abrams et al. 2007; Quelhas et al. 2014; Walsh et al. 2017), material mechanical properties (e.g., masonry compressive strength, elastic modulus, and shear strength) often govern the in-plane and the dynamic behavior of URM structures (Quelhas et al. 2014; Pir et al. 2015). The determination of the mechanical properties – especially in historic buildings with non-homogeneous construction due to expansions and retrofits over time – is process-dependent on the adopted assessing technique, especially when non-destructive testing (NDT) techniques are applied, which are generally and inherently less precise and less accurate than destructive and semi-destructive techniques (McCann and Forde 2001). Nonetheless, the current research was targeted to the development of a dependable NDT assessment methodology for three primary reasons:

- Historic buildings are often subject to regulatory and architectural constraints that prohibit the extraction of specimens to be studied in laboratory testing using destructive techniques unless a retrofitting intervention is in progress;
- NDT techniques are generally more rapid and less cost-demanding than semi-destructive and destructive techniques, and hence more suitable for use in a time-efficient risk assessment methodology (Pirchio et al., 2020a); and
- Although several studies have been conducted using different NDT techniques on masonry buildings (Brozovsky 2013; Ohtsu 2016; Roknuzzaman et al. 2017), the authors are aware of only limited research in which the discrepancies amongst different NDT techniques are considered (Arduini, Di Leo, and Pascale 1994; Conde et al. 2017).

3.3 Churches, Macro-blocks, and Materials

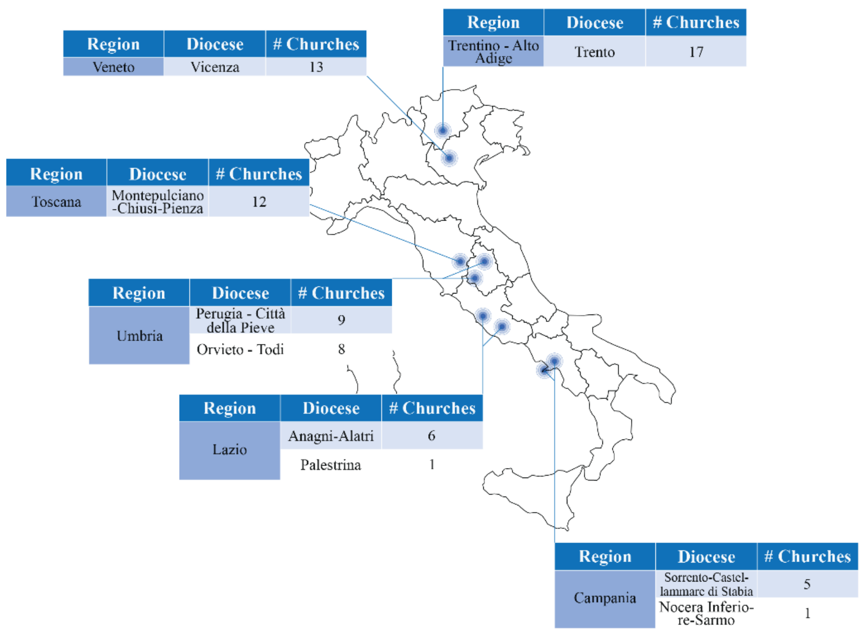

Figure 3.2: Map of Italy indicating the six regions and the nine dioceses in which churches were surveyed.

Within the current research, 72 churches in six different regions were surveyed (Figure 3.2). The complete list of the churches is tabulated in Table A.1 of Appendix A. The surveyed churches were selected to be a representative sample of the stock of URM churches in each surveyed region based on four criteria, which were described in detail in Pirchio et al. (2020a):

- The geographic location (considering the seismicity, the density of churches, the climate and geologic/topographic conditions, and the cultural and historic features);
- The churches' active functionality;
- The original construction period; and
- The urban and planimetric layout.

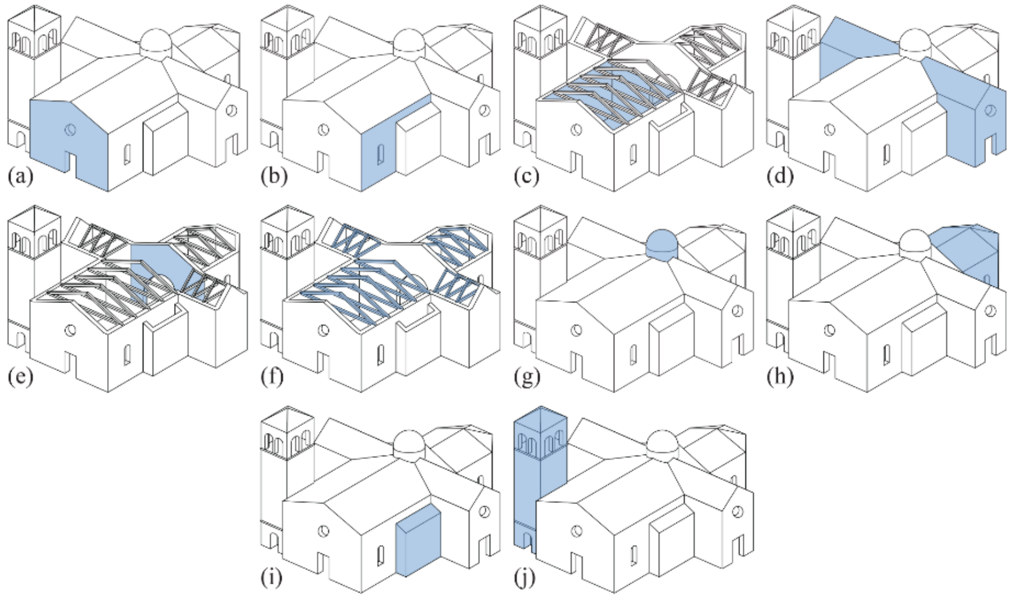

Figure 3.3: Macro-blocks considered: (a) façade; (b) lateral walls; (c) naves; (d) transept; (e) triumphal arch; (f) roof; (g) dome; (h) apse; (i) chapels; (j) bell tower.

Due to the slenderness of church walls compared to most other types of buildings, subdividing URM churches into units called "macro-blocks" is the preferred method to assess churches and other complex URM buildings (Doglioni, Moretti, and Petrini 1994; Marotta et al. 2017; Gàlvez et al. 2018). In general, in URM churches ten different macro-blocks types can be recognized (Figure 3.3). Most of the macro-blocks types – with the exception of the roof, which is usually in timber – are constructed in URM. In the current research, only the nine URM macro-block types were addressed, and, wherever visible (e.g., not covered in plaster), the URM type of each macro-block component was identified and assessed via NDT techniques.

The following four general URM types were found to be used in the construction the macro-blocks components of the surveyed churches:

- Rubble stones (Fiure 3.4a);
- Split stones with good texture (Figure 3.4b);
- Squared stone blocks (Figure 3.4c); and
- Solid fired clay bricks with lime mortar (Figure 3.4d).

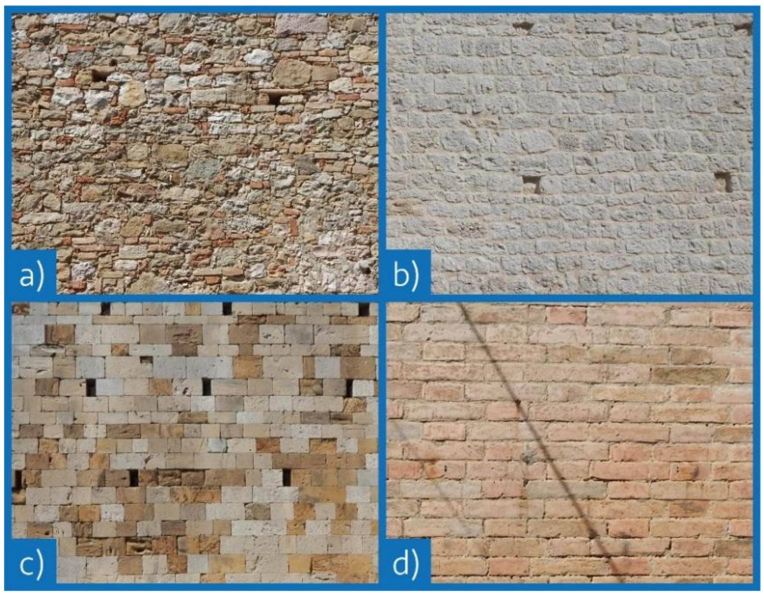

Figure 3.4: Prototypical examples of URM types identified: a) rubble stones; b) split stones with good texture; c) squared stone blocks; d) solid fired clay bricks with lime mortar.

In total, 424 individual macro-blocks components were surveyed amongst the 72 churches (roughly six macro-blocks types for each church, in average). Given that some macro-blocks components were composed by different URM types due the retrofits over the time, 1.11 URM specimens were identified (in average) for each macro-block component resulting in 471 URM specimens. However, 268 masonry URM specimens (the 57%) were classified as “unknown” since the corresponding macro-blocks components resulted completely plastered. Although all the remaining 203 URM specimens were categorized accordingly with the four URM types (Figure 3.4), only the specimens in which all the NDT techniques could be applied (i.e., accessible) were considered in the current research, resulting in 170 tested URM specimens. In Table 3.1, the 170 tested URM specimens were categorized basing on the recognized URM type.

TABLE 3.1

TOTAL NUMBER OF TESTED SPECIMENS AND CORRESPONDING URM TYPE

URM type	**Total tested specimens**
Rubble stones	20
Split stones with good texture	41
Squared stone blocks	75
Solid fired clay bricks with lime mortar	34

Furthermore, since the 78% of the surveyed churches were composed of at least five macro-blocks types (close to the average, which is six macro-blocks type per church), and given that roughly one URM specimen was tested for each macroblock, larger curches were not overly represented in the current research. In Figure 3.5 – Figure 3.10, the distribution amongst the regions of the number of surveyed churches, the number of macro-blocks components identified for each one of the nine considered macro-blocks types, the number of different URM types identified in each macro-block component, and the total number of URM specimens for each one of the four URM type are illustrated.

Region	Diocese	# Churches
Trentino - Alto Adige	Trento	17

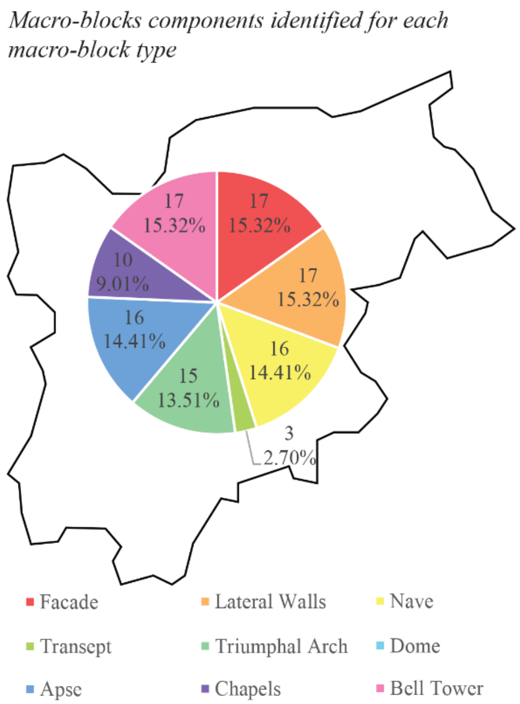

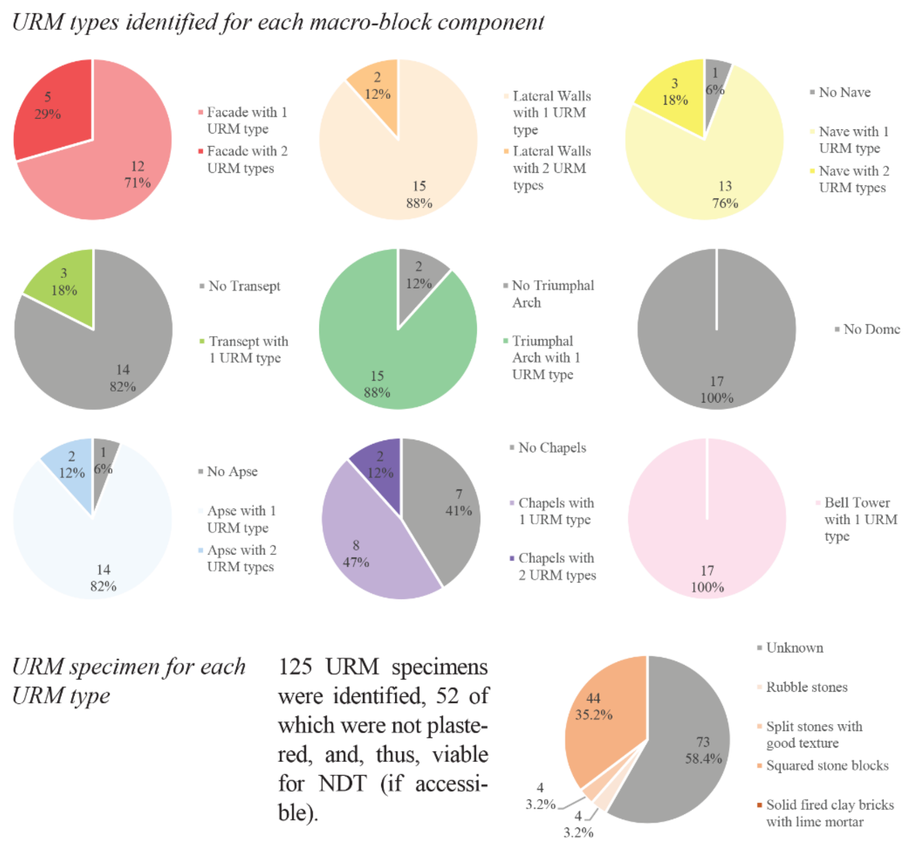

Figure 3.5: Region: Trentino – Alto Adige; top left: number of surveyed churches; bottom left: number of macro-blocks components identified for each macro-block type; top right: number of URM types identified for each macro-block component; bottom right: number of URM specimen for each URM type.

Region	Diocese	# Churches
Veneto	Vicenza	13

Macro-blocks components identified for each macro-block type

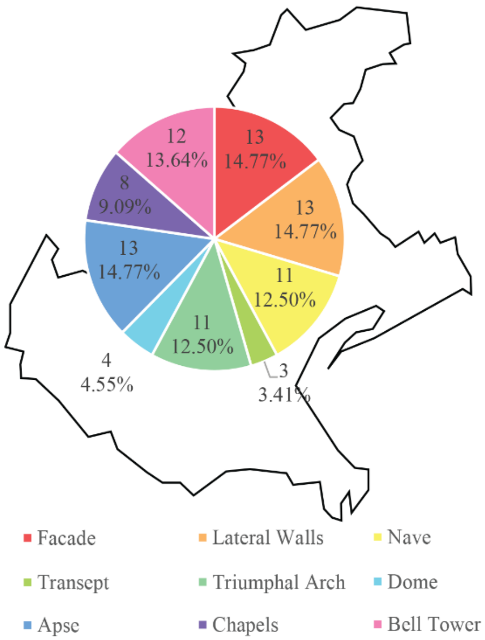

URM types identified for each macro-block component

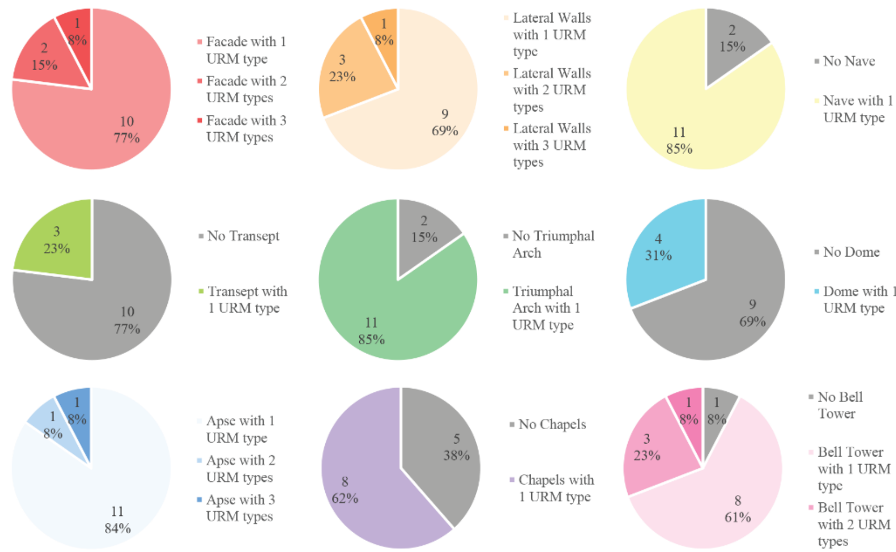

URM specimen for each URM type

105 URM specimens were identified, 27 of which were not plastered, and, thus, viable for NDT (if accessible).

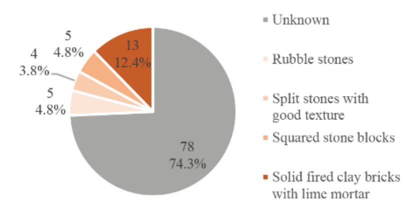

Figure 3.6: Region: Veneto; top left: number of surveyed churches; bottom left: number of macro-blocks components identified for each macro-block type; top right: number of URM types identified for each macro-block component; bottom right: number of URM specimen for each URM type.

Region	Diocese	# Churches
Toscana	Montepulciano -Chiusi-Pienza	12

Macro-blocks components identified for each macro-block type

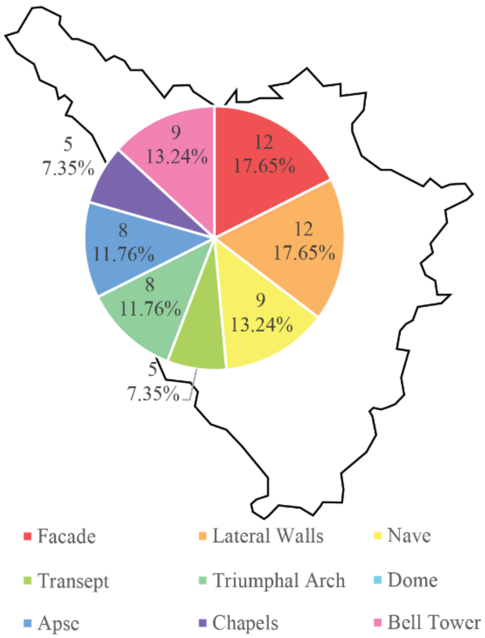

URM types identified for each macro-block component

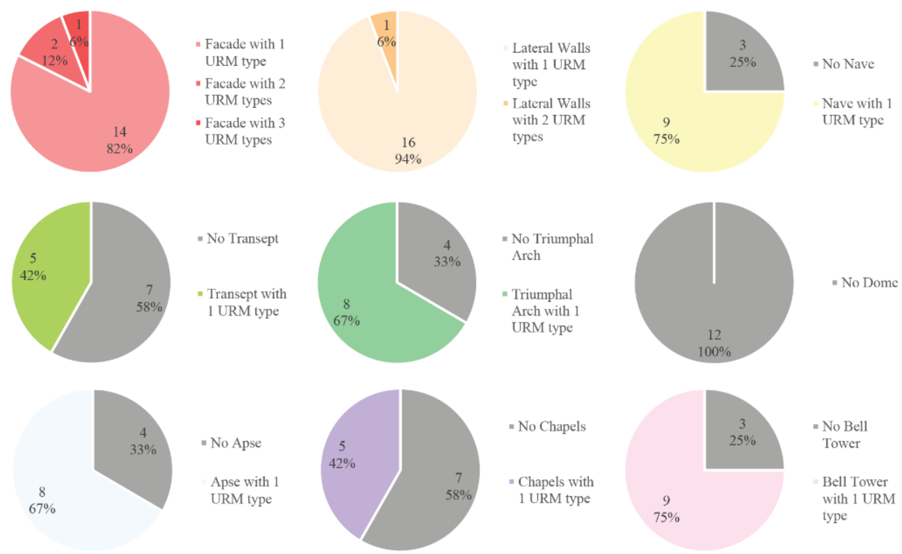

URM specimen for each URM type

71 URM specimens were identified, 42 of which were not plastered, and, thus, viable for NDT (if accessible).

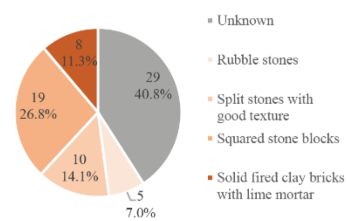

Figure 3.7: Region: Toscana; top left: number of surveyed churches; bottom left: number of macro-blocks components identified for each macro-block type; top right: number of URM types identified for each macro-block component; bottom right: number of URM specimen for each URM type.

Region	Diocese	# Churches
Umbria	Perugia - Città della Pieve	9
	Orvieto - Todi	8

Macro-blocks components identified for each macro-block type

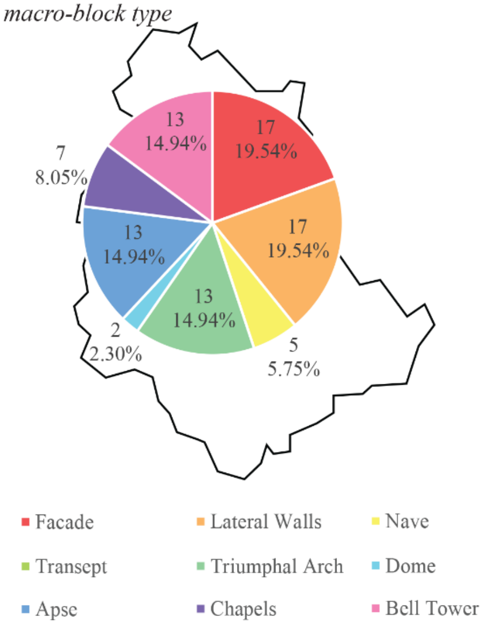

URM types identified for each macro-block component

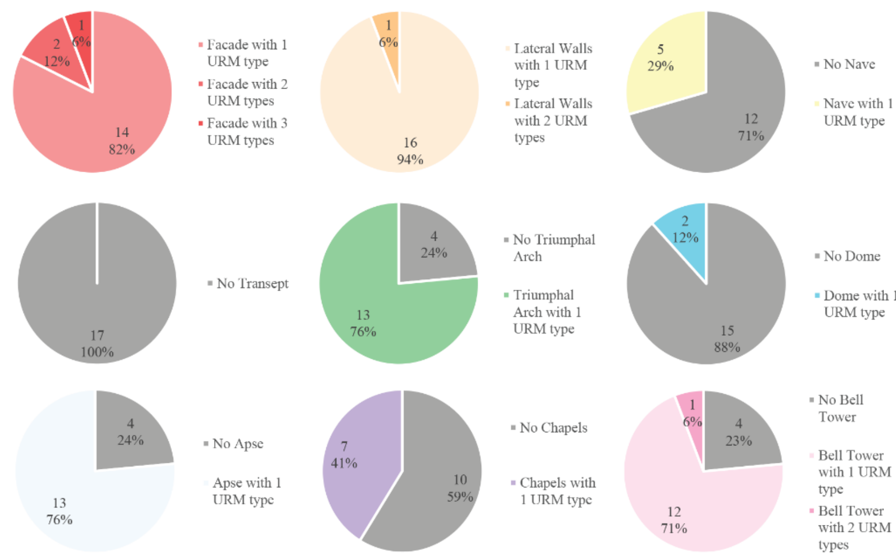

URM specimen for each URM type

93 URM specimens were identified, 61 of which were not plastered, and, thus, viable for NDT (if accessible).

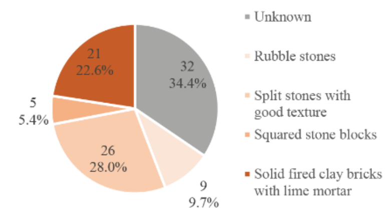

Figure 3.8: Region: Umbria; top left: number of surveyed churches; bottom left: number of macro-blocks components identified for each macro-block type; top right: number of URM types identified for each macro-block component; bottom right: number of URM specimen for each URM type.

Region	Diocese	# Churches
Lazio	Anagni-Alatri	6
	Palestrina	1

Macro-blocks components identified for each macro-block type

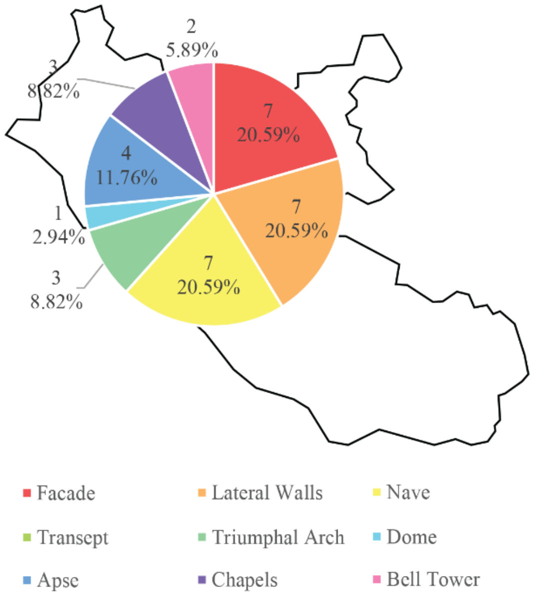

URM types identified for each macro-block component

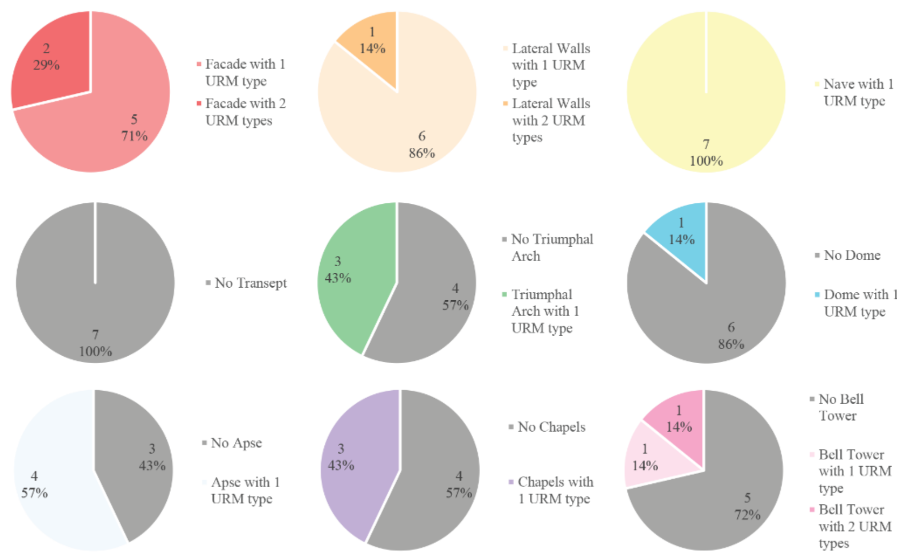

URM specimen for each URM type

38 URM specimens were identified, 13 of which were not plaste-red, and, thus, viable for NDT (if accessi-ble).

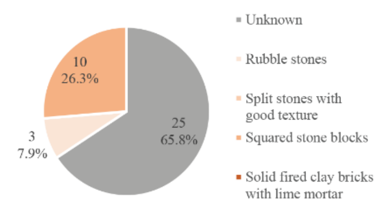

Figure 3.9: Region: Lazio; top left: number of surveyed churches; bottom left: number of macro-blocks components identified for each macro-block type; top right: number of URM types identified for each macro-block component; bottom right: number of URM specimen for each URM type.

Region	Diocese	# Churches
Campania	Sorrento-Castellammare di Stabia	5
	Nocera Inferiore-Sarmo	1

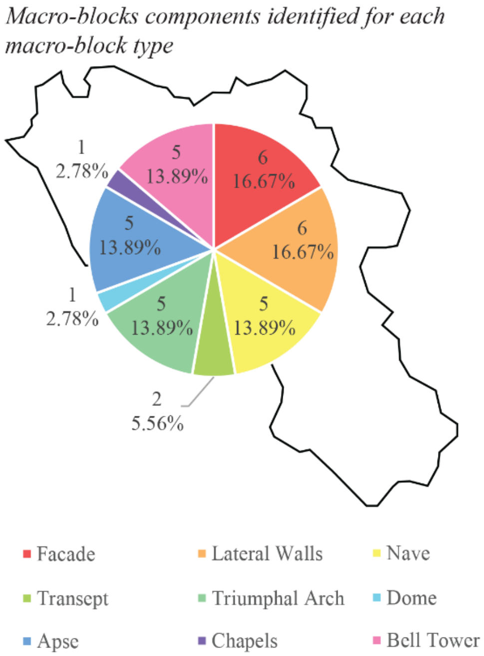

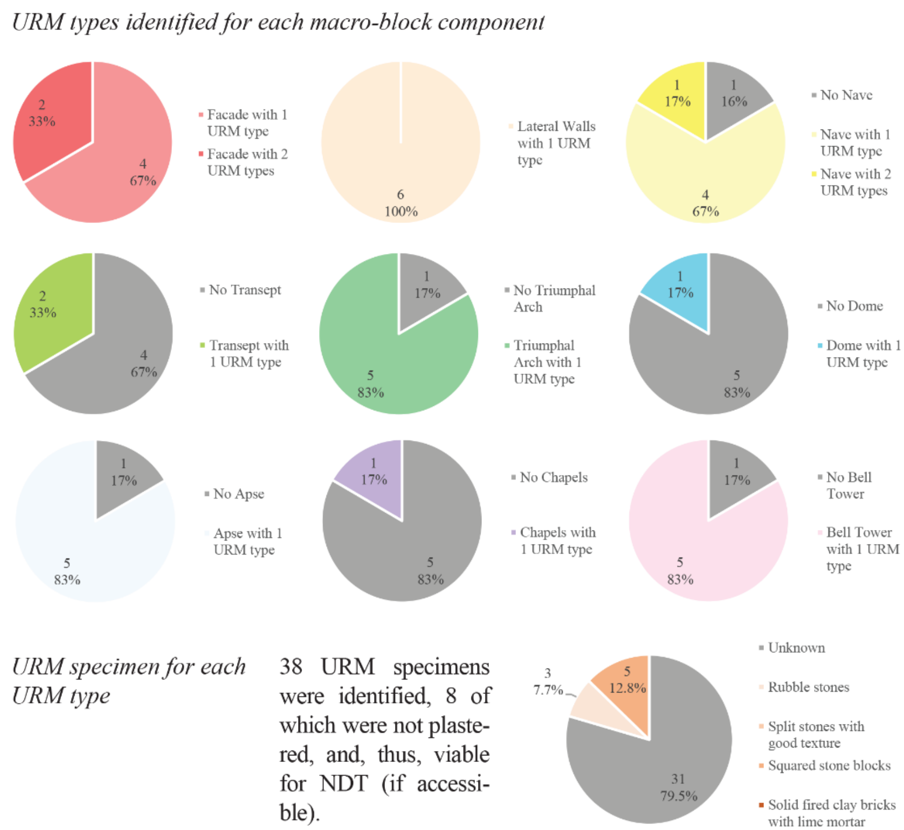

Figure 3.10: Region: Campania; top left: number of surveyed churches; bottom left: number of macro-blocks components identified for each macro-block type; top right: number of URM types identified for each macro-block component; bottom right: number of URM specimen for each URM type.

Four NDT techniques were applied on the 170 tested URM specimens: 1) URM type mechanical properties' range; 2) masonry quality index (*MQI*); 3) Schmidt hammer test; and 4) pulse velocity test. While the NDT techniques were described in the following section, the considered criteria were selected listed and related to each NDT in Table 3.2.

TABLE 3.2

SELECTION CRITERIA OF THE APPLIED NDT TECHNIQUE

Criteria	**URM type mechanical properties' range**	***MQI***	**Schmidt hammer test**	**Pulse velocity test**
Execution time	n/a	Moderate	Very low	Low
Test cost	n/a	n/a	Very low	Low
Damage to the structure	n/a	n/a	Very low	n/a
Independent of engineering judgment	✗	✗	✓	✓
Equations based on large statistical base of destructive tests performed in the same country where the specimens were assessed (i.e, Italy)	✓	✓	✗	✗
Negligible variation of the outputs due to non-homogeneity or discontinuity of the masonry	✓	✓	✗	✗
Applicable when the masonry is not visible (i.e., plastered surface)	✗	✗	✗	✓ (Although the plaster may affect the results)
Mechanical properties categorized by URM type	✓	✗	✗	✗
Multiple parameters are accounted for (with respect of both constitutive materials and construction technique)	✗	✓	✗	✗
Discrete values for the mechanical properties of a given specimen are recognizable, rather than a probabilistic range	✗	✗	✓	✓

The four NDT techniques have complementary benefits, as identified in Table 3.2 providing, therefore, a basis for the methodology proposed in the current research to assess the mechanical properties (i.e., masonry compressive strength, Young's modulus, and shear strength) of unreinforced masonry used to construct Italian medieval churches.

3.4 Non-destructive Testing (NDT) Techniques

3.4.1 URM Type Mechanical Properties' Range

The Italian technical standard for construction (MIT 2018) and its commentary (MIT 2019) provide a qualitative method to determine ranges for the assessment of the mechanical properties of existing URM and corrective coefficients to apply for different scenarios.

While the mechanical properties' ranges, the corrective coefficients, and their application according to the criteria listed in the MIT (2019) were summarized in Table E.1 and Table E.2 of Appendix E, the resulting strengths and moduli ranges for the URM types considered in the current research are shown in Table 3.3.

TABLE 3.3

RANGES OF THE MECHANICAL PROPERTIES FOR THE CONSIDERED URM TYPES ACCORDING TO THE ITALIAN TECHNICAL STANDARDS FOR CONSTRUCTION (MIT 2018, 2019)

URM type	***f'$_m$*** **[MPa]**	***c*** **[MPa]**	***E_m*** **[MPa]**	***G_m*** **[MPa]**	**w [kN/m^3]**
	min – max	**min – max**	**min – max**	**min – max**	
Rubble stones	1.00 – 7.00	0.018 – 0.112	690 – 3675	230 – 1225	19
Split stones with good texture	2.60 – 9.12	0.056 – 0.178	1500 – 3861	500 – 1287	20
Squared stone blocks	5.80 – 11.48	0.090 – 0.168	1540 – 4620	800 – 1540	21
Solid fired clay bricks with lime mortar	2.60 – 7.74	0.050 – 0.234	1200 – 2700	400 – 900	18

3.4.2 Masonry Quality Index (MQI)

The masonry quality index (*MQI*) is a qualitative method developed by Borri et al. (2015) to classify the mechanical properties of the assessed materials. The *MQI* accounts for seven different parameters related to the composing materials of the URM (i.e., the blocks and the mortar) and constructive characteristics of the macro-blocks. Each parameter is defined by three possible outcomes: 1) fulfilled, *F*; 2) partially fulfilled, *PF*; and 3) not fulfilled, *NF*. The seven assessed parameters were defined as follows by Borri et al. 2015:

- The state of the masonry (*SM*) accounts for the conservation and the mechanical properties of the masonry units (bricks or stones);
- The stone/brick dimension properties (*SD*);
- The stone/brick shape (SS);

- The wall leaves connection (*WC*);
- The horizontal bed joints characteristics (*HJ*);
- The vertical joint characteristics (*VJ*); and
- The mortar mechanical properties (*MM*).

The *MQI* was determined for each loading direction using Equation 3.1 (Borri et al. 2015) by converting the qualitative outcomes of the assessment (i.e., *NF*, *PF*, and *F*) into quantitative values according to the criteria listed in Table F.1 of Appendix F.

$$MQI = SM(SD + SS + WC + HJ + VJ + MM) \tag{3.1}$$

Additionally, the authors (Borri et al. 2015) also proposed correlations between the *MQI* and the mechanical properties of the masonry (i.e., the masonry compressive strength (f'_m), the mortar cohesion (c), and the elastic modulus (E_m). Other researchers (Marino et al. 2014) also showed a correlation between the *MQI* and the friction coefficient of masonry (μ_f). The correlations are shown in Equation 3.2 – 3.5 (Marino et al. 2014; Borri et al. 2015).

$$0.937^{0.2232MQI} \leq f'_m \leq 1.6882^{0.1998MQI} \tag{3.2}$$

$$548.31^{0.1738MQI} \leq E_m \leq 821.24^{0.1634MQI} \tag{3.3}$$

$$0.018913^{0.2168MQI} \leq c \leq 0.030253^{0.1992MQI} \tag{3.4}$$

$$\mu = 0.303^{0.124MQI} \tag{3.5}$$

In Figure 3.11, the *MQI* for the 170 URM specimens in the current research are shown grouped by URM type and region. The values of the *MQI* for each URM specimen are also listed in Table G.1 – Table G.4 in Appendix G grouped by URM type.

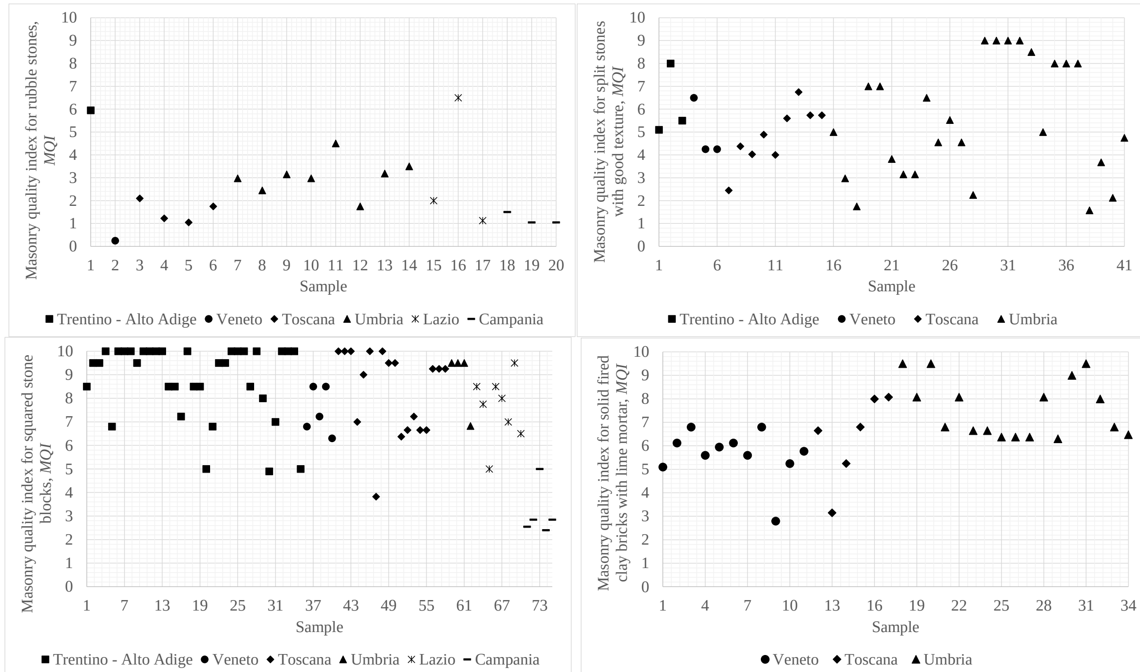

Figure 3.11: MQI values grouped by URM type and region.

3.4.3 Rebound Hammer Testing

The Schmidt hammer test is one of the most applied NDT techniques (Masi 2005, Aydın and Saribiyik 2010). The test results in the measurement of the superficial hardness of the construction material (i.e., the bricks or the stones) based on the principle that the elastic energy absorbed by the material is correlated with its strength. However, the results may be affected by several factors (e.g., the roughness of the surface, the temperature, and the non-homogeneity of the material); thus, a strategic selection and preparation of the tested surface might be desirable.

In the current study, the tests were performed on any accessible and unplastered macro-block element in accordance with international standards (ASTM C805/C805M, EN 12504-2:2012). A Type L Schmidt hammer with a lens-shaped punch ending was used (Figure 3.12a), while the testing area was selected as the area most visually representative of the entire macro-block surface and was smoothed with an abrasive stone where necessary. To increase the consistency of the testing results among different specimens, an 80 x 80 cm grid with 20 cm spacing was applied to each tested surface (Figure 3.12b), and the test was performed at the center of each square of the grid resulting in 16 rebound numbers that were averaged to determine the mean rebound number of the specimen, *R*.

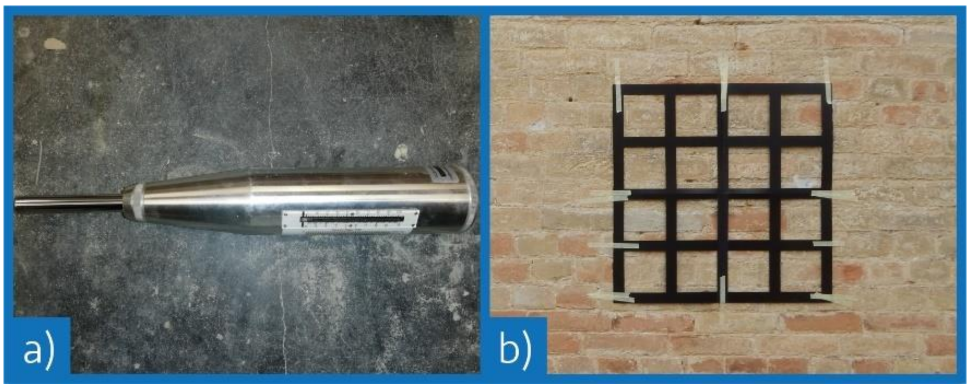

Figure 3.12: a) type L Schmidt hammer; b) grid utilized for Schmidt hammer tests.

The average rebound numbers, *R*, for the 170 tested URM specimens are shown grouped by URM type and region in Figure 3.13. The values of *R* for each URM specimen are also listed in Table G.1 – Table G.4 in Appendix G grouped by URM type.

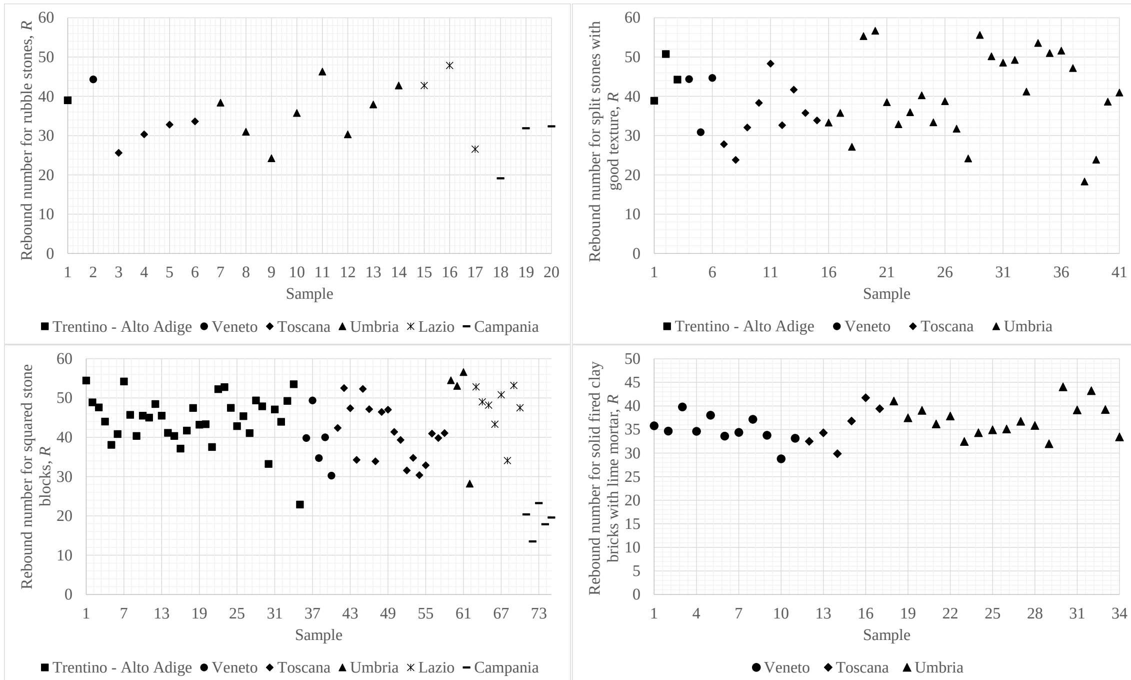

Figure 3.13: Mean rebound numbers grouped by URM type and region.

3.4.4 Pulse Velocity Test

The pulse velocity test is an NDT technique used to measure the velocity of the ultrasonic waves passing through a masonry wall. The ultrasonic pulse is emitted by and received by two transducers (Figure 3.14a) while the average velocity of the pulse is determined dividing the distance between the centers of the transducers by the time interval between the signal emission from the first transducer and the signal reception by the second transducer. While the pulse velocity test might be applied to evaluate the uniformity of the masonry, to estimate the depth of cracks, and to detect the presence of internal voids (McCann and Forde 2001), in the current research it was applied to determine the compressive strength of the masonry, f'_m, and the Young's modulus, E_m.

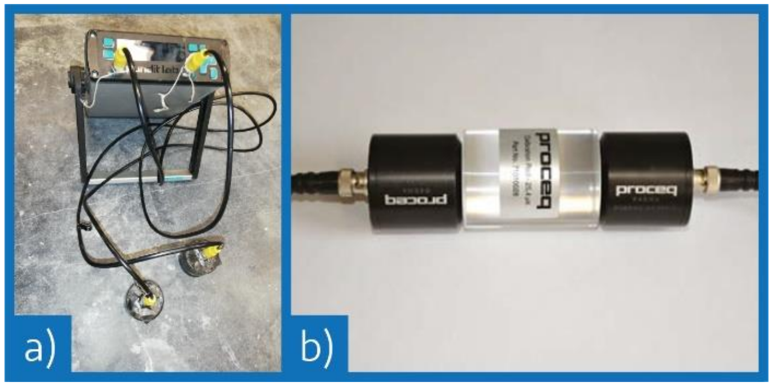

Figure 3.14: a) Ultrasonic pulse velocity tester; b) Calibration control sample.

The pulse velocity tests were performed on any accessible macro-block element in accordance with international standards (ASTM C597-2, EN 12504-4:2005). The ultrasonic pulse velocity tests were conducted in the same wall area in which the Schmidt hammer test was performed for each element. Plasticine medallions (Figure 3.14b) were applied on the transducer surface after proving that the resulting pulse velocity would be unaffected based on a calibration sample. Due to the infeasibility in most cases of reaching simultaneously two faces of the tested macro-block elements, the direct and the semi-direct configurations of the test (Figure 3.15a and b) could not be performed. Hence, the tests were conducted using the indirect configuration (Figure 3.15c) with a pulse frequency of 54 kHz to allow a deeper penetration of the sonic wave into the masonry. The distance between the centers of the transducers was varied specimen-by-specimen based on the different URM types (i.e., bricks or stones) to ensure that the pulse velocity waves passed through both the masonry units and the mortar beds, ranging between 15 cm and 40 cm. At least three measurements were taken for each specimen, and the final pulse velocity, v_i, was taken as the average of the measurements.

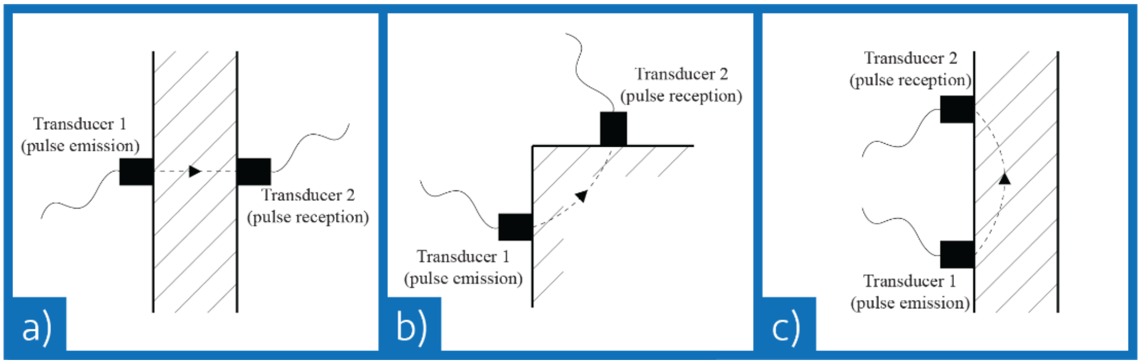

Figure 3.15: Pulse velocity test configuration: a) direct; b) semi-direct; c) indirect.

The average indirect pulse velocities, v_i, for the 170 tested URM specimens are shown grouped by URM type and region in Figure 3.16. The values of v_i for each URM specimen are also listed in Table G.1 – Table G.4 in Appendix G grouped by URM type.

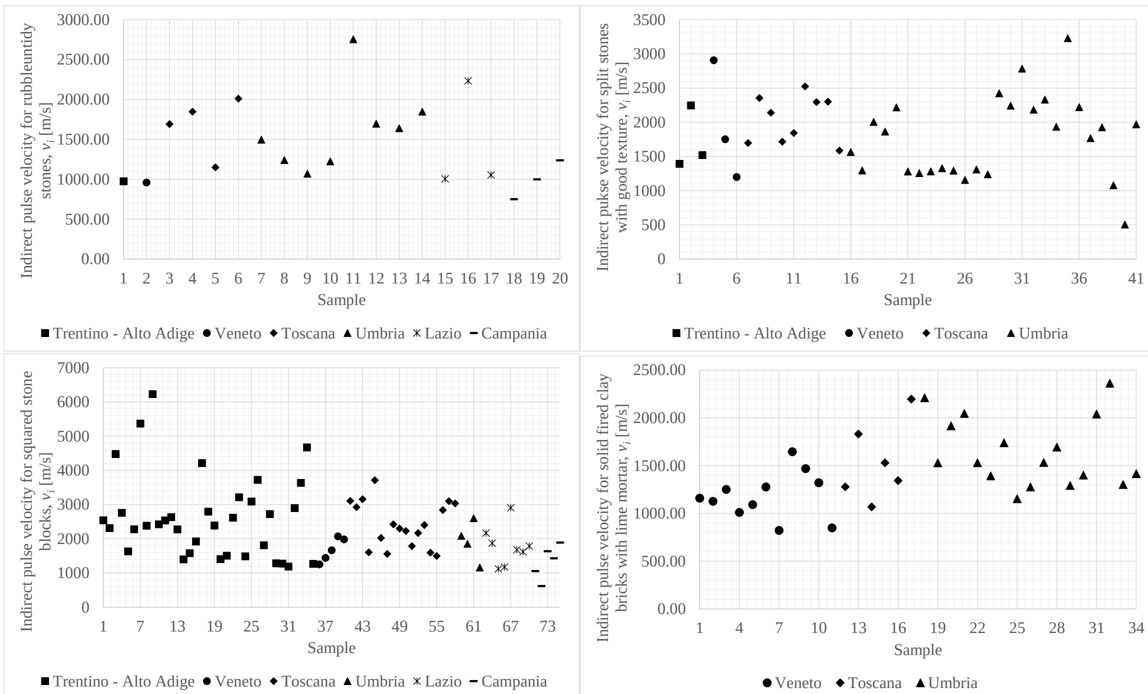

Figure 3.16: Indirect pulse velocity grouped by URM type and region.

3.5 Aggregation of the four NDT techniques

3.5.1 Masonry Compressive Strength, f'_m

According to several authors (Gasparik 1992; Di Leo and Pascale 1994; RILEM 1994), the results of the Schmidt hammer test and the pulse velocity test can be combined into the SonReb method, a combined NDT technique which increases the reliability of the two test when considered separately (Masi 2005; Nobile and Bonagura 2013). Thus, the rebound number and the pulse velocity were combined using Equation 3.6.

$$f'_m = a{v_i}^b R^c \tag{3.6}$$

where: f'_m is the compressive strength of the masonry in MPa;

v_i is the pulse indirect velocity measured through the pulse velocity test in *m/s*;

R is the rebound number measured through the Schmidt hammer test;

a, b, and c are correlation coefficients to best-fit the equation.

Although different authors proposed values for the correlation coefficients (Gasparik 1992; Di Leo and Pascale 1994; RILEM 1994), the proposed values were based on concrete material testing. The authors of the current research are not aware of reliable values to be applied to URM. Given that the URM type mechanical properties' range and the *MQI* have both been extensively tested against more reliable destructive techniques, the ranges shown in Table 3.3 and Equation 3.2 were used to define the feasible upper and lower limits of the masonry compressive strength, f'_m. Thus, the correlation coefficients a, b, and c were determined to obtain the best-fitting shape for Equation 3.6 combined with the determined limits. The coefficients to apply in Equation 3.6 were determined for each URM type resulting in the values listed in Table 3.4.

TABLE 3.4

CORRELATION COEFFICIENTS A, B, AND C FOR EACH URM TYPE

URM type	**Correlation coefficients**		
	a	**b**	**c**
Rubble stones	1.314×10^{-2}	0.317	0.825
Split stones with good texture	2.188×10^{-3}	0.599	0.846
Squared stone blocks	2.766×10^{-1}	0.313	0.249
Solid fired clay bricks with lime mortar	7.960×10^{-5}	0.597	1.856

In Figure 3.17, the compressive strength, f'_m, of the 170 URM specimens obtained by using the described technique are shown grouped by URM type.

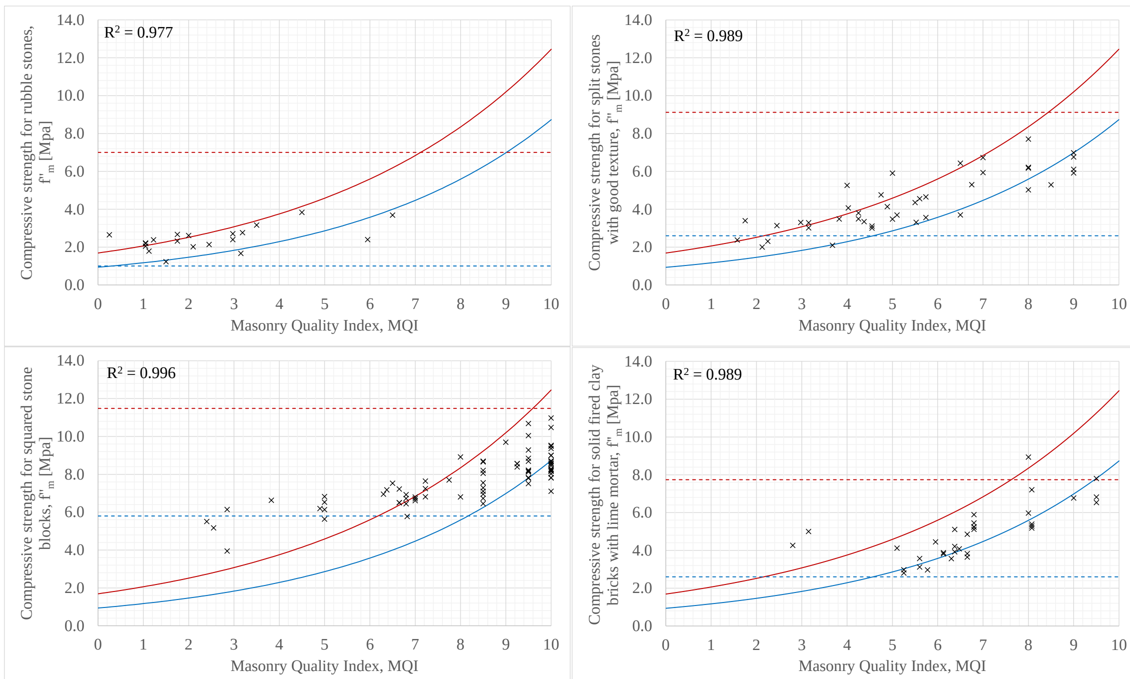

Figure 3.17: The compressive strength f'_m of the URM specimens grouped by URM type.

3.5.2 Masonry Young's Modulus, E_m

The pulse velocity, v_i, and the dynamic elastic modulus, E_{dm}, can be related using the theoretical relationship shown in Equation 3.7 (Masi 2005; Brozovsky 2013; Makoond, Pelà, and Molins 2019).

$$E_{dm} = \frac{w}{1000g} {v_i}^2 \frac{(1+\nu)(1-2\nu)}{1-\nu} \tag{3.7}$$

where: E_{dm} is the dynamic elastic modulus of the masonry in MPa;

w is the density of the masonry in kN/m^3;

g is the gravitation acceleration in m/s^2;

v_i is the pulse indirect velocity in *m/s*;

ν is the Poisson's ratio.

However, Equation 3.7 was modified in the current research for two reasons: 1) the equation is only valid for homogeneous, isotropic, and elastic materials (Masi 2005), while the masonry tested in the current research cannot be considered homogeneous since it is composed of at least two materials with different mechanical characteristic (i.e., the bricks/stones, and the mortar); and 2) the dynamic elastic modulus is usually larger than the static elastic modulus (i.e., Young's modulus) due to the rapid variation of stress within the specimen causing a smaller deformation (Brotons et al. 2014). Thus, Equation 3.8 was developed to account for the non-homogeneity of the material tested in the current research and to convert the dynamic modulus into the static one.

$$E_m = \frac{E_{dm}}{k} = \frac{w}{1000g}\frac{{v_i}^2}{k}\frac{(1+\nu)(1-2\nu)}{1-\nu} \tag{3.8}$$

where: E_m is the static elastic modulus (i.e., Young's modulus) of the masonry in MPa;

k is a correlation factor accounting for the non-homogeneity of the masonry and the conversion from dynamic to static elastic modulus.

The Poisson's ratio, ν, was considered within a range of 0.2 and 0.4 (Francis, Horman, and Jerrems 1971; Harris 1988; Middleton, Pande, and Kralj 1998; Bakhteri, Makhtar, and Sambasivam 2004; Makoond, Pelà, and Molins 2019).

While the URM type mechanical properties' range and the *MQI* were also used to define the feasible upper and lower limits of the masonry Young's modulus, E_m, using the ranges shown in Table 3.3 and Equation 3.3, the values the Poisson's ratio, ν, and the correlation factor, k, were determined to obtain the best-fitting shape for Equation 3.8. The

Poisson's ratio, ν, and the correlation factor, k, to apply in Equation 3.8 were determined for each URM type resulting in the values listed in Table 3.5.

TABLE 3.5

POISSON'S RATIO, ν, AND THE CORRELATION FACTOR, k, FOR EACH URM TYPE

URM type	**Poisson's ratio, ν**	**Correlation factor, k**
Rubble stones	0.299	4.193
Split stones with good texture	0.300	3.611
Squared stone blocks	0.277	6.589
Solid fired clay bricks with lime mortar	0.300	1.844

In Figure 3.18, the Young's modulus, E_m, based on Equation 3.8 of the 170 URM specimens obtained by using the described technique are shown grouped by URM type.

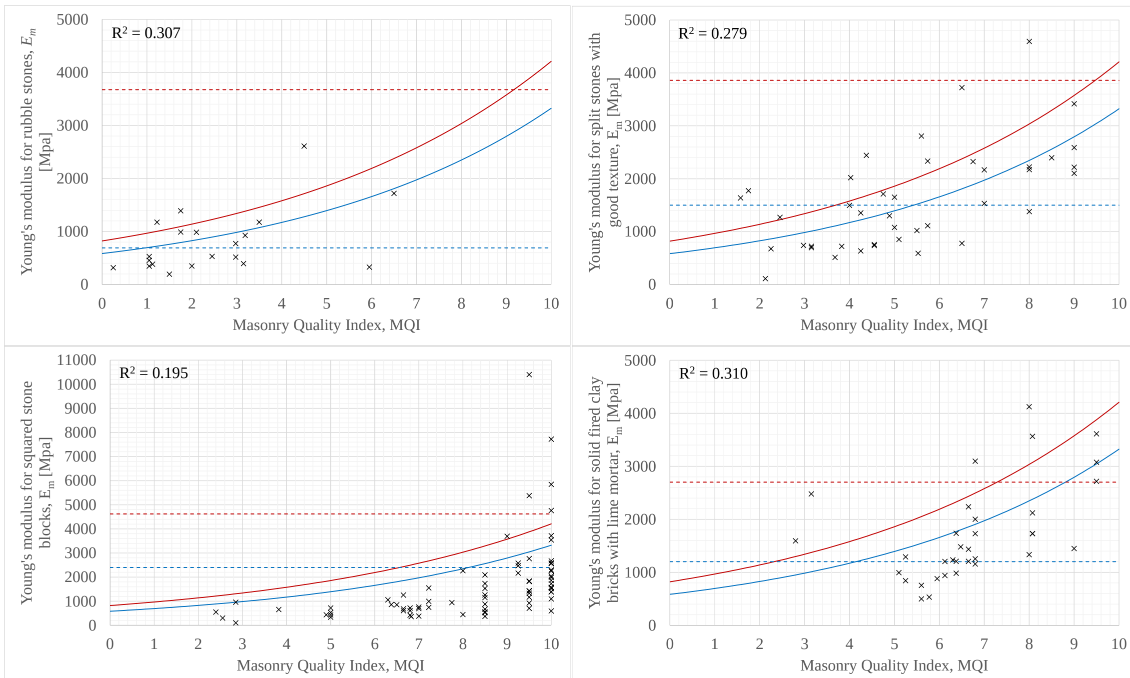

Figure 3.18: The Young's modulus, E_m, based on Equation 3.8 of the URM specimens grouped by URM type.

However, given the low value of the regression coefficient, R^2, another technique was proposed. In fact, accordingly to different international standards (FEMA 306; EN 1996-1-1:2006) and authors (Drysdale, Hamid, and Baker 1999; Kaushik, Rai, and Jain 2007), the Young's modulus of the masonry, E_m, can be determined proportionally to the compressive strength, f'_m, as shown in Equation 3.9.

$$E_m = K_{em} f'_m \tag{3.9}$$

where: E_m is the static elastic modulus (i.e., Young's modulus) of the masonry in MPa;

K_{em} is the proportion coefficient for the elastic modulus.

Thus, given the feasible upper and lower limits from Table 3.3 and Equation 3.3, the proportion coefficient, K_{em}, was determined to obtain the best-fitting shape for Equation 3.9. The values of K_{em} to apply in Equation 3.9 were determined for each URM type resulting in the values listed in Table 3.6.

TABLE 3.6

ELASTIC MODULUS PROPORTION COEFFICIENT, K_{em}, FOR EACH URM TYPE

URM type	**Elastic modulus proportion coefficient, K_{em}**
Rubble stones	463
Split stones with good texture	426
Squared stone blocks	385
Solid fired clay bricks with lime mortar	397

In Figure 3.19, the Young's modulus, E_m, based on Equation 3.9 of the 170 URM specimens obtained by using the described technique are shown grouped by URM type. The determined proportion coefficients for the Young's modulus, K_{em}, are in accordance with the values proposed by other sources, as shown in Table 3.7.

.

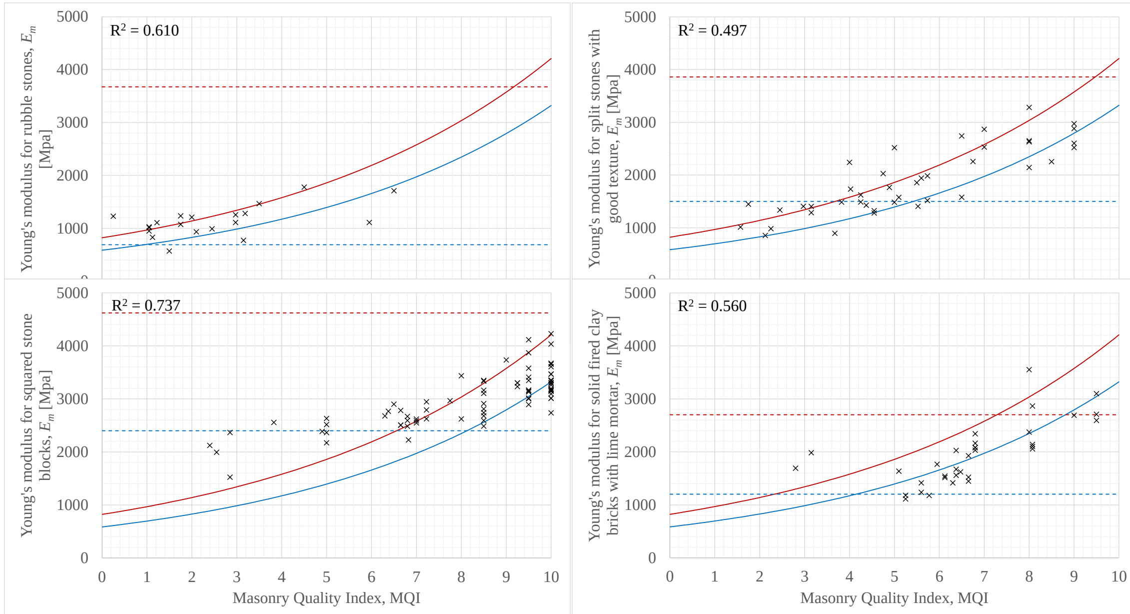

Figure 3.19: The Young's modulus, E_m, based on Equation 3.9 of the URM specimens grouped by URM type.

TABLE 3.7

PROPOSED ELASTIC MODULUS PROPORTION COEFFICIENT, K_{em}, COMPARED WITH OTHER AUTHORS

URM type	**Proposed proportion coefficient for the Young's modulus, K_{em}**	K_{em} (FEMA 306)	K_{em} (EN 1996-1-1:2006)	K_{em} (Drysdale, Hamid and Baker 1999)	K_{em} (Kaushik, Rai and Jain 2007)
Rubble stones	463	550	1000	210 - 1670	250 - 1100
Split stones with good texture	426				
Squared stone blocks	385				
Solid fired clay bricks with lime mortar	397				

3.5.3 Masonry Shear Modulus, *Gm*

According to the Eurocode (EN 1996-1-1:2006) and to Bosiljkov, Totoev and Nichols (2005) the shear modulus for URM, G_m, can be determined as proportional to the Young's modulus, E_m, as shown in Equation 3.10.

$$G_m = K_{es}E_m \tag{3.10}$$

where: G_m is the shear modulus of the masonry in MPa;

K_{es} is the proportion coefficient for the shear modulus.

Since the *MQI* technique has no known correlation with the shear modulus, G_m, only the URM type mechanical properties' range (Table 3.3) was used to set the feasible upper and lower limits for G_m. Thus, basing on the determined limits, the proportion coefficient for the shear modulus, K_{es}, was determined to obtain the best-fitting shape for Equation 3.10. The values of K_{es} to apply in Equation 3.10 were determined for each URM type resulting in the values listed in Table 3.8.

TABLE 3.8

SHEAR MODULUS PROPORTION COEFFICIENT, K_{es}, FOR EACH URM TYPE

URM type	**Proportion coefficient for the shear modulus, K_{es}**
Rubble stones	0.406
Split stones with good texture	0.426
Squared stone blocks	0.381
Solid fired clay bricks with lime mortar	0.281

In Figure 3.20, the shear modulus, G_m, of the 170 URM specimens obtained by using the described technique are shown grouped by URM type.

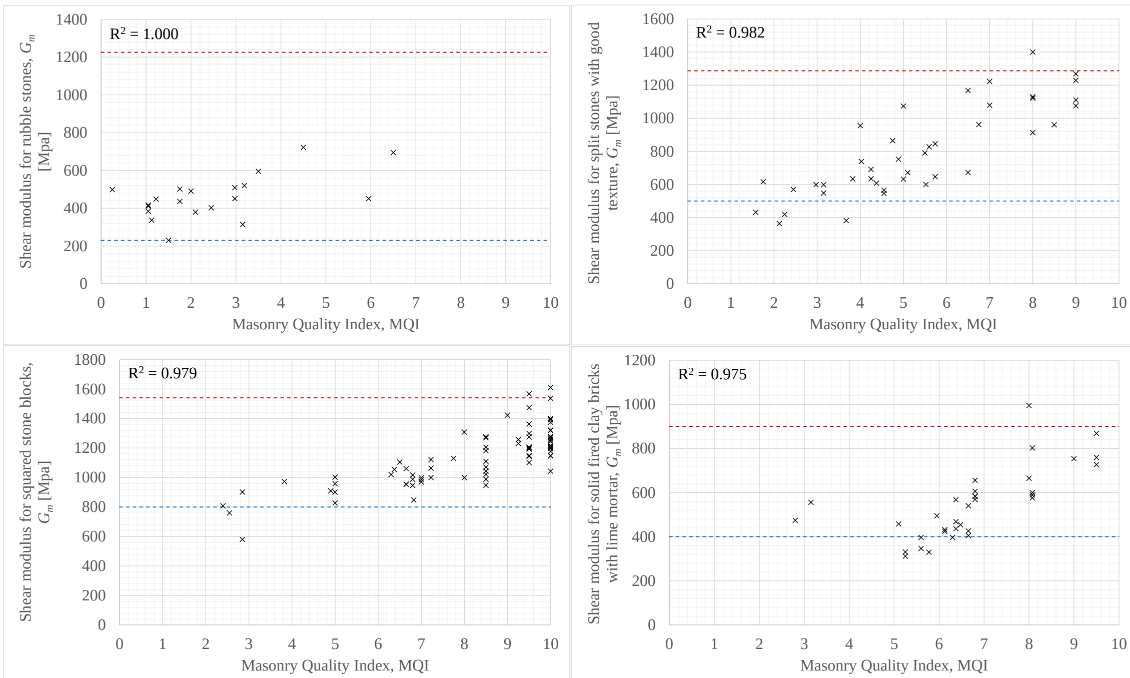

Figure 3.20: The shear modulus, G_m, of the URM specimens grouped by URM type.

The determined proportion coefficients for the shear modulus, K_{es}, are in accordance with the values proposed by other sources, as shown in Table 3.9.

TABLE 3.9

PROPOSED SHEAR MODULUS PROPORTION COEFFICIENT, K_{es}, COMPARED WITH OTHER AUTHORS

URM type	**Proposed proportion coefficient for the shear modulus, K_{es}**	K_{es} (EN 1996-1-1:2006)	K_{es} (Bosiljkov, Totoev and Nichols 2005)
Rubble stones	0.406	0.4	0.45
Split stones with good texture	0.426		
Squared stone blocks	0.381		
Solid fired clay bricks with lime mortar	0.281		

3.5.4 Masonry Cohesion, c, and the Friction Coefficient, μ

The masonry cohesion, c, represents the shear strength of the masonry in absence of compressive stresses acting on the macroblock (Marino et al. 2014). According to the Mohr-Coulomb failure criterion, the masonry cohesion, c, and friction coefficient, μ, are related to the shear strength of the macroblock as shown in Equation 3.11 (Marino et al. 2014).

$$f_{vm} = c + \mu\sigma \tag{3.11}$$

where: f_{vm} is the masonry shear strength in MPa;

c is the masonry cohesion in MPa;

μ is the friction coefficient;

σ is the compressive stress (in *MPa*) acting on the macroblock at the position of the considered section of failure.

The authors are not aware of any known relationship between the values of the c and μ, and the Schmidt hammer test, nor the pulse velocity test. Furthermore, although there some semi-destructive techniques to assess the cohesion and the friction coefficient of a URM wall (e.g., flat jack test), the authors are not aware of any other NDT technique – except for the URM type mechanical properties' range and the *MQI* – to assess the values of c and μ. Thus, in the current research, the values of the masonry cohesion, c, were assumed as the average between the feasible upper and lower limits given in Table 3.3 and Equation 3.4, while the friction coefficients of the URM specimens, μ, were determined using Equation 3.5. The cohesion values, c, and the friction coefficients, μ, of the 170 URM specimens obtained by using the described technique are shown grouped by URM type in Figure 3.21 and Figure 3.22, respectively.

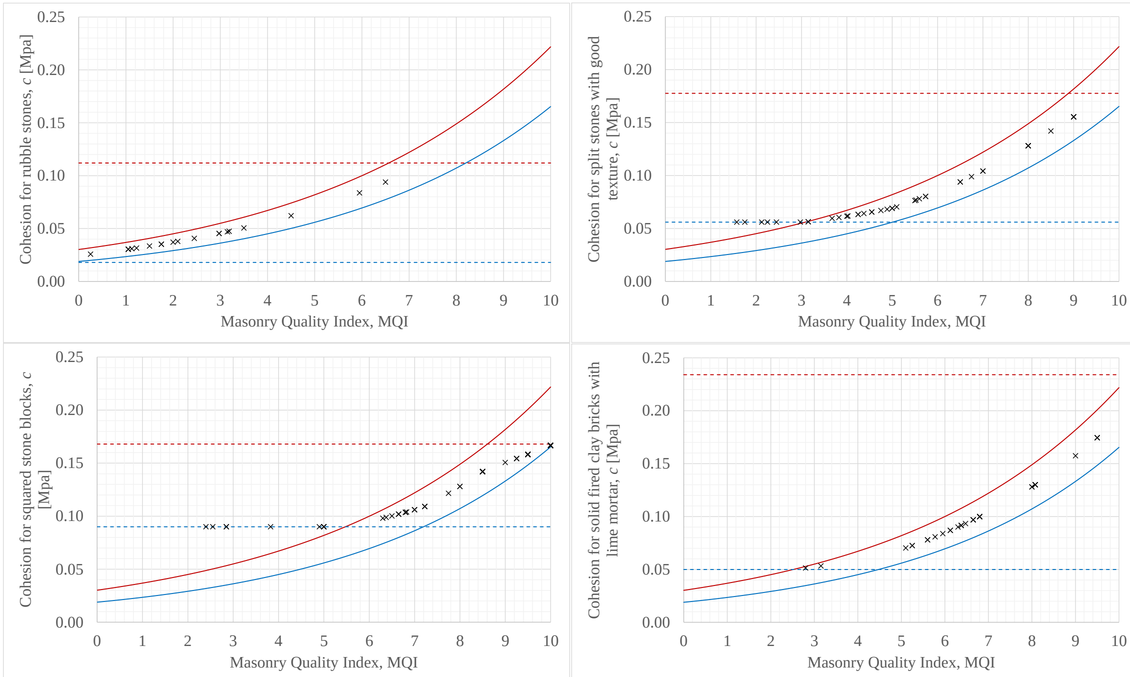

Figure 3.21: The cohesion, c, of the URM specimens grouped by URM type.

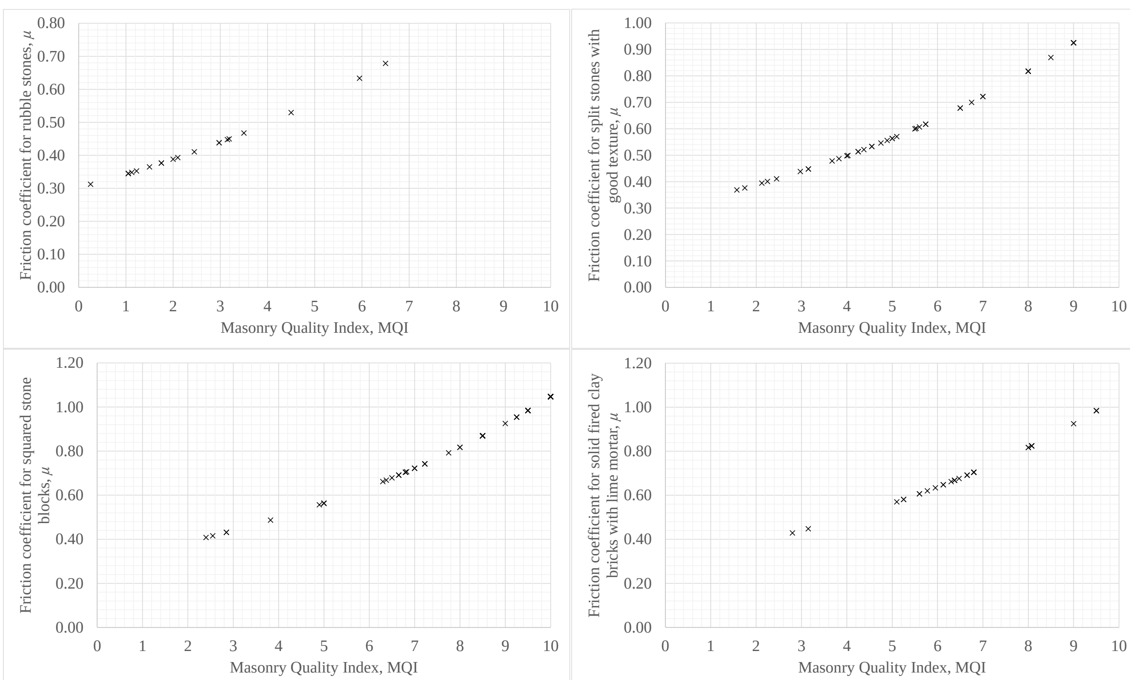

Figure 3.22: The friction coefficient, μ, of the URM specimens grouped by URM type.

3.6 Correlations Between the MQI, the Schmidt Hammer Test, the Pulse Velocity Test

The proposed technique requires to perform three different types of NDTs (i.e., the masonry quality index, the Schmidt hammer test, and the pulse velocity test) and to check their interaction with the URM type mechanicals properties' range offered by the Italian technical standard for construction (MIT 2018) and its commentary (MIT 2019). Although the authors strongly suggest performing all the NDT techniques whenever possible, in some cases (e.g., lack of resources, instrument, time, or favorable conditions of the survey) not all the described tests can be executed. Thus, some correlations between the output of the different performed tests were developed to allow the applicability of the technique described in the previous section also in those scenarios in which only some of the required NDT techniques could be performed. Two possible scenarios were addresses:

1. Two out of three NDT techniques could be performed; and
2. One out of three NDT techniques could be performed.

3.6.1 Scenario 1: Two out of Three NDT Techniques could be Performed

A multilinear regression was performed between the measured values of the three NDT techniques. The multilinear regression was centred in the origin since all the considered techniques should give a close-to-zero output for extremely weak masonry. Thus, the relationship is shown in Equation 3.12, while the values of the regression coefficients are given in Table 3.10 grouped for URM type.

$$MQI = \alpha_{S1} v_i + \beta_{S1} R \leq 10 \tag{3.12}$$

where: α_{S1} (in *s/m*) and β_{S1} are the regression coefficients for scenario 1.

TABLE 3.10

REGRESSION COEFFICIENTS, α_{S1} AND β_{S1}, FOR SCENARIO 1

URM type	$\boldsymbol{\alpha_{S1}}$	$\boldsymbol{\beta_{S1}}$
Rubble stones	7.302×10^{-4}	4.370×10^{-2}
Split stones with good texture	1.010×10^{-3}	9.196×10^{-2}
Squared stone blocks	6.630×10^{-4}	1.558×10^{-1}
Solid fired clay bricks with lime mortar	1.045×10^{-3}	1.438×10^{-1}

In Figure 3.23, the relationship in Equation 3.12 is shown grouped by URM type.

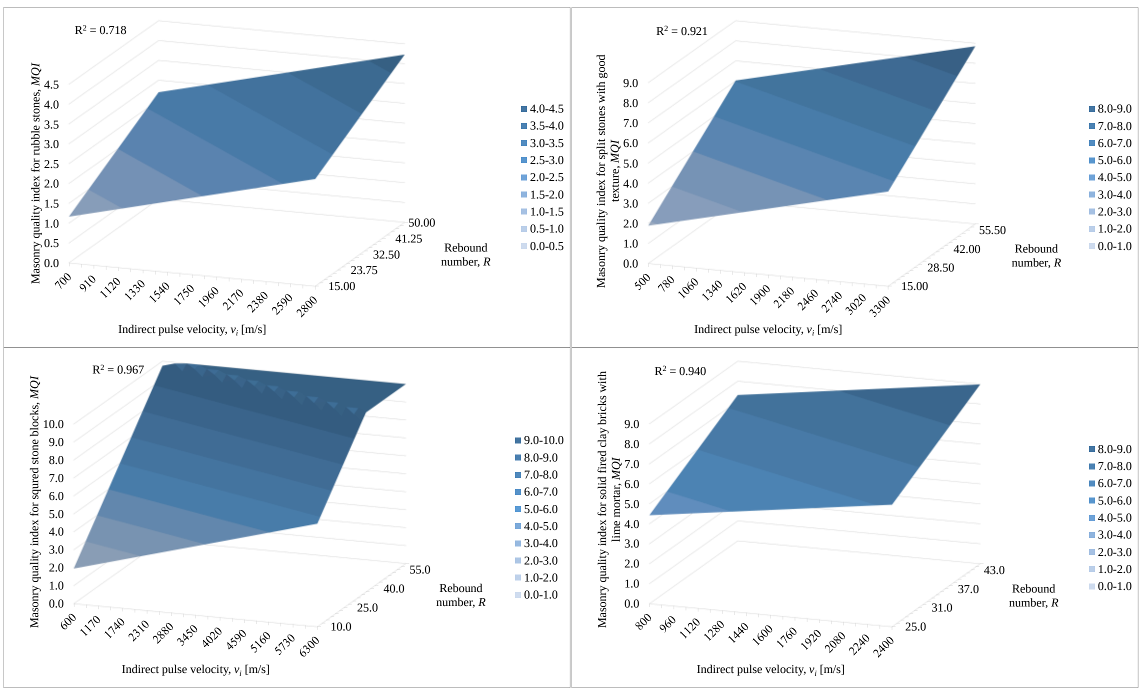

Figure 3.23: Correlation between the pulse indirect velocity, the rebound number, and the masonry quality index.

3.6.2 Scenario 2: One out of Three NDT Techniques could be Performed

Three linear regressions for each couple of NDT techniques were performed between. The linear regressions were centred in the origin since all the considered techniques should give a close-to-zero output for extremely weak masonry. Thus, the relationship between the *MQI*-v_i, *MQI*-*R*, and v_i-*R* are shown in Equations 3.13 – 3.15, respectively, while the values of the regression coefficients are given in Table 3.11 grouped for URM type.

$$MQI = \alpha_{S2,a} v_i \leq 10 \tag{3.13}$$

$$MQI = \alpha_{S2,b} R \leq 10 \tag{3.14}$$

$$v_i = \alpha_{S2,c} R \tag{3.15}$$

where: $\alpha_{S2,a}$ is the regression coefficient of the *MQI*-v_i relationship (in *s/m*);

$\alpha_{S2,b}$ is the regression coefficient of the *MQI*-*R* relationship;

$\alpha_{S2,c}$ is the regression coefficient of the v_i-*R* relationship (in *m/s*).

TABLE 3.11

REGRESSION COEFFICIENTS, $\alpha_{S2,a}$, $\alpha_{S2,b}$, $\alpha_{S2,c}$, FOR SCENARIO 2

URM type	$\boldsymbol{\alpha_{S2,a}}$	$\boldsymbol{\alpha_{S2,b}}$	$\boldsymbol{\alpha_{S2,c}}$
Rubble stones	0.074	1.699×10^{-3}	41.155
Split stones with good texture	0.137	2.877×10^{-3}	45.000
Squared stone blocks	0.192	3.155×10^{-3}	54.317
Solid fired clay bricks with lime mortar	0.186	4.397×10^{-3}	40.827

In Figure 3.24 – Figure 3.26, relationship between the *MQI*-v_i, *MQI*-*R*, and v_i-*R* are shown, respectively.

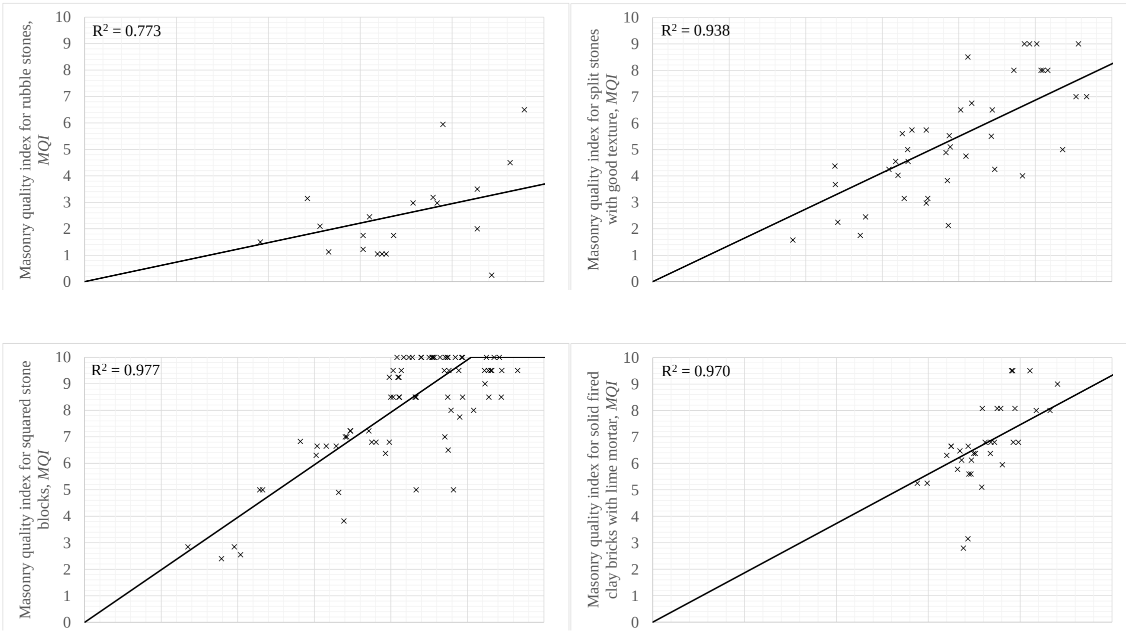

Figure 3.24: Correlation between the masonry quality index, and the rebound number.

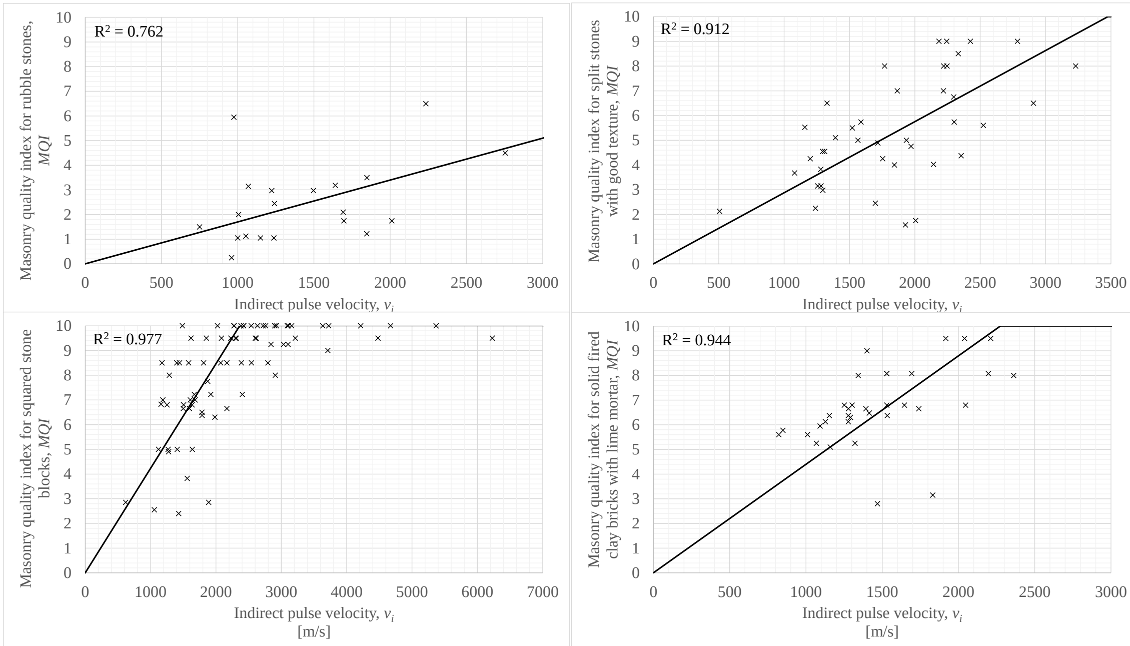

Figure 3.25: Correlation between the masonry quality index, and the pulse indirect velocity.

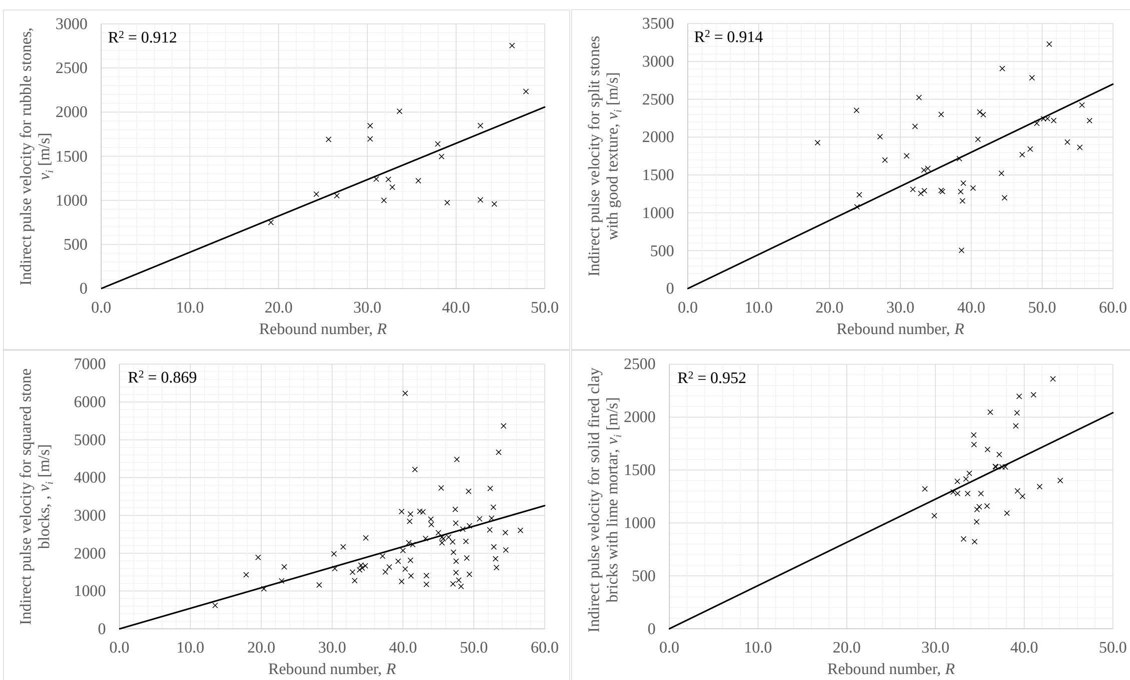

Figure 3.26: Correlation between the pulse indirect velocity, and the rebound number.

3.7 Results

No close form equation was determined for the cohesion, *c*, and the friction coefficient, μ, as a function of all the NDTs applied, however, the relationships to calculate the compressive strength, f'_m, the Young's modulus, E_m, and the shear modulus, G_m, determined in the proposed aggregated technique are summarized in Equation 3.16, Equation 3.17 (relating Equations 3.6 and 3.9), and Equation 3.18 (relating Equations 3.6, 3.9, and 3.10).

$$f'_m = a{v_i}^b R^c \tag{3.16}$$

$$E_m = K_{em}(a{v_i}^b R^c) \tag{3.17}$$

$$G_m = K_{es}K_{em}(a{v_i}^b R^c) \tag{3.18}$$

While the values of a, b, c, K_{em}, and K_{es} for each URM type can be found in Table 3.4, Table 3.6, and Table 3.8, respectively, the mechanical properties of the 170 URM specimens (i.e., f'_m, E_m, G_m, c, and μ) are respectively shown in Figure H.1 – H.5 in Appendix H grouped by URM type and region.

3.8 Summary, Conclusions, and Further Research

In the current research, 170 URM specimens belonging to 72 URM Medieval Italian churches were tested using four commonly applied NDT techniques. The results of the four NDT techniques were aggregated to develop a more comprehensive non-destructive methodology to assess the mechanical properties of the URM (i.e., compressive strength, Young's modulus, shear modulus, cohesion, and friction coefficient). In fact, given that each NDT has both weaknesses and strengths, the NDT techniques selected for the current research were found to positively interact in balancing each other deficiencies.

Solely a partial validation was possible through destructive testing due to architectural and historical constraints acting on the studied churches, however, the results of the proposed methodology were found to have a satisfying alignment with previous studies based on semi-destructive and destructive assessment techniques (FEMA 306; EN 1996-1-1:2006; Drysdale, Hamid, and Baker 1999; Bosiljkov, Totoev, and Nichols 2005; Kaushik, Rai, and Jain 2007). Although the authors are aware that destructive tests are preferable for achieving more reliable results, the proposed methodology might be potentially useful for all those situations in which, for any given reason, only NDT are feasible.

The proposed aggregated technique could be applied to improve previously developed qualitative risk assessment methods (e.g., Pirchio et al. 2020), in fact, the seismic robustness of six out of 28 collapse mechanisms (roughly the 23%) identified for the macro-blocks approach for determining the vulnerability of URM churches are directly affected by the quality of the composing URM materials (DPCM 2011). Furthermore, the determined mechanical properties will be further used to develop complete structural building information models (BIM) of select churches case study, and to achieve an exhaustive structural analysis to compare the results of the detailed analysis with the results of previous assessments (Pirchio et al., 2020a).

CHAPTER 4:

INTEGRATED FRAMEWORK TO STRUCTURALLY MODEL UNREINFORCED MASONRY ITALIAN MEDIEVAL CHURCHES: FROM PHOTOGRAMMETRY TO FINITE ELEMENT MODEL ANALYSIS THROUGH BUILDING INFORMATION MODEL

Medieval churches constructed of unreinforced masonry (URM) are often assessed for structural performance in earthquakes using macro-block elements. However, obtaining the necessary geometric information to correctly conduct the macro-block assessment of such complex buildings requires time-demanding and expensive surveying campaigns. Furthermore, accurately and precisely identifying the local failure mechanisms most influential to macro-block behaviour is challenging. Thus, a complete framework is proposed to assess the vulnerability of a case study URM Italian Medieval church by applying interacting modern tools including unmanned aircraft systems (UAS), photogrammetric survey equipment and software, and finite element model (FEM) analysis software in a complete building information modelling (BIM) package.

4.1 Introduction

Medieval churches are a critical component of Italian Heritage due to their inherent historic value, ongoing community usage, and the large quantity and significance of artwork housed therein. According to Cagnana (1997), most of the remaining Medieval churches were constructed using unreinforced masonry (URM) given the wide dispersion of the URM constructing technique during the High and Late Middle Ages and the durability of URM. However, slender URM elements are especially vulnerable to damage and collapse under high lateral load demands, and the vulnerability of this construction type was widely observed during past earthquakes such as in Friuli-Venezia Giulia in 1976 (Doglioni, Moretti, and Petrini 1994), in Basilicata and Campania in 1980 (Proietti 1994), in Umbria-Marche in 1997 (Doglioni 2000; Lagomarsino 2012), in L'Aquila in 2009 (Cimellaro et al. 2010, da Porto et al. 2012), and in central Italy in 2016 (Penna et al. 2019).

A holistic risk assessment methodology to guide the decision-making processes of the dioceses concerning prioritizing retrofitting interventions was previously proposed (Pirchio et al. 2020a). Given the regional scale of the holistic methodology and its intended rapid application, the holistic methodology relied on simplistic and imprecise methods to quantify structural vulnerabilities which the intention that churches ranking highly (i.e., poorly) in the holistic risk index would subsequently be assessed with more sophisticated and precise analytical methods. The church of *Santa Maria Maggiore* (Figure 4.1) was identified in the holistic study as the church in the Lazio region with the highest risk rating, i_R (Pirchio et al. 2020a), and was thus identified as the most pertinent candidate in the region for the subsequent detailed assessment described herein. The church is located in the main square of Alatri, in the diocese of Anagni – Alatri (province of Frosinone, Lazio). Construction of the church was completed in the 13th century, and it was constructed atop the ruins of a pagan temple dating from the 5th century A.D.

Figure 4.1: Church of Santa Maria Maggiore, Alatri, Lazio (Italy).

The material mechanical properties (e.g., masonry compressive strength, elastic modulus, and shear strength) often govern the in-plane and dynamic behavior of URM structures (Quelhas et al. 2014; Pir et al. 2015) and were determined for the church case study using an aggregation of non-destructive test techniques conducted by Pirchio et al. (2020b). The geometric properties of the building components are the governing parameters for the out-of-plane behavior of URM structures (Abrams et al. 2007; Quelhas et al. 2014; Walsh et al. 2017). Thus, an adequate understanding of the three-dimensional (3D) configuration of the church is critical for a proper detailed analysis.

The proposed framework addresses the complete modelling procedure of a URM church starting from the acquisition of the geometric configuration to the global structural analysis of the church and the local structural analysis of its components (herein referred to as "macro-blocks"). The framework was developed with the main aim of being generalizable for similar cases and applicable using software widely used in engineering practice. Three steps were identified to describe the framework generally:

- Step 1: Acquisition of the geometry of the church via photogrammetry-based surveys using unmanned aircraft systems (UAS) and development of the dense point cloud;
- Step 2: Development of a solid 3D model comprising geometric information, material properties, and various other risk-related information collected from site investigations (Pirchio et al. 2020a, 2020b). This information is aggregated into a complete building information modelling (BIM); and
- Step 3: Structural analysis of the church, with respect to both global and local behaviors, using finite element model (FEM) analysis software.

4.2 Step 1: Definition of the Geometry of the Church using Photogrammetric Techniques

Photogrammetric techniques are increasingly applied in building surveys to procure geometric information (Achille et al. 2015; Daftry, Hoppe, and Bischof 2015; Faltynovà et al. 2016). Geometric information (e.g., walls' height-to-thickness ratio) is especially relevant to the accurate assessment of URM buildings, especially for out-of-plane behavior (Abrams et al. 2007; Daftry, Hoppe, and Bischof 2015; Ragone et al. 2017). Given the complex geometry of churches, traditional survey techniques and tools (e.g., triangulation method, total station, and laser scanner) may be inadequate due to inaccessible church macro-block elements such as the bell tower, nave vaults, or roofs. Therefore, an unmanned aircraft system (UAS, colloquially referred to as a "drone") with an on-board high-resolution camera was used to photograph different perspectives of the church in a relatively short time. For the interior of the church, stationary cameras were used.. Subsequently, those images were processed using photogrammetric software, resulting in a high-density point cloud in which each point's position is defined in a three-dimensional reference system.

Figure 4.2: Examples of photographs taken both using UAS and stationary cameras to realize a high-density points cloud.

A large number of photographs both outside and inside the building (Figure 4.2) are required to create a complete 3D model. The photographic acquisition was performed following three best-practice requirements (Luhmann, et al. 2013):

- Completeness: The entire building was captured. Any unphotographed "blank" areas could compromise the accuracy of the model and the point cloud density;
- Overlap: Adjacent photographs were overlapped for at least 40% of their planar dimensions to catch the same objects with different perspectives, allowing the photogrammetric software to process the photographs with less distortion; and

- Redundancy: “Key-points” of the building, such as wall corners or opening vertices were captured in several different photographs in case some of the photographs were discarded for any reason (e.g., blurriness).

A schematic drawing representing the configuration of the photograph acquisition is shown in Figure 4.3a and b. A *Typhoon H* UAS (Figure 4.3c) was used during the exterior photogrammetric survey, due to the increased stability in wind scenarios guaranteed by the six-rotors configuration and the 360° rotational freedom of the camera. The exterior camera resolution was 3840x2160 pixels with a focal lens length of 35mm. The exterior photographs were acquired with a lens opening of f/2.8 and ISO-100. A digital camera *NIKON COOLPIX L830* (Figure 4.3d) was used for the stationary interior photographs. The digital camera resolution size was 4608x3456 pixels with a focal lens length of 22mm. The interior photographs were acquired with a lens opening of f/3 and ISO-720.

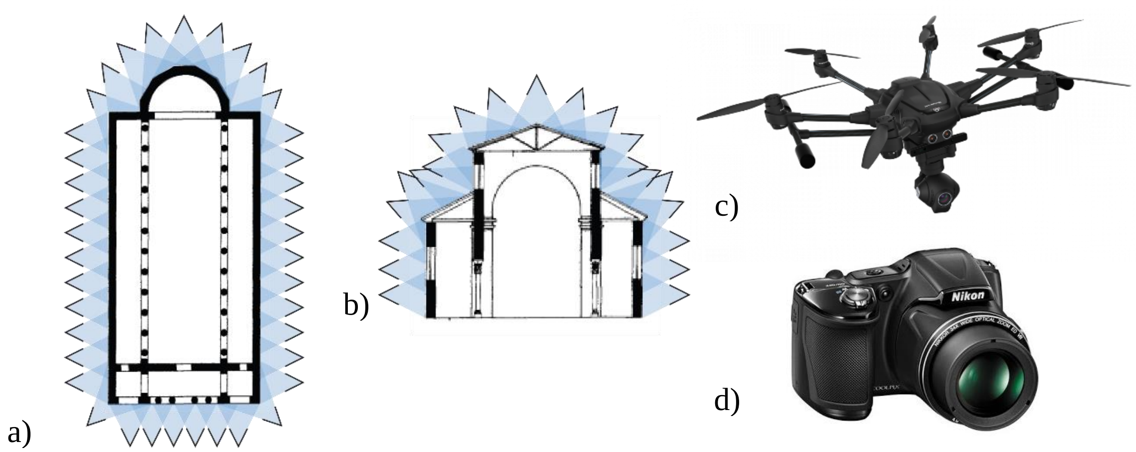

Figure 4.3: a) Schematic plan view of the UAS photographic survey; b) schematic elevation of the UAS photographic survey c) the UAS utilized during the current study; d) the digital camera utilized during the current study.

The photographs were processed using photogrammetric software (e.g., *Autodesk ReCap Pro®* or *Agisoft Photoscan®*) which utilizes georeferenced meta-data in the photographs to auto-scale the point cloud, thus reducing the post-process time for the scaling of the model. A few measurements of some church components (e.g., doors width and height, façade length, and arches net span) were taken manually to confirm the accuracy of the auto-scaled point cloud from the photogrammetric survey, with an error of approximately 1%. The models produced at the end of the photogrammetric process are shown in Figure 4.4a (exterior) and Figure 4.4b (interior) for the church case study.

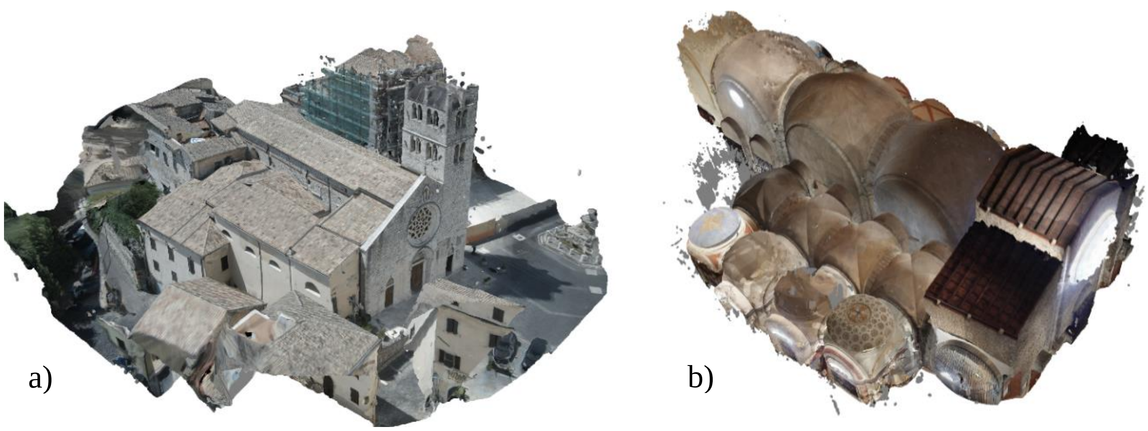

Figure 4.4: a) high-density point cloud with applied texture of the exterior of the church of Santa Maria Maggiore; b) high-density point cloud with applied texture of the interior of the church of Santa Maria Maggiore

4.3 Step 2: 3D Modelling of the Church using BIM

4.3.1 The BIM Approach to the Seismic Risk Assessment

Building information modelling (BIM) represents a software tool as well as a holistic approach in the management of the design-related information for a building (Osello 2012). A BIM package for a building may contain not only the 3D geometric shape of the building and its components but also various other data types (e.g., mechanical material properties, structural shell and linear elements, and photographs and worksheets collected during the surveys) that might warrant exchange amongst various designers and facility managers (Deng and Chang 2006). Thus, “integration” (i.e., integrating in one single model large amount of multi-source data) and “interoperability” (i.e., comprehensive and bi-lateral interaction with other software) should be considered the key words to apply to the BIM approach (Osello 2012). The information regarding the seismic risk assessment of the church of Santa Maria Maggiore developed by Pirchio et al. (2020a) and the mechanical properties of the macro-blocks of the church defined using aggregated non-destructive test techniques (Pirchio et al., 2020b) were included in the multi-dimensional BIM-based model as shown in Figure 4.5.

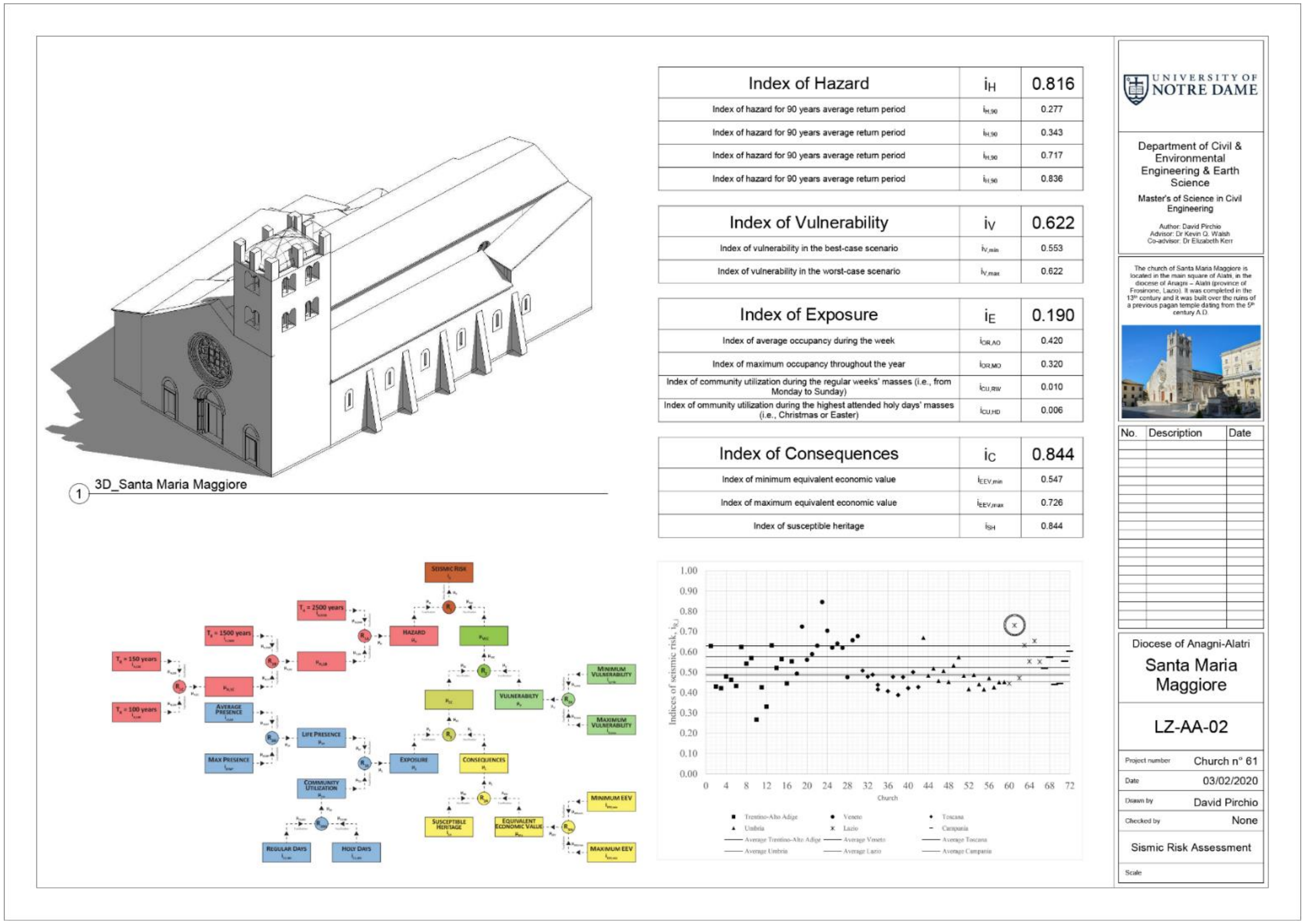

Figure 4.5: Overview of the seismic risk assessment of the church of Santa Maria Maggiore.

4.3.2 The BIM Approach to the Macro-Blocks Analysis

Due to the height and slenderness of church walls, as well as the poor quality of connections between different URM walls compared to most other types of buildings, subdividing URM churches into units called “macro-blocks” is the preferred method to assess churches and other complex URM buildings (Doglioni, Moretti, and Petrini 1994; Marotta et al. 2017; Gàlvez et al. 2018). In the Italian seismic assessment guidelines for heritage buildings (DPCM 2011) ten different macro-blocks types are identified for URM churches (Figure 4.6).

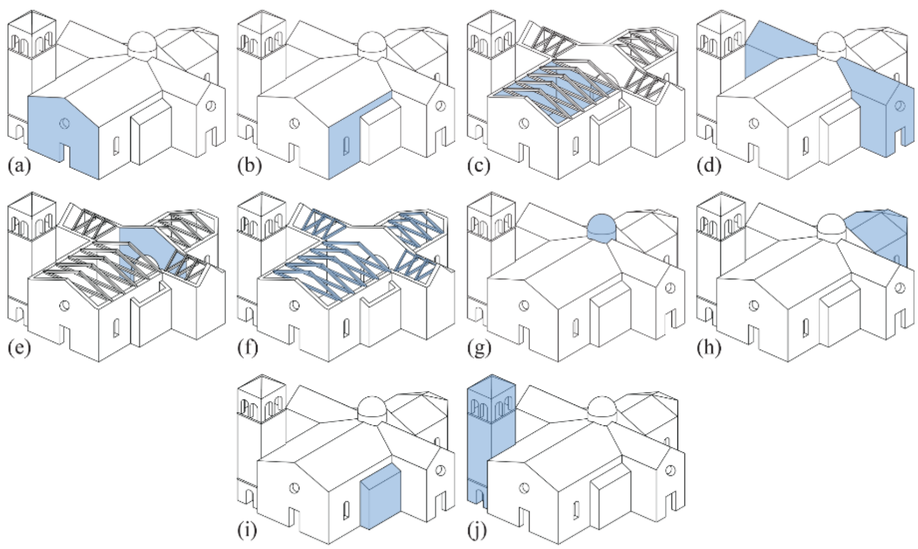

Figure 4.6: Macro-blocks considered: (a) façade; (b) lateral walls; (c) naves; (d) transept; (e) triumphal arch; (f) roof; (g) dome; (h) apse; (i) chapels; (j) bell tower.

Each macro-block of the church of Santa Maria Maggiore was identified in the BIM-based approach, and each single sub-component (e.g., one of the vaults of the macro-block “nave”) could be classified and assigned within the BIM file with particular data regarding the macro-block’s material properties and geometry.

Thus, starting from the high-density point clouds developed in step 1, each macroblock was defined and singularly modelled (Figure 4.7), for use in subsequent analysis of the entire church building.

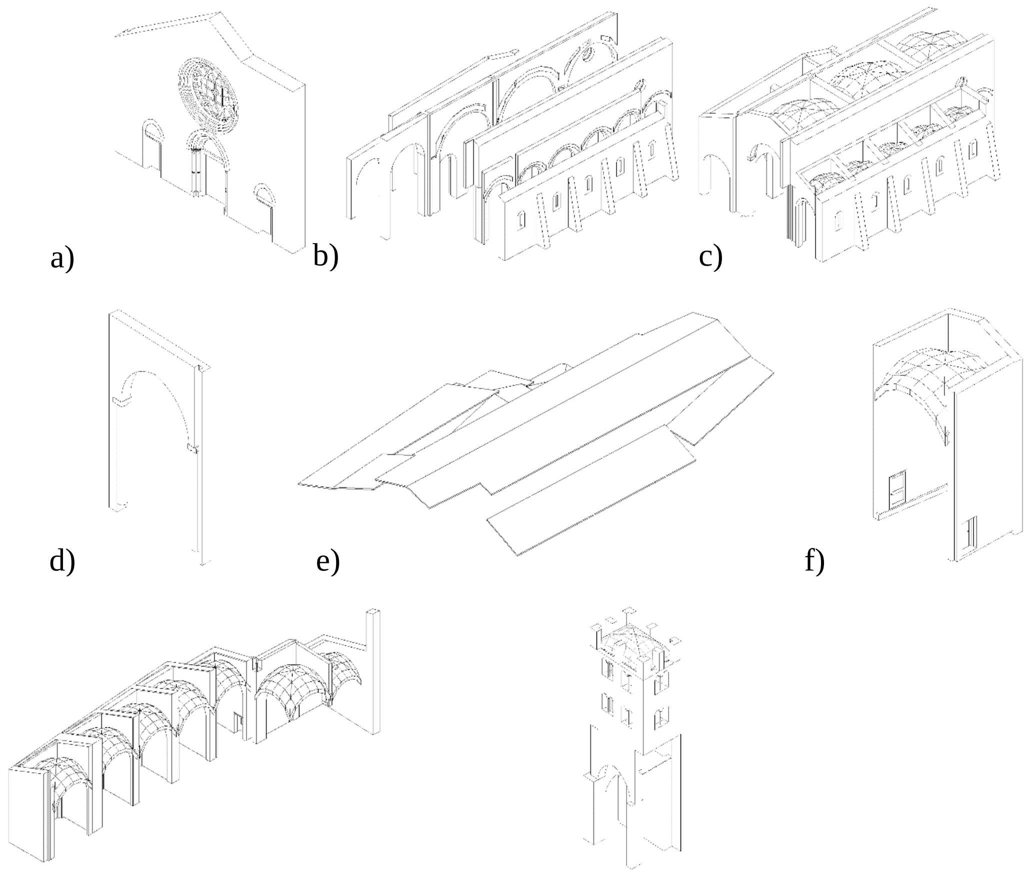

Figure 4.7: The macro-blocks of the church of Santa Maria Maggiore: a) façade; b) lateral walls; c) naves; d) triumphal arch; e) roofs; f) apse; g) chapels; h) bell tower.

4.4 Step 3: Structural Analysis of the Church using Finite Element Model (FEM) Analysis

Simplified analysis techniques (e.g., linear equivalent static or modal response spectrum) and FEM analysis are not suitable for particularly complex URM buildings (such as churches) due to the discontinuity and non-homogeneity of the URM (Ip et al. 2018),. Alternative structural modelling approaches based on finite-discrete elements (FDE) and discrete elements (DE) were proposed by different authors (Cundall 1971; Lemos 1995; Lourenço 1996). However, these alternative approaches require a niche expertise as well as specific software that is not common to the industry at large.

Given the practice limitations of highly specialized analysis, the current research shared the aim of other authors (Ragone et al. 2017; Angjeliu, Coronelli, and Cardani 2018; Valente and Milani 2018) to explore the possibilities of FEM analysis and modal response spectrum analysis to approximate reasonable results for complex URM structures like the selected church case study.

4.4.1 The BIM Approach to the FEM Analysis

In addition to being a useful storage of information regarding the composing material, the macro-blocks, and the provisional regional-scale qualitative seismic risk assessment of the church case study, the developed BIM-based model (Figure 4.8a) was also implemented as a base for a FEM of the church. In fact, accordingly with the principle of "interoperability" (Deng and Chang 2006; Osello 2012), the model contains also structural information regarding the approximated shell elements representing the walls of the church (Figure 4.8b).

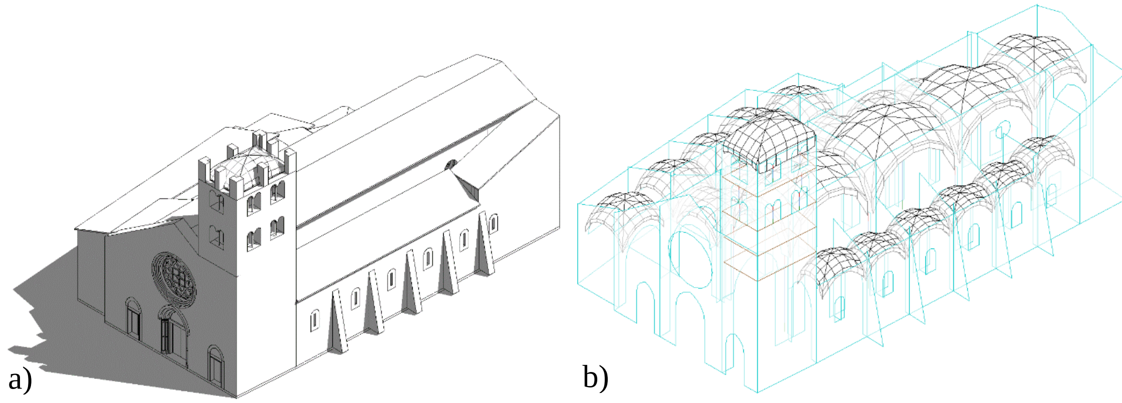

Figure 4.8: a) geometric BIM-based model of the church of Santa Maria Maggiore; b) structural BIM-based shell elements model of the church of Santa Maria Maggiore.

The shell elements for the model could be directly exported to the FEM software through the .ifc file (Deng and Chang 2006) with limited data-loss regarding the modeled macro-blocks (e.g., few shell elements could not be exported due to their large amount of geometric complexity).

4.4.2 Design Response Spectra

The response spectrum analysis was performed assuming an earthquake with 1-in-2475 years average return period to address the largest resulting stresses and the dominating modal shapes (in terms of participating mass) for each macro-block, as a necessary premise to any retrofitting intervention proposal. Although the vertical component of the ground acceleration is often neglected in common practice structural analysis, it was included in the current study because of the presence of thrusting members (e.g., arches and vaults) whose lateral thrust can be affected by a variation of the self-weight. The resulting seismic inertial forces were combined using Equation 4.1 – 4.2

provided by the Italian Technical Standard for Construction (MIT 2018) and its commentary (MIT 2019):

$$1.00E_x + 0.30E_y \tag{4.1}$$

$$0.30E_x + 1.00E_y \tag{4.2}$$

where: E_x, and E_y are the resulting seismic inertial forces in x-direction, and y-direction.

The elastic and design response spectra were determined accordingly with the NTC (2018) using the assumptions in Table 4.1, and they are shown in Figure 4.9. Please note that the corresponding elastic spectral acceleration at the plateau of the elastic response spectrum for the 1-in-500 years earthquake, S_{DS}, would correspond to a moderate level of seismicity according to the American Standards (ASCE 41-17), since $S_{DS} = 0.41g > 0.33g$.

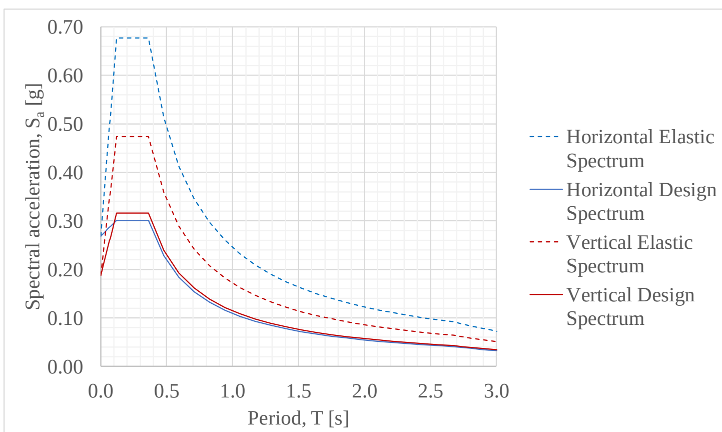

Figure 4.9: Horizontal and vertical design response spectra.

TABLE 4.1

ASSUMPTIONS TO DETERMINE THE ELASTIC AND DESIGN RESPONSE SPECTRA (BOTH FOR HORIZONTAL AND VERTICAL COMPONENTS OF THE ACCELERATION) ACCORDING TO THE NTC (2018)

Variable		**Value**
Reference life in which the earthquake might happen	V_R [years]	150
Probability of overcoming of the considered earthquake intensity within the reference period	P_{V_R} [%]	5
Soil category	-	A
Topographic category	-	T1
Peak ground acceleration	a_g [g]	0.2687
Magnification factor	F_0	2.5206
Reference period	T_C^* [s]	0.3616
Response modification coefficient for horizontal acceleration (corresponding to the *R* factor in the ASCE 7)	q_h	2.25
Response modification coefficient for vertical acceleration (corresponding to the *R* factor in the ASCE 7)	q_v	1.5

4.4.3 The Finite Element Model (FEM)

The BIM-based model was exported into *CSi SAP2000®*, and the FEM graphic is shown in Figure 4.10. The walls were initially modeled as shell elements fully “fixed” (i.e., translationally and rotationally restrained in all three axes) at the base. The masonry piers were initially assumed as fixed both at the top and at the bottom. The masonry columns were modeled as frame elements assumed as hinged both at the top and at the bottom. The masonry vaults were modelled consistently with their geometric imperfections such that the edges were not perfectly coincident with the centerlines of the walls. Thus, translationally rigid connectors were added to link the vaults and the walls. Nonetheless, the rotation of the vault edges around their weak axis was allowed. Given that it was not possible to survey the reinforced concrete roof, the connection between the roof and the top of the walls was conservatively assumed to be poor, consistent with observation in late 20th century following retrofitting interventions (Binda, Saisi, and Tedeschi 2006; Sorrentino et al. 2019). Thus, the roof was modeled only as an additional dead load and assumed to provide no diaphragm action, although additional frictional resistance was considered at the interface between the concrete roof and the top of the walls.

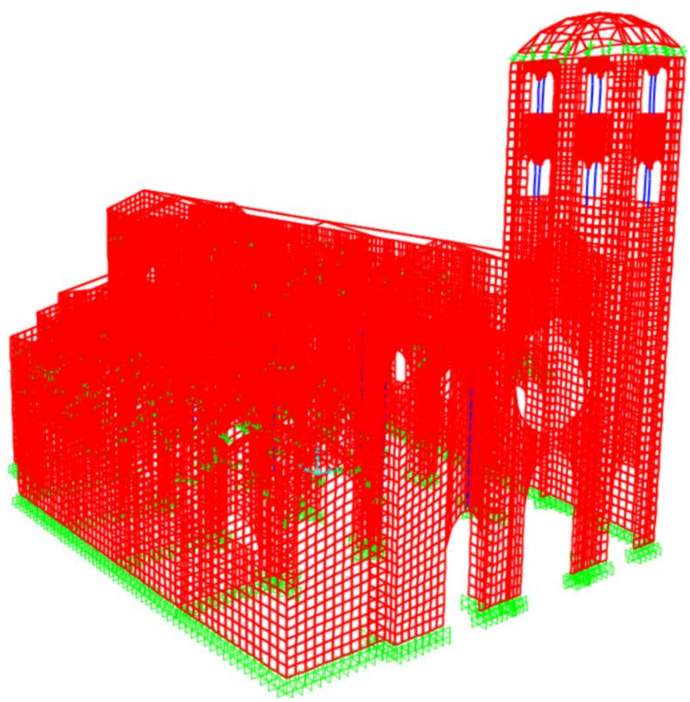

Figure 4.10: FEM of the church of Santa Maria Maggiore.

Both the connections between the different masonry walls and the base restrains of the walls were initially assumed as fixed; however, partial releases were applied when the stress demand was larger than the stress strength. The analysis was applied iteratively, assuming the released boundary conditions determined at the end of each step of the analysis as a starting point for the following step. The sum of the resulting out-of-plane shear stresses, τ_{13} and τ_{23} in Figure 4.11 (σ_3 is assumed equal to zero in *CSi SAP2000®*), were checked against the frictional shear capacity of the wall determined accordingly with the Mohr-Coulomb theory (Labuz and Zang 2012) in Equation 4.:3

$$\tau_{13} + \tau_{23} \leq f_{vn} = c + \mu\sigma_0 \tag{4.3}$$

where: f_{vn} is the shear capacity of the wall;

c is the cohesion of the URM;

μ is the coefficient of friction of the URM;

σ_0 is the compressive stress acting at the considered section of the wall.

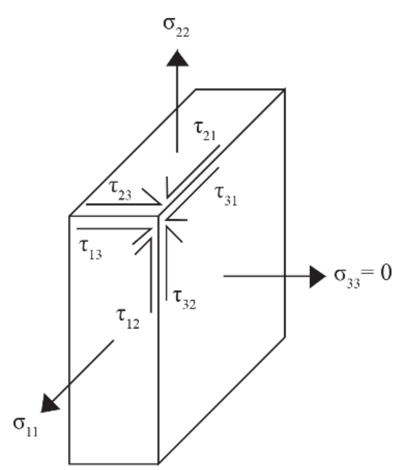

Figure 4.11: Positive direction of the stresses on a typical wall shell element in CSi SAP2000®.

Both sides of the connection were controlled (i.e., the two edges of the connected walls). If the condition expressed in Equation 4.3 was satisfied, then the fixed connection between the connected walls was retained in the model. Otherwise, horizontal translational releases were applied to the connection in the out-of-plane direction of the wall as well as rotational releases with respect of the out-of-plane rotation. The condition provided by Equation 4.4 was checked iteratively until all the wall-to-wall connection tensile demands satisfied the shear friction capacity. In Table 4.2 the mechanical material properties of each macroblock of the church case study are shown. The material properties were determined by Pirchio et al. (2020b).

TABLE 4.2

MECHANICAL MATERIAL PROPERTIES ASSUMED FOR THE ANALYSIS

Macroblock	**Compressive strength, f'_m [Mpa]**	**Young's modulus, E_m [MPa]**	**Shear modulus, G_m [MPa]**	**Cohesion, c [MPa]**	**Coefficient of friction, μ**
Façade	8.92	3434	1309	0.128	0.817
Lateral Walls	5.21	2087	833	0.090	0.563
Naves	6.45	2485	947	0.142	0.869
Triumphal Arch	8.04	3098	1181	0.142	0.869
Roofs	25kN/m^3 normal weight concrete was assumed for determining the dead load				
Apse	5.21[1]	2087[1]	833[1]	0.090[1]	0.563[1]
Chapels	5.21[1]	2087[1]	833[1]	0.090[1]	0.563[1]
Bell Tower	8.16	3141	1197	0.128	0.817

[1]Since no measurements were taken at these locations, the worst material properties measured in other locations on the church case study were assumed.

4.4.4 Dynamic Properties and Stressed Status of the Structure

A modal analysis was performed on the FEM of the case study both for the initial condition (i.e., fixed wall-to-wall connections) and for the final condition (following the end of the process of iteratively releasing the connections). Sixteen modes were analyzed to achieve at least 70% of participating mass in *x* and *y* direction. The first eight mode shapes are shown both for the initial and final conditions (Figure 4.12 and Figure 4.13). The periods of vibration and the corresponding participating masses for each of the first eight modes are shown in Table 4.3.

TABLE 4.3

DYNAMIC PROPERTIES OF THE FIRST EIGHT MODE SHAPES FOR BOTH THE INITIAL AND THE ITERATED CONDITIONS

Condition	**Dynamic property**	**Mode 1**	**Mode 2**	**Mode 3**	**Mode 4**	**Mode 5**	**Mode 6**	**Mode 7**	**Mode 8**
Initial	Period, T [s]	0.250	0.222	0.170	0.142	0.135	0.111	0.100	0.093
	Participating mass, U_x [%]	23.86	0.84	38.86	0.45	0.11	0.62	5.82	4.77
	Participating mass, U_y [%]	1.68	21.19	0.54	34.86	9.88	2.33	0.01	0.21
	Participating mass, U_z [%]	0.02	0.00	0.00	0.03	0.00	0.07	0.13	0.02
Final	Period, T [s]	0.252	0.222	0.170	0.142	0.135	0.111	0.101	0.094
	Participating mass, U_x [%]	24.02	0.64	38.99	0.52	0.10	0.75	5.95	4.22
	Participating mass, U_y [%]	1.55	21.34	0.60	35.00	9.61	2.44	0.02	0.23
	Participating mass, U_z [%]	0.02	0.00	0.00	0.03	0.00	0.07	0.11	0.02

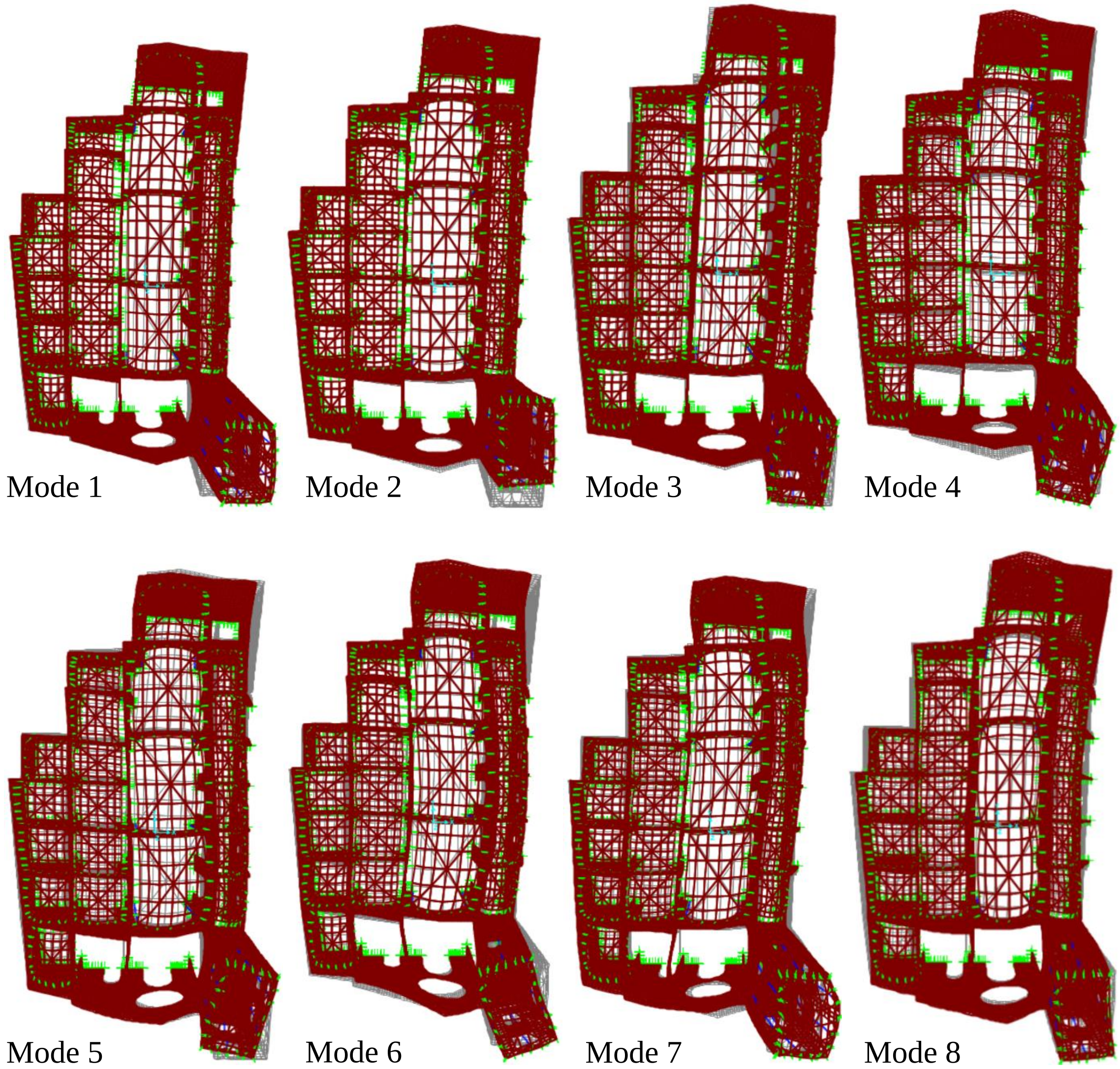

Figure 4.12: First eight mode shapes for the initial condition.

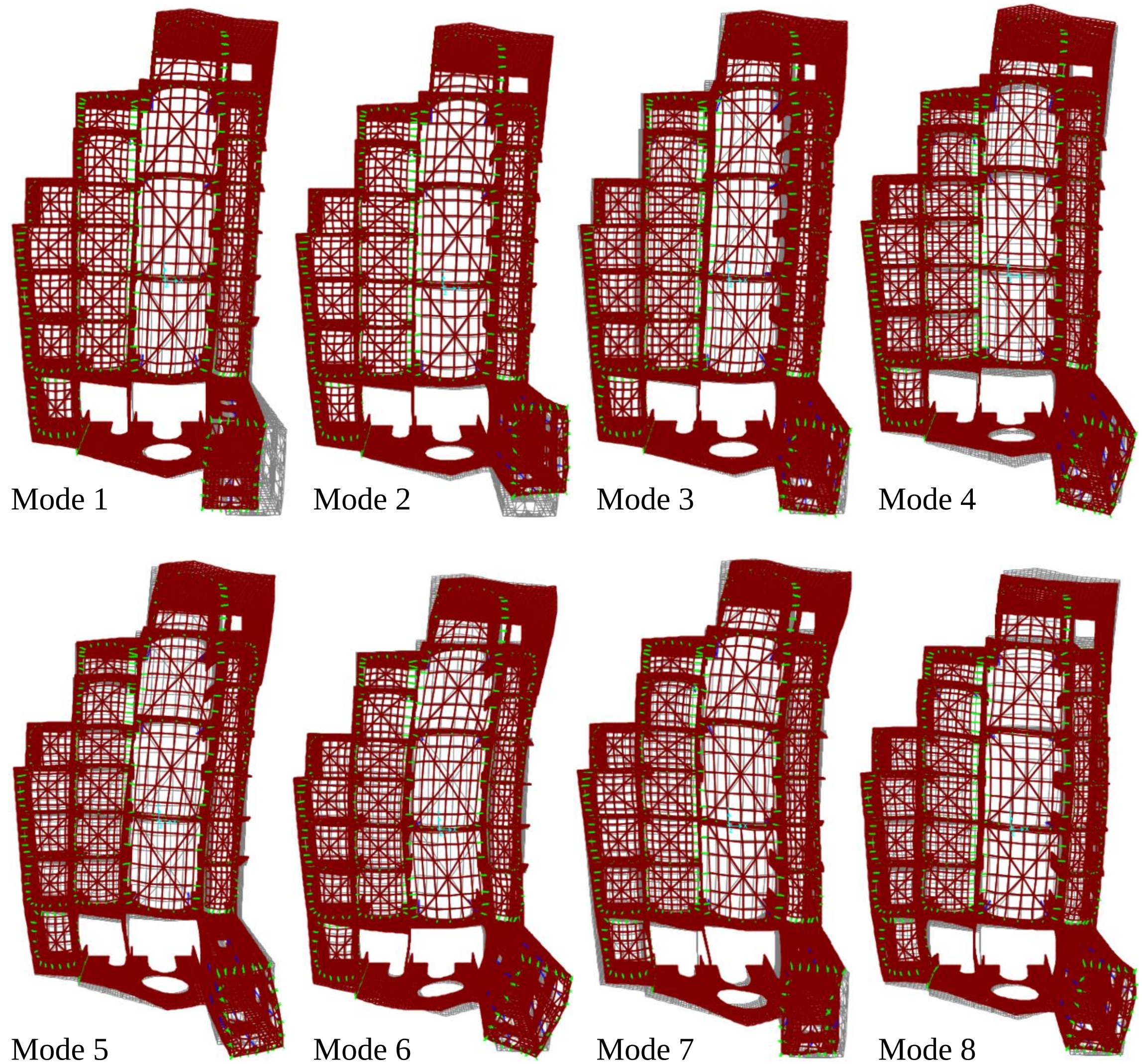

Figure 4.13: First eight mode shapes for the final condition.

As can be observed in Figure 4.12 and Figure 4.13, the first four modes are dominated by the vibration of the bell tower and the façade, explaining why so little participating mass ratios were identified for these modes (Table 4.3). Furthermore, although the translational releases applied to the wall-to-wall slightly affected the dynamic behaviour of the building (Table 4.3), the differences are almost negligible.

Subsequently, a modal response spectrum analysis was performed to compute the design elastic demands associated with a 1-in-2475 years earthquake. The compressive stresses and the shear stresses (both in-plane and out-of-plane) were determined to identify critical zones of stress concentration. In general, the compressive stresses determined in the worst-case scenario (Figure 4.14a) were smaller than the compressive capacity of the URM material (Table 4.2). Nonetheless, the piers of the façade and of the bell tower were found to be subjected to large shear-stresses (Figure 4.14b, c, and d), and thus, these macro-block elements were analysed in greater detail, as discussed in the next section.

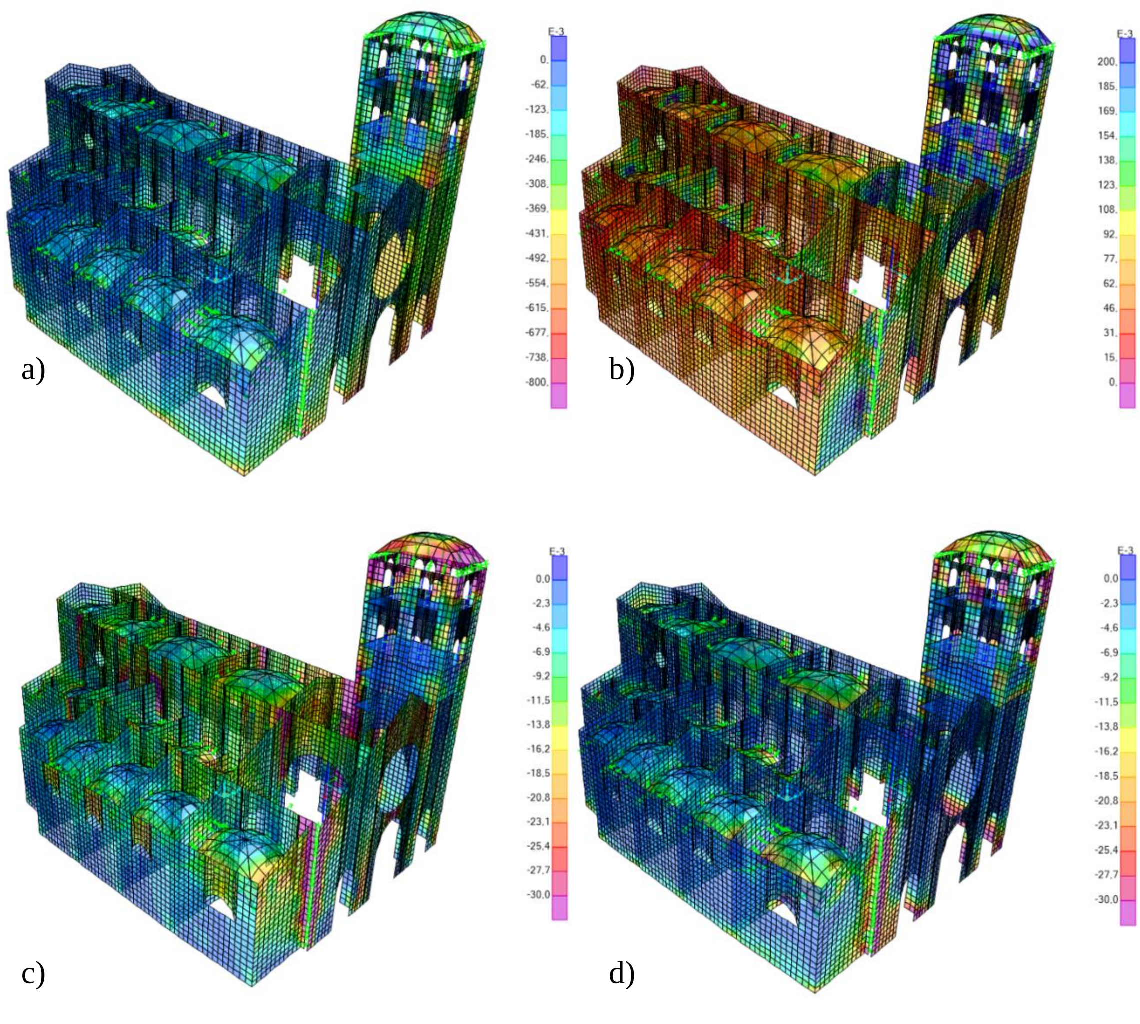

Figure 4.14: a) σ_2 stresses; b) τ_{12} stresses; c) τ_{13} stresses; d) τ_{23} stresses. Please note that the units are in MPa and that the stress directions are in accordance with Figure 4.11.

Although the FEM analysis is not suitable to simulate the actual failure mechanisms of the macro-blocks, in the current research it was used (given its wide practitioner acceptance) to determine the resulting stresses which can be used to identify where yield lines governing macro-block failure would most-likely develop. The likely yield lines of the gable mechanism on the façade were identified using the FEM (Figure 4.15) and assessed via the virtual works approach as discussed in the next section.

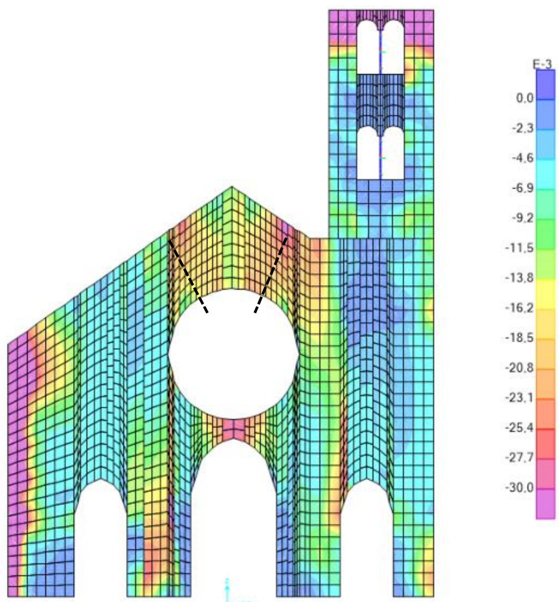

Figure 4.15: Out-of-plane shear stresses on the façade with likely yield lines for the gable mechanism identified.

4.4.5 Local Macro-blocks Failure Mechanisms

4.4.5.1 Pier Mechanism

URM piers should be checked against three mechanisms: rocking failure and toe crushing, diagonal shear, and sliding shear (Magenes and Calvi 1997; Tomaževič 1999; EN 1996-1-1:2012; MIT 2018) resulting in Equation 4.4 – 4.6.

$$M_{d,rocking} = \frac{Dt\sigma_0}{2\psi\frac{H}{D\,(or\,t)}}\left(1 - \frac{\sigma_0}{0.85f'_m}\right) \tag{4.4}$$

$$V_{d,diagonal} = Dt(c + \mu\sigma_0) \tag{4.5}$$

$$V_{d,sliding} = Dt\mu\sigma_0 \tag{4.6}$$

where: D is the depth of the URM pier;

t is the thickness of the URM pier;

H is the height of the URM pier;

ψ is a coefficient equal to 1 for fixed-fixed piers and 0.5 for fixed-pinned piers.

The FEM might be used to determine the forces and the moments acting at the base and at the top of each URM pier in order to perform a demand versus capacity check. As an example, the capacity of the piers of the façade and the bell towers were checked against the force demand obtained by the modal response spectrum analysis. The results are shown in Figure 4.16.

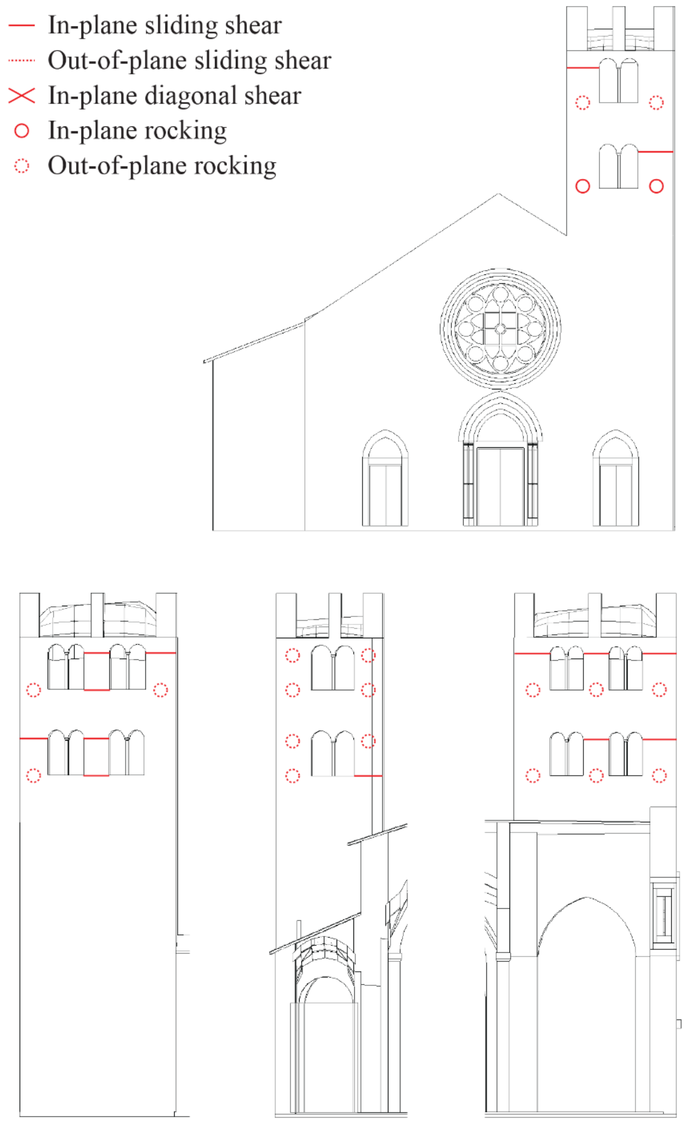

Figure 4.16: Failure mechanisms of the piers of the façade and of the bell tower.

4.4.5.2 Gable Mechanism

The gable mechanism is identified as one on the most affecting macro-blocks failure mechanism for the façade (DPCM 2011). Due to the rose-window (i.e., the large circular opening on the façade), the gable of the façade of the church of Santa Maria Maggiore is subjected to significant out-of-plane stresses (Figure 4.15) which might likely lead to the out-of-plane collapse of the gable (Figure 4.17, Figure 4.18a and b).

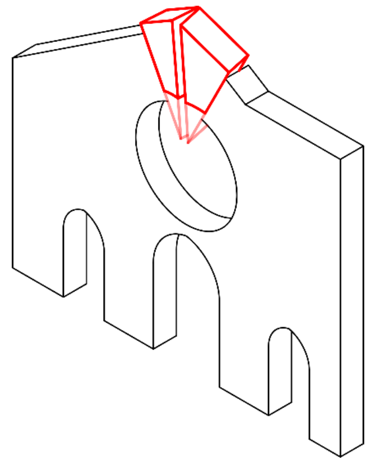

Figure 4.17: Schematic representation of the gable mechanism.

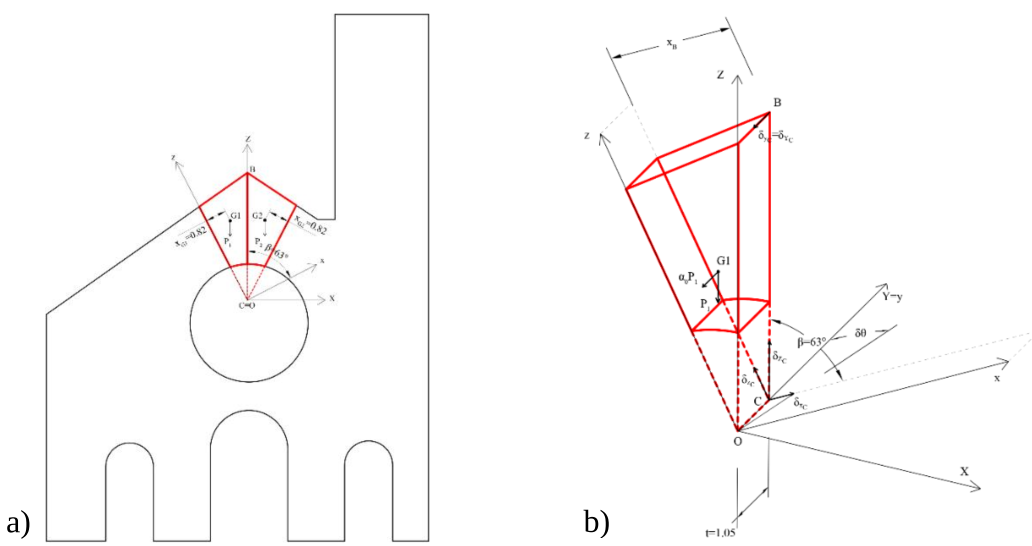

Figure 4.18: a) elevation of the gable mechanism; b) isometric representation of one of the rigid blocks and relative displacements.

To determine if the gable might collapse under the inertial forces imposed by the considered design response spectrum (Figure 4.9), the linear kinematic approach was used (Vinci 2012), which is a type of analysis based on the virtual work principle. The horizontal inertial forces acting on the gable are considered equal to the self-weight multiplied by an inertial multiplier α_0, as shown in Figure 4.18b (in which one single block is shown considering the second one symmetric). Considering the two blocks composing the mechanism as rigid (Figure 4.17), the external work produced by the inertial forces was equated to the internal work produced by the self-weights of the rigid blocks in Equation 4. (Vinci 2012):

$$\alpha_0\left(\sum_{i=1}^{2} P_i \cdot \delta_{Y,P_i}\right) = \sum_{i=1}^{2} P_i \cdot \delta_{Z,P_i} \tag{4.7}$$

where: P_i is the self-weight of the i-*th* block;

δ_{Y,P_i} is the translation along the Y-axis of the center of gravity of the i-*th* block;

δ_{Z,P_i} is the translation along the Z-axis of the center of gravity of the i-*th* block.

To solve Equation 4.8 the rigid blocks are assumed to rotate against and to displace parallel to the inclined yield lines with negligible friction after the mechanism has been activated. The two blocks are considered symmetric and the ideal point C is considered to displace only vertically because of symmetry (Figure 4.18a). The point O displaces parallel to the yield lines (Figure 4.18b). Once the virtual rotation, $\delta\vartheta$, is applied the displacements of point C and B with respect of the reference system x-y-z can be determined accordingly to Equation 4.8 – 4.11.

$$\delta_{x_C} = t\delta\vartheta \tag{4.8}$$

$$\delta_{y_C} = 0 \tag{4.9}$$

$$\delta_{z_C} = \delta_{x_C} \tan\beta = t \tan\beta\, \delta\vartheta \tag{4.10}$$

$$\delta_{y_B} = -x_B\delta\vartheta \tag{4.11}$$

The displacements were converted to the X-Y-Z reference system accordingly to Equations 4.12 – 4.13.

$$\delta_{Y_B} = \delta_{y_B} - x_B \delta\vartheta \tag{4.12}$$

$$\delta_{Z_C} = \delta_{x_C} \cos\beta + \delta_{z_C} \sin\beta = [t \cos\beta + t \tan\beta \sin\beta]\delta\vartheta \tag{4.13}$$

Finally, the displacements for a generic point P were determined using Equation 4.14 – 4.15.

$$\delta_{Y_P} = \delta_{y_P} = -x_P \delta\vartheta \tag{4.14}$$

$$\delta_{Z_P} = [y_P \cos\beta + t \tan\beta \sin\beta]\delta\vartheta \tag{4.15}$$

By substituting Equation 4.14 – 4.15 in Equation 4.7, the inertial coefficient, α_0, necessary to develop the mechanism can be determined using Equation 4.16.

$$\alpha_0 = \frac{(P_1+P_2)\left[\frac{t}{2}\cos\beta + t\tan\beta\sin\beta\right]\delta\vartheta}{(P_1 x_{G1} + P_2 x_{G2})\delta\vartheta} \tag{4.16}$$

In general, given that the position and the inclination of the yield lines would be unknown, Equation 4.16 would have too many variables (i.e., α_0, β, and x_{G1}=x_{G2}) and a relatively complex optimization problem would be required to determine the minimum value of α_0. However, thanks to the FEM analysis, the most likely configuration of the yield lines was determined already (Figure 4.15), thus, the value of the inertial multiplier can be easily determined to be $\alpha_0 = 1.26$.

Another FEM-related advantage is the identification of which mode shape would most-likely affect the macro-block's mechanisms. Focusing on the gable of the façade

(Figure 4.18) the period of the mode shape in which stresses in the gable macro-block element are highest, and the corresponding design spectral acceleration (respectively T_{GM} and $S_{d,a,GM}$ in Figure 4.19) were determined. The gable mechanism would be assumed to not develop under the applied spectral demands if the condition in Equation 4.17 is satisfied.

$$\alpha_0 \geq \frac{S_{d,a,GM}}{g} \tag{4.17}$$

Mode 13
T_{GM} = 0.081s
$S_{d,a,GM}$=0.29g

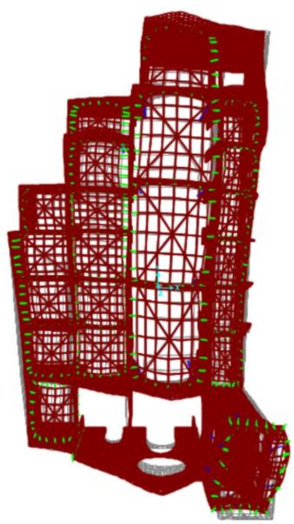

Figure 4.19: Gable mode shape.

In solving Equation 17 for the church case study, the inertial multiplier $\alpha_0 = 1.26 > \frac{S_{d,a,GM}}{g} = 0.29$ meaning that the required acceleration to activate the gable macro-block mechanism is much larger than the spectral acceleration imposed on the mechanism itself, correlating with the comparative demand and capacity stresses of the URM materials in the gable per the FEM (Figure 4.15). Note that the ratio $\frac{S_{d,a,GM}/g}{\alpha_0} = 0.23$ is similar to the demand-to-capacity ratio for the out-of-plane stresses in the most highly stressed portion of the gable (i.e., at the top of the gable, where the shear capacity is equal to the cohesion, *c*, given the absence of any compressive stress) $\frac{\tau_{13}+\tau_{23}}{c} = 0.27$.

4.5 Pushover Analysis via SAA

To confirm the results and the observations obtained via the simplified response spectrum analysis, a non-linear static analysis (i.e. pushover analysis) was performed on the structure. Although recently a new function to define non-linear stress-strain relationships was implemented in *CSi SAP2000®* (i.e., layered elements), the application to complex models still causes large computational demand and, eventually, lack of convergency. Therefore, a procedure defined as "stiffness adaptation analysis" (SAA) was performed.

The SAA, originally proposed by De Boer (2010), consists in a iterative linear pushover analysis in which at the end of each step the shell elements that experienced tensile stresses or exceeded the compressive strength of the material are removed. In Figure 4.20 and Figure 4.21 a graphic representation of different steps was shown, while in Figure 4.22 the algorithm applied in the iterative process was described.

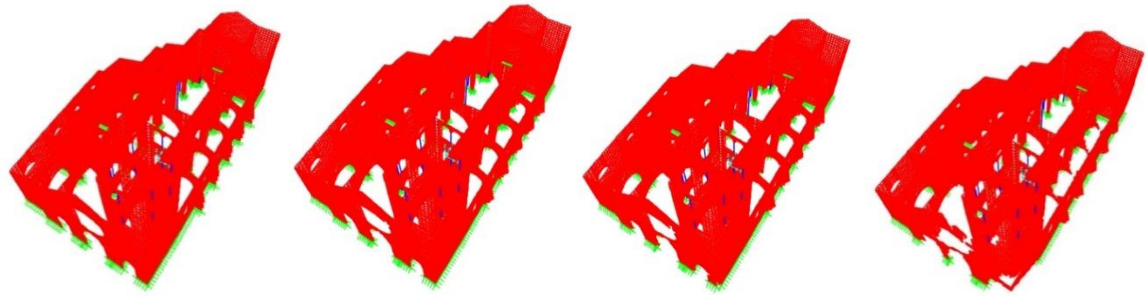

Figure 4.20 – SAA in N-S direction.

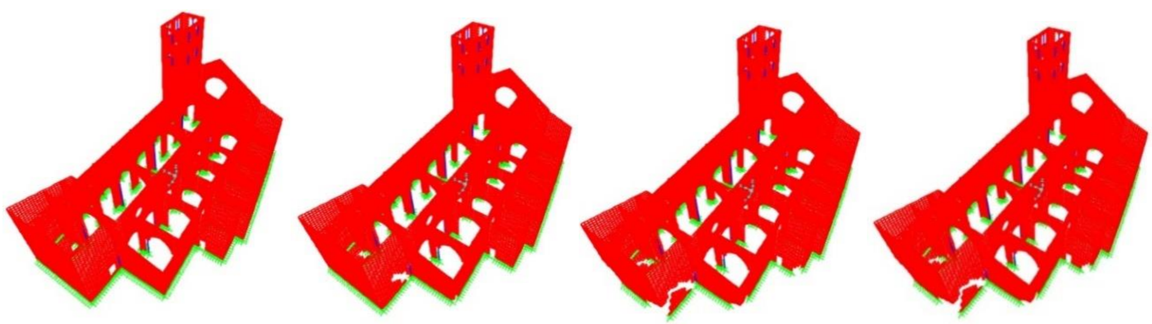

Figure 4.21 – SAA in E-W direction.

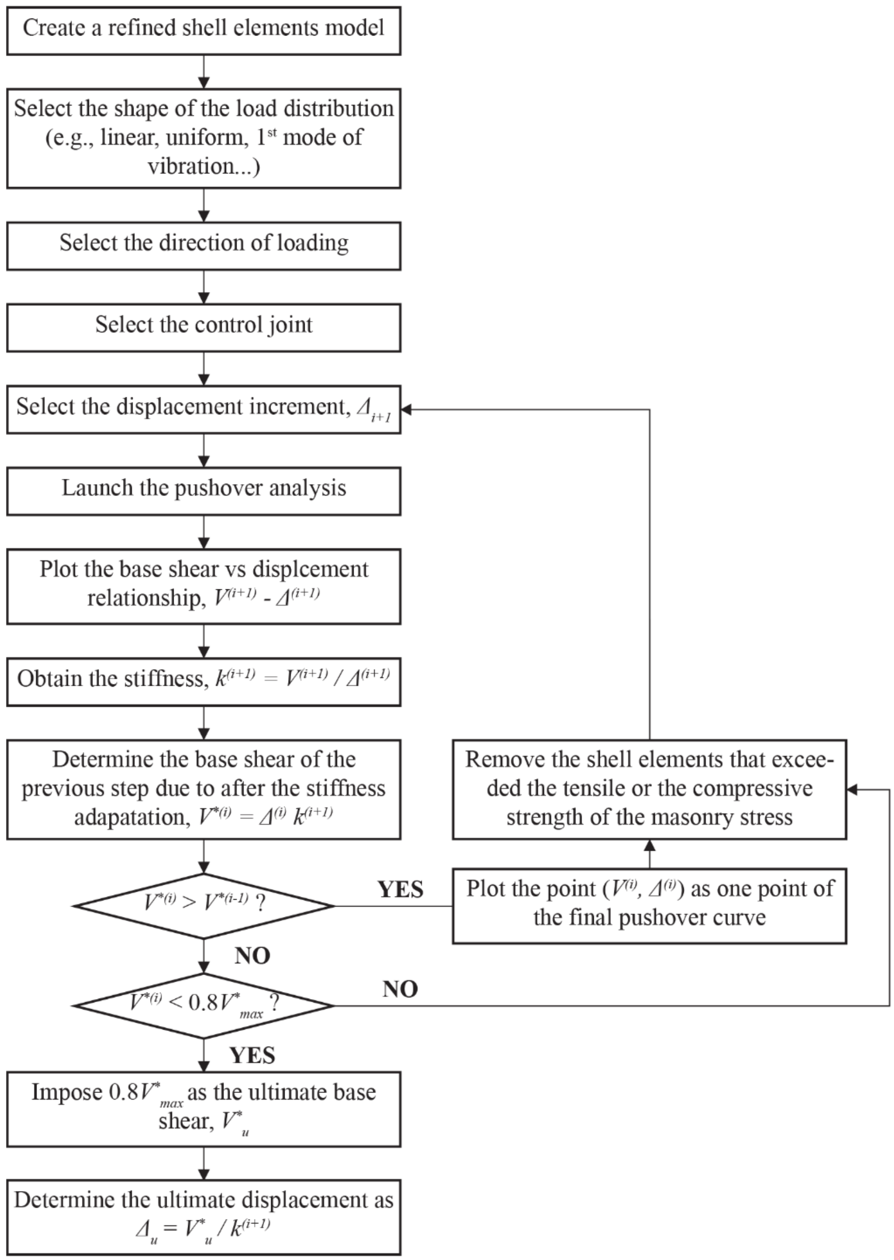

Figure 4.22 – Algorithm of the SAA iterative process.

Thus, the capacity curves in North-South and East-West direction (respectively x and y) were determined for the multi-degree of freedom (MDoF) as shown in Figure 4.23. Please note that the displacement was expressed in terms of drift of the top of the walls.

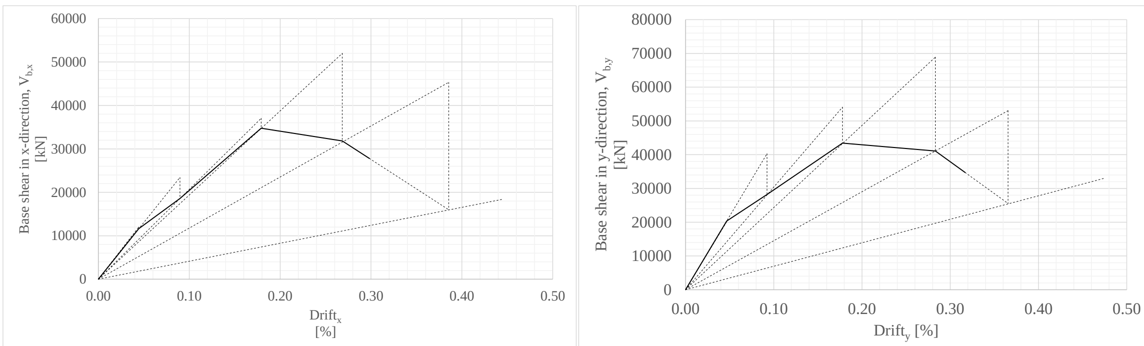

Figure 4.23 – On the left: capacity curve for the MDoF system in N-S direction (x); On the right: capacity curve for the MDoF system in E-W direction (y).

To allow the comparison with the demand spectrum, an equivalent single degree of freedom (SDoF) capacity curve was developed from the MDoF one. The equivalent curve was obtained, accordingly with the provisions of the MIT (2019) by scaling both the coordinates (drift) and the ordinates (base shear, V_{base}) of the original curve using the modal participation factor, Γ, as described in Equation 4.18.

$$\begin{cases} Drift^{(SDoF)} = {Drift^{(MDoF)}}/{\Gamma} \\ {V_{base}}^{(SDoF)} = {{V_{base}}^{(MDoF)}}/{\Gamma} \end{cases} \tag{4.18}$$

where: Γ is the modal participation factor as defined in Equation 4.19.

$$\Gamma = \sum_{i=1}^{n} \frac{{\varphi^T}_i M \tau}{{\varphi^T}_i M \varphi_i} \tag{4.19}$$

where: φ_i is the vector of the modal *i-th* mode of vibration;

M is mass matrix of the structure;

τ is the influence vector corresponding to the direction of the considered earthquake;

n is the total number of considered modes of vibration (16 in the current manuscript).

In Figure 4.24 the equivalent capacity curve relative to the SDoF system was shown.

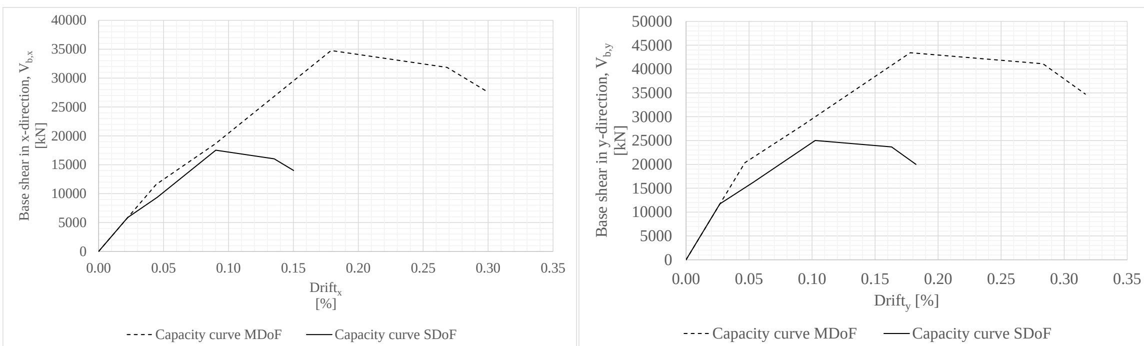

Figure 4.24 – On the left: capacity curve for the SDoF system in N-S direction (x); On the right: capacity curve for the SDoF system in E-W direction (y).

Once the capacity curve for the SDoF system was obtained, the performance point (PP) for all the limit states (i.e., immediate occupancy, damage control, life safety, and collapse prevention) was determined comparing the capacity curve with the corresponding demand spectrum. The comparison was based on a iterative process in order to find the equivalent damping ratio, ξ_{eq}, to be used for each limit state to scale the demand spectrum. While the MIT (2019) proposed Equation 4.20 to determine ξ_{eq}, the iterative process to obtain the PP was described in

Figure 4.25.

$$\xi_{eq}{}^{(i+1)} = k\,\frac{63.7\left(F_y{}^{*(i)} d_{PP}{}^{*(i)} - F_{PP}{}^{*(i)} d_y{}^{*(i)}\right)}{F_{PP}{}^{*(i)} d_{PP}{}^{*(i)}} + 5 \qquad (4.20)$$

where: $\xi_{eq}{}^{(i+1)}$ is the equivalent damping ratio to be used in the *i+1-th* step;

$F_y{}^{*(i)}$ and $d_y{}^{*(i)}$ are the coordinates of the equivalent yielding point of the bilinear curve;

$F_{PP}{}^{*(i)}$ and $d_{PP}{}^{*(i)}$ are the coordinates of the equivalent PP of the bilinear curve;

k is 0.33 for structures with low dissipation capacity.

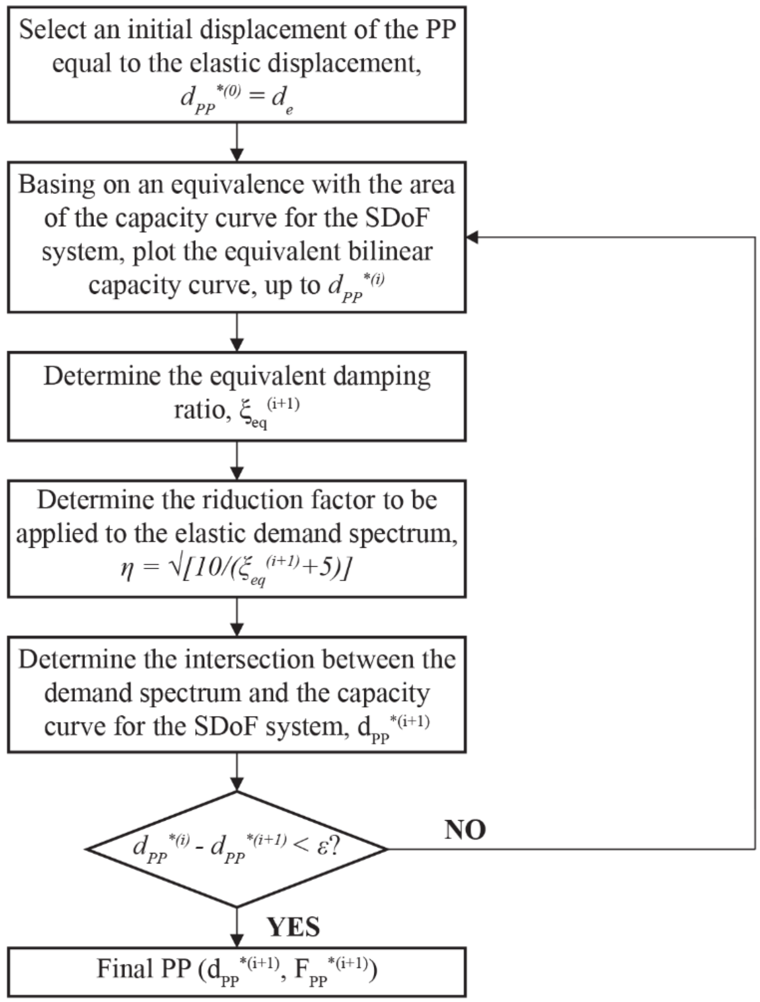

Figure 4.25 – Algorithm for the iterative process to determine the PP.

Applying the procedure shown in Figure 4.25 for each limit state resulted in the PP shown in Figure 4.26. It might be noticed that the poorest performance corresponded to an earthquake excitation in North-South direction. In fact, the PP corresponding to the collapse prevention limit state was identified in the part of the capacity curve with negative stiffness, meaning that the structure might likely reach the collapse. Furthermore, focusing on Figure 4.20, it might be noticed that, according to the analysis, the damage was concentrated on the façade and the bell tower. This observation is consistent with the results of the modal analysis (Figure 4.13) and the response spectrum analysis (Figure 4.14 – Figure 4.16).

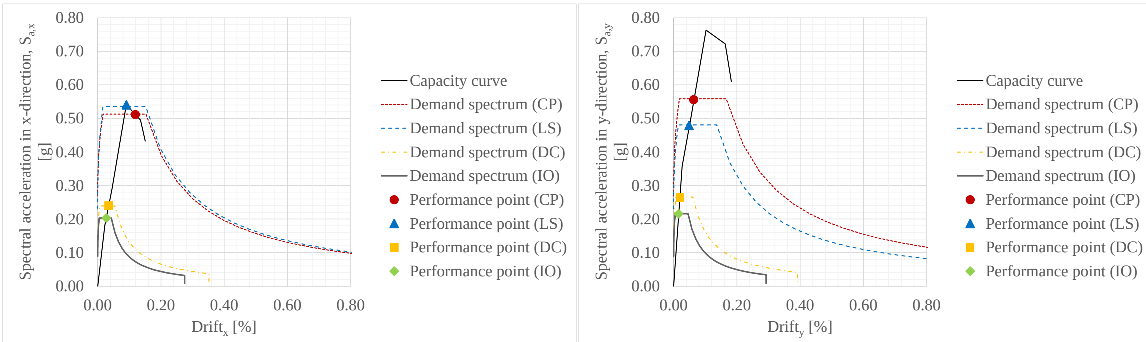

Figure 4.26 – On the left: PP in N-S direction (x); On the right: PP in E-W direction (y).

In Table 4.4, the equivalent damping ratio, ξ_{eq} , the reduction factor to be applied to the elastic demand spectrum, η, and the response modification coefficient for horizontal acceleration (corresponding to the R factor in the ASCE 7), q_h, related with each PP were shown. Please note that, although they have different definitions, the factor η and the coefficient q_h are applied for the same purpose and with the same physical meaning (i.e., reducing the demand spectrum due to the capability of dissipating energy of the structure), and they can be considered as reciprocal values in the equations offered by the MIT (2018).

It might be noticed that the maximum response spectrum modification factor, q_h, resulting from the pushover SAA was smaller than the one assumed in the response spectrum analysis as suggested by the MIT (2018) in general for URM buildings.

TABLE 4.4

EQUIVALENT DAMPING RATIO AND REDUCTION FACTORS RELATED WITH THE STRUCTURE PERFORMANCE POINTS

Considered direction	**Limit state considered for the PP**	**Equivalent damping ratio, ξ_{eq} [%]**	**Reduction factor, η**	**Response spectrum modification coefficient, q_h**
North-South	Immediate occupancy, IO	6.33	0.94	1.06
	Damage control, DC	7.33	0.90	1.11
	Life Safety, LS	7.01	0.91	1.10
	Collapse prevention, CP	12.44	0.76	1.32
East-West	Immediate occupancy, IO	5.00	1.00	1.00
	Damage control, DC	5.00	1.00	1.00
	Life Safety, LS	9.35	0.83	1.20
	Collapse prevention, CP	9.70	0.82	1.21

Although in the current study the pushover analysis via SAA was applied in order to describe the global behavior of the church, the authors wanted to highlight the possibility of application also for addressing the failure mechanisms of the single macro-block by selecting adequately the control joint as shown in previous research (Milani and Valente 2015). As the global SAA pushover was used to valid the response spectrum analysis, the local pushover SAA might be used as a validation for the kinematic analysis shown in Figure 4.17 and Figure 4.18.

4.6 Summary and Conclusion

A framework to perform a structural analysis of a Medieval Italian URM church was proposed herein, with the goal of establishing a complete and relatively rapid procedure for professional engineers approaching the detailed modeling of complex URM buildings when no drawings are available,. A three-step procedure was applied to the case study of the URM church of Santa Maria Maggiore in the diocese of Anagni-Alatri (Lazio, Italy) to acquire the necessary geometric dimensions in form of a high-density point cloud

(1), to convert the point cloud into a solid 3D BIM-based model attached with data regarding the material properties and the structural elements (2), and to export the latter into FEM software to perform a modal response spectrum analysis (3).

Beneficial features of the proposed framework could be identified for each step as follows:

- Step 1: the use of UAS and stationary cameras to perform a photogrammetric survey of the church case study represented a cost-efficient in-site data gathering campaign. A complete geometrical survey of a complex building such as a church could be performed in a few hours by moving most of the survey into post-processing operations (e.g., creation of the high-density point cloud). Furthermore, the accuracy of the photogrammetric survey could be easily customized by increasing (or decreasing) the number of captured photographs basing on the requirements of the project;
- Step 2: the use of BIM-based modelling effectuated an optimal interoperability between step 1 (i.e., point cloud development) and step 3 (FEM). Furthermore, the parametric modelling integrated data coming from different sources (e.g., the point cloud, the mechanical material properties, the geometry of the macro-blocks, the results of previous provisional risk assessment, and the structural model) and to store them in a single file reducing the risk of loss of information between the different steps;
- Step 3: the use of FEM analysis effectuated the detailed seismic assessment of a very complex structure. The modal analysis, which can be carried out by most experienced structural engineers, was used to identify the most highly stressed

macro-blocks in an earthquake scenario. The forces and moments demand could be easily obtained via modal response spectrum analysis, exported, and used to classify the failure mechanisms of the masonry piers. Eventually, the stress condition of the shell elements in the FEM was used to identify the most-likely yield lines of the local collapse mechanisms establishing a logical connection between FEM analysis and the more appropriate, but time-demanding and highly specialized, macro-block modeling approach. The simplified linear modal response spectrum analysis was further checked via non-linear pushover SAA resulting in a validation of the identified main collapse mechanism. However, the response modification factor, qh, suggested by the MIT (2018) for URM buildings was larger than the one obtained for the collapse prevention performance point through the comparison of the capacity curve for the SDoF system with the demand spectrum. Other sources (New Zealand Society for Earthquake Engineering and Structural Engineering Society New Zealand 2016, American Society of Civil Engineers 2017) suggested smaller values for the response modification factor that might be more appropriate for the modeling of churches. The authors encourage for further research on the topic for allowing a larger number of practicing engineers to be able to approach the simplified modeling of complex URM buildings such as churches.

Although the proposed three-step framework has room for improvements in terms of automatization of the process and accuracy of the results, the authors forecast that it might be serve as a useful methodology for the detailed analysis of complex, historic URM buildings that can be applied by the practicing engineering community.

CHAPTER 5:

SUMMARY AND CONCLUSIONS

In this manuscript, a holistic and generalizable seismic risk assessment methodology was established based on surveys of 72 URM Italian medieval churches. Indices to address the different components of risk (i.e., hazard, vulnerability, exposure, and consequences) were developed and assessed with statistical bases. The indices were then processed through the “Fuzzy Set Theory” (FST) to account for statistical variations (including unknowns) result in a final comparative rating of seismic risk for each church. Finally, a set of ready-to-use multilinear equations was developed to facilitate further assessment for similar scenarios conducted by others.

All the proposed indices were based on easily accessible data, resulting in efficient and effective surveys for each church. Using this procedure, one single person could survey several churches per day to obtain the necessary information for the assessment, saving time and money for portfolio managers. Given the limited funding at the disposal of the selected communities, the developed seismic risk ratings are expected to offer a reliable but provisional basis to assist the decision-making process resulting in a cost-efficient management of the dioceses’ property portfolio and funding allocations. The seismic risk ratings shown in Figure 2.26 will be provided to the portfolio managers of the respective dioceses and used to prioritize the churches for further detailed analysis and retrofits of the identified vulnerabilities.

Subsequently, 170 URM specimens belonging to 72 URM Medieval Italian churches were tested using four commonly applied NDT techniques. The results of the four

NDT techniques were aggregated to develop a more comprehensive non-destructive methodology to assess the mechanical properties of the URM (i.e., compressive strength, Young's modulus, shear modulus, cohesion, and friction coefficient). In fact, given that each NDT has both weaknesses and strengths, the NDT techniques selected for the current research were found to positively interact in balancing each other deficiencies.

The results of the proposed methodology were found to have a satisfying alignment with previous studies based on semi-destructive and destructive assessment techniques (FEMA 306; EN 1996-1-1:2006; Drysdale, Hamid, & Baker, 1999; Bosiljkov, Totoev, & Nichols, 2005; Kaushik, Rai, & Jain, 2007). Although the authors are aware that destructive tests are preferable for achieving more reliable results, the proposed methodology might be potentially useful for all those situations in which, for any given reason, only NDT are feasible.

The proposed aggregated technique could be applied to improve the previously developed provisional risk assessment methods, in fact, the seismic robustness of six out of 28 collapse mechanisms (roughly the 23%) identified for the macro-blocks approach for determining the vulnerability of URM churches are directly affected by the quality of the composing URM materials (D.P.C.M. 9 febbraio 2011).

Finally, a framework to perform a structural analysis of a Medieval Italian URM church was proposed herein, with the goal of establishing a complete and relatively rapid procedure for professional engineers approaching the detailed modeling of complex URM buildings when no drawings are available. A three-step procedure was applied to the case study of the URM church of Santa Maria Maggiore in the diocese of Anagni-Alatri (Lazio, Italy) to acquire the necessary geometric dimensions in form of a high-density point cloud

(1), to convert the point cloud into a solid 3D BIM-based model attached with data regarding the material properties and the structural elements (2), and to export the latter into FEM software to perform a modal response spectrum analysis (3).

Beneficial features of the proposed framework could be identified for each step as follows:

- Step 1: the use of UAS and stationary cameras to perform a photogrammetric survey of the church case study represented a cost-efficient in-site data gathering campaign. A complete geometrical survey of a complex building such as a church could be performed in a few hours by moving most of the survey into post-processing operations (e.g., creation of the high-density point cloud). Furthermore, the accuracy of the photogrammetric survey could be easily customized by increasing (or decreasing) the number of captured photographs basing on the requirements of the project;
- Step 2: the use of BIM-based modelling effectuated an optimal interoperability between step 1 (i.e., point cloud development) and step 3 (FEM). Furthermore, the parametric modelling integrated data coming from different sources (e.g., the point cloud, the mechanical material properties assessed during the surveys, the geometry of the macro-blocks, the results of previous provisional risk assessment, and the structural model) and to store them in a single file reducing the risk of loss of information between the different steps;
- the use of FEM analysis effectuated the detailed seismic assessment of a very complex structure. The modal analysis, which can be carried out by most experienced structural engineers, was used to identify the most highly stressed

macro-blocks in an earthquake scenario. The forces and moments demand could be easily obtained via modal response spectrum analysis, exported, and used to classify the failure mechanisms of the masonry piers. Eventually, the stress condition of the shell elements in the FEM was used to identify the most-likely yield lines of the local collapse mechanisms establishing a logical connection between FEM analysis and the more appropriate, but time-demanding and highly specialized, macro-block modeling approach. The simplified linear modal response spectrum analysis was further checked via non-linear pushover SAA resulting in a validation of the identified main collapse mechanism. However, the response modification factor, qh, suggested by the MIT (2018) for URM buildings was larger than the one obtained for the collapse prevention performance point through the comparison of the capacity curve for the SDoF system with the demand spectrum. Other sources (NZSEE and SESNZ 2016, ASCE 41-17) suggested smaller values for the response modification factor that might be more appropriate for the modeling of churches. The authors encourage for further research on the topic for allowing a larger number of practicing engineers to be able to approach the simplified modeling of complex URM buildings such as churches.

Although the proposed three-step framework has room for improvements in terms of automatization of the process and accuracy of the results, the authors forecast that it might be serve as a useful methodology for the detailed analysis of complex, historic URM buildings that can be applied by the practicing engineering community.

The sum of the methodology herein proposed represents a complete and consistent seismic assessment procedure from a broad national-scale assessment to the building-scale structural analysis. The methodology in its entirety achieved the initial target of being relatively rapid, holistic, and reproducible. Furthermore, it offers a guideline to the approach of complex engineering challenges using instruments, knowledge, and technical competency available to the most in the practice engineering environment, fulfilling the primary aim of the author as he approached writing the herein presented manuscript.

APPENDIX A:

SELECTED CHURCHES

TABLE A.1

SELECTED CHURCHES

#	Church Name	Region	Diocese	Settlement / City	Coordinates WGS84 GD	Role	Original Construction Year
1	Santi Dioniso, Rustico ed Eleuterio Martiri	Trentino – Alto Adige	Trento	Santa Croce	46.066530 10.839030	Parish church	1155
2	Santa Maria Assunta	Trentino – Alto Adige	Trento	Tavodo	46.066530 10.893080	Parish church	1160
3	San Giovanni Apostolo ed Evangelista	Trentino – Alto Adige	Trento	Poia	46.028870 10.884130	Parish church	1200
4	San Marcello	Trentino – Alto Adige	Trento	Lundo	46.011910 10.884130	Parish church	1200
5	Santa Maria Assunta	Trentino – Alto Adige	Trento	Dasindo	46.010960 10.860530	Subsidiary church	1200
6	San Lorenzo	Trentino – Alto Adige	Trento	Vigo Lomaso	46.012050 10.872040	Parish church	1210
7	San Nicolò	Trentino – Alto Adige	Trento	Comighello	46.034260 10.849410	Parish church	1250
8	Santa Maria Assunta e San Giovanni Battista	Trentino – Alto Adige	Trento	Tione	46.034190 10.729450	Parish church	1300
9	Annunciazione di Maria	Trentino – Alto Adige	Trento	Rango	46.018330 10.811640	Parish church	1400
10	San Felice	Trentino – Alto Adige	Trento	Bono	46.026080 10.848670	Parish church	1480
11	Santi Pietro e Paolo	Trentino – Alto Adige	Trento	Sclemo	46.055610 10.882940	Subsidiary church	1490
12	San Vigilio	Trentino – Alto Adige	Trento	Stenico	46.052460 10.854170	Parish church	1500
13	San Giorgio	Trentino – Alto Adige	Trento	Dorsino	46.072690 10.896920	Subsidiary church	1500
14	Santi Pietro e Paolo	Trentino – Alto Adige	Trento	Cares	46.032700 10.866660	Parish church	1500
15	San Biagio Vescovo e Martire	Trentino – Alto Adige	Trento	Favrio	45.999920 10.858800	Subsidiary church	1500

TABLE A.1 (CONTINUED)

#	Church Name	Region	Diocese	Settlement / City	Coordinates WGS84 GD	Role	Original Construction Year
16	Sant'Antonio Abate	Trentino – Alto Adige	Trento	Bivedo	46.028170 10.827460	Parish church	1530[2]
17	Immacolata e Santi Fabiano e Sebastiano	Trentino – Alto Adige	Trento	Fiavè	46.004600 10.842050	Parish church	1540 (1880)[1]
18	Santa Maria Etiopissa	Veneto	Vicenza	Polegge	45.605930 11.557180	Subsidiary church	1000
19	Santa Maria e Santa Fosca	Veneto	Vicenza	Dueville	45.634970 11.548010	Parish church	1050 (1955)[1]
20	Santa Maria Annunziata	Veneto	Vicenza	Poia	45.530100 11.423720	Parish church	1300
21	San Pietro Apostolo	Veneto	Vicenza	Monticello Conte Otto	45.594130 11.585370	Parish church	1350
22	Santa Margherita Vergine e Martire	Veneto	Vicenza	Posina	45.790430 11.261480	Parish church	1400
23	Santissima Trinità	Veneto	Vicenza	Bassano del Grappa	45.724970 11.721980	Parish church	1400
24	Santi Pietro e Paolo	Veneto	Vicenza	Nove	45.724970 11.680790	Parish church	1440
25	Santi Girolamo e Bernardino	Veneto	Vicenza	Vivaro	45.610720 11.544320	Parish church	1460
26	Santo Stefano Protomartire	Veneto	Vicenza	Lupia	45.640930 11.608730	Parish church	1470
27	San Matteo Apostolo	Veneto	Vicenza	Cavazzale	45.600760 11.569250	Parish church	1480
28	San Michele Arcangelo	Veneto	Vicenza	Sarmego	45.599800 11.671670	Parish church	1500
29	Santa Cristina	Veneto	Vicenza	Poianella	45.632870 11.625320	Parish church	1560[2]
30	Beata Vergine di Monte Berico	Veneto	Vicenza	Vivaro	45.621370 11.560270	Subsidiary church	1770[1]
31	San Secondiano	Toscana	Montepulciano – Chiusi - Pienza	Chiusi	43.015560 11.949120	Parish church	550[1]
32	San Lorenzo	Toscana	Montepulciano – Chiusi - Pienza	Valiano	43.148320 11.901600	Parish church	1100
33	Santa Croce	Toscana	Montepulciano – Chiusi - Pienza	Abbadia San Salvatore	42.880090 11.678360	Parish church	1100
34	Santi Pietro e Paolo	Toscana	Montepulciano – Chiusi - Pienza	Petroio	43.141490 11.688210	Parish church	1180
35	Santi Leonardo e Cassiano	Toscana	Montepulciano – Chiusi - Pienza	San Casciano dei Bagni	42.871630 11.875230	Parish church	1200

TABLE A.1 (CONTINUED)

#	Church Name	Region	Diocese	Settlement / City	Coordinates WGS84 GD	Role	Original Construction Year
36	Santissima Annunziata	Toscana	Montepulciano – Chiusi - Pienza	Montisi	43.156690 11.651720	Parish church	1200
37	San Francesco	Toscana	Montepulciano – Chiusi - Pienza	Chiusi	43.016640 11.947110	Parish church	1210
38	San Leonardo	Toscana	Montepulciano – Chiusi - Pienza	Montefollonico	43.128120 11.745330	Parish church	1215
39	San Pietro	Toscana	Montepulciano – Chiusi - Pienza	Radicofani	42.896360 11.767490	Parish church	1220
40	Santi Leonardo e Cristoforo	Toscana	Montepulciano – Chiusi - Pienza	Monticchiello	43.068370 11.725680	Parish church	1300
41	Sant'Apollinare	Toscana	Montepulciano – Chiusi - Pienza	San Francesco	43.016000 11.946030	Subsidiary church	1400
42	San Vincenzo e Anasiasio	Toscana	Montepulciano – Chiusi - Pienza	Ascianello	43.139580 11.797180	Subsidiary church	1450
43	San Giovanni Battista	Umbria	Perugia – Città della Pieve	Castiglione della Valle	43.018110 12.253970	Parish church	1100
44	San Feliciano	Umbria	Perugia – Città della Pieve	San Feliciano	43.119030 12.166770	Parish church	1170
45	Sant'Ansano Martire	Umbria	Perugia – Città della Pieve	Petrignano del Lago	43.148450 11.937900	Parish church	1190
46	Crocifisso	Umbria	Perugia – Città della Pieve	Torgiano	43.018380 12.437670	Parish church	1200
47	San Martino di Fontana	Umbria	Perugia – Città della Pieve	Fontana	43.113110 12.324470	Parish church	1300
48	Santissimo Salvatore e Santa Maria Assunta	Umbria	Perugia – Città della Pieve	Paciano	43.023420 12.070170	Parish church	1480
49	San Lorenzo	Umbria	Perugia – Città della Pieve	Gioiella	43.093580 11.971890	Parish church	1500
50	Santa Maria delle Grazie	Umbria	Perugia – Città della Pieve	Montepetriolo	43.016910 12.229730	Subsidiary church	1500
51	Annunziata	Umbria	Perugia – Città della Pieve	Fontignano	43.026540 12.191760	Subsidiary church	1500
52	San Terenziano	Umbria	Orvieto - Todi	San Terenziano	42.863510 12.471800	Parish church	1200
53	Santi Giacomo e Marco	Umbria	Orvieto - Todi	Castel dell'Aquila	42.633830 12.406490	Parish church	1200
54	San Lorenzo Martire	Umbria	Orvieto - Todi	Montegiove	42.917050 12.144030	Subsidiary church	1270

TABLE A.1 (CONTINUED)

#	Church Name	Region	Diocese	Settlement / City	Coordinates WGS84 GD	Role	Original Construction Year
55	San Biagio Vescovo e Martire	Umbria	Orvieto - Todi	Porano	42.686550 12.101730	Parish church	1270
56	Sant'Andrea Apostolo	Umbria	Orvieto - Todi	Marcellano	42.872980 12.520790	Parish church	1300
57	Santa Maria Assunta	Umbria	Orvieto - Todi	Montecchio	42.663140 12.286270	Parish church	1300
58	San Nicolò	Umbria	Orvieto - Todi	Farnetta	42.648420 12.453280	Parish church	1400
59	San Pancrazio Martire	Umbria	Orvieto - Todi	Castel Giorgio	42.704710 11.979650	Parish church	1520[2]
60	Maddalena	Lazio	Anagni-Alatri	Alatri	41.716550 13.352380	Subsidiary church	1100
61	Santa Maria Maggiore	Lazio	Anagni Alatri	Alatri	41.726150 13.342160	Parish church	1100
62	Santa Maria al Colle	Lazio	Anagni Alatri	Fiuggi	41.804120 13.218100	Parish church	1200
63	Santi Nicola e Giovanni	Lazio	Anagni Alatri	Filettino	41.889500 13.319210	Subsidiary church	1200
64	Sant'Antonio	Lazio	Anagni Alatri	Filettino	41.890270 13.328870	Subsidiary church	1274
65	San Michele Arcangelo e San Gaurico	Lazio	Anagni Alatri	Fumone	41.727160 13.290440	Parish church	1350
66	Santa Maria Maddalena	Lazio	Palestrina	Capranica Prenestina	41.862310 12.952400	Parish church	1400
67	Santissima Annunziata	Campania	Sorrento – Castellammare di Stabia	Vico Equense	40.663880 14.423930	Subsidiary church	1330
68	San Renato Vescovo	Campania	Sorrento – Castellammare di Stabia	Moiano	40.650660 14.466020	Parish church	1340
69	Santa Maria Assunta	Campania	Sorrento – Castellammare di Stabia	Vico Equense	40.655540 14.435040	Subsidiary church	1400
70	Santa Maria di Casarlano	Campania	Sorrento – Castellammare di Stabia	Casarlano	40.623250 14.391680	Parish church	1425
71	San Giovanni Evangelista	Campania	Sorrento – Castellammare di Stabia	Vico Equense	40.662960 14.436400	Parish church	1490
72	Sant'Antonio	Campania	Nocera Inferiore - Sarno	Nocera Inferiore	40.746980 14.645720	Parish church	1260

[1]The church was selected beyond specific request of the diocese.
[2]Although the original construction year is slightly outside of the selected limits, the church was selected because it was respecting the other criteria.

APPENDIX B:

CRITERIA TO DETERMINE THE INFLUENCE SCORE OF THE VULNERABILITY INDICATORS, $I_{I,KI}$, AND THE EFFECTIVENESS SCORE OF THE ROBUSTNESS IMPROVERS, $I_{E,KP}$

Given the subjectivity of the criteria to determine the score for the vulnerability indicators and the robustness improvers, v_{ki} and v_{kp} (DPCM 2011), more extensive criteria were developed to address the influence score of the vulnerability indicators, $I_{e,kp}$, and the effectiveness score of the robustness improvers, $I_{i,ki}$, of the selected churches. The authors underline that the applied criteria were developed for the purposes of a rapid and effective visual survey, based on the recurrent characteristics of the analyzed churches. The criteria might still have a subjective component and further research to achieve more scientific criteria would be desirable.

Whenever uncertainties regarding the assessment of any macro-block occurred (due to impossibility of accessing directly the element, or to the difficulty of establishing a correct score) a conservative approach was applied by considering both the worst and the best-case scenario. While the application of the criteria is related to the correspondent collapse mechanism (Figure B.1) of each macro-block in Table B.1, a description of each criterion is listed in Table B.2 and Table B.3.

.

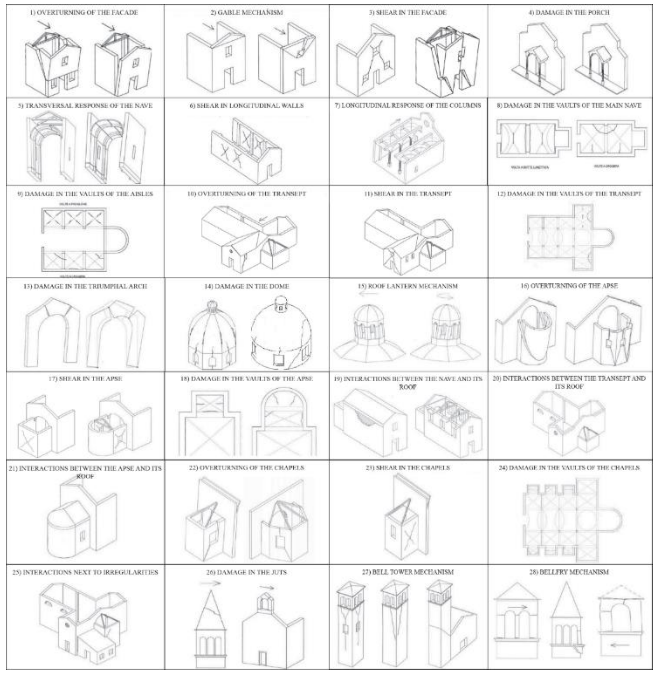

Figure B.1: Collapse mechanisms (D.P.C.M. 9 febbraio 2011).

TABLE B.1

APPLICATION OF THE CRITERIA FOR THE DIFFERENT COLLAPSE MECHANISMS OF THE MACRO-BLOCKS

Macro-block (Figure 2.7)	**Collapse Mechanism (Figure B.1)**	**Criteria applied for vulnerability indicators**	**Criteria applied for robustness improvers**
Façade	1) Overturning of the façade	V1; V2	R1; R2; R3
	2) Gable mechanism	V2; V3; V4	R4; R5; R6
	3) Shear in the façade	V2; V5	R1; R7
	4) Damage in the porch	V1	R1; R8
Lateral Walls	5) Transversal response of the nave	V1; V5	R1; R2; R7
	6) Shear in the longitudinal walls	V2; V5	R6; R9; R10
Nave	7) Longitudinal response of the columns	V1; V6	R1; R2
	8) Damage in the vaults of the main nave	V7; V8; V9	R1; R2

TABLE B.1 (CONTINUED)

Macro-block (Figure 2.7)	**Collapse Mechanism (Figure B.1)**	**Criteria applied for vulnerability indicators**	**Criteria applied for robustness improvers**
	9) Damage in the vaults of the aisles	V7; V8; V9	R1; R2
Transept	10) Overturning of the transept	V2; V3; V4	R1; R2; R3; R4; R6
	11) Shear in the transept	V2; V4	R6; R9; R10
	12) Damage in the vaults of the transept	V7; V8; V9	R1; R2
Triumphal Arch	13) Damage in the triumphal arch	V1; V6	R1; R7; R11
Dome	14) Damage in the dome	V7; V10	R2; R12; R13
	15) Roof lantern mechanism	V5	R2; R12; R14
Apse	16) Overturning of the apse	V1; V2; V4	R2; R5; R12
	17) Shear in the apse	V2; V4	R6; R9; R10
	18) Damage in the vaults of the apse	V7; V8; V9	R1; R2
Chapels	22) Overturning of the chapels	V2	R1; R2; R3
	23) Shear in the chapels	V2; V4	R6; R9; R10
	24) Damage in the vaults of the chapels	V7; V8; V9	R1; R2
Projections	26) Damage in the juts	V5; V11; V12	R4; R9; R15
Bell Tower	27) Bell tower mechanism	V2; V13; V11	R1; R3; R9; R16
	28) Belfry mechanism	V1; V6	R1; R8; R17
Interactions	19) Interaction between the nave and its roof	V1; V4	R4; R5; R6; R18
	20) Interaction between the transept and its roof	V1; V4	R4; R5; R6; R18
	21) Interaction between the apse and its roof	V1; V4	R4; R5; R6; R18
	25) Interaction next to irregularities	V7; V14	R1; R19

TABLE B.2

CRITERIA FOR THE INFLUENCE SCORE OF THE VULNERABILITY INDICATOR, $I_{I,KI}$

Criteria for the influence score of the vulnerability indicator, $I_{i,ki}$	**Description**
V1: Thrusting elements	Thrusting elements will always exist when there are vaults, arches, or any element causing horizontal loading. The amount of the thrust would depend on the length of the span, the rise of the vault (or the arch), the overall geometry, the depth, and the composing material. However, in most cases only the span and rise can be quickly and directly assessed and the intensity of the horizontal thrust can be estimated consequently. Thus, a scoring approach similar to V8 (long spans) was applied.
V2: Large openings	The presence of openings might significantly affect a masonry wall by creating a system of piers, instead of a solid wall behavior. A score of 5 might be assigned if the openings area (considering also their vertical projections) affect an area larger than the 50% of the area of the wall. A score of 4 might be assigned if the openings area (considering also their vertical projections) affect an area ranging between the 40% and the 50% of the area of the wall. A score of 3 might be assigned if the openings area (considering also their vertical projections) affect an area ranging between the 30% and the 40% of the area of the wall. A score of 2 might be assigned if the openings area (considering also their vertical projections) affect an area ranging between the 20% and the 30% of the area of the wall. A score of 1 might be assigned if the openings area (considering also their vertical projections) affect an area smaller than the 10% of the area of the wall. A score of 0 might be assigned only if the openings are absent or their dimension is negligible.
V3: Large and heavy groin/rib vault panels	This criterion has several similarities with V1 (thrusting elements) and it was assessed in a similar way.
V4: Stiff ring-beam	Stiff ring-beams exist where there is a concrete bond beam. This may or may not be visible. Roof retrofits that involve reinforced concrete provide a stiff ring-beams. There may be a reinforced concrete beam around the roof elements. Tell-tale marks of the presence of a reinforced concrete ring-beams might be noticed from the outside of the church. If joists are not visible outside the wall and the latter is plastered, then it might be tentatively assumed a concrete ring-beam is existing. A score of 5 might be assigned if there is a concrete ring-beam. The score should be lowered basing on the divergence from the worst-case scenario.
V5: Slenderness	The slenderness of an element negatively affects the out-of-plane performance. Given the difficulty of measuring directly the thickness of several macro-blocks, the score was based on the perceived geometry of the element.
V6: Excessively stiff or heavy roof	A stiff or heavy roof exists where there is a concrete roof or masonry vaults. A score of 5 might be assigned if there is a concrete roof or masonry vaults. A score not lower than 2 should be assigned for this criterion, unless the entire roof system (roof covering included) is constructed in timber and the connections can be assumed as effective.
V7: Concentrated loads	A large concentrated load might likely negatively affect the response of the loaded element by creating a “punching load” effect. Furthermore, the position might affect the distribution of the load towards the support. Asymmetric loads might cause an

TABLE B.2 (CONTINUED)

Criteria for the influence score of the vulnerability indicator, $I_{i,ki}$	**Description**
	unequal loading of the supports and differential responses. A score of 5 might be assigned to large and asymmetric concentrated loads. The score should be lowered basing on the divergence from the worst-case scenario.
V8: Span length of arches/vaults	LThis criterion is associated with the presence of vaults or arches. A score of 5 might be assigned to span longer than 8 m. A score of 4 might be assigned to spans with length ranging between 6 and 8 m. A score of 3 might be assigned to spans with length ranging between 4 and 6 m. A score of 2 might be assigned to spans with length ranging between 2 and 4 m. A score of 1 might be assigned to spans shorter than 2 m.
V9: Irregular profile	Any asymmetry in the geometry of a vault (or an arch) might cause an increasing bending moment on the section, while arches are designed to take compressive stresses. The score was based on the perceived irregularity in the geometry of the vault (or arch).
V10: Large openings in the dome drum	This criterion has several similarities with V2 (large openings) and it was assessed in a similar way.
V11: False supports	False support might happen when a secondary element is not resting on a structural element, such as a load bearing wall, or on appropriate foundations system. A score of 0 might be assigned if the element is fully supported by a vertical bearing element or if it lays on its own foundations. The score should be increased basing on the divergence from the best-case scenario.
V12: Eccentric position	Secondary elements that are not symmetrically resting on primary vertical bearing elements might cause a differential response of the supports. A score of 0 might be assigned to elements that are symmetrical resting on the primary bearing element with respect both to the depth and the length. The score should be increased basing on the divergence from the best-case scenario.
V13: Asymmetric position of the bell tower	An asymmetric position of the bell tower coupled with a very stiff roof strongly connected to walls may lead to increased torsional action within the structure. A score of 0 might be assigned if the bell tower is properly separated from the church. The score should be increased basing on the divergence from the optimal scenario.
V14: Stiffness differences	Stiffness differences might exist if a structure or element that is either incorporated into the structure of the church or next to the church is of a different height and/or width and/or material. A score of 5 might be assigned if the two structures (i.e., the church and the considered irregularity) have significant differences in terms of material and geometry. The score should be lowered basing on the divergence from the worst-case scenario.

TABLE B.3

CRITERIA FOR THE EFFECTIVENESS SCORE OF THE ROBUSTNESS IMPROVER, $I_{E,KP}$

Criteria for the effectiveness score of the robustness improver, $I_{e,kp}$	**Description**
R1: Tie rods	For being fully effective tie rods must: 1) span in the direction perpendicular to the macroblock motion at location (height) that is effective for resisting motion, and 2) must extend through exterior walls or the member that it is supporting. If a tie rod exists in a direction that is not perpendicular to the macroblock motion or not providing restraint to motion of the specific element, then the tie rod may be considered absent for that category. If there is no evidence of a tie rod extending through a wall or member in which it is supporting, then it is not very effective. Also, look for signs of weakness or damage in the tie rod that may impact the effectiveness. Additonally, consider spacing between tie rods and size of the wall anchor. A score of 5 might be assigned if the criterion is fully respected. The score should be lowered basing on the divergence from the optimal scenario.
R2: Buttresses	Elements other than traditional buttresses may act as a buttress on an element of the structure. To be effective, buttresses must be providing resistance in the direction in which the macro-block needs support for. An element also needs to transfer loads into the foundation (or in the closest vertical bearing element) in order to be acting as a buttress. This may exist as another component of the church. There may be instances where a chapel serves as a buttress to the main nave or the aisle. To be serving as a buttress, the element must be interlocked as a component of the structure/element in which it is supporting. A score of 5 might be assigned if the buttresses are uniformly distributed along the direction of the vault, or at the exact position of the arches, and if the footprint is large enough to accommodate the inclined forces coming from the thrusting elements. The score should not be larger than 2 if there are buttresses just on one side of the thrusting element. The score should be lowered basing on the divergence from the optimal scenario.
R3: Connection to lateral walls	The criterion depends on how well connected the walls that are subject to overturning are connected to the walls perpendicular to them. For example, the façade and transept would both have some type of connection to a lateral wall. A well-connected lateral wall means that the masonry is interlocked as a consequence of dressed units and staggered head joints. The mortar should also be strong and in good condition for full effectiveness. A lateral wall that would not be well connected would be a wall that does not have interconnected masonry blocks. Hooping elements or diagonal tie rods crossing the connecting walls increase the effectiveness of the connection. A score of 5 might be assigned if the criterion is fully respected. The score should not be larger than 4 if the connection is only based on masonry bond. The score should be lowered basing on the divergence from the optimal scenario.
R4: Connection to roof	All churches will have some type of connection to the roof. Newly renovated roofs will likely have a stronger connection and a score of 4 or 5 can be assigned in some instances. It is possible that newly renovated roofs in some churches were only renovated over certain sections of the church and may not include chapels, the apse, or

TABLE B.3 (CONTINUED)

Criteria for the effectiveness score of the robustness improver, $I_{e,kp}$	**Description**
	transepts. Be certain that the entire roof has been retrofitted before giving all elements a full effective score for roof connections. A score of 5 might be assigned if devices to increase the effectiveness of the connection are applied (e.g., steel bars drilled in the bond beam and resins-filled holes). The score should not be larger than 3 if the connection between the roof and the vertical bearing elements is mainly based on friction. The score should be lowered basing on the divergence from the optimal scenario.
R5: Braced roof pitch	The braced roof pitch exists when there are adequate bracing elements connecting the roof frames. The more bracing there are, and the shorter the span between the bracing is, the more effective the braced roof pitch will be. This may not be visible. A score of 4 might be assigned if the roof is composed of concrete beams and a collaborating concrete slab, and a score of 5 if a lighter and properly designed bracing system is connecting the roof beams. The score should not be larger than 2 if a single layer of timber board is overlapped transversely to the roof beams. The score should be lowered basing on the divergence from the optimal scenario. If it is not something visible from inside the church, a conservative score of 0 might be assumed.
R6: Light ring-beam	The ring-beam should be light (timber, steel, reinforced masonry or FRP stripes), continuous, and well-connected to the vertical bearing element. A score of 5 might be assigned if the criterion is fully respected. The score should not be larger than 3 if the ring-beam is not continuous or if the connection with the vertical bearing element is mainly based on friction. In newly renovated roofs, a concrete beam may exist to ensure (if properly designed) a stronger connection between the roof and other building components. In this case, even though the connections are strong, the ring-beam is still heavy and stiff, and a score of 0 might be assigned.
R7: Lateral restraints	The criterion refers to components (other than buttresses) that are serving as lateral restraints. These components are not always part of the church structure and may not have a structural attachment. Lateral restraints of transverse motion may be in the form of surrounding structures that abut the element. Lateral restraints may also be interior elements that are not structural, but that may help to prohibit motion in direction specified in each category of the specified element. A score of 5 might be assigned if the lateral restraints are continuously restraining the transversal motion. The score should not be larger than 2 if there are lateral restraints just on one side of the thrusting element. The score should be lowered basing on the divergence from the optimal scenario.
R8: Columns dimension	This is only applicable for churches that have columns. Columns that are only located integral with lateral walls in a church that only has a main nave and no aisles are not considered in this criterion. The dimensions refer to how thick they are with respect to the height and span length of arch(es) converging into them. A score of 5 might be assigned if the footprint is large enough to accommodate the inclined forces coming from the thrusting elements. The score should be lowered basing on the divergence from the optimal scenario.
R9: Quality of masonry	For the purposes of this criterion, the quality of the masonry is based on the qualitative approach of the masonry quality index (Borri et al. 2015). The score for this criterion can be 1, 2, or 3 and equation 2.8 should be changed with $v_{kp,i} = \frac{I_{e,kp,R9}}{n_{kp}} + \frac{3}{5n_{kp}} \sum_{j=1}^{n_{kp}-1} I_{e,kp,j}$. A score of 3 might be assigned to a corresponding to masonry category "A" in the in-plane direction. A score of 2 might be assigned to a

TABLE B.3 (CONTINUED)

Criteria for the effectiveness score of the robustness improver, $I_{e,kp}$	Description
	corresponding to masonry category "B" in the in-plane direction. A score of 1 might be assigned to a corresponding to masonry category "C" in the in-plane direction. The score should not be larger than 1 if the wall has extensive cracks.
R10: Lintels	Lintels should either look like beams, stonework, or brickwork around openings. These must be in good shape to transfer loads appropriately through masonry walls. A score of 5 might be assigned if the lintel has a properly large support on the vertical bearing elements surrounding the opening and no cracks are evident on the lintels or on the immediately surrounding area. The score should be lowered basing on the divergence from the optimal scenario. If any evidence of the absence of lintels might be noticed (extensive cracks surrounding the openings) a score of 0 might be assigned.
R11: Large thickness	This criterion refers to how thick triumphal arch is with respect of its length. The score was based on the perceived geometry of the triumphal arch.
R12: Radial bracing	This criterion has several similarities with R1 (tie rods). The main difference is the radial distribution of the tie rods to counteract the transversal forces. Also steel, timber, or FRP hooping members should be considered in this criterion and, if they exist, a score of 5 might be assigned.
R13: Connection to the triumphal arch	This criterion has several similarities with R4 (connection to roof) and it was assessed in a similar way.
R14: Lantern dimension	This criterion refers to the dimension of the lantern above the dome. The bigger the lantern is, the larger would be the load on the dome. Furthermore, slender lanterns could be likely affected by overturning. Given the difficulty of accessing the lantern directly, the score was based on the perceived geometry of the element.
R15: Elements dimension	This criterion has several similarities with R14 (lantern dimension) and it was assessed in a similar way.
R16: Distance of the bell tower from church walls	If the bell tower is not integral with the church or adjacent the actual church structure, then it will have some distance from the church. It may still be adjacent another structure that may be adjacent to the church, but not the church itself. A score of 5 might be assigned if there are no forms of connections between the bell tower and the church, and the minimum distance between the two structure is larger H/100, where H is the height of the church wall adjacent to the bell tower. The score should be lowered based on the divergence from the optimal scenario.
R17: Span length of the belfry arches	Short span arches provide better support than longer span arches. This is applicable if there are one or more arches in the belfry. Given the difficulty of accessing the belfry of each church, the score was based on the perceived geometry of the arch. A score of 5 might be assigned if the arch span was less than one third of the horizontal dimension of the belfry. The score should be lowered basing on the divergence from the optimal scenario.
R18: Connection to bond beams	This criterion has several similarities with R4 (connection to roof) and it was assessed in a similar way.
R19: Connection with later interventions	This criterion exists if there is a connection between the irregularity (other buildings typically) and the church structure. It has several similarities with R3 (connection to lateral walls) and it has been assessed in a similar way. If there is not clear integral connection, a score of 0 might be assigned. For example, if the other building/structure has a clear vertical joint without stones or bricks going into both the church and the

TABLE B.3 (CONTINUED)

Criteria for the effectiveness score of the robustness improver, $I_{e,kp}$	Description
	other structure (i.e., two distinct construction phases can be clearly recognized) A score of 5 might be assigned if there is no connection between the church and the other building/structure, and structural breaks were interposed between the two structures.

APPENDIX C:

WORKED EXAMPLE FOR THE CALCULATION OF SEISMIC RISK RATING, I_R, OF A CASE STUDY CHURCH

A worked example for the calculation of the seismic risk rating is offered in the following appendix. The case of the church of “Santa Maria Maggiore” (Figure C.1) was used for this example (church # 61 in Table A.1 of Appendix A). The church is located in the main square of Alatri, in the diocese of Anagni – Alatri (province of Frosinone, Lazio). It was completed in the 13th century A.D. and it was constructed over the ruins of a previous pagan temple dating from the 5th century A.D.

Figure C.1: Church of Santa Maria Maggiore, Alatri, Lazio (Italy).

C.1 Seismic Risk Components

C.1.1 Hazard

While the peak ground accelerations (PGA_{90}, PGA_{151}, PGA_{1424}, and PGA_{2475}) were determined using the online tool offered by the Italian High Council of Public Work (MIT and CSLP 2020), Equations 2.2 – 2.5 were used to determine the indices of hazard components $i_{H,90}$, $i_{H,151}$, $i_{H,1424}$, and $i_{H,2475}$. The results are shown in Table C.1.

TABLE C.1

INDICES OF HAZARD COMPONENTS

Scenario	**Peak ground acceleration, PGA_i [g]**	**5th percentile [g]**	**95th percentile [g]**	**Index of hazard component, $i_{H,i}$**
T_R = 90 years	0.088	0.044	0.310	0.277
T_R = 151 years	0.109			0.343
T_R = 1424 years	0.228			0.717
T_R = 2475 years	0.266			0.836

C.1.2 Vulnerability

An example for the calculation of one of the collapse mechanisms based on Table B 1 of Appendix B is offered below:

- Macro-block: Nave
  - Collapse mechanism: 8) Damage in the vaults of the main nave

- V7: During the survey no concentrated loads were noticed on the vaults of the main nave, thus, a score of 0 was assigned to this criterion ($I_{i,8i,1}$ = 0);
- V8: The spans of the vaults of the main nave were measured to be included in the range 6-8 meters, thus, a score of 3 was assigned to this criterion ($I_{i,8i,2}$ = 3);
- V9: No irregularity on the profile of the vaults of the main nave was noticed during the survey, thus, a score of 0 was assigned to this criterion ($I_{i,8i,3}$ = 0);
- R1: No tie rods were noticed on the vaults of the main nave, thus, a score of 0 was assigned to this criterion ($I_{e,8p,1}$ = 0);
- R2: Given the presence of aisles on both sides of the vaults, the main nave was considered fully laterally restrained, thus, a score of 5 was assigned to this criterion ($I_{e,8p,2}$ = 5).

Hence, the score for the vulnerability indicators and the robustness improvers, v_{ki} and v_{kp}, were determined using Equations 2.7 and 2.8:

$$v_{8i} = \frac{3}{5n_{8i}} \sum_{j=1}^{n_{8i}} I_{i,8i,j} = \frac{3}{5(3)}(0 + 3 + 0) = 0.6 \tag{2.7}$$

$$v_{8p} = \frac{3}{5n_{8p}} \sum_{j=1}^{n_{8p}} I_{e,8p,j} = \frac{3}{5(2)}(0 + 5) = 1.5 \tag{2.8}$$

Since there were no unknown data, $v_{8i,max} = v_{8i,min} = v_{8i} = 0.6$ and $v_{8p,max} = v_{8p,min} = v_{8p} = 1.5$. While in Table 3 it might be noticed that $\rho_{8,max} = \rho_{8,min} = \rho_8 = 1.0$.

Finally, the index of minimum and maximum vulnerability, $i_{V,min}$ and $i_{V,max}$, were determined using Equations 2.6 – 2.10 and the criteria expressed in Appendix B, assessing also the other collapse mechanisms. The results are shown in Table C.2.

TABLE C.2

INDICES OF VULNERABILITY COMPONENTS

Scenario	Index of vulnerability component, $i_{v,i}$
Minimum	0.553
Maximum	0.622

C.1.3 Exposure

C.1.3.1 Indices of Occupancy Rate

While the average and the maximum occupancy (p_{av} and p_{max}) were determined during the survey, the indices of occupancy rate were calculated using Equation 2.11 – 2.13. The results are shown in Table C.3.

TABLE C.3

INDICES OF OCCUPANCY RATE

Scenario	Occupancy, p_i [people]	5th percentile [people]	95th percentile [people]	Index of occupancy rate, $i_{OR,i}$
Average occupancy, p_{av}	57	2.05	136.20	0.420
Maximum occupancy, p_{max}	200	49.026	624.64	0.320

C.1.3.2 Indices of Community Utilization

While the utilization during the regular days and the holy days (k_{av} and k_{max}) were determined during the survey, the indices of community utilization were calculated using Equations 2.14 – 2.17. The results are shown in Table C.4.

TABLE C.4

INDICES OF COMMUNITY UTILIZATION

Scenario	**Occupancy, p_i [people]**	**City residents [people]**	**Community utilization, k_i**	**5th percentile**	**95th percentile**	**Index of community utilization, $i_{CU,i}$**
Regular days, k_{av}	57	28884	0.00198	0.0016	0.193	0.010
Holy day, k_{max}	200	28884	0.00692	0.014	2.368	0.006

C.1.4 Consequences

C.1.4.1 Indices of Equivalent Economic Value

The indices of minimum and maximum equivalent economic value were determined using Equations 2.18 – 2.21. The results are shown in Table C.5.

TABLE C.5

INDICES OF EQUIVALENT ECONOMIC VALUE

Scenario	**Surface, S_i [m^2]**	**Equivalent unitarian value, $C_{eq,i}$ [€/m^2]**	**Economic impact of the land, $i_{a,i}$**	**Equivalent economic value, $V_{eq,i}$ [€]**	**5th percentile [€]**	**95th percentile [€]**	**Index of equivalent economic value, $i_{EEV,i}$**
Minimum	854	810	0.30	1,452,461	207,225	970,545	0.547
Maximum		1076		1,928,546			0.762

C.1.4.2 Index of Susceptible Heritage

The index of susceptible heritage was determined using Equation 2.22 and the criteria expressed in Table 2.4. The results are shown in Table C.6.

TABLE C.6

INDEX OF SUSCEPTIBLE HERITAGE

Scenario	Total score of the church, $Score_i$	Maximum possible score	Index of Susceptible Heritage, $i_{SH,i}$
Susceptible heritage	38	45	0.844

C.2 Fuzzy Set Theory

C.2.1 Step 1: Membership Ratio and Fuzzification of the Inputs

The indices of risk subcomponents were fuzzified using Equation 2.23. A graphical representation of the fuzzification process is shown in

Figure C.2 through Figure C.7, while the resulting five-tuples sets $\boldsymbol{\mu_i}$ are summarized in Table C.7 (please, refer to Table 2.3 for the notations).

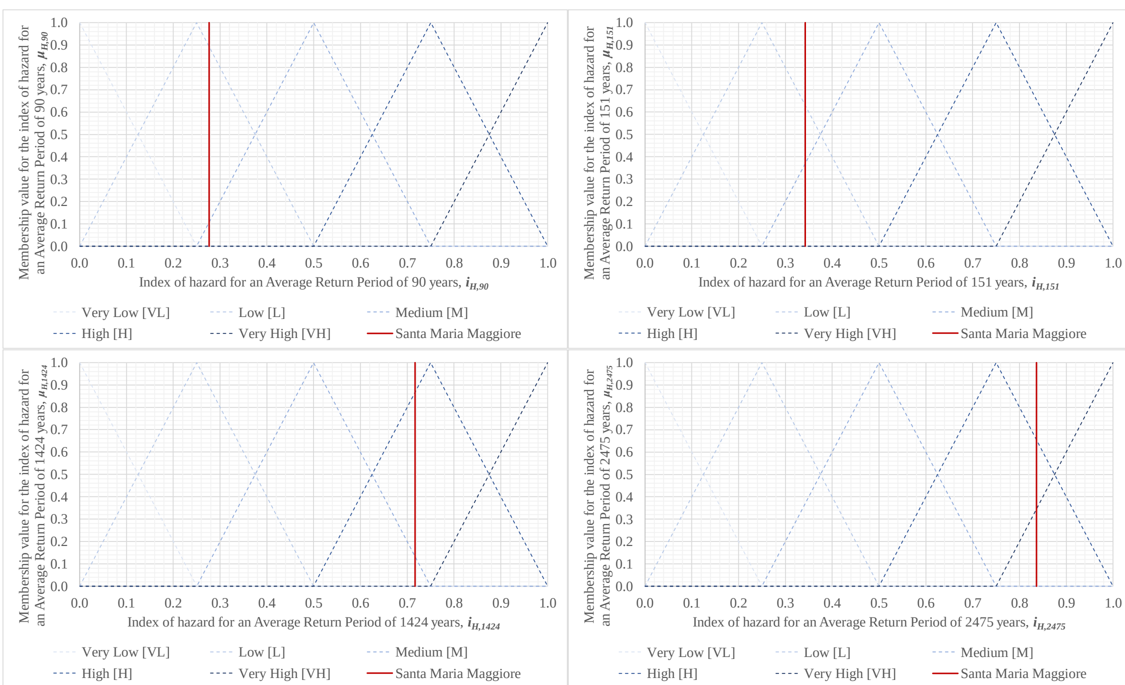

Figure C.2: Fuzzification of the indices of hazard components.

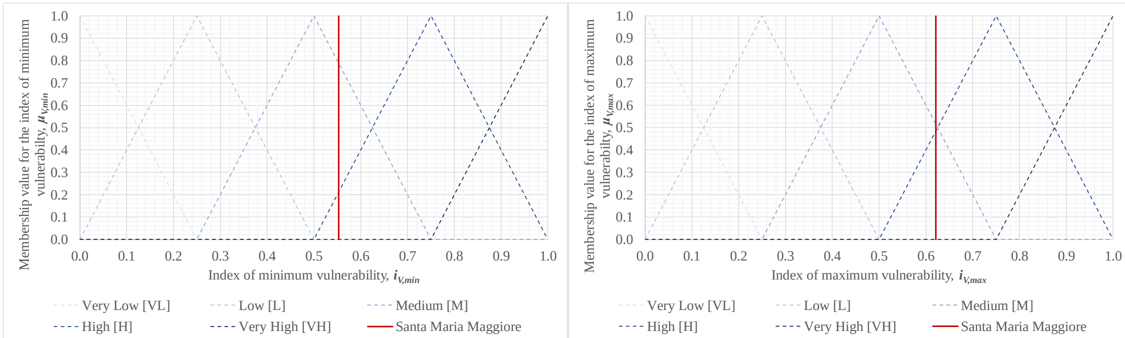

Figure C.3: Fuzzification of the indices of vulnerability components.

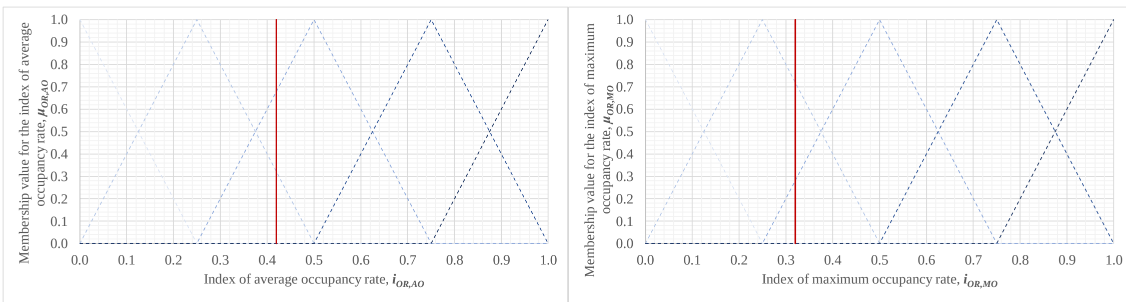

Figure C.4: Fuzzification of the indices of occupancy rate.

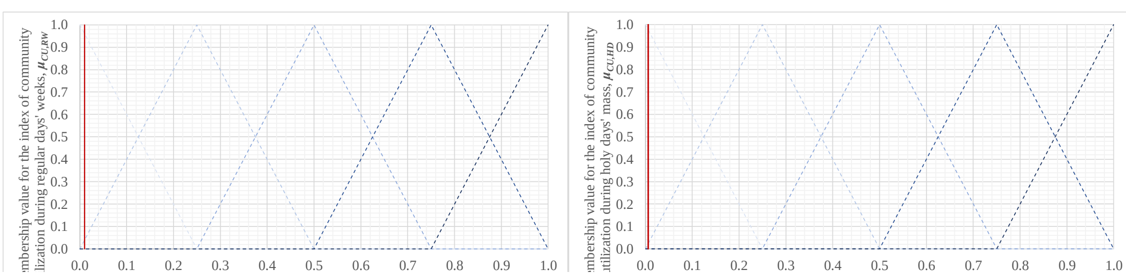

Figure C.5: Fuzzification of the indices of community utilization.

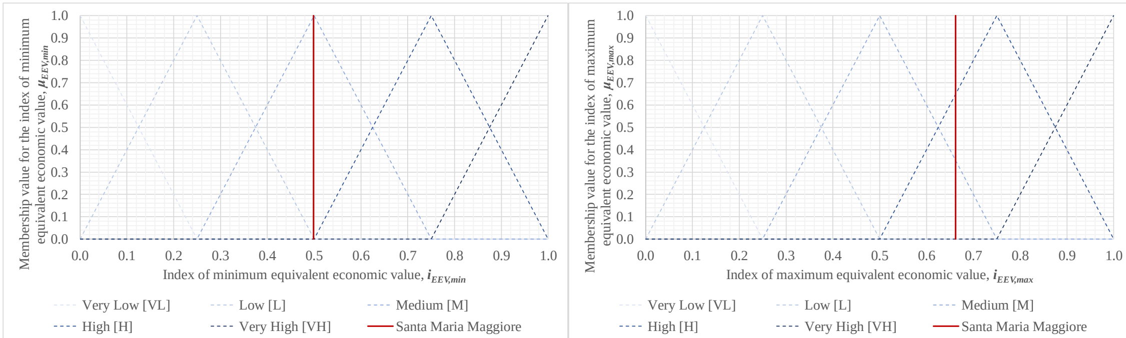

Figure C.6: Fuzzification of the indices of equivalent economic value.

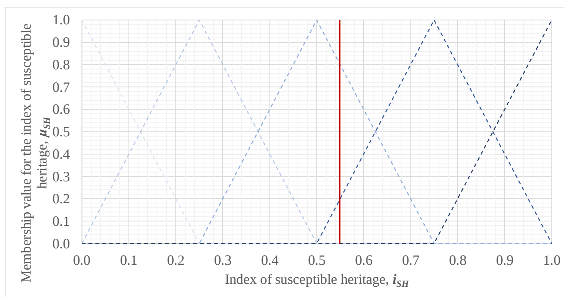

Figure C.7: Fuzzification of the index of susceptible heritage.

TABLE C.7

FUZZIFICATION OF THE INDICES OF RISK COMPONENTS

Indices, i_i		**Fuzzified five-tuple set, μ_i**	**Very Low [VL]**	**Low [L]**	**Medium [M]**	**High [H]**	**Very High [VH]**
$i_{H,90}$	0.277	$\mu_{H,90}$	0	0.894	0.106	0	0
$i_{H,151}$	0.343	$\mu_{H,151}$	0	0.630	0.370	0	0
$i_{H,1424}$	0.717	$\mu_{H,1424}$	0	0	0.134	0.866	0
$i_{H,2475}$	0.836	$\mu_{H,2475}$	0	0	0	0.656	0.344
$i_{V,min}$	0.553	$\mu_{V,min}$	0	0	0.787	0.213	0
$i_{V,max}$	0.622	$\mu_{V,max}$	0	0	0.514	0.486	0
$i_{OR,AO}$	0.420	$\mu_{OR,AO}$	0	0.322	0.678	0	0
$i_{OR,MO}$	0.320	$\mu_{OR,MO}$	0	0.719	0.281	0	0
$i_{CU,RW}$	0.010	$\mu_{CU,RW}$	0.959	0.041	0	0	0
$i_{CU,HD}$	0.006	$\mu_{CU,HD}$	0.975	0.025	0	0	0
$i_{EEV,min}$	0.499	$\mu_{EEV,min}$	0	0.005	0.995	0	0
$i_{EEV,max}$	0.649	$\mu_{EEV,max}$	0	0	0.351	0.649	0
i_{SH}	0.844	μ_{SH}	0	0	0	0.622	0.378

C.2.2 Step 2: Aggregation of Two Five-tuple Sets

The five-tuple sets $\boldsymbol{\mu_i}$ were aggregated two-by-two in an iterative process as shown in Figure 2.24. The aggregation was obtained by using Equations 2.26 and 2.27 and the rules of aggregation shown in Table 2.6.

C.2.2.1 Aggregation for the Hazard Rating

The results of the aggregation for the hazard rating are shown in Table C.8.

TABLE C.8

AGGREGATION FOR THE HAZARD RATING

Input five-tuple sets		**Output five-tuple set**	**Very Low [VL]**	**Low [L]**	**Medium [M]**	**High [H]**	**Very High [VH]**
$\mu_{H,90}$	$\mu_{H,151}$	$\mu_{H,1C}$	max[min(0;0] = **0**	max[min(0;0.630) ; min(0;0.370); min(0.894;0); min(0.894;0.630); min(0.106;0)] = **0.630**	max[min(0;0); min(0;0); min(0.894;0.370); min(0.894;0); min(0.106;0.630); min(0.106;0.370); min(0;0); min(0;0.630); min(0;0)] = **0.370**	max[min(0.894;0) ; min(0.106;0); min(0.106;0); min(0;0.370); min(0;0); min(0;0.630); min(0;0.370)] = **0**	max[min(0;0); min(0;0); min(0;0)] = **0**
$\mu_{H,1C}$	$\mu_{H,1424}$	$\mu_{H,1B}$	**0**	**0**	**0.630**	**0.370**	**0**
$\mu_{H,1B}$	$\mu_{H,2475}$	μ_{H}	**0**	**0**	**0**	**0.630**	**0.344**

C.2.2.2 Aggregation for the Vulnerability Rating

The results of the aggregation for the vulnerability rating are shown in Table C.9.

TABLE C.9

AGGREGATION FOR THE VULNERABILITY RATING

Input five-tuple sets		**Output five-tuple set**	**Very Low [VL]**	**Low [L]**	**Medium [M]**	**High [H]**	**Very High [VH]**
$\mu_{V,min}$	$\mu_{V,max}$	μ_V	max[min(0;0] = **0**	max[min(0;0); min(0;0.514); min(0;0); min(0;0); min(0.787;0)] = **0**	max[min(0;0.486); min(0;0); min(0;0.514); min(0;0.486); min(0.787;0); min(0.787;0.514); min(0.213;0); min(0.213;0); min(0;0)] = **0.514**	max[min(0;0); min(0.787;486); min(0.787;0); min(0.213;0.514); min(0.213;486); min(0;0); min(0;0.514)] = **0.486**	max[min(0.213;0); min(0;0.486); min(0;0)] = **0**

C.2.2.3 Aggregation for the Exposure Rating

The results of the aggregation for exposure rating are shown in Table C.10.

TABLE C.10

AGGREGATION FOR THE EXPOSURE RATING

Input five-tuple sets		**Output five-tuple set**	**Very Low [VL]**	**Low [L]**	**Medium [M]**	**High [H]**	**Very High [VH]**
$\mu_{OR,AO}$	$\mu_{OR,MO}$	μ_{OR}	max[min(0;0] = **0**	max[min(0;0.719) ; min(0;0.281); min(0;0); min(0.322;0); min(0.322;719)] = **0.322**	max[min(0;0); min(0;0); min(0.322;0.281); min(0.322;0); min(0.678;0.719); min(0.678;0.281); min(0;0); min(0;0.719); min(0;0)] = **0.678**	max[min(0.322;0) ; min(0.678;0); min(0.678;0); min(0;0.281); min(0;0); min(0;0.719); min(0;0.281)] = **0**	max[min(0;0); min(0;0); min(0;0)] = **0**
$\mu_{CU,RW}$	$\mu_{CU,HD}$	μ_{CU}	**0.959**	**0.041**	**0**	**0**	**0**
μ_{CU}	μ_{OR}	μ_{E}	**0**	**0.678**	**0.041**	**0**	**0**

C.2.2.4 Aggregation for the Consequences Rating

The results of the aggregation for consequences rating are shown in Table C.11.

TABLE C.11

AGGREGATION FOR THE CONSEQUENCES RATING

Input five-tuple sets		**Output five-tuple set**	**Very Low [VL]**	**Low [L]**	**Medium [M]**	**High [H]**	**Very High [VH]**
$\mu_{EEV,min}$	$\mu_{EEV,max}$	μ_{EEV}	max[min(0;0] = **0**	max[min(0;0); min(0;0.096); min(0;0); min(0;0); min(0.813;0)] = **0**	max[min(0;0.904) ; min(0;0); min(0;0.096); min(0;0.904); min(0.813;0); min(0.813;0.096); min(0;0); min(0;0); min(0;0)] = **0.096**	max[min(0;0); min(0.813;0.904); min(0.813;0); min(0.187;0.096); min(0.187;0.904); min(0;0); min(0;0.096)] = **0.813**	max[min(0.187;0) ; min(0;0.904); min(0;0)] = **0**
μ_{SH}	μ_{EEV}	μ_C	**0**	**0**	**0**	**0.622**	**0.378**

C.2.2.5 Aggregation for the Seismic Risk Rating

The results of the aggregation for the seismic risk rating are shown in Table C.12.

TABLE C.12

AGGREGATION FOR THE SEISMIC RISK RATING

Input five-tuple sets		**Output five-tuple set**	**Very Low [VL]**	**Low [L]**	**Medium [M]**	**High [H]**	**Very High [VH]**
μ_E	μ_C	μ_{EC}	max[min(0;0] = **0**	max[min(0;0); min(0;0); min(0.678;0); min(0.678;0); min(0.041;0)] = **0**	max[min(0;0.622); min(0;0.378); min(0.678;0); min(0.678;0.622); min(0.041;0); min(0.041;0); min(0;0); min(0;0); min(0;0)] = **0.622**	max[min(0.678;0.378); min(0.041;0.622); min(0.041;0.378); min(0;0); min(0;0.622); min(0;0); min(0;0)] = **0.378**	max[min(0;0.378); min(0;0.622); min(0;0.378)] = **0**
μ_{EC}	μ_V	μ_{VEC}	**0**	**0**	**0.514**	**0.486**	**0**
μ_{VEC}	μ_H	μ_R	**0**	**0**	**0**	**0.514**	**0.344**

C.2.3 Step 3: Defuzzification

The defuzzification of the aggregated five-tuples was obtained by using Equation 2.28. The results are shown in Table C.13.

TABLE C.13

RATINGS OF SEISMIC RISK AND RISK COMPONENTS

	Aggregate five-tuple set, μ_i	**Rating, i_i**	
Hazard	μ_H = [0; 0; 0; 0.630; 0.344]	i_H	0.816
Vulnerability	μ_V = [0; 0; 0.514; 0.486; 0]	i_V	0.622
Exposure	μ_E = [0; 0.678; 0.041; 0; 0]	i_E	0.190
Consequences	μ_C = [0; 0; 0; 0.622; 0.378]	i_C	0.844
Seismic Risk	μ_R = [0; 0; 0; 0.514; 0.344]	i_R	0.730

The resulting seismic risk rating was i_R = 0.730.

C.3 Multilinear Regression

The ratings obtained via FST were compared with the ones determined using Equations 2.29 – 2.33 (resulting from the multilinear regression). The comparison is shown in Table C.14.

TABLE C.14

COMPARISON BETWEEN FST RATING AND MULTILINEAR REGRESSION RATINGS

Rating	**FST**	**Multilinear regression**
Hazard, $\boldsymbol{i_H}$	0.816	0.697
Vulnerability, $\boldsymbol{i_V}$	0.622	0.611
Exposure, $\boldsymbol{i_E}$	0.190	0.183
Consequences, $\boldsymbol{i_C}$	0.844	0.770
Seismic Risk, $\boldsymbol{i_R}$	0.730	0.663

APPENDIX D:

FUZZYFICATION OF THE INDICES OF THE RISK SUBCOMPONENT (PROCEDURAL EXAMPLE BASED ON THE INDEX OF SUSCEPTIBLE HERITAGE)

As a procedural example, the graphic fuzzification of the indices of susceptible heritage for each assessed church, $i_{SH,i}$, is shown herein.

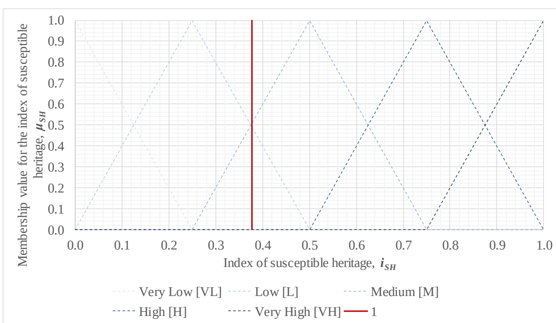

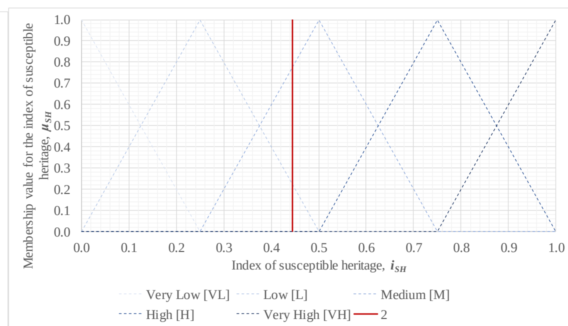

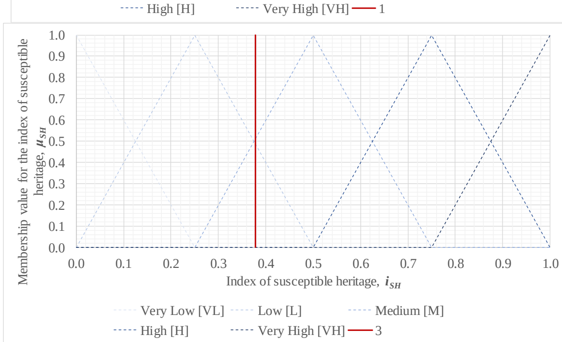

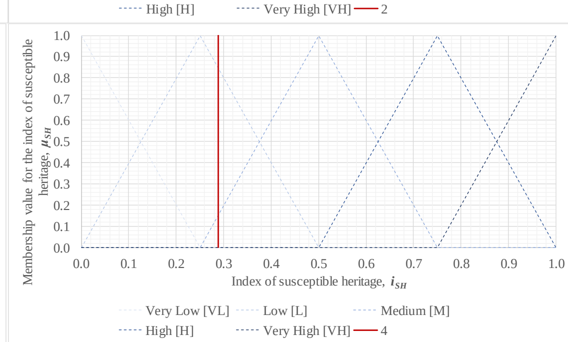

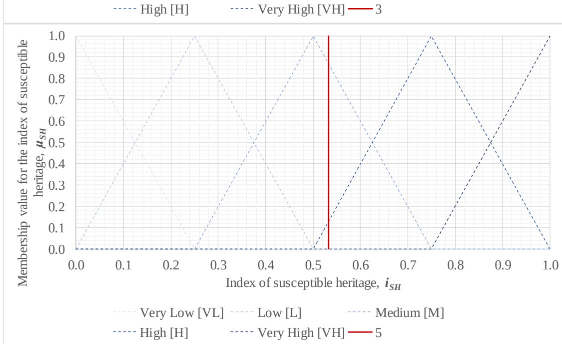

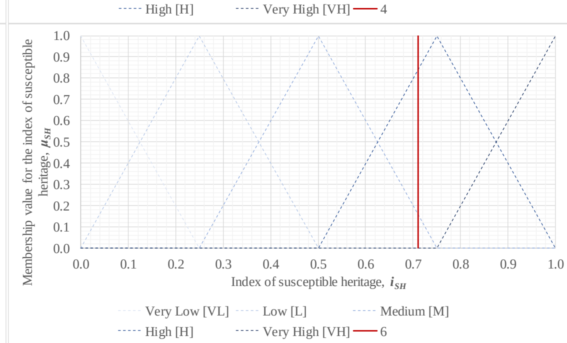

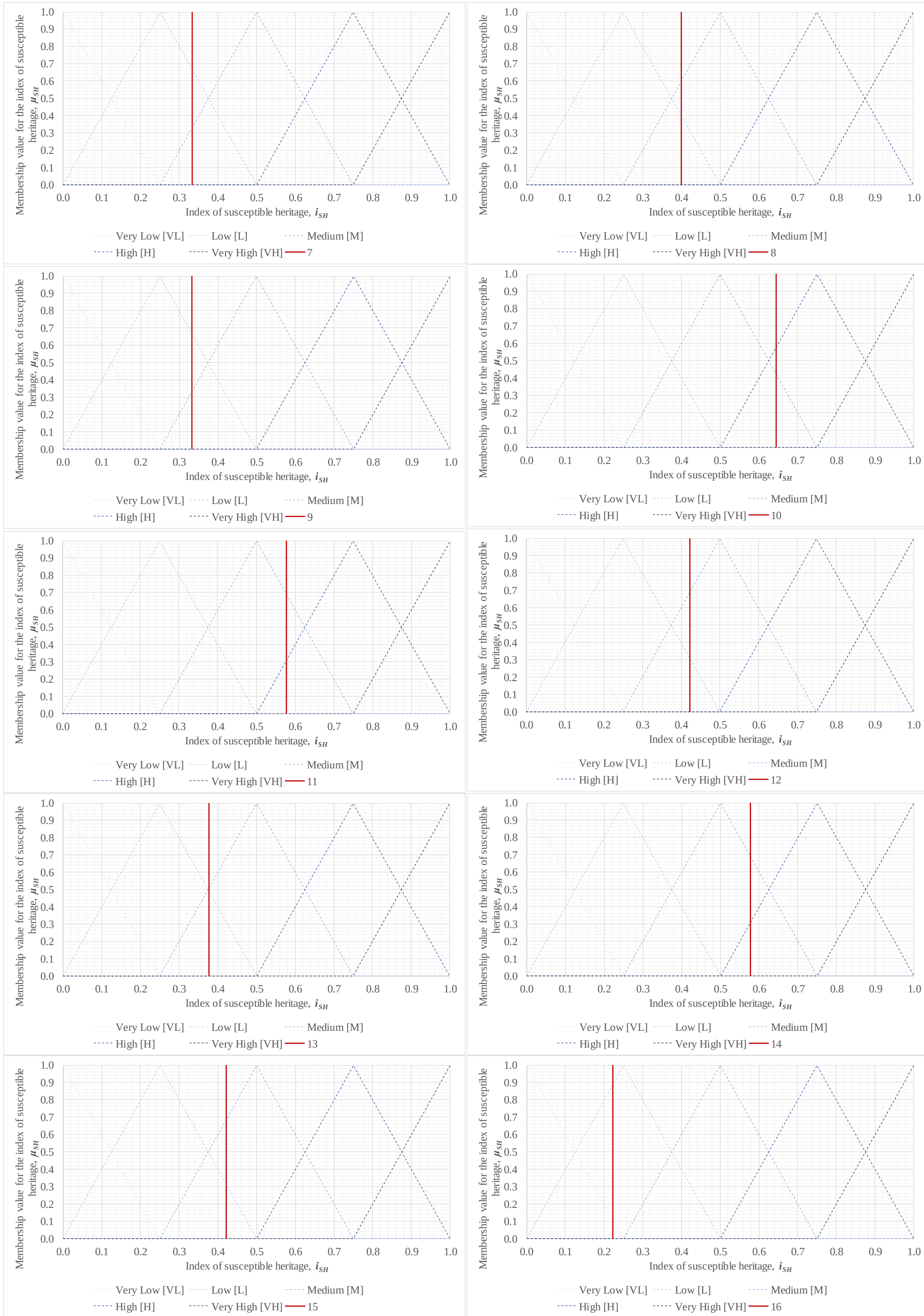
Membership value for the index of susceptible heritage, μ_{SH}
Index of susceptible heritage, i_{SH}
Very Low [VL]
Low [L]
Medium [M]
High [H]
Very High [VH]
7
8
9
10
11
12
13
14
15
16

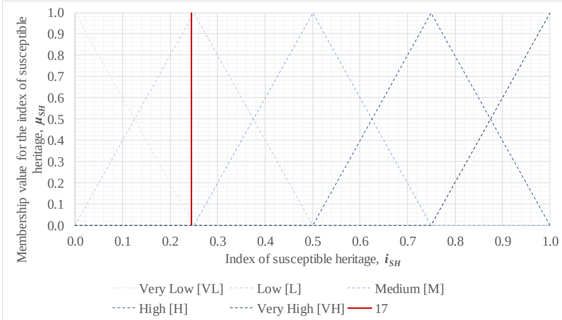
Membership value for the index of susceptible heritage, μ_{SH}
Index of susceptible heritage, i_{SH}
Very Low [VL]
Low [L]
Medium [M]
High [H]
Very High [VH]
17

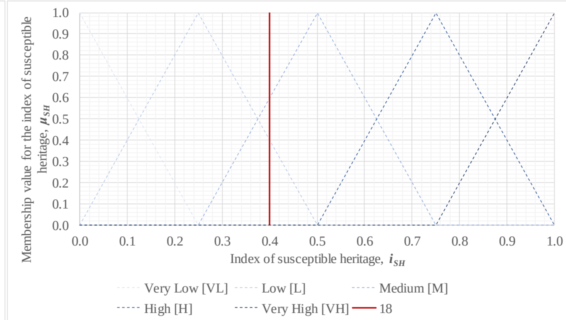
Membership value for the index of susceptible heritage, μ_{SH}
Index of susceptible heritage, i_{SH}
Very Low [VL]
Low [L]
Medium [M]
High [H]
Very High [VH]
18

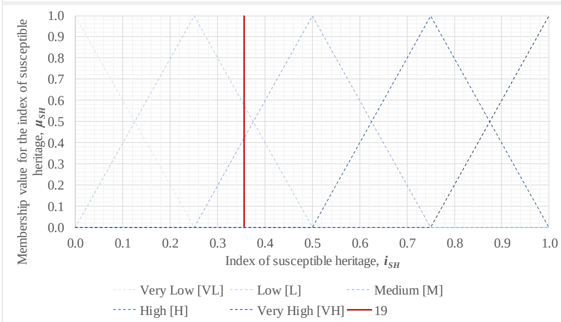
Membership value for the index of susceptible heritage, μ_{SH}
Index of susceptible heritage, i_{SH}
Very Low [VL]
Low [L]
Medium [M]
High [H]
Very High [VH]
19

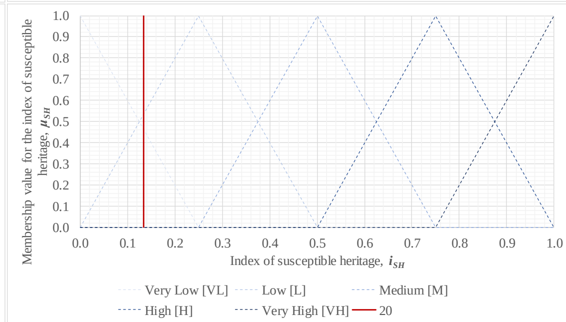
Membership value for the index of susceptible heritage, μ_{SH}
Index of susceptible heritage, i_{SH}
Very Low [VL]
Low [L]
Medium [M]
High [H]
Very High [VH]
20

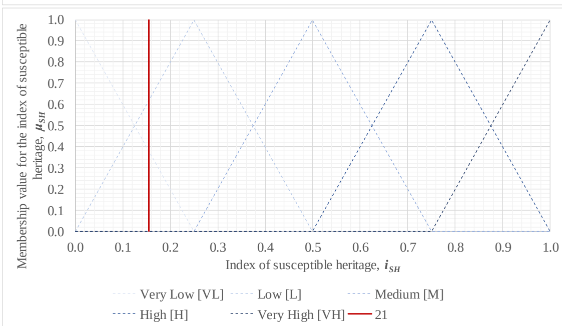
Membership value for the index of susceptible heritage, μ_{SH}
Index of susceptible heritage, i_{SH}
Very Low [VL]
Low [L]
Medium [M]
High [H]
Very High [VH]
21

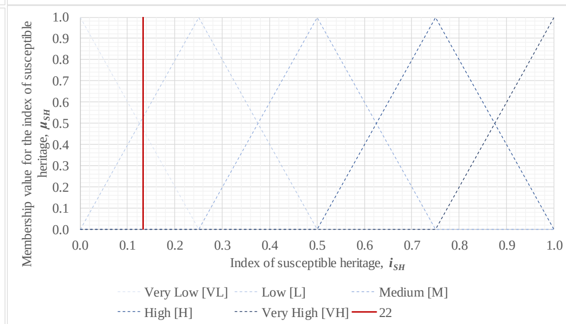
Membership value for the index of susceptible heritage, μ_{SH}
Index of susceptible heritage, i_{SH}
Very Low [VL]
Low [L]
Medium [M]
High [H]
Very High [VH]
22

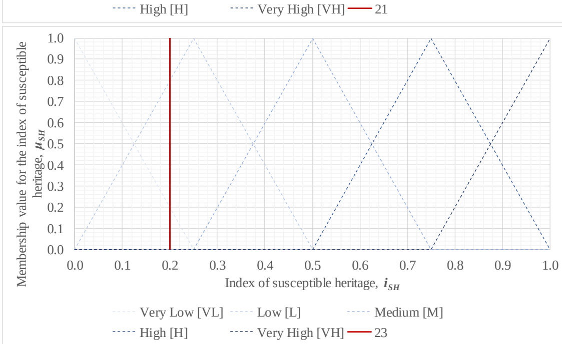
Membership value for the index of susceptible heritage, μ_{SH}
Index of susceptible heritage, i_{SH}
Very Low [VL]
Low [L]
Medium [M]
High [H]
Very High [VH]
23

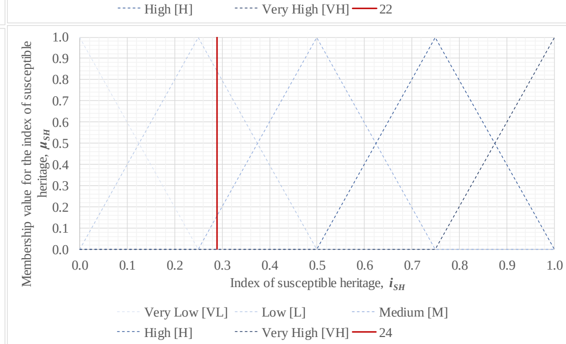
Membership value for the index of susceptible heritage, μ_{SH}
Index of susceptible heritage, i_{SH}
Very Low [VL]
Low [L]
Medium [M]
High [H]
Very High [VH]
24

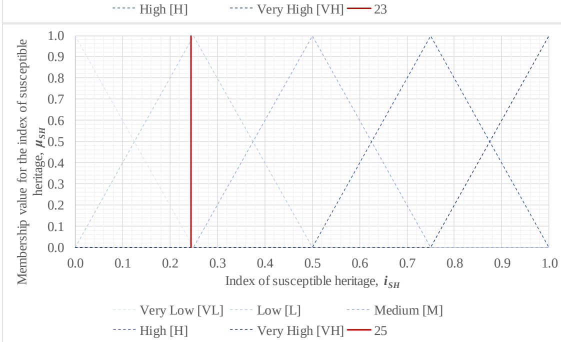
Membership value for the index of susceptible heritage, μ_{SH}
Index of susceptible heritage, i_{SH}
Very Low [VL]
Low [L]
Medium [M]
High [H]
Very High [VH]
25

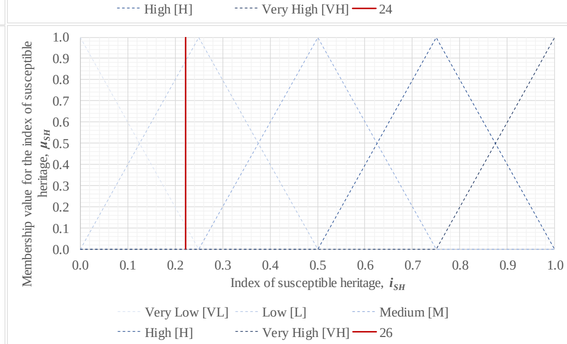
Membership value for the index of susceptible heritage, μ_{SH}
Index of susceptible heritage, i_{SH}
Very Low [VL]
Low [L]
Medium [M]
High [H]
Very High [VH]
26

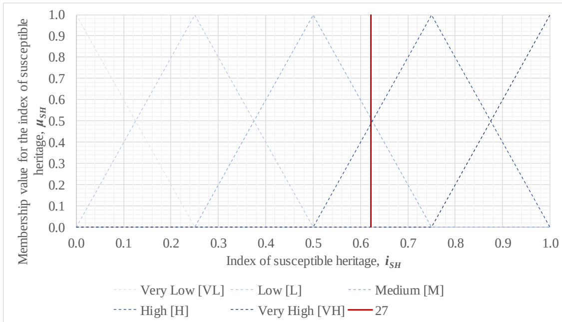
Membership value for the index of susceptible heritage, μ_{SH}
Index of susceptible heritage, i_{SH}
Very Low [VL]
Low [L]
Medium [M]
High [H]
Very High [VH]
27

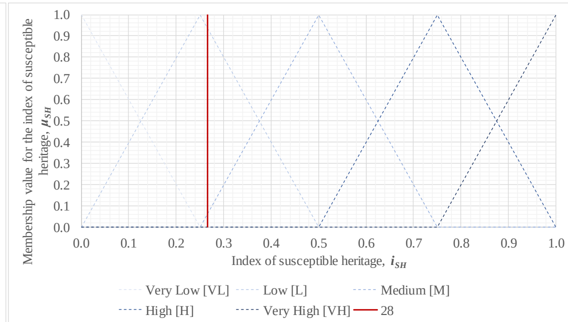
Membership value for the index of susceptible heritage, μ_{SH}
Index of susceptible heritage, i_{SH}
Very Low [VL]
Low [L]
Medium [M]
High [H]
Very High [VH]
28

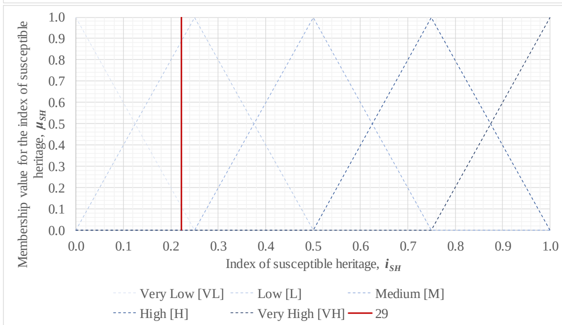
Membership value for the index of susceptible heritage, μ_{SH}
Index of susceptible heritage, i_{SH}
Very Low [VL]
Low [L]
Medium [M]
High [H]
Very High [VH]
29

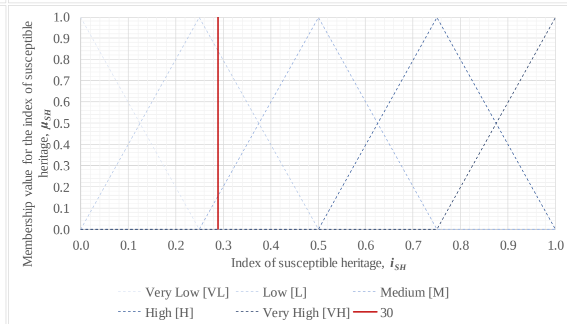
Membership value for the index of susceptible heritage, μ_{SH}
Index of susceptible heritage, i_{SH}
Very Low [VL]
Low [L]
Medium [M]
High [H]
Very High [VH]
30

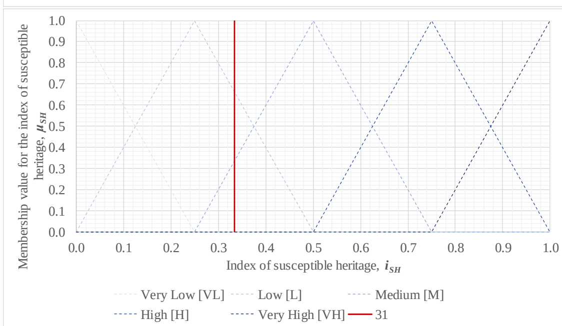
Membership value for the index of susceptible heritage, μ_{SH}
Index of susceptible heritage, i_{SH}
Very Low [VL]
Low [L]
Medium [M]
High [H]
Very High [VH]
31

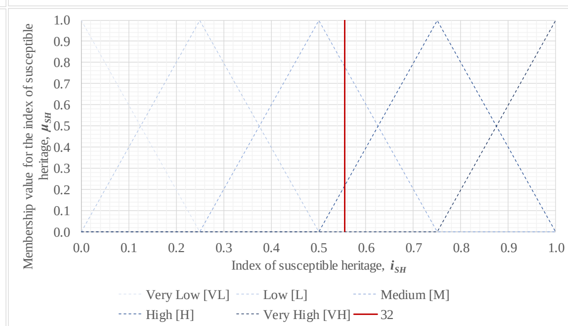
Membership value for the index of susceptible heritage, μ_{SH}
Index of susceptible heritage, i_{SH}
Very Low [VL]
Low [L]
Medium [M]
High [H]
Very High [VH]
32

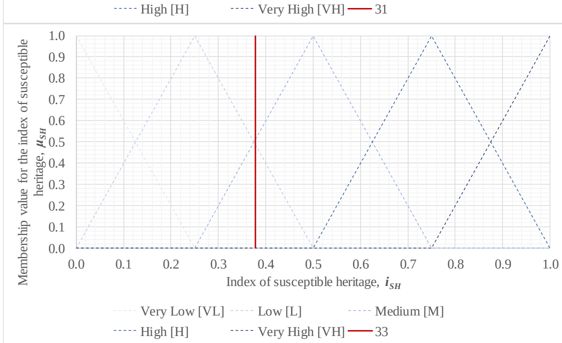
Membership value for the index of susceptible heritage, μ_{SH}
Index of susceptible heritage, i_{SH}
Very Low [VL]
Low [L]
Medium [M]
High [H]
Very High [VH]
33

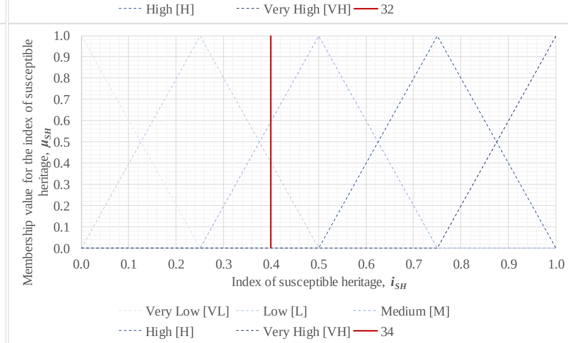
Membership value for the index of susceptible heritage, μ_{SH}
Index of susceptible heritage, i_{SH}
Very Low [VL]
Low [L]
Medium [M]
High [H]
Very High [VH]
34

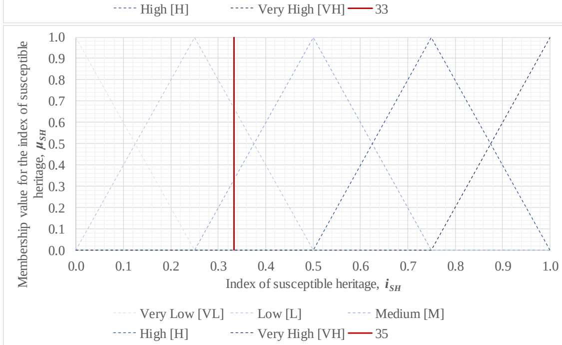
Membership value for the index of susceptible heritage, μ_{SH}
Index of susceptible heritage, i_{SH}
Very Low [VL]
Low [L]
Medium [M]
High [H]
Very High [VH]
35

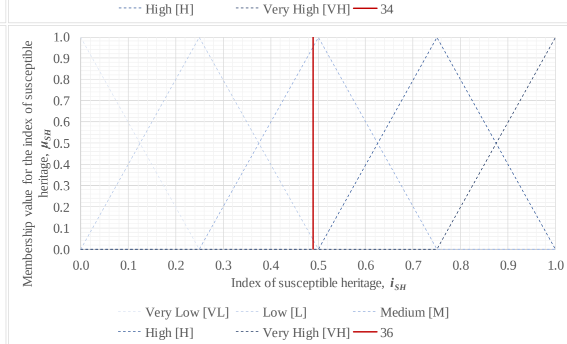
Membership value for the index of susceptible heritage, μ_{SH}
Index of susceptible heritage, i_{SH}
Very Low [VL]
Low [L]
Medium [M]
High [H]
Very High [VH]
36

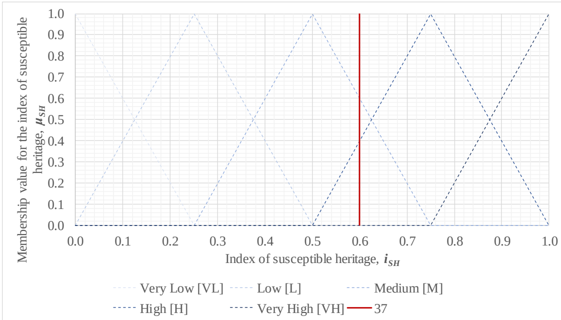
Membership value for the index of susceptible heritage, μ_{SH}
Index of susceptible heritage, i_{SH}
Very Low [VL]
Low [L]
Medium [M]
High [H]
Very High [VH]
37

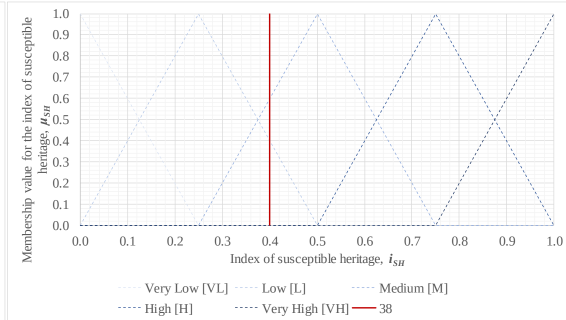
Membership value for the index of susceptible heritage, μ_{SH}
Index of susceptible heritage, i_{SH}
Very Low [VL]
Low [L]
Medium [M]
High [H]
Very High [VH]
38

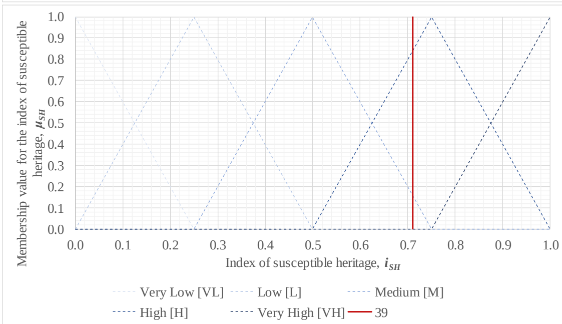
Membership value for the index of susceptible heritage, μ_{SH}
Index of susceptible heritage, i_{SH}
Very Low [VL]
Low [L]
Medium [M]
High [H]
Very High [VH]
39

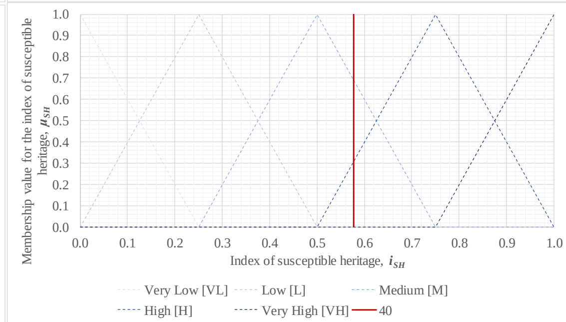
Membership value for the index of susceptible heritage, μ_{SH}
Index of susceptible heritage, i_{SH}
Very Low [VL]
Low [L]
Medium [M]
High [H]
Very High [VH]
40

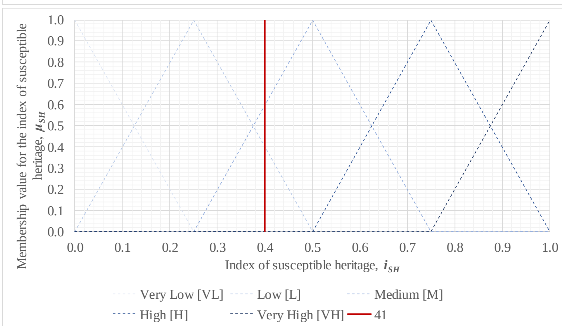
Membership value for the index of susceptible heritage, μ_{SH}
Index of susceptible heritage, i_{SH}
Very Low [VL]
Low [L]
Medium [M]
High [H]
Very High [VH]
41

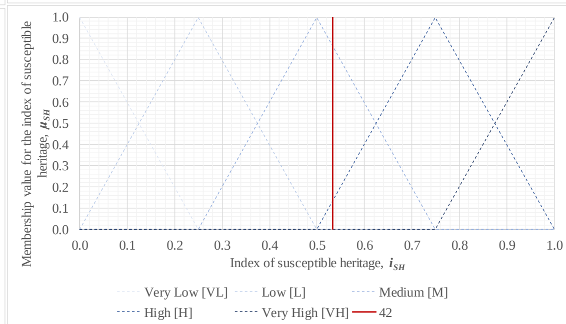
Membership value for the index of susceptible heritage, μ_{SH}
Index of susceptible heritage, i_{SH}
Very Low [VL]
Low [L]
Medium [M]
High [H]
Very High [VH]
42

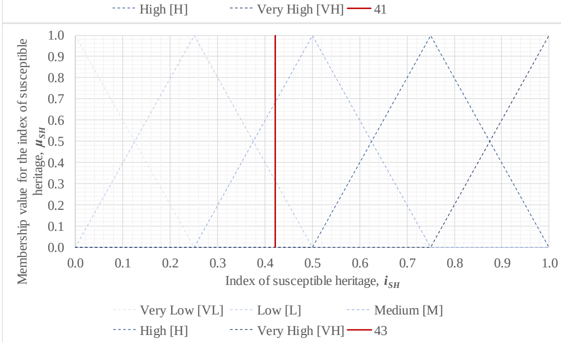
Membership value for the index of susceptible heritage, μ_{SH}
Index of susceptible heritage, i_{SH}
Very Low [VL]
Low [L]
Medium [M]
High [H]
Very High [VH]
43

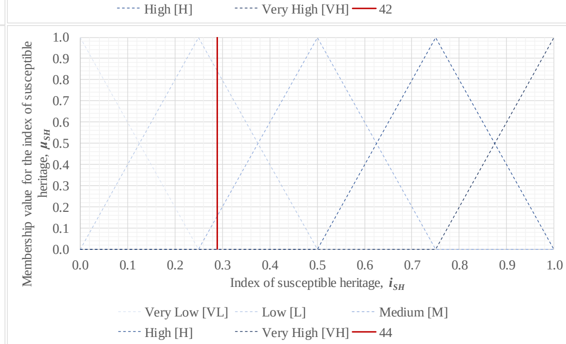
Membership value for the index of susceptible heritage, μ_{SH}
Index of susceptible heritage, i_{SH}
Very Low [VL]
Low [L]
Medium [M]
High [H]
Very High [VH]
44

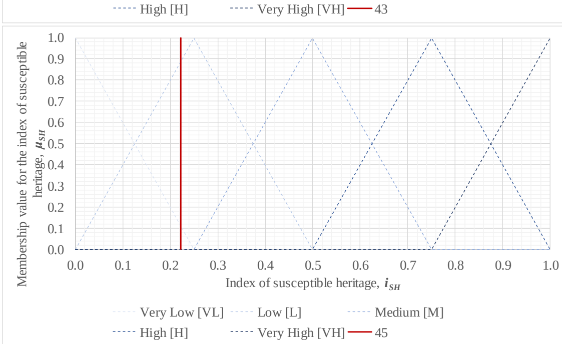
Membership value for the index of susceptible heritage, μ_{SH}
Index of susceptible heritage, i_{SH}
Very Low [VL]
Low [L]
Medium [M]
High [H]
Very High [VH]
45

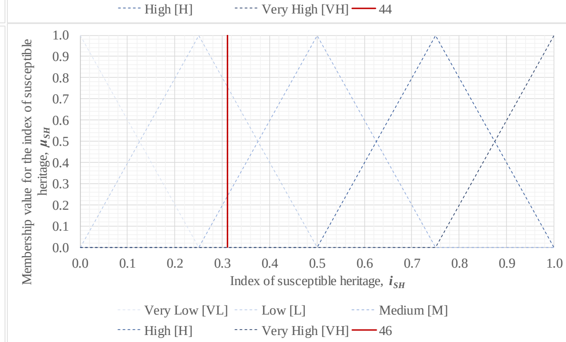
Membership value for the index of susceptible heritage, μ_{SH}
Index of susceptible heritage, i_{SH}
Very Low [VL]
Low [L]
Medium [M]
High [H]
Very High [VH]
46

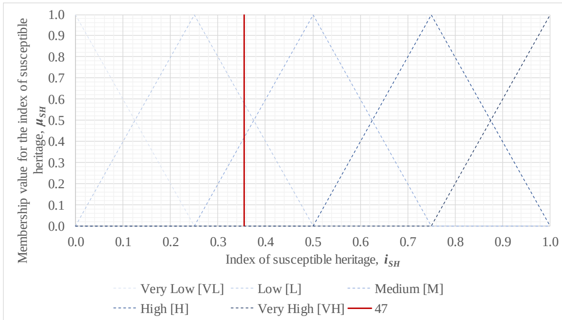
Membership value for the index of susceptible heritage, μ_{SH}
Index of susceptible heritage, i_{SH}
Very Low [VL]
Low [L]
Medium [M]
High [H]
Very High [VH]
47

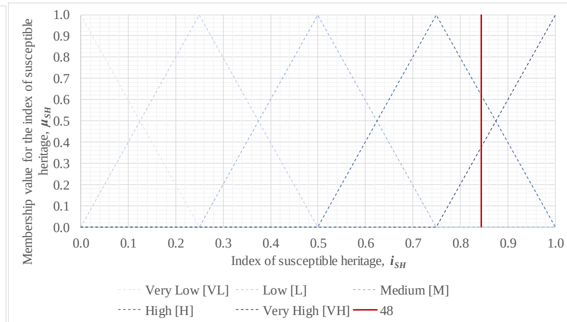
Membership value for the index of susceptible heritage, μ_{SH}
Index of susceptible heritage, i_{SH}
Very Low [VL]
Low [L]
Medium [M]
High [H]
Very High [VH]
48

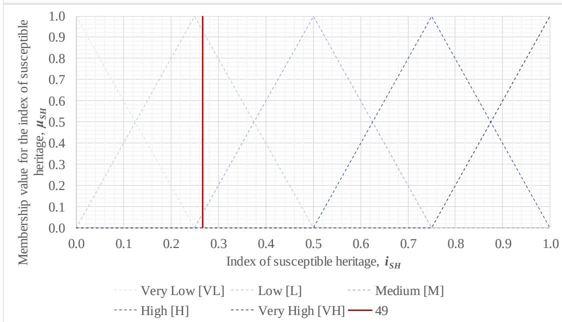
Membership value for the index of susceptible heritage, μ_{SH}
Index of susceptible heritage, i_{SH}
Very Low [VL]
Low [L]
Medium [M]
High [H]
Very High [VH]
49

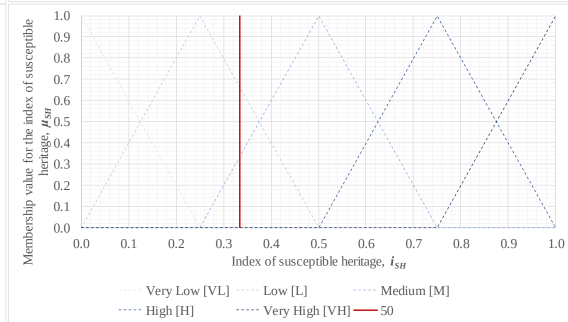
Membership value for the index of susceptible heritage, μ_{SH}
Index of susceptible heritage, i_{SH}
Very Low [VL]
Low [L]
Medium [M]
High [H]
Very High [VH]
50

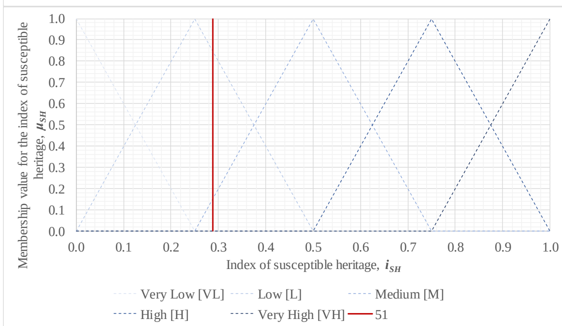
Membership value for the index of susceptible heritage, μ_{SH}
Index of susceptible heritage, i_{SH}
Very Low [VL]
Low [L]
Medium [M]
High [H]
Very High [VH]
51

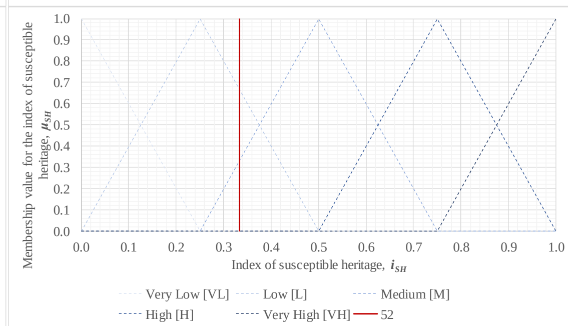
Membership value for the index of susceptible heritage, μ_{SH}
Index of susceptible heritage, i_{SH}
Very Low [VL]
Low [L]
Medium [M]
High [H]
Very High [VH]
52

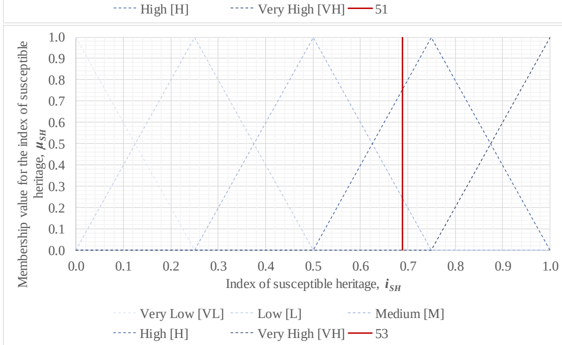
Membership value for the index of susceptible heritage, μ_{SH}
Index of susceptible heritage, i_{SH}
Very Low [VL]
Low [L]
Medium [M]
High [H]
Very High [VH]
53

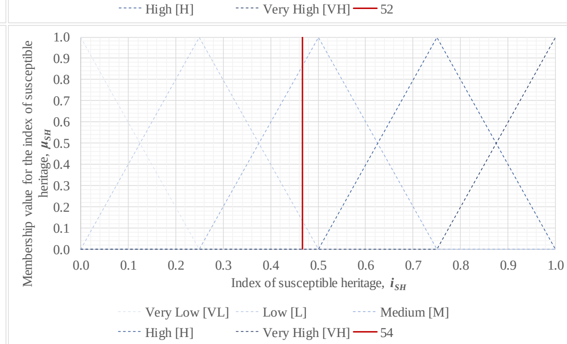
Membership value for the index of susceptible heritage, μ_{SH}
Index of susceptible heritage, i_{SH}
Very Low [VL]
Low [L]
Medium [M]
High [H]
Very High [VH]
54

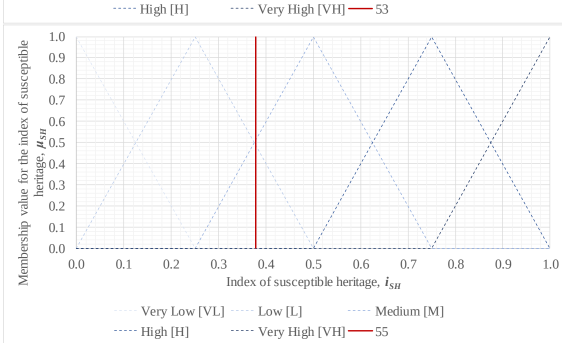
Membership value for the index of susceptible heritage, μ_{SH}
Index of susceptible heritage, i_{SH}
Very Low [VL]
Low [L]
Medium [M]
High [H]
Very High [VH]
55

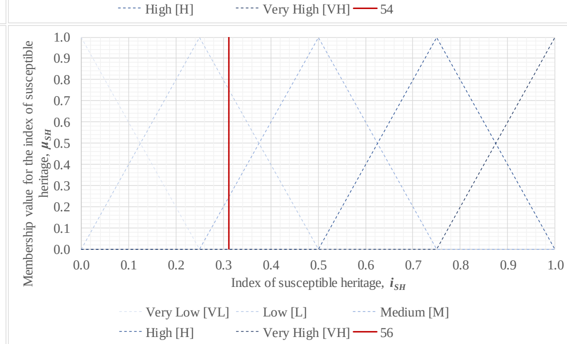
Membership value for the index of susceptible heritage, μ_{SH}
Index of susceptible heritage, i_{SH}
Very Low [VL]
Low [L]
Medium [M]
High [H]
Very High [VH]
56

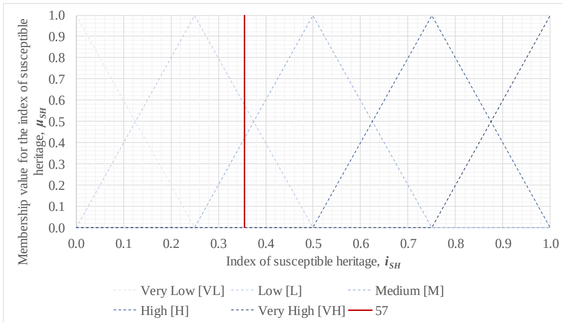
Membership value for the index of susceptible heritage, μ_{SH}
Index of susceptible heritage, i_{SH}
Very Low [VL]
Low [L]
Medium [M]
High [H]
Very High [VH]
57

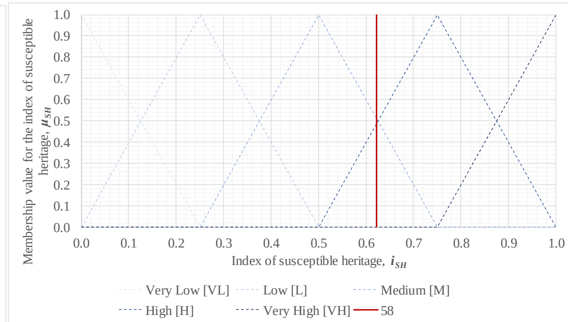
Membership value for the index of susceptible heritage, μ_{SH}
Index of susceptible heritage, i_{SH}
Very Low [VL]
Low [L]
Medium [M]
High [H]
Very High [VH]
58

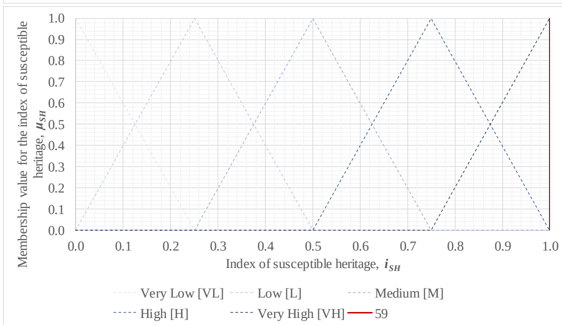
Membership value for the index of susceptible heritage, μ_{SH}
Index of susceptible heritage, i_{SH}
Very Low [VL]
Low [L]
Medium [M]
High [H]
Very High [VH]
59

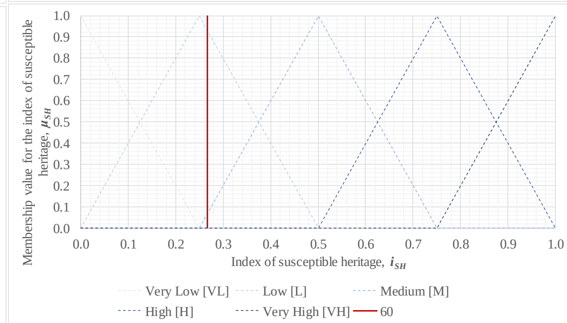
Membership value for the index of susceptible heritage, μ_{SH}
Index of susceptible heritage, i_{SH}
Very Low [VL]
Low [L]
Medium [M]
High [H]
Very High [VH]
60

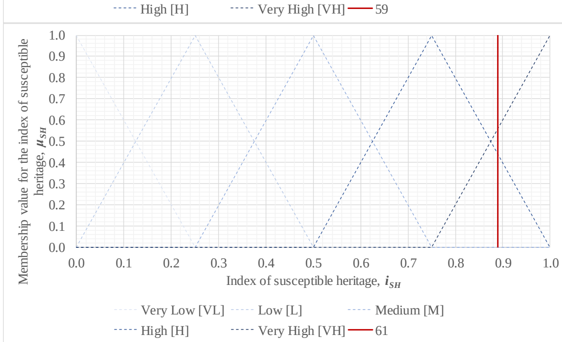
Membership value for the index of susceptible heritage, μ_{SH}
Index of susceptible heritage, i_{SH}
Very Low [VL]
Low [L]
Medium [M]
High [H]
Very High [VH]
61

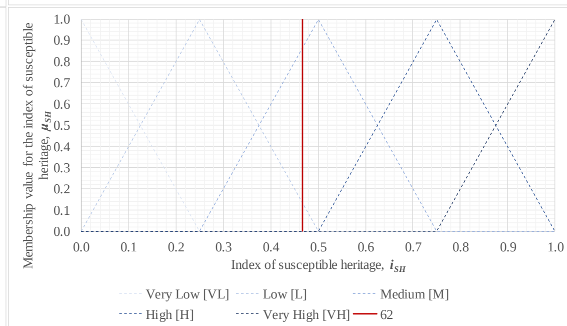
Membership value for the index of susceptible heritage, μ_{SH}
Index of susceptible heritage, i_{SH}
Very Low [VL]
Low [L]
Medium [M]
High [H]
Very High [VH]
62

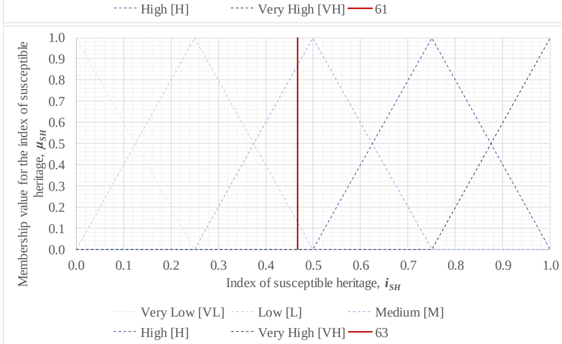
Membership value for the index of susceptible heritage, μ_{SH}
Index of susceptible heritage, i_{SH}
Very Low [VL]
Low [L]
Medium [M]
High [H]
Very High [VH]
63

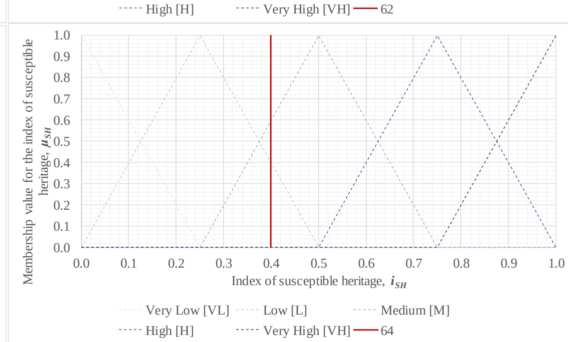
Membership value for the index of susceptible heritage, μ_{SH}
Index of susceptible heritage, i_{SH}
Very Low [VL]
Low [L]
Medium [M]
High [H]
Very High [VH]
64

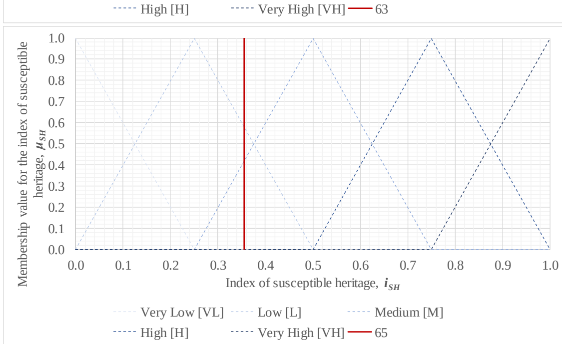
Membership value for the index of susceptible heritage, μ_{SH}
Index of susceptible heritage, i_{SH}
Very Low [VL]
Low [L]
Medium [M]
High [H]
Very High [VH]
65

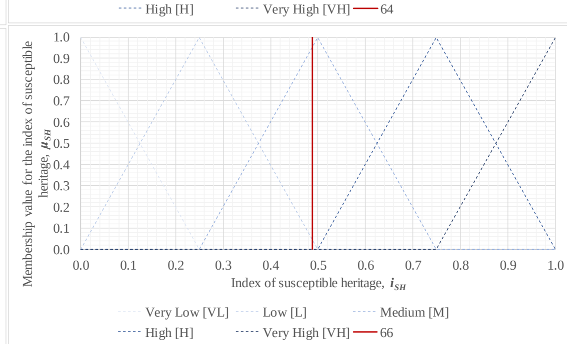
Membership value for the index of susceptible heritage, μ_{SH}
Index of susceptible heritage, i_{SH}
Very Low [VL]
Low [L]
Medium [M]
High [H]
Very High [VH]
66

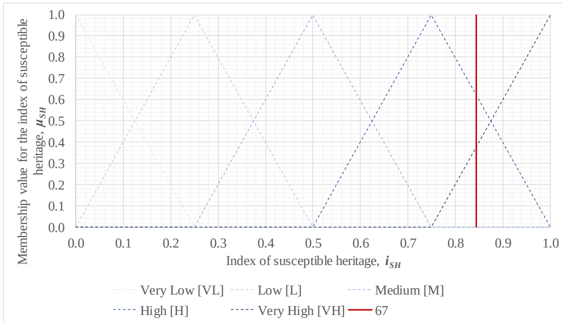
Membership value for the index of susceptible heritage, μ_{SH}
Index of susceptible heritage, i_{SH}
Very Low [VL]
Low [L]
Medium [M]
High [H]
Very High [VH]
67

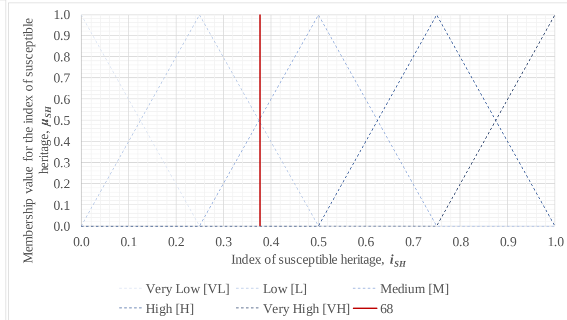
Membership value for the index of susceptible heritage, μ_{SH}
Index of susceptible heritage, i_{SH}
Very Low [VL]
Low [L]
Medium [M]
High [H]
Very High [VH]
68

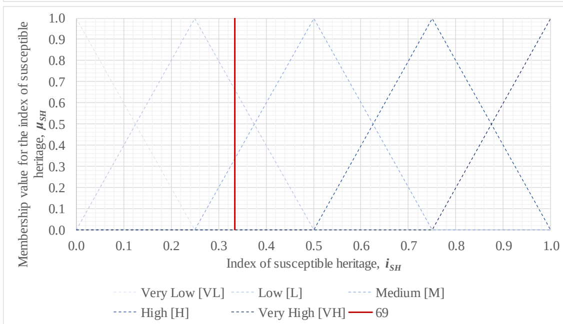
Membership value for the index of susceptible heritage, μ_{SH}
Index of susceptible heritage, i_{SH}
Very Low [VL]
Low [L]
Medium [M]
High [H]
Very High [VH]
69

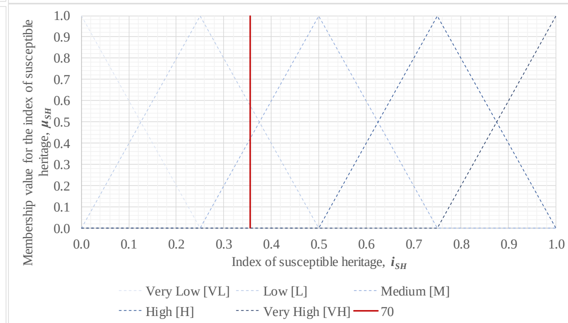
Membership value for the index of susceptible heritage, μ_{SH}
Index of susceptible heritage, i_{SH}
Very Low [VL]
Low [L]
Medium [M]
High [H]
Very High [VH]
70

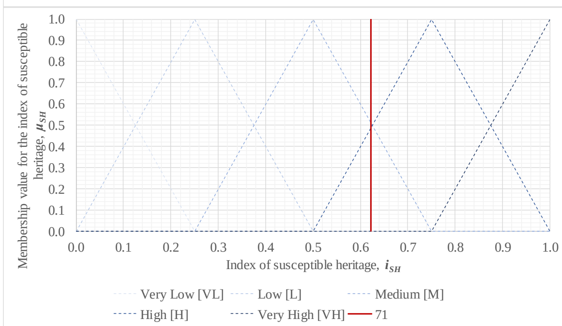
Membership value for the index of susceptible heritage, μ_{SH}
Index of susceptible heritage, i_{SH}
Very Low [VL]
Low [L]
Medium [M]
High [H]
Very High [VH]
71

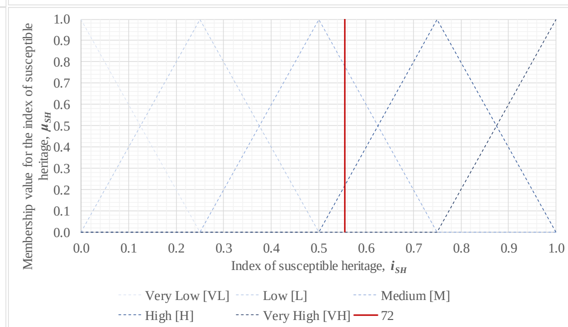
Membership value for the index of susceptible heritage, μ_{SH}
Index of susceptible heritage, i_{SH}
Very Low [VL]
Low [L]
Medium [M]
High [H]
Very High [VH]
72

APPENDIX E:

MECHANICAL PROPERTIES AND CORRECTIVE COEFFICIENTS FOR EACH URM TYPE

The mechanical properties' range and the corrective coefficients proposed by the Italian Standards for Construction and its commentary for the assessment of different existing URM types are listed in Table E.1 and Table E.2.

TABLE E.1

MECHANICAL PROPERTIES OF DIFFERENT URM TYPES. VALUES ADOPTED BY THE ITALIAN TECHNICAL STANDARD FOR CONSTRUCTION (NTC, 2018) AND ITS COMMENTARY (C.S.LL.PP. 2019)

URM type	f'_m **[MPa]**	c **[MPa]**	E_m **[MPa]**	G_m **[MPa]**	**w [kN/m^3]**
	min – max	**min – max**	**min – max**	**min – max**	
Rubble stones	1.0 – 2.0	0.018 – 0.032	690 – 1050	230 – 350	19
Hewn ashlar, with non-homogenous leaves	2.0	0.035 – 0.051	1020 – 1440	340 – 480	20
Split stones with good texture	2.6 – 3.8	0.056 – 0.074	1500 – 1980	500 – 660	21
Irregular masonry with soft stone blocks (tuff, calcarenite, etc.)	1.4 – 2.2	0.028 – 0.042	900 – 1260	300 – 420	13 – 16
Regular masonry with soft stone blocks (tuff, calcarenite, etc.)	2.0 – 3.2	0.04 – 0.08	1200 – 1620	400 – 500	
Squared stone blocks	5.8 – 8.2	0.09 – 0.12	2400 – 3300	800 – 1100	22
Solid fired clay bricks with lime mortar	2.6 – 4.3	0.05 – 0.13	1200 – 1800	400 – 600	18
Semi-solid fired clay bricks with cement mortar	5.0 – 8.0	0.08 – 0.17	3500 – 5600	875 – 1400	15

TABLE E.2

MAXIMUM CORRECTIVE COEFFICIENTS FOR DIFFERENT URM TYPES. VALUES ADOPTED BY THE ITALIAN TECHNICAL STANDARD FOR CONSTRUCTION (NTC, 2018) AND ITS COMMENTARY (C.S.LL.PP. 2019)

URM type	State of the art			Consolidation intervention			
	Good Mortar (c_1)	**Regular horizontal joints (c_2)**	**Leaves connectors (c_3)**	**Binding Mixture Injections (c_4)**	**Reinforced Plaster (c_5)**	**Reinforced joints and leaves connections (c_6)**	**Maximum coefficient (c_{max})**
Rubble stones	1.5	1.3	1.5	2.0	2.5	1.6	3.5
Hewn ashlar, with non-homogenous leaves	1.4	1.2	1.5	1.7	2.0	1.5	3.0
Split stones with good texture	1.3	1.1	1.3	1.5	1.5	1.4	2.4
Irregular masonry with soft stone blocks (tuff, calcarenite, etc.)	1.5	1.2	1.3	1.4	1.7	1.1	2.0
Regular masonry with soft stone blocks (tuff, calcarenite, etc.)	1.6	-	1.2	1.2	1.5	1.2	1.8
Squared stone blocks	1.2	-	1.2	1.2	1.2	-	1.4
Solid fired clay bricks with lime mortar	-	-	1.3	1.2	1.5	1.2	1.8
Semi-solid fired clay bricks with cement mortar	1.2	-	-	-	1.3	-	1.3

According to the MIT (2018, 2019), the coefficients listed in Table E.2 should be applied to the basic mechanical material properties (Table E.1) accordingly with the following criteria:

- The coefficient c_1 can be applied both to the strengths (f'_m and c) and to the elastic moduli (E_m and G_m);
- The coefficient c_2 can be applied only to the strengths (f'_m and c);

- The coefficient c_3 can be applied only to the strengths (f'_m and c);
- The coefficient c_4 can be applied both to the strengths (f'_m and c) and to the elastic moduli (E_m and G_m), but the benefit might be neglected if the original mortar has a good quality;
- The coefficient c_5 can be applied both to the strengths (f'_m and c) and to the elastic moduli (E_m and G_m), but the benefit might be neglected if the wall has widespread leaves connectors;
- The coefficient c_6 can be fully applied to the strengths (f'_m and c) and with a 50% reduction to the elastic moduli (E_m and G_m), but the benefit might be neglected if reinforced plaster is applied to the wall; and
- More than one coefficient might be applied to the same URM type without exceeding the maximum increment c_{max}.

APPENDIX F:

CRITERIA TO DETERMINE THE MASONRY QUALITY INDEX

The criteria used to convert the qualitative outcomes of the assessment (i.e, NF, PF, and F) into numerical values to be applied in Equation 3.1 to determine the *MQI* are listed in Table F.1.

TABLE F.1

NUMERICAL VALUES FOR DETERMINING THE MQI. VALUES ADOPTED FROM BORRI, ET AL. (2015)

Parameter	**Vertical loading (*V*)**			**Horizontal in-plane loading (*I*)**			**Horizontal out-of-plane loading (*O*)**		
	NF	***PF***	***F***	***NF***	***PF***	***F***	***NF***	***PF***	***F***
SM	0.3	0.7	1.0	0.3	0.7	1.0	0.5	0.7	1.0
SD	0	0.5	1.0	0	0.5	1.0	0	0.5	1.0
SS	0	1.5	3.0	0	1.0	2.0	0	1.0	2.0
WC	0	1.0	1.0	0	1.0	2.0	0	1.5	3.0
HJ	0	1.0	2.0	0	0.5	1.0	0	1.0	2.0
VJ	0	0.5	1.0	0	1.0	2.0	0	0.5	1.0
MM	0	0.5	2.0	0	1.0	2.0	0	0.5	1.0

TABLE F.2

MASONRY CATEGORIES AS A FUNCTION OF THE MQI. VALUES ADOPTED FROM BORRI ET AL. (2015)

Loading direction	**URM category**		
	A	***B***	***C***
Vertical loading (*V*)	$10 \geq MQI > 5$	$5 \geq MQI > 2.5$	$2.5 \geq MQI \geq 0$
In-plane loading (*I*)	$10 \geq MQI > 5$	$5 \geq MQI > 3$	$3 \geq MQI \geq 0$
Out-of-plane loading (*O*)	$10 \geq MQI > 7$	$7 \geq MQI > 4$	$4 \geq MQI \geq 0$

The *MQI* may be also used for a qualitative classification of the macroblock behavior with respect to the direction of loading (Table F.2), which might have applications in qualitative risk assessment. Basing on the response to the different loading direction, three URM categories were identified: 1) good response, *A*; 2) response of average quality, *B*; and 3) inadequate response, *C*.

APPENDIX G:

COLLECTED DATA FOR EACH NON-DESTRUCTIVE TESTING (NDT) TECHNIQUE

TABLE G.1

COLLECTED DATA FOR 20 URM SPECIMENS FOR URM TYPE: RUBBLE STONES

URM type: Rubble stones					
Specimen #	**Church #**	**Macroblock**	**Masonry quality index, (*MQI*)**	**Pulse indirect velocity, v_i [m/s]**	**Rebound number, *R***
1	8	Bell Tower	5.950	975.000	39.000
2	18	Facade	0.250	959.600	44.308
3	31	Lateral Wall	2.100	1691.800	25.625
4	34	Apse	1.225	1846.600	30.313
5		Bell Tower	1.050	1149.400	32.813
6	36	Lateral Wall	1.750	2010.333	33.625
7	43	Lateral Wall	2.975	1496.667	38.375
8		Apse	2.450	1241.250	31.000
9	44	Lateral Wall	3.150	1070.250	24.250
10		Bell Tower	2.975	1223.333	35.750
11	47	Bell Tower	4.500	2754.333	46.313
12	55	Bell Tower	1.750	1696.250	30.313
13	56	Facade	3.188	1639.400	37.938
14		Lateral Wall	3.500	1847.333	42.750
15	62	Lateral Wall	2.000	1005.500	42.750
16	65	Lateral Wall	6.500	2234.250	47.875
17	66	Bell Tower	1.125	1053.667	26.563
18	67	Apse	1.500	750.333	19.125
19	69	Facade	1.050	999.750	31.875
20		Lateral Wall	1.050	1237.333	32.375

TABLE G.2

COLLECTED DATA FOR 41 URM SPECIMENS FOR URM TYPE: SPLIT STONES WITH GOOD TEXTURE

URM type: split stones with good texture					
Specimen #	**Church #**	**Macroblock**	**Masonry quality index, (*MQI*)**	**Pulse indirect velocity, v_i [m/s]**	**Rebound number, *R***
1	5	Bell Tower	5.100	1392.000	38.875
2	13	Lateral Wall	8.000	2246.000	50.750
3	16	Bell Tower	5.500	1521.600	44.250
4	18	Facade	6.500	2907.200	44.375
5	29	Bell Tower	4.250	1753.167	30.875
6		Bell Tower	4.250	1199.667	44.688
7	31	Chapels	2.450	1697.333	27.813
8		Bell Tower	4.375	2354.333	23.813
9	34	Lateral Wall	4.025	2142.000	32.063
10		Transept	4.888	1717.000	38.313
11	35	Bell Tower	4.000	1843.000	48.313
12	36	Facade	5.600	2523.750	32.625
13	39	Lateral Wall	6.750	2297.000	41.688
14		Apse	5.738	2300.800	35.750
15		Chapels	5.738	1587.500	33.875
16	43	Bell Tower	5.000	1565.000	33.313
17	44	Facade	2.975	1295.667	35.750
18		Facade	1.750	2006.000	27.125
19	47	Facade	7.000	1865.333	55.313
20		Lateral Wall	7.000	2218.333	56.688
21	48	Facade	3.825	1280.000	38.500
22		Lateral Wall	3.150	1256.667	32.875
23		Chapels	3.150	1281.667	35.938
24	50	Facade	6.500	1328.000	40.250
25		Lateral Wall	4.550	1293.667	33.375
26	51	Facade	5.525	1158.000	38.750
27		Lateral Wall	4.550	1309.750	31.750
28		Apse	2.250	1238.667	24.188
29	52	Facade	9.000	2424.333	55.625
30		Lateral Wall	9.000	2243.333	50.188
31		Nave	9.000	2785.333	48.563

TABLE G.2 (CONTINUED)

URM type: split stones with good texture					
Specimen #	**Church #**	**Macroblock**	**Masonry quality index, (*MQI*)**	**Pulse indirect velocity, v_i [m/s]**	**Rebound number, *R***
32		Triumphal Arch	9.000	2184.000	49.250
33		Bell Tower	8.500	2332.000	41.188
34	54	Facade	5.000	1935.333	53.563
35		Lateral Wall	8.000	3230.250	51.000
36		Apse	8.000	2220.667	51.625
37		Bell Tower	8.000	1768.500	47.188
38	55	Apse	1.575	1927.750	18.313
39		Chapels	3.676	1079.333	23.875
40	57	Apse	2.125	505.000	38.625
41		Bell Tower	4.750	1971.000	40.938

TABLE G.3

COLLECTED DATA FOR 75 URM SPECIMENS FOR URM TYPE: SQUARED STONE BLOCKS

URM type: squared stone blocks					
Specimen #	**Church #**	**Macroblock**	**Masonry quality index, (*MQI*)**	**Pulse indirect velocity, v_i [m/s]**	**Rebound number, *R***
1	2	Facade	8.500	2543.000	54.438
2	3	Facade	9.500	2312.333	48.875
3		Bell Tower	6.800	1635.333	38.063
4		Nave	9.500	4479.000	47.594
5		Triumphal Arch	10.000	2760.000	44.000
6	4	Nave	10.000	2276.667	40.813
7		Nave	10.000	5367.667	54.188
8		Chapels	10.000	2383.333	45.688
9		Bell Tower	9.500	6229.500	40.313
10	5	Nave	10.000	2424.333	45.500
11		Transept	10.000	2539.333	45.000

TABLE G.3 (CONTINUED)

URM type: squared stone blocks					
Specimen #	**Church #**	**Macroblock**	**Masonry quality index, (*MQI*)**	**Pulse indirect velocity, v_i [m/s]**	**Rebound number, *R***
12		Triumphal Arch	10.000	2635.667	48.438
13		Chapels	10.000	2274.667	45.500
14	6	Facade	8.500	1399.750	41.125
15		Facade	8.500	1581.000	40.313
16		Lateral Wall	7.225	1921.750	37.125
17		Nave	10.000	4214.750	41.688
18		Triumphal Arch	8.500	2794.000	47.438
19		Apse	8.500	2389.500	43.188
20		Bell Tower	5.000	1407.400	43.313
21	9	Bell Tower	6.800	1505.500	37.500
22	11	Lateral Wall	9.500	2617.333	52.250
23	12	Facade	9.500	3214.000	52.750
24	13	Triumphal Arch	10.000	1486.667	47.471
25	14	Nave	10.000	3091.000	42.813
26		Triumphal Arch	10.000	3724.250	45.375
27		Bell Tower	8.500	1811.333	41.063
28	15	Chapels	10.000	2723.500	49.375
29		Bell Tower	8.000	1285.667	47.875
30	16	Facade	4.900	1274.750	33.188
31		Nave	7.000	1188.000	47.063
32		Nave	10.000	2898.600	43.938
33		Triumphal Arch	10.000	3635.333	49.250
34	17	Nave	10.000	4670.400	53.500
35		Triumphal Arch	5.000	1267.333	22.875
36	19	Lateral Wall	6.800	1252.000	39.813
37		Chapels	8.500	1441.600	49.375
38	20	Bell Tower	7.225	1667.333	34.688
39	27	Bell Tower	8.500	2071.800	40.000
40	28	Bell Tower	6.300	1984.167	30.250
41	31	Facade	10.000	3106.600	42.375
42		Nave	10.000	2924.600	52.500
43	32	Facade	10.000	3158.000	47.375
44	34	Facade	7.000	1606.667	34.250
45	35	Facade	9.000	3711.667	52.313
46	36	Nave	10.000	2024.000	47.125

TABLE G.3 (CONTINUED)

URM type: squared stone blocks					
Specimen #	**Church #**	**Macroblock**	**Masonry quality index, (*MQI*)**	**Pulse indirect velocity, v_i [m/s]**	**Rebound number, *R***
47		Chapels	3.825	1559.000	33.875
48	37	Bell Tower	10.000	2424.333	46.438
49	38	Facade	9.500	2299.800	47.000
50		Lateral Wall	9.500	2227.000	41.375
51		Transept	6.375	1787.250	39.313
52		Bell Tower	6.650	2166.333	31.563
53	39	Facade	7.225	2403.333	34.750
54		Nave	6.650	1594.600	30.375
55		Triumphal Arch	6.650	1499.200	32.875
56	40	Facade	9.250	2842.500	40.938
57		Lateral Wall	9.250	3102.500	39.813
58		Transept	9.250	3034.000	41.063
59	57	Facade	9.500	2084.600	54.500
60		Lateral Wall	9.500	1853.250	53.063
61		Chapels	9.500	2602.667	56.563
62	59	Facade	6.825	1159.750	28.188
63	60	Facade	8.500	2167.000	52.813
64		Lateral Wall	7.750	1873.000	49.000
65	61	Lateral Wall	5.000	1121.143	48.188
66		Nave	8.500	1174.667	43.313
67		Bell Tower	8.000	2908.000	50.813
68	62	Facade	7.000	1681.000	34.063
69	65	Facade	9.500	1619.000	53.188
70		Nave	6.500	1785.667	47.500
71	67	Triumphal Arch	2.550	1057.333	20.375
72	68	Bell Tower	2.850	618.667	13.500
73	70	Facade	5.000	1638.667	23.250
74		Bell Tower	2.400	1429.333	17.875
75	72	Triumphal Arch	2.850	1889.000	19.563

TABLE G.3 (CONTINUED)

TABLE G.4

COLLECTED DATA FOR 34 URM SPECIMENS FOR URM TYPE: SOLID FIRED CLAY BRICKS WITH LIME MORTAR

URM type: Solid fired clay bricks with lime mortar					
Specimen #	**Church #**	**Macroblock**	**Masonry quality index, (*MQI*)**	**Pulse indirect velocity, v_i [m/s]**	**Rebound number, *R***
1	18	Facade	5.100	1160.000	35.813
2		Lateral Wall	6.125	1127.600	34.688
3	19	Lateral Wall	6.800	1252.000	39.813
4		Apse	5.600	1010.600	34.643
5		Bell Tower	5.950	1092.667	38.063
6	21	Bell Tower	6.125	1277.333	33.625
7	25	Lateral Wall	5.600	822.600	34.417
8		Bell Tower	6.800	1646.000	37.200
9	26	Bell Tower	2.800	1469.000	33.813
10	28	Bell Tower	5.250	1321.600	28.813
11	30	Bell Tower	5.775	849.200	33.176
12	32	Facade	6.650	1278.333	32.500
13	36	Lateral Wall	3.150	1831.333	34.313
14	37	Facade	5.250	1068.667	29.875
15		Lateral Wall	6.800	1530.000	36.813
16		Transept	8.000	1343.333	41.750
17	41	Facade	8.075	2196.000	39.438
18	43	Facade	9.500	2211.000	41.063
19	45	Facade	8.075	1530.000	37.500
20		Lateral Wall	9.500	1917.000	39.063
21		Bell Tower	6.800	2046.667	36.188
22	46	Facade	8.075	1530.167	37.875
23		Lateral Wall	6.650	1393.500	32.469
24		Lateral Wall	6.650	1739.833	34.344
25	49	Facade	6.375	1153.667	34.938
26		Lateral Wall	6.375	1277.667	35.125

TABLE G.4 (CONTINUED)

URM type: Solid fired clay bricks with lime mortar					
Specimen #	**Church #**	**Macroblock**	**Masonry quality index, (*MQI*)**	**Pulse indirect velocity, v_i [m/s]**	**Rebound number, *R***
27		Chapels	6.375	1533.000	36.750
28		Bell Tower	8.075	1694.000	35.875
29	52	Apse	6.300	1292.000	32.000
30		Chapels	9.000	1400.667	44.063
31	53	Facade	9.500	2040.000	39.188
32	58	Facade	8.000	2362.000	43.250
33		Lateral Wall	6.800	1303.000	39.250
34	59	Facade	6.475	1415.667	33.438

APPENDIX H:

RESULTING URM MECHANICAL PROPERTIES

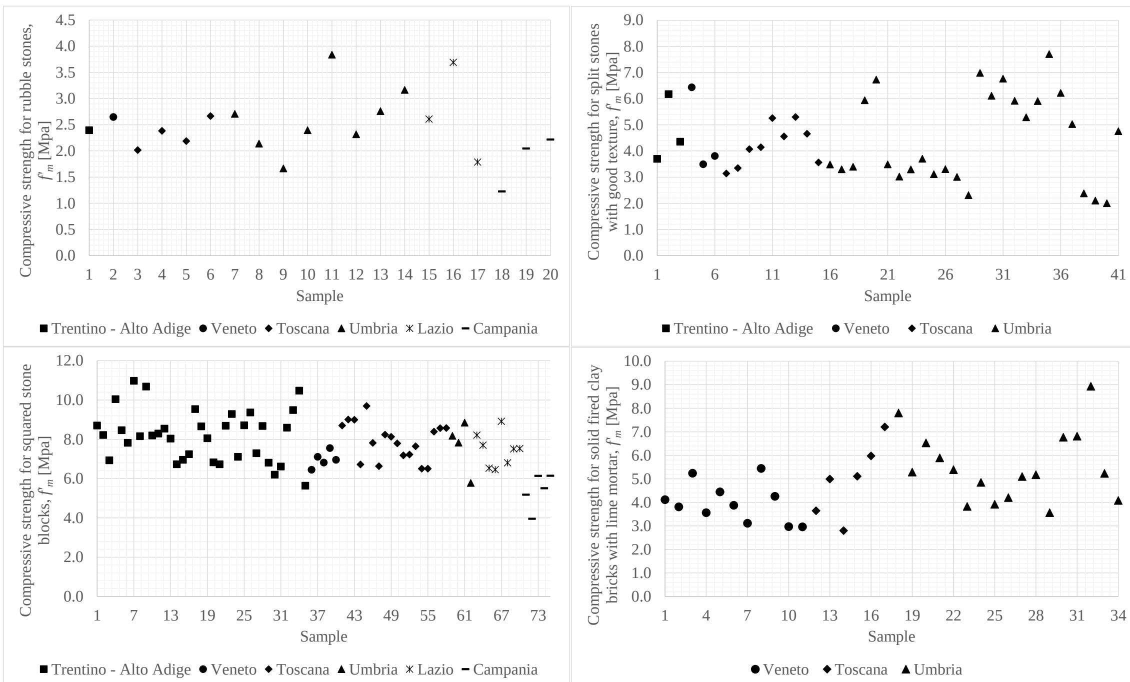

Figure H.1: Compressive strength, f'$_m$, grouped by URM type and region.

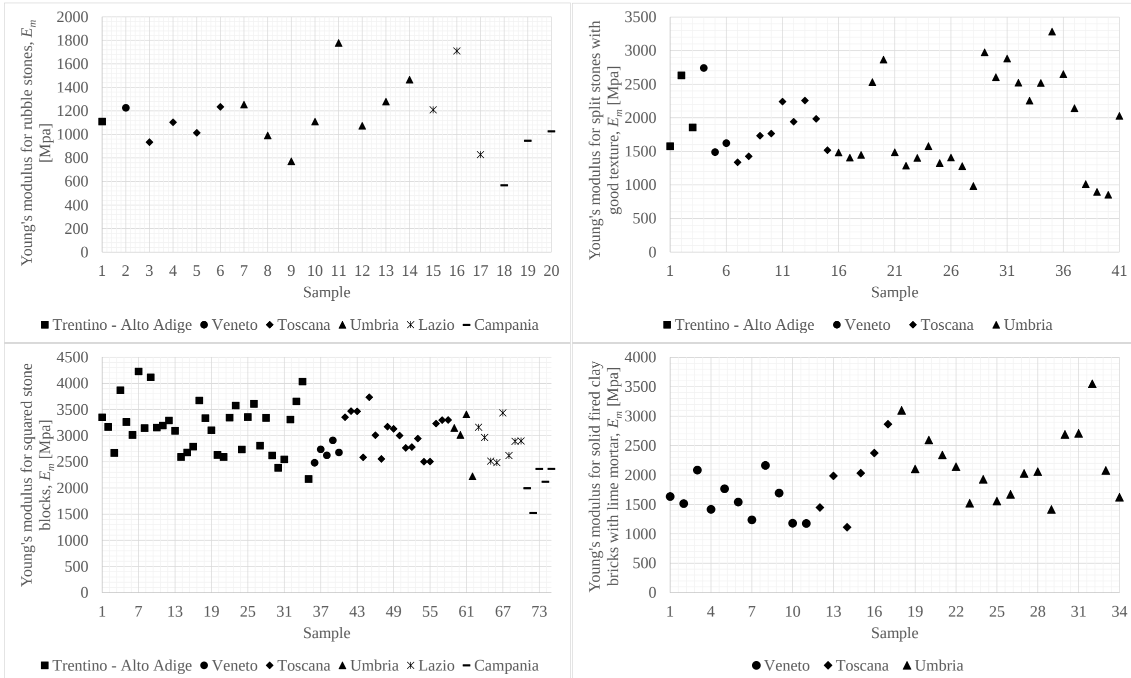

Figure H.2: Young's modulus, E_m, grouped by URM type and region.

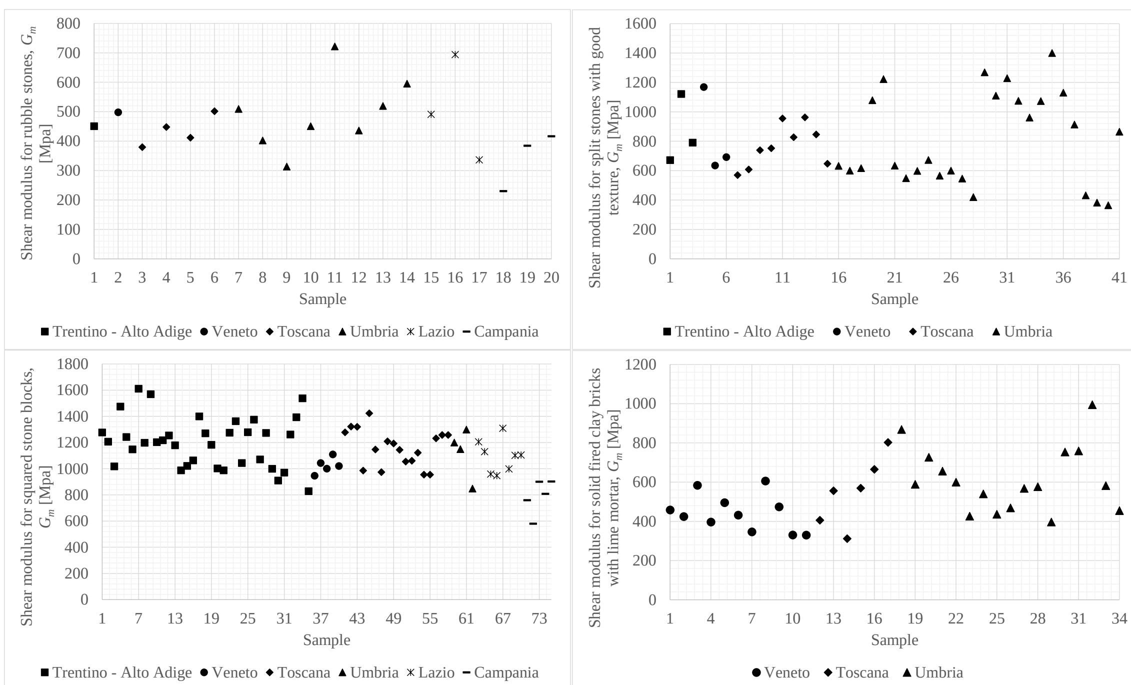

Figure H.3: Shear modulus, G_m, grouped by URM type and region.

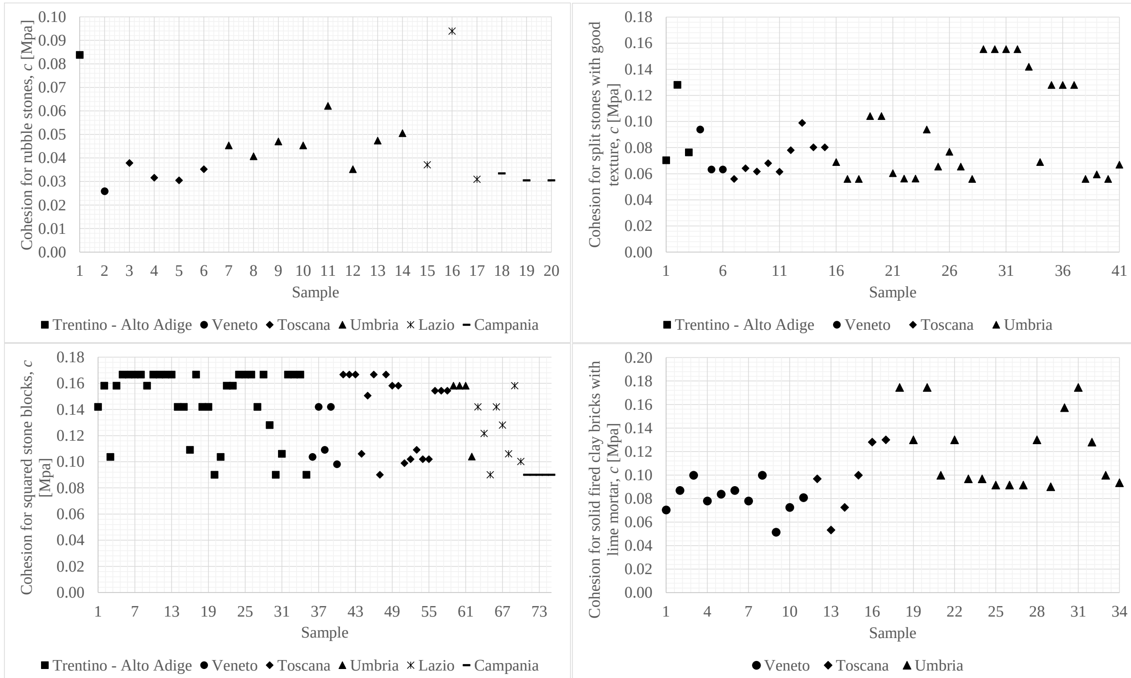

Figure H.4: Cohesion, c, grouped by URM type and region.

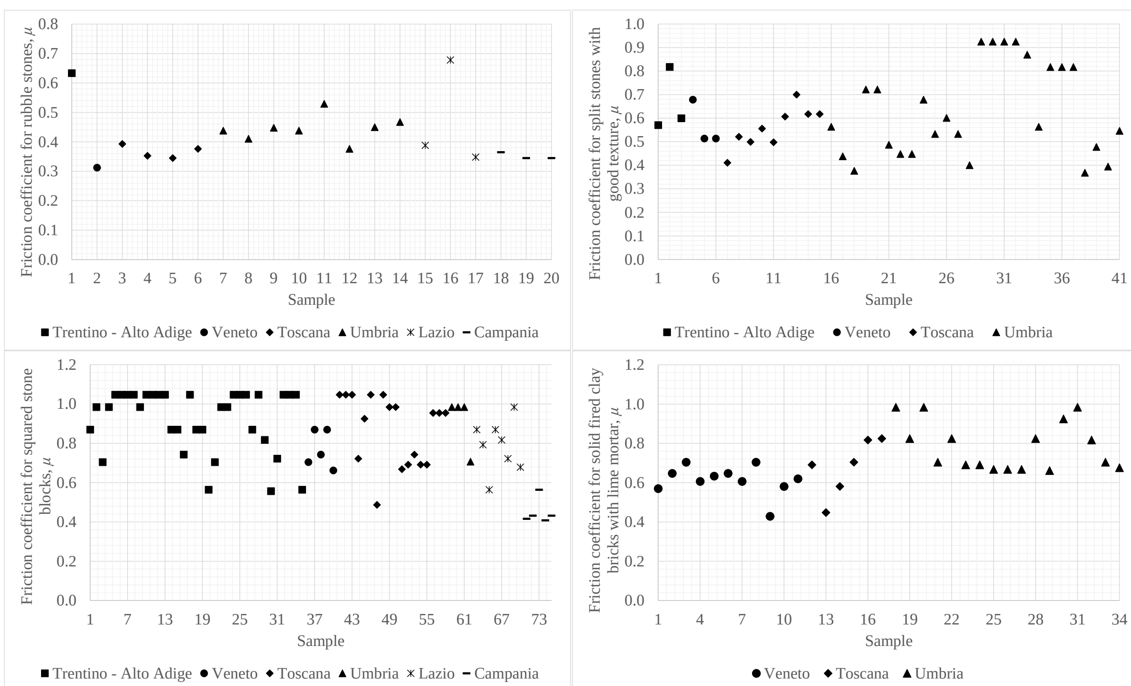

Figure H.5: Friction coefficient, μ, grouped by URM type and region.

BIBLIOGRAPHY

Abeling, S. R., S. Vallis, T. Goded, S. Giovinazzi, and J.M. Ingham. 2018. Seismic Risk Assessment of New Zealand URM Church. Paper presented at the 10th Australian Masonry Conference. Sydney, Australia, February 12-14.

Abrams, D. P., O. AlShawa, P. B. Lourenço, and L. Sorrentino. 2007. Out-of-plane seismic response of unreinforced masonry walls: conceptual discussion, research needs, and modeling issues. *International Journal of Architectural Heritage* 11(1): 22-30.

Achille, C., A. Adami, S. Chiarini, S. Cremonesi, F. Fassi, L. Fregonese, and L. Taffurelli. 2015. UAV-Based Photogrammetry and Integrated Technologies for Architectural Applications - Methodological Strategies for the After-Quake Survey of Vertical Structures in Mantua (Italy). *Sensor* 15(7): 15520-15539.

ACI (American Concrete Society) Committee, and International Organization for Standardization. 2019. *Building code requirement for structural concrete (ACI 318-19)*. American Concrete Institute.

Adam, J. P., M. P. Guidobaldi, M. Torelli, and M. Torelli. (1984). *L'arte di costruire presso i Romani: materiali e tecniche.* Milano (Italy): Longanesi.

Agenzia delle Entrate. Banca dati delle quotazioni immobiliari. Accessed September 8, 2019. https://wwwt.agenziaentrate.gov.it/servizi/Consultazione/ricerca.htm.

Altman, C. F. 1980. The medieval marquee: Church portal sculpture as publicity. *The Journal of Popular Culture* 14(1): 37-46.

American Society of Civil Engineers. 2017. ASCE 41-17. *Seismic Evaluation and Retrofit of Existing Buildings*. Reston, VA: ASCE.

American Society for Testing and Materials. 2016. *"ASTM C597-2." Standard Test Method for Pulse Velocity Through Concrete.* USA: ASTM.

American Society for Testing and Materials. 2018. *"ASTM C805/C805M." Standard Test Method for Rebound Number of Hardened Concrete.* USA: ASTM.

Angjeliu, G., D. Coronelli, and G. Cardani. 2018. Structural modelling of complex historic masonry buildings. Paper presented at the 10th International Masonry Conference. Milan, Italy, July 9-11.

Arduini, M., A. Di Leo, and G. Pascale. 1994. Experimental methods for on site evaluation of the mechanical properties of masonry. Paper presented at the Tenth International Brick & Block Masonry Conference. Calgary, Canada, July 5-7.

Aydın, F., and M. Saribiyik. 2010. Correlation between Schmidt Hammer and destructive compressions testing for concretes in existing buildings. *Scientific Research and Essays* 5(13): 1644-1648.

Bakhteri, J., A. M. Makhtar, and S. Sambasivam. 2004. Finite element modelling of structural clay brick masonry subjected to axial compression. *Jurnal Teknologi* 41(1): 57-68.

Basaglia, A., A. Aprile, E. Spacone, and F. Pilla. 2018. Performance-based seismic risk assessment of urban systems. *International Journal of Architectural Heritage* 12(7-8): 1131-1149.

Benvenuti, A., and M. Simonotti. 2005. Incidenza dell'area in un segmento di mercato immobiliare. *Estimo e territorio* 12: 7-11.

Binda, L., A. Saisi, and C. Tedeschi. 2006. Masonry. In *Fracture and failure of natural building stones*, ed. S. K. Kourkoulis, 167-182. Dordrecht, Netherland: Springer.

Bosiljkov, V. Z., Y. Z. Totoev, and J. M. Nichols. 2005. Shear modulus and stiffness of brickwork masonry: an experimental perspective. *Structural Engineering and Mechanics* 20(1): 21-44.

Borri, A., M. Corradi, G. Castori, and A. De Maria. 2015. A method for the analysis and classification of historic masonry. *Bulletin of Earthquake Engineering* 13(9): 2647-2665.

Brotons, V., R. Tomás, S. Ivorra, and A. Grediaga. 2014. Relationship between static and dynamic elastic modulus of calcarenite heated at different temperatures: the San Julián's stone. *Bulletin of Engineering Geology and the Environment* 73(3): 791-799.

Brozovsky, J. (2013). Use of non-destructive ultrasonic pulse testing methods in evaluation of brick parameters. In *Proceedings of the 3rd International Conference on Sustainable Construction Materials & Technologies (SCMT'13)*, ed. P. Claisse, E. Ganjian, and T. Naik, 1-10. Coventry, UK: Coventry University.

Cagnana, A. 1997. La transizione al Medioevo attraverso la storia delle tecniche murarie: dall'analisi di un territorio ad un problema sovraregionale. In *I Congresso Nazionale di Archeologia Medievale*, ed. S. Gelichi, 445-448. Pisa, Italy: All'Insegna del Giglio.

CCIAA (Camera di Commercio, Industria, Artigianato e Agricoltura). Borsino Immobiliare. Last Modified June 22, 2020. Accessed September 9, 2019. https://www.borsinoimmobiliare.it/.

Chiesa Cattolica. BeWeb. Last Modified April 24, 2020. Accessed October 21, 2018. https://beweb.chiesacattolica.it/edificidiculto/.

Chiesa Cattolica. Diocesi e Parrocchie. Accessed June 2, 2019. https://www.chiesacattolica.it/annuario-cei/regioni-diocesi-e-parrocchie/.

Cimellaro, G. P., I. P. Christovasilis, A. M. Reinhorn, A. De Stefano, and T. Kirova. 2010. L'Aquila earthquake of April 6, 2009 in Italy: Rebuilding a resilient city to withstand multiple hazards. Technical Report MCEER-10-0010, MCEER (Multidisciplinary Center for Earthquake Engineering Research), Buffalo, NY.

Ciuna, M. 2010. L'Allocation Method nella stima delle aree edificabili. Aestimum 57(171): 171-184.

Conde, B., L. F. Ramos, D. V. Oliveira, B. Riveiro, and M. Solla. 2017. Structural assessment of masonry arch bridges by combination of non-destructive testing techniques and three-dimensional numerical modelling: Application to Vilanova bridge. *Engineering structures* 148: 621-638.

Cosenza, E., and G. Manfredi. 2000. Damage indices and damage measures. *Progress in Structural Engineering and Materials* 2(1): 50-59.

Cundall, P. A. 1971. A computer model for simulating progressive, large scale movements in blocky rock systems. In *Proceedings of the international symposium on rock fractures*, ed. Rubrecht, 1-12. Nancy, France: International Society for Rock Mechanics.

da Porto, F., B. Silva, C. Costa, and C. Modena. 2012. Macro-scale analysis of damage to churches after earthquake in Abruzzo (Italy) on April 6, 2009. *Journal of Earthquake Engineering* 16(6): 739-758.

Daftry, S., C. Hoppe, and H. Bischof. 2015. Building with Drones: Accurate 3D Facade Reconstruction using MAVs. Paper presented at the IEEE International Conference on Robotics and Automation. Seattle, WA, May 26-30.

De Boer, A. 2010. *Design strategy structural concrete in 3D focusing on uniform force results and sequential analysis*. Delft, Netherlands: Delft University of Technology.

De Matteis, G., E. Criber, and G. Brando. 2016. Damage probability matrices for three-nave masonry churches in Abruzzi after the 2009 L'Aquila earthquake. *International Journal of Architectural Heritage* 10(2-3): 120-145.

De Matteis, G., G. Brando, V. Corlito, E. Criber, and M. Guadagnuolo. 2019. Seismic vulnerability assessment of churches at regional scale after the 2009 L'Aquila earthquake. *International Journal of Masonry Research and Innovation* 4(1-2): 174–96.

De Matteis, G., V. Corlito, M. Guadagnuolo, and A. Tafuro. 2019. Seismic Vulnerability Assessment and Retrofitting Strategies of Italian Masonry Churches of the Alife-Caiazzo Diocese in Caserta. *International Journal of Heritage Architecture*: 1-16.

Deng, X. Y., and T. P. Chang. 2006. Creating structural model from IFC-based architectural model. Paper presented at the Joint International Conference on Computing and Decision Making in Civil and Building Engineering. Montreal, Canada, June 14-16.

Dikmen, I., M. T. Birgonul, and S. Han. 2007. Using fuzzy risk assessment to rate cost overrun risk in international construction projects. *International Journal of Project Management* 25(5): 494-505.

Disposizioni concernenti la concessione di contributi finanziari della CEI per i beni culturali ecclesiastici e l'edilizia di culto e il relativo regolamento attuativo. CEI 5 Giugno 2018. Rome, Italy: CEI (Conferenza Episcopale Italiana), 2018.

Doglioni, F. 2000. *Codice di pratica (Linee Guida) per la progettazione degli interventi di riparazione, miglioramento sismico e restauro dei beni architettonici danneggiati dal terremoto umbro-marchigiano del 1997*. Ancona, Italy: Bollettino Ufficiale della Regione Marche (Tipolitografia DBS).

Doglioni, F., A. Moretti, and V. Petrini. 1994. *Le chiese e il territorio. Dalla vulnerabilità constatata nel terremoto del Friuli al miglioramento antisismico nel restauro. Verso una politica di prevenzione*. Trieste, Italy: Edizioni Lint.

Dong, W. 1987. Applications of fuzzy set theory in structural and earthquake engineering (Approximate reasoning, expert systems). PhD diss., Stanford University.

Drysdale, R., A. Hamid, and L. Baker. 1999. *Masonry Structures: Behavior and Design.* Boulder, Colorado: The Masonry Society.

European Committee for Standardization. 2005. *"EN 12504-4:2005." Testing concrete. Determination of the ultrasonic puls velocity*. Brussels, Belgium: European Committee for Standardization.

European Committee for Standardization. 2006. *"EN 1996-1-1:2006." Design of masonry structures - Part 1-1: General rules for reinforced and unreinforced masonry structures.* Brussels, Belgium: European Committee for Standardization.

European Committee for Standardization. 2012. *"EN 12504-2:2012." Testing concrete in structures - part 2: non-destructive testing - determination of rebound number*. Brussels, Belgium: European Committee for Standardization.

Faltynovà, M., E. Matouskovà, J. Sedina, and K. Pavelka. 2016. Building Facade Documentation Using Laser Scanning and Photogrammetry and Data

Implementation into BIM. *The International Archives of the Photogrammetry, Remote Sensing and Spatial Information Sciences* 41(B3): 215-220.

Federal Emergency Management Agency. 1999. *"FEMA 306." Evaluation of earthquake damaged concrete and masonry wall buildings, basic procedures manual, ATC-43*. Redwood City, CA: Applied Technology Council (ATC-43 Project).

Ferraiuolo, S. 1991. *La chiesa sorrentina e i suoi pastori*. Sorrento, Italy: Venerabile Congregazione dei Servi di Maria.

Fitchen, J. 1981. *The construction of Gothic cathedrals: a study of medieval vault erection.* Chicago, IL: University of Chicago Press.

Francis, A. J., C. B. Horman, and L. E. Jerrems. 1971. The effect of joint thickness and other factors on the compressive strength of brickwork. In *Proceedings of the second international brick masonry conference*, 31-37. Trent, UK: British Ceramic Research Association, and Stoke-on-Trent.

Frantzich, H. 1988. Risk and fire safety engineering. *Fire Safety Journal* 31(4): 313-329.

Galliani, B. 1832. *Dell'Architettura, Libri Dieci di M.Vitruvio Pollione.* Milano, Italy: A. Dozio.

Gàlvez, F., S. R. Abeling, K. Ip, S. Giovinazzi, D. Dizhur, and J. M. Ingham. 2018. Using themacro-element method to seismically assess complex URM buildings. Paper presented at the 10th Australian Masonry Conference. Sydney, Australia, February 12-14.

Gasparik, J. 1992. Prove non distruttive nell'edilizia. *Quaderno didattico AIPnD (Associazione Italiana Prove non Distruttive)*.

Giuffrè, A. 1989. Philological restoration of historical monuments. The cathedral of "Sant'Angelo dei Lombardi" in Irpinia. In *Structural Conservation of Stone Masonry. International Technical Conference*, ed. International Centre for the Study of the Preservation and the Restoration of Cultural Properties (ICCROM), 567-578. Athens, Greece: ICCROM.

Gloria, C. 1976. *Evoluzione storica dei leganti e dei conglomerati: dall'empirismo alla loro conoscenza razionale. Cemento: Storia, Tecnologia, Applicazioni*. Milano, Italy: Ed Fratelli Fabbri Editori.

Harris, H. A. 1988. *Masonry: Materials, design, construction, and maintenance.* Conshohocken, PA: ASTM International.

Hofer, L., P. Zampieri, M. A. Zanini, F. Faleschini, and C. Pellegrino. 2018. Seismic damage survey and empirical fragility curves for churches after the August 24, 2016 Central Italy earthquake. *Soil Dynamics and Earthquake Engineering* 111: 98-109.

Ip, K., D. Dizhur, L. Sorrentino, M. Masia, M. Griffith, and J. M. Ingham. (2018). Critical review of numerical modelling techniques for seismic response of complex URM buildings. Paper presented at the *10th Australasian Masonry Conference*. Sydney, Australia, February 12-14.

Italian Guidelines for Built Heritage. DPCM 9 febbraio 2011. Rome, Italy: Gazzetta Ufficiale, 2011.

Jordan, W. C. 2002. *Europe in the Middle Ages*. London, UK: Penguin Books.

Kappos, A. J. 2016. An overview of the development of the hybrid method for seismic vulnerability assessment of buildings. Structure and Infrastructure Engineering 12(12): 1573-1584.

Kaushik, H. B., D. C. Rai, and S. K. Jain. 2007. Stress-strain characteristics of clay brick masonry under uniaxial compression. *Journal of materials in Civil Engineering* 19(9): 728-739.

Klir, G. J., and B. Yuan. 1996. *Fuzzy sets and fuzzy logic: Theory and applications*. Upper Saddle River, NJ: Prentice Hall PTR.

Labuz, J. F., and A. Zang. 2012. Mohr–Coulomb failure criterion. *Rock mechanics and rock engineering*, 45(6): 975-979.

Lagomarsino, S. 2006. On the vulnerability assessment of monumental buildings. *Bulletin of Earthquake Engineering* 4(4): 445-463.

Lagomarsino, S. 2012. Damage assessment of churches after l'Aquila eartquake (2009). Bulletin of Earthquake Engineering 10(1): 73-92.

Lagomarsino, S., A. Brencich, F. Bussolino, A. Moretti, L. C. Pagnini, and S. Podestà. 1997. Una nuova metodologia per il rilievo del danno alle chiese: prime considerazioni sui meccanismi attivati dal sisma. *Ingegneria sismica* 3: 70-82.

Lagomarsino, S., and S. Giovinazzi. 2006. Macroseismic and mechanical models for the vulnerability and damage assessment of current buildings. *Bulletin of Earthquake Engineering* 4(4): 415-443.

Lagomarsino, S., and S. Podestà. 2004. Seismic vulnerability of ancient churches: II. Statistical analysis of surveyed data and methods for risk analysis. *Earthquake Spectra* 20(2): 395-412.

Lagomarsino, S., S. Podestà, G. Cifani, and A. Lemme. 2004. The 31st October 2002 earthquake in Molise (Italy): a new methodology for the damage and seismic vulnerability survey of churches. Paper presented at the 13th World Conference on Earthquake Engineering. Vancouver, Canada, August 1-6.

Lavin, M. A. 1990. The place of narrative: mural decoration in Italian churches, 431-1600. Chicago, IL: University of Chicago Press.

Lemos, J. V. 1995. Assessment of the ultimate load of a masonry arch using discrete elements. *Computer methods in structural masonry* 3: 294-302.

Lourenço, P. B. (1996). *Computational strategies for masonry structures.* Delft, Netherlands: Delft University of Technology.

Luhmann, T., S. Robson, S. Kyle, and J. Boehm. 2013. *Close-range photogrammetry and 3D imaging.* Leck, Germany: CPI books GmbH.

MacCulloch, D. 2010. *Christianity: The first three thousand years.* New York, NY: Penguin.

Made. Come calcolare il valore di un terreno edificabile in pochi passi. Last Modified January 2, 2018. Accessed September 16, 2019. https://ristrutturaconmade.it/come-calcolare-il-valore-di-un-terreno-edificabile/.

Magenes, G., and A. Penna. 2009. Existing masonry buildings: general codes issues and methods of analysis and assessment. *Eurocode 8:* 185-198.

Magenes, G., and G. M. Calvi. 1997. In-plane seismic response of brick masonry walls. *Earthquake engineering & structural dynamics*, 26(12): 1091-1112.

Makoond, N., L. Pelà, and C. Molins. 2019. Dynamic elastic properties of brick masonry constituents. *Construction and Building Materials* 199: 756-770.

Mamdani, E. H. 1976. Advances in the linguistic synthesis of fuzzy controllers. *International Journal of Man-Machines Studies* 8(6): 669-678.

Marino, M., F. Neri, A. Borri, and A. De Maria. (2014). Experimental data of friction coefficient for some types of masonry and its correlation with an index of quality of Masonry (IQM). In *Proceedings of the 2nd European conference on earthquake engineering and seismology*, ed. European Association for Earthquake Engineering (EAEE), 25-29. Istanbul, Turkey: Curran Associates, Inc.

Marotta, A., L. Sorrentino, D. Liberatore, and J. M. Ingham. 2018. Seismic risk assessment of New Zealand unreinforced masonry churches using statistical procedures. *International Journal of Architectural Heritage* 12(3): 448-464.

Marotta, A., S. Sorrentino, D. Liberatore, and J. M. Ingham. 2017. Vulnerability Assessment of Unreinforced Masonry Churches Following the 2010-2011 Canterbury Earthquake Sequence. *Journal of Earthquake Engineering* 21(6): 912-934.

Martinez, J. C. 2009. Methodology for conducting discrete-event simulation studies in construction engineering and management. *Journal of Construction Engineering and Management* 136(1): 3-16.

Masi, A. 2005. La stima della resistenza del calcestruzzo in situ mediante prove distruttive e non distruttive. *Il Giornale delle Prove non Distruttive Monitoraggio Diagnostica* 1: 1-10

McCann, D. M., and M. C. Forde. 2001. Review of NDT methods in the assessment of concrete and masonry structures. *NDT & E International* 34(2): 71-84.

Medasani, S., J. Kim, and R. Krishnapuram. 1998. An overview of membership function generation techniques for pattern recognition. *International Journal of approximate reasoning* 19(3-4): 391-417.

Middleton, J., G. N. Pande, and B. Kralj. 1998. Computer Methods in Structural Masonry-4. Presented at the Fourth International Symposium on Computer Methods in Structural Masonry. London, UK, September 3-5.

Milani, G., and M. Valente. 2015. Comparative pushover and limit analyses on seven masonry churches damaged by the 2012 Emilia-Romagna (Italy) seismic events: Possibilities of non-linear finite elements compared with pre-assigned failure mechanisms. *Engineering Failure Analysis* 47: 129-161.

Mistakidis, E. S., and D. N. Georgiou. 2003. Fuzzy sets in seismic inelastic analysis and design of reinforced concrete frames. *Advances in Engineering Software* 34(10): 589-599.

MIT (Ministero delle Infrastrutture e dei Trasporti). 2018. *Aggiornamento delle "Norme tecniche per le costruzioni"*. Rome, Italy: Gazzetta Ufficiale.

MIT (Ministero delle Infrastrutture e dei Trasporti), and CSLP (Consiglio Superiore dei Lavori Pubblici). Spettri NTC. Last Modified May 8, 2020. Accessed September 23, 2019.

Narendra, T. 2010. *Design of reinforced masonry structures.* Ann Arbor, MI: McGraw-Hill.

The National Academies. 2012. *Disaster Resilience: A National Imperative.* Washington, D.C.: The National Academies Press.

NZSEE (New Zealand Society for Earthquake Engineering), and SESNZ (Structural Engineering Society New Zealand). 2016. *The Seismic Assessment of Existing Building*. Aukland, New Zeland: NZSEE.

Nobile, L., and M. Bonagura. 2013. Accuracy of non-destructive evaluation of concrete compression strength. Paper presented at the 12th International Conference of the

Slovenian Society for Non-Destructive Testing. Portorož, Slovenia, September 4-6.

Ohtsu, M. 2016. Innovative AE and NDT techniques for on-site measurement of concrete and masonry structures. *RILEM State-of-the-Art Reports* 20: 89-103.

Osello, A. 2012. *Il futuro del disegno con il BIM per ingegneri e architetti, The future of Drawing with BIM for Engineers and Architects.* Palermo, Italy: Dario Flaccovio Editore.

Parducci, A. 2011. *Fondamenti di ingegneria sismica in 80 lezioni*. Naples, Italy: Liguori Editore.

Parisi, M. A. V., C. Tardini, and E. Maritato. 2016. Seismic behaviour and vulnerability of church roof structures. *Structural Analysis of Historical Constructions*, 1582-1589.

Penna, A., C. Calderini, L. Sorrentino, C. F. Carocci, E. Cescatti, R. Sisti, A. Borri, C. Modena, and A. Prota. 2019. Damage to churches in the 2016 central Italy earthquakes. *Bulletin of Earthquake Engineering* 10(17): 1-28.

Pir, A., L. S. Hogan, D. Y. Dizhur, K. Q. Walsh, and J. M. Ingham. 2015. A comparison of numerically and experimentally obtained in-plane responses of a full-scale unreinforced masonry building frame. Paper presented at the Tenth Pacific Conference on Earthquake. Auckland, New Zealand, August 6-8.

Pirchio, D., K. Q. Walsh, E. Kerr, I. Giongo, M. Giaretton, B. D. Weldon, L. Ciocci, and L. Sorrentino. 2020a. Seismic Risk Assessment and Intervention Prioritization for Italian Medieval Churches (submitted). *International Journal of Architectural Heritage*.

Pirchio, D., K. Q. Walsh, E. Kerr, I. Giongo, M. Giaretton, B. D. Weldon, L. Ciocci, and L. Sorrentino. 2020b. Aggregated Non-destructive Test Technique for the Assessment of Mechanical Properties of Unreinforced Masonry Italian Medieval Churches (internally reviewed). *Construction and Building Materials*.

Pirchio, D., K. Q. Walsh, E. Kerr, I. Giongo, M. Giaretton, B. D. Weldon, L. Ciocci, and L. Sorrentino. 2020c. Integrated framework to structurally model unreinforced masonry Italian Medieval churches: from photogrammetry to finite element model analysis through building information modeling (internally reviewed). *Engineering Structures*.

Pirenne, J. H., and K. F. Wallace. 1963. *Europe in Transition 1300–1520.* Boston, *MA*: Houghton Mifflin Company.

Pitilakis, K., H. Crowley, and A. M. Kaynia. 2014. SYNER-G: Typology definition and fragility functions for physical elements at seismic risk: buildings, lifelines, transportation networks and critical facilities. *Geotechnical, Geological and Earthquake Engineering* 27: 1-28.

Proietti, G. 1994. *"Dopo la polvere". Rilevazione degli interventi di recupero (1985-1989) del patrimoni artistico-monumentale danneggiato dal terremoto del 1980-1981*. Roma, Italy: Istituto Poligrafico e Zecca dello Stato.

PCN (Protezione Civile Nazionale). Classificazione sismica. Last Modified June 6, 2020. Accessed October 15, 2019. http://www.protezionecivile.gov.it/attivita-rischi/rischio-sismico/attivita/classificazione-sismica.

Quelhas, B., L. Cantini, J. M. Guedes, F. da Porto, and C. Almeida. 2014. Characterization and reinforcement of stone masonry walls. S*tructural Rehabilitation of Old Buildings*: 131-155.

Ragone, A., A. Ippolito, D. Liberatore, and L. Sorrentino. (2017). Emerging technologies for the seismic assessment of historical churches: The case of the bell tower of the cathedral of Matera, Southern Italy. In *Handbook of research on emerging technologies for architectural and archeological heritage*, ed. A. Ippolito, 159-196. Hershey, PA: IGI Global.

Regione Lazio. Tariffa dei Prezzi (Lavori Pubblici). Accessed November 2, 2019. http://www.regione.lazio.it/binary/rl_main/tbl_documenti/INF_DGR_412_06_08_2012_Allegato3.pdf.

RILEM. 1994. NDT 4 Recommendation for in situ concrete strength determination by combined non-destructive methods, 1993. In *RILEM Recommendations for the Testing and Use of Constructions Materials*, ed. Systems and Structures International Union of Laboratories and Experts in Construction Materials, 92-98. E & FN SPON.

Roknuzzaman, M., M. B. Hossain, M. I. Mostazid, and M. R. Haque. 2017. Application of rebound hammer method for estimating compressive strength of bricks. *Journal of Civil Engineering Research* 7(3): 99-104.

Romão, X., and E. Paupério. 2019. An indicator for post-disaster economic loss valuation of impacts on cultural heritage. *International Journal of Architectural Heritage*: 1-20.

Ross, T. 2005. *Fuzzy logic with engineering applications*. Albuquerque, NM: John Wiley & Sons.

Sánchez-Silva, M., and L. Garcia. 2001. Earthquake damage assessment based on fuzzy logic and neural networks. *Earthquake Spectra* 17(1): 89-112.

Sorrentino, L., S. Cattari, F. da Porto, G. Magenes, and A. Penna. 2019. Seismic behaviour of ordinary masonry buildings during the 2016 central Italy earthquakes. *Bulletin of Earthquake Engineering*, 17(10): 5583-5607.

Sorrentino, L., L. Liberatore, L. D. Decanini, and D. Liberatore. 2014. "The performance of churches in the 2012 Emilia earthquakes." *Bulletin of Earthquake Engineering* 12(5): 2299-2331.

Stanghellini, S., A. Mascarello, and V. Ruaro. La stima del valore di trasformazione: definizione e stima. Accessed September 9, 2019. http://www.iuav.it/Ateneo1/docenti/architettu/docenti-st/Stefano-St/archivio-p/CLASA-08-0/LEZIONI/La-stima-del-valore-di-trasformazione.pdf.

Tah, J. H., and V. Carr. 2000. A proposal for construction project risk assessment using fuzzy logic. *Constrution Management & Economics* 18(4): 491-500.

Tesfamaraim, S., and M. Saatcioglu. 2008. Seismic risk assessment of RC building using fuzzy synthetic evaluation. *Journal of Earthquake Engineering* 12(7): 1157-1184.

Tomaževič, M. 1999. *Earthquake-resistant design of masonry buildings.* London, UK: Imperial College Press.

Touring Club Italiano. 1982 - 2015. *Guide Rosse.* Torino, Italy: Touring Club Italiano.

Valente, M., and G. Milani. 2018. Seismic response evaluation and strengthening intervention of two historical masonry churches. Paper presented at the 10th International Masonry Conference. Milan, Italy, July 9-11.

Valente, M., and G. Milani. 2019. Damage survey, simplified assessment, and advanced seismic analyses of two masonry churches after the 2012 Emilia earthquake. *International Journal of Architectural Heritage* 13(6): 901-924.

Vinci, M. 2012. *Metodi di calcolo e tecniche di consolidamento per edifici in muratura*. Palermo, Italy: Universal Book.

Walsh, K. Q., D. Y. Dizhur, I. Giongo, H. Derakhshan, and J. M. Ingham. 2017. Effect of boundary conditions and other factors on URM wall out-of-plane behaviour: design demands, predicted capacity, and in situ proof test results. *Sesoc Journal 30*(1): 57-81.

White, J. 1993. *Art and architecture in Italy 1250-1400*. New Haven, CT: Yale University Press.

Whitehead, A. N. 1898. *A treatise on universal algebra: with applications.* Cambridge, UK: Cambridge University Press.

Yates, F. A. 1944. Paolo Sarpi's "History of the Council of Trent". *Journal of the Warburg and Courtauld Institutes*: 123-143.

Zadeh, L. A. 1965. Fuzzy sets. *Information and control* 8(3): 338-353.

Zucconi, M., R. Ferlito, and L. Sorrentino. 2020. Validation and extension of a statistical usability model for unreinforced masonry buildings with different ground motion intensity measures. *Bulletin of Earthquake Engineering* 18(2): 767-795.